

Aus der Fachrichtung Physiologie
Theoretische Medizin und Biowissenschaften
der Medizinischen Fakultät
der Universität des Saarlandes, Homburg

Functional characterization of vomeronasal receptors using a Herpes Simplex Virus type 1 (HSV-1)-derived amplicon

*Dissertation zur Erlangung des Grades eines Doktors der Naturwissenschaften
der Medizinischen Fakultät
der UNIVERSITÄT DES SAARLANDES*

2017

vorgelegt von: Benjamin Stein
geb. am: 06.10.1983 in Ottweiler

Tag des Prüfungskolloquiums:

Dekan:

Vorsitzender:

Berichterstatter:

Wissenschaft: Es ist nicht ihr Ziel, der unendlichen Weisheit eine Tür zu öffnen, sondern eine Grenze zu setzen dem unendlichen Irrtum.

Bertolt Brecht

The following manuscripts emerged from this thesis:

Stein B, Alonso MT, Zufall F, Leinders-Zufall T, Chamero P (2016) Functional Overexpression of Vomeronasal Receptors Using a Herpes Simplex Virus Type 1 (HSV-1)-Derived Amplicon. PLoS One 19; 11: e0156092.

Pérez-Gómez A, Bleyemehl K, **Stein B**, Pyrski M, Birnbaumer L, Munger SD, Leinders-Zufall T, Zufall F, Chamero P (2015) Innate Predator Odor Aversion Driven by Parallel Olfactory Subsystems that Converge in the Ventromedial Hypothalamus. Curr Biol 25: 1340-1346.

Pérez-Gómez A, **Stein B**, Leinders-Zufall T, Chamero P (2014) Signaling mechanisms and behavioral function of the mouse basal vomeronasal neuroepithelium. Front Neuroanat 26, 8: 135.

Table of Contents

Table of Contents	I
List of Figures	IV
List of Tables	VI
Abstract	VII
Zusammenfassung	VIII
Abbreviations	IX
1 INTRODUCTION	1
1.1 The olfactory system	1
1.1.1 Main olfactory system (MOS)	2
1.1.1.1 Canonical olfactory sensory neurons (OSNs).....	3
1.1.1.2 The guanylyl cyclase D (GC-D) system and necklace glomeruli	6
1.1.1.3 Trace amine-associated receptor (Taar) neurons	7
1.1.1.4 Other OSN subgroups	7
1.1.1.5 Behavior mediated by the MOE	8
1.1.2 Grüneberg ganglion (GG).....	9
1.1.3 Septal organ of Masera (SOM)	9
1.1.4 Vomeronasal organ (VNO).....	9
1.1.4.1 VNO structure.....	9
1.1.4.2 Vomeronasal receptor family 1 (V1r).....	10
1.1.4.3 Vomeronasal receptor family 2 (V2r).....	12
1.1.4.4 Formyl peptide receptors (Fprs)	17
1.1.4.5 Canonical olfactory receptors in the VNO.....	18
1.1.4.6 Signal transduction.....	18
1.1.4.7 Projection of VSNs.....	20
1.1.4.8 Behavior mediated by the VNO	21
1.1.5 Deorphanizing receptor-ligand interactions	23
1.1.5.1 Heterologous system.....	23
1.1.5.2 Gene delivery in sensory neurons by viral vectors.....	25
1.1.5.3 Gene-targeted mouse models as a Vr-deorphanizing tool.....	26
2 AIMS	27
3 MATERIALS AND METHODS	28
3.1 Molecular cloning	28
3.1.1 RNA extraction from tissue	28
3.1.2 cDNA synthesis.....	28
3.1.3 Vomeronasal receptor cloning into pHSV-IRES-GFP vector.....	29
3.1.3.1 Amplification of receptor genes.....	29
3.1.3.2 Gel electrophoresis	30
3.1.3.3 Gel Band extraction.....	31
3.1.3.4 DNA and RNA concentration measurements	31
3.1.3.5 Sequencing	31
3.1.3.6 Subcloning into pGEM®-T Easy and TOPO®-TA vectors	31
3.1.3.7 Preparation of competent Escherichia coli (E. coli).....	32
3.1.3.8 Transformation of E. coli.....	32
3.1.3.9 Isolation of bacterial clones and plasmid amplification.....	33
3.1.3.10 Restriction analysis for receptor cloning.....	33
3.1.3.11 Subcloning into pHSV-IRES-GFP expression vector.....	34

3.1.3.12	<i>Ligation</i>	34
3.1.3.13	<i>Preparation of glycerol stocks</i>	34
3.1.4	Cloning procedure mCherry	34
3.1.4.1	<i>Cloning pHSV-IRES-mCherry constructs</i>	34
3.1.4.2	<i>pHSV-Vmn2r74-IRES-mCherry construct</i>	35
3.1.5	Cloning of the recombinant major urinary protein 20 (MUP20)	35
3.1.6	Production of recombinant major urinary proteins (MUPs)	36
3.1.7	Sodium dodecyl sulfate polyacrylamide gel electrophoresis (SDS-PAGE)	37
3.2	Calcium imaging measurements using ratiometric calcium indicator dye fura-2 AM	37
3.2.1	Fura-2 loading	37
3.2.2	Live cell calcium imaging measurement	38
3.2.3	Data processing and analysis	38
3.2.4	Chemostimuli	39
3.2.4.1	<i>High molecular weight urine fraction (HMW) preparation</i>	40
3.2.4.2	<i>Cat fur odor solution (CFO) preparation</i>	40
3.3	Single cell RT-PCR	40
3.3.1	Low cell RT-PCR	42
3.4	Cell-line culture	43
3.4.1	HEK293 cell culture	43
3.4.2	2-2 cell-line	43
3.5	Primary cell culture	43
3.5.1	Dissociation of mouse vomeronasal sensory neurons (VSNs)	43
3.5.2	Dissociation of mouse olfactory sensory neurons (OSNs)	44
3.6	Generation of HSV-1-derived amplicons	44
3.6.1	Amplification of helper virus stock	46
3.6.2	Amplicon titration	46
3.7	Viral infection	47
3.8	Transient Transfection	47
3.9	Mice	47
3.9.1	Animal care and housing	47
3.9.2	C57BL/6 wild type mice	48
3.9.3	Omp-GFP mice	48
3.9.4	<i>Gnao1/OMP-Cre conditional G_o knockout mice</i>	48
3.10	Computational analysis and tools	48
3.10.1	Software	48
3.10.1.1	<i>Microsoft office Word 2007</i>	48
3.10.1.2	<i>CorelDRAW Graphics suite X7</i>	49
3.10.1.3	<i>XcellencePro software (Olympus)</i>	49
3.10.1.4	<i>Origin 8.6 (OriginLab) and ImageJ 1.50i (NIH)</i>	49
3.10.1.5	<i>Chromas Lite (Technelysium Pty Ltd) and AnnHyb (Bioinformatics Organization)</i>	49
3.10.2	Computational analysis	49
3.10.2.1	<i>GFP fluorescence intensity comparison</i>	49
3.10.3	Online tools	50
3.11	Statistics and mathematics	50
3.12	Media and buffers	50

4 RESULTS 52

4.1	Functional overexpression of vomeronasal receptors	52
4.1.1	Heterologous expression of <i>Vmn1r89 (V1rj2)</i> in HEK293 cells	52

4.1.2	Herpes Simplex Virus type 1 (HSV-1)-derived amplicon system.....	54
4.1.2.1	<i>Cloning strategy</i>	54
4.1.2.2	<i>Time course of GFP expression in amplicon-infected HEK293 cells</i>	57
4.1.2.3	<i>HSV-1-Vmn1r89-GFP amplicon infection in HEK293 cells</i>	58
4.1.2.4	<i>Culture of vomeronasal sensory neurons (VSNs)</i>	59
4.1.2.5	<i>HSV-1-GFP amplicon infection of native VSNs</i>	63
4.1.2.6	<i>HSV-1-mCherry amplicon infection in native VSNs</i>	64
4.1.3	Functional validation of the HSV-1-derived expression system in VSNs	65
4.1.3.1	<i>Vmn1r89 expression in VSNs</i>	65
4.1.3.2	<i>Expression of Vmn1r237 in native VSNs</i>	69
4.1.3.3	<i>Functional expression of a V2r (Vmn2r26) in native VSNs</i>	72
4.1.3.4	<i>Expression of Fpr3 in native VSNs</i>	74
4.2	A putative high molecular weight fraction (HMW) receptor	76
4.2.1	HMW-induced activation of <i>Vmn2r74</i>	76
4.2.2	Dose-dependent activation of <i>Vmn2r74-GFP</i> amplicon-infected cells	81
4.2.3	HMW activation of <i>Vmn2r74-GFP</i> amplicon-infected <i>Omp-GFP</i> VSNs	84
4.2.4	<i>Vmn2r74</i> expression in olfactory sensory neurons (OSNs).....	85
4.2.5	Strain-dependent difference in HMW activation of <i>Vmn2r74-GFP</i> -expressing VSNs	87
4.2.6	Single MUP activation of <i>Vmn2r74-GFP</i> -expressing VSNs	91
4.3	Receptor identification by Calcium imaging and single cell RT-PCR	93
4.3.1	Identification of specific gene transcripts in whole VNO using RT-PCR	93
4.3.2	Detection of gene-specific transcripts from individual VSNs	94
4.3.3	RT-PCR of HMW-activated native VSNs.....	95
4.3.4	Detection of gene transcripts in single VSNs after stimulus activation.....	96
4.4	Kairomone activation of VSNs	99
5	DISCUSSION	102
5.1	<i>Vr expression in heterologous cells</i>	102
5.2	<i>HSV-1-derived amplicon system to transduce Vrs to intact VSNs</i>	104
5.3	<i>Infection efficiency and natural tropism of HSV-1 for VSNs</i>	104
5.4	<i>GFP expression properties of HSV-1-derived amplicon-infected cells</i>	105
5.5	<i>Functional validation of Vr expression</i>	106
5.6	<i>Vmn2r74 receptor expression increases responses to HMW</i>	108
5.7	<i>Single cell RT-PCR to decipher receptor-ligand pairs</i>	111
5.8	<i>VSN detection of the cat MUP Feld4</i>	113
6	CONCLUSIONS	114
7	LITERATURE	115
8	ACKNOWLEDGEMENTS	143
9	COPYRIGHT PERMISSION	145

List of Figures

Figure 1:	Schematic sagittal section of the mouse head with its different olfactory subsystems.	2
Figure 2:	Schematic drawing of olfactory receptor (Or) topology.	5
Figure 3:	Schematic coronal section of the VNO and receptors located in the sensory epithelium.	14
Figure 4:	Proposed VNO signal transduction pathway.	20
Figure 5:	Production of HSV-1-derived amplicons in 2-2 cells.	46
Figure 6:	Fura-2 calcium imaging assay of transfected HEK293 cells.	54
Figure 7:	pHSV expression vectors.	56
Figure 8:	<i>GFP</i> expression in infected HEK293 cells.	57
Figure 9:	Viral transduction of <i>Vmn1r89-GFP</i> in HEK293 cells.	59
Figure 10:	Culture of freshly dissociated VSNs and infection with HSV-1-derived amplicons.	60
Figure 11:	VSN culture after amplicon infection.	61
Figure 12:	HSV-1 transgene expression profile at different time points in VSNs.	62
Figure 13:	Alternative gene delivery system in VSNs.	63
Figure 14:	HSV-1- <i>GFP</i> amplicon infection of VSNs followed by fura-2 loading.	64
Figure 15:	HSV-1-derived amplicon infection of heterozygous <i>Omp-GFP</i> VSNs.	65
Figure 16:	Functional expression of <i>Vmn1r89</i> in HSV-1-derived amplicon-infected VSNs.	67
Figure 17:	Response profile of VSNs responding to E mix.	69
Figure 18:	<i>Vmn1r237</i> expression in VSNs increases responsivity to E mix.	71
Figure 19:	Viral transduction of <i>Vmn2r26</i> in VSNs.	73
Figure 20:	Viral transduction of <i>Vmn2r26</i> in <i>cG_o^{-/-}</i> VSNs.	74
Figure 21:	Viral transduction of <i>Fpr3</i> in VSNs.	75
Figure 22:	Expression of <i>Vmn2r74</i> in HSV-1-derived amplicon-infected VSNs.	77
Figure 23:	Viral transduction of 3 <i>V2rs</i> in native VNSs.	79
Figure 24:	Response profile of <i>Vmn2r74-GFP</i> amplicon-infected VSNs.	80
Figure 25:	Viral transduction of <i>Vmn2r74</i> in <i>cG_o^{-/-}</i> VSNs.	81
Figure 26:	Summary of GFP-positive cell activation for different dilutions of HMW.	82
Figure 27:	Calcium imaging of VSNs infected with <i>Vmn2r74-GFP</i> amplicons and stimulated with different HMW dilutions.	83
Figure 28:	Expression of <i>Vmn2r74</i> in <i>Omp-GFP</i> cells.	84
Figure 29:	HSV-1-derived amplicon infection in olfactory sensory neurons (OSNs).	86
Figure 30:	Viral transduction of <i>Vmn2r74</i> in OSNs.	87
Figure 31:	Calcium imaging measurements of <i>Vmn2r74-GFP</i> -expressing cells to HMW from different mouse strains.	88
Figure 32:	Summary of GFP+ cell activation by HMW fractions from different mouse strains.	90

Figure 33:	Recombinant MUP (rMUP) stimulation of <i>Vmn2r74</i> -transduced VSNs.	92
Figure 34:	Ethidium bromide-stained agarose gels of RT-PCR products of whole VNO cDNA.	94
Figure 35:	RT-PCRs for olfactory marker protein (<i>Omp</i>) and transient receptor potential channel <i>c2</i> (<i>Trpc2</i>).	95
Figure 36:	Gene-specific RT-PCR for <i>Trpc2</i> and <i>Vmn2r1</i> in isolated VSNs after HMW stimulation in calcium imaging.	96
Figure 37:	Cell picking of VSNs activated by the sulfated steroid E1050.	97
Figure 38:	Single cell RT-PCR of VSNs responding to the sulfated steroid E1050 in calcium imaging.	98
Figure 39:	Representative F340/F380 ratio traces from B6 and <i>cG_o^{-/-}</i> VSNs.	100
Figure 40:	Summary of VSN kairomone activation in mice lacking <i>G_o</i> (<i>cG_o^{-/-}</i>).	101

List of Tables

Table 1. List of selected signaling molecules with proposed receptors and behavioral output.	21
Table 2. Gene-specific primers.	30
Table 3. Gene-specific primers for Single and Low cell RT-PCR.	42

Abstract

Mammals are equipped with several anatomically and functionally distinct sensory systems to communicate with the external world. The accessory olfactory system (also known as the vomeronasal system) is specialized to detect socially relevant chemosignals and transmit sensory information to higher brain areas. Chemoperception is mediated by vomeronasal sensory neurons (VSNs) expressing chemoreceptors out of three major families of G protein-coupled receptors (GPCRs): vomeronasal receptors (*Vrs*) type 1 (*V1rs/Vmn1rs*), type 2 (*V2rs/Vmn2rs*), and a subgroup of formyl peptide receptors (*Fprs*). *V1rs* and some *Fprs* are expressed in VSNs localized in the apical zone of the sensory epithelium and coexpress with the G protein subunit G_{i2} . Basal VSNs express *V2rs* or one *Fpr* and overlap with the expression of the G protein subunit G_o . Thus far, only a limited number of *Vrs* out of the almost 400 receptor genes were matched with their potential ligands, at least partially due to a tremendous amount of potential agonists as well as the lack of robust heterologous expression assays to analyze receptor-ligand interactions. To overcome this limitation, I hypothesized that a Herpes Simplex Virus type 1 (HSV-1)-derived amplicon delivery system can facilitate expression of all three groups of vomeronasal receptor genes in native VSNs to characterize cell responses to potential ligands. To test this hypothesis, I validated the functionality of the expression system with proposed receptor-ligand interactions. I showed through calcium imaging measurements in infected VSNs that amplicon-induced expression of *Vmn1r89*, *Vmn1r237*, *Vmn2r26*, and *Fpr3* caused a robust increase in responsivity to sulfated steroids, a MHC-peptide, or the hexapeptide W-peptide. Suggested receptor-ligand interactions were partially confirmed by combining calcium imaging measurements with a single cell Reverse Transcriptase-Polymerase Chain Reaction (RT-PCR) approach. Furthermore, the developed expression system allowed me to propose for the first time a potential receptor (*Vmn2r74*) to detect the high molecular weight urine fraction (HMW), a source of major urinary proteins (MUPs). HMW is linked to various behavioral outputs like aggression, attraction, or countermarking.

In summary, I provide a novel tool to deorphanize VNO ligand detection; an important requirement to understand chemosignal-based mammalian communication.

Zusammenfassung

Um mit ihrem äußeren Umfeld zu kommunizieren, sind Säugetiere mit mehreren anatomisch und funktionell unterschiedlichen Sensorik-Systemen ausgestattet. Das akzessorische olfaktorische System (auch bekannt als Vomeronasalorgan) ist darauf spezialisiert sozial relevante chemische Signalstoffe zu erkennen und an höhere Hirnzentren weiterzuleiten. Die Perzeption chemischer Signalstoffe wird von sensorischen Vomeronasalneuronen vermittelt, die Chemorezeptoren der drei Hauptfamilien von G Protein-gekoppelten Rezeptoren (GPCRs), nämlich den Vomeronasalrezeptoren Typ 1 (*V1rs/Vmn1rs*), Typ 2 (*V2rs/Vmn2rs*) und eine Untergruppe von Formyl Peptid Rezeptoren (*Fprs*), exprimieren. *V1rs* und einige *Fprs* werden zusammen mit der G Protein Untereinheit G_{i2} in apikal gelegenen VSNs expremiert. Basale VSNs hingegen expremieren *V2rs* oder einen *Fpr* zusammen mit der G Protein Untereinheit G_o . Bisher konnte nur für eine begrenzte Anzahl *Vrs* der beinahe 400 Rezeptorgenen der passende Ligand identifiziert werden, was zumindest teilweise darin begründet ist, dass es eine schier unendliche Anzahl an möglichen Agonisten gibt, sowie dem Fehlen eines robusten heterologen Testsystems zum Entschlüsseln von Rezeptor-Liganden Interaktionen. Um dieses Problem zu lösen, habe ich die Hypothese aufgestellt, dass ein Herpes Simplex Virus Typ 1 (HSV-1) basiertes Amplicon Transfer System zur Expression aller drei Gruppen von vomeronasalen Rezeptorgenen in natürlichen VSNs genutzt werden kann, um zelluläre Antworten auf potentielle Liganden zu untersuchen. Um diese Hypothese zu testen, habe ich die Funktionalität des Expressionssystems mit bekannten Rezeptor-Liganden Interaktionspartnern validiert. Ich habe durch Calcium Imaging Experimente in infizierten VSNs gezeigt, dass die virale Expression von *Vmn1r89*, *Vmn1r237*, *Vmn2r26* und *Fpr3* zu einem deutlichen Anstieg der Antworten auf sulfatierte Steroide, auf ein MHC-bindendes Peptid und das Hexapeptid W-Peptid führt. Die vorgeschlagenen Rezeptor-Liganden Interaktionen wurden teilweise durch eine Kombination von Calcium Imaging Messungen mit der Einzelzell Reverse Transcriptase-Polymerase Chain Reaction (RT-PCR) bestätigt. Darüber hinaus konnte ich mit diesem Expressionssystem zum ersten Mal einen potentiellen Rezeptor (*Vmn2r74*) zur Detektion der Urinfraction ermitteln, die Komponenten eines höheren Molekulargewichtes (High Molecular Weight; HMW) beinhaltet. Die HMW Fraktion enthält die *Major Urinary Proteins* (MUPs) und steuert zahlreiche Verhalten wie z.B. Aggression, Attraktion oder Markierungsverhalten. Zusammenfassend stelle ich ein neues Hilfsmittel vor um die Detektion von VNO-Liganden zu entschlüsseln; eine wichtige Voraussetzung zum Verständnis der Kommunikation von Säugetieren mittels chemischer Signalstoffe.

Abbreviations

2,5-DMP	2,5-dimethylpyrazine
2,3-DHB	2,3-dehydro-exo-brevicommin
A ₂₆₀	absorption at a wavelength of 260 nm
A ₂₈₀	absorption at a wavelength of 280 nm
A7864	5-androsten-3 , 17 -diol disulfate
AA	arachidonic acid
ACIII	adenylyl cyclase III
AM	acetoxymethyl ester
Amp	ampicillin
ANO1/2	anoctamin 1/2 channels
ANOVA	analysis of variance
AOB	accessory olfactory bulb
AOS	accessory olfactory system
ATP	adenosine triphosphate
a.u.	arbitrary units
AV	adenovirus
AAV	adeno-associated virus
C57BL/6 (B6)	C57BL/6 mouse strain
BALB/c (B/c)	BALB/c mouse strain
BES	N,N-bis (2-hydroxyethyl)-2-aminoethanesulfonic acid
BF	bright field
BK	big potassium channel
BSA	bovine serum albumin
bidest.	bidestillated
°C	degree Celsius
C1	ligation mix without insert
C2	ligation mix without insert and T4 DNA ligase
cAMP	cyclic adenosine-3',5'-monophosphate
CAN	calcium-activated non-selective cation channel
CCD	charge-coupled device
cDNA	complementary deoxyribonucleic acid
CFO	cat fur odor
cG _o ^{-/-}	conditional G _o gene ablation

cG _o ^{+/-}	conditional heterozygous G _o gene ablation
cGMP	cyclic guanosine-3',5'-monophosphate
CNG	cyclic nucleotide-gated channel
CNGA2/A3	cyclic nucleotide-gated channel subunit A2/A3
Co.	company
ColE1	sequence (origin of replication) derived from colicin E1 plasmid
CPE	cytopathic effect
CRAMP	cathelicidin-related antimicrobial peptide
cre	cre recombinase
<i>cursive lettering</i>	gene name
DAG	diacylglycerol
dATP	2'-deoxyadenosine 5'-triphosphate
dCTP	2'-deoxycytidine 5'-triphosphate
D-cysteine HCl	cysteine hydrogen chloride D-enantiomer
DEPC	diethyl dicarbonate
D-glucose	glucose D-enantiomer
dGTP	2'-deoxyguanosine 5'-triphosphate
DMEM	Dulbecco's modified Eagle's medium
DMEM- GlutaMAX TM -I	Dulbecco's modified Eagle's medium supplement with GlutaMAX TM -I
DMSO	dimethyl sulfoxide
DNA	deoxyribonucleic acid
dNTP	2'-deoxynucleoside 5'-triphosphate
DTT	dithiothreitol
dTTP	2'-deoxythymidine 5'-triphosphate
E1050	1,3,5(10)-estratrien-3, 17 -diol disulphate
E1100	1,3,5(10)-estratrien-3, 17 -diol 3-sulphate
E0893	1,3,5(10)-estratrien-3, 17 -diol 3-sulphate
E0588	1,3,5(10)-7-estratetraen-3, 17 -diol 3-sulphate
E2734	1,3,5(10)-estratrien-3, 16 , 17 -triol 17-sulphate
EBV	Epstein-Barr virus
EDTA	ethylenediaminetetraacetic acid
E mix	estrogen mix
E. coli	Escherichia coli

ESP	exocrine gland-secreting peptide
ESP1/22	exocrine gland-secreting peptide 1/22
EVG	electrovomerogram
<i>EX Taq</i> ® HS DNA Polymerase	<i>EX Taq</i> ® Hot start DNA Polymerase
f-	functional formyl group (-CHO) at the N-terminus of a protein
F340	fluorescence intensity at 340 nm
F380	fluorescence intensity at 380 nm
FBS	fetal bovine serum
Flag-tag	Flag octapeptide
f-MLF	N-formyl-methionine-leucine-phenylalanine
F ₀	baseline fluorescence ratio value
F _P	peak fluorescence ratio value
Fpr	formyl peptide receptor
Fpr-rs	formyl peptide receptor-related sequence
fura-2	ratiometric calcium dye fura-2 AM
g	acceleration due to gravity
G α_{i2} (G _i)	G protein alpha i2 subunit
G $\alpha_{i2 \ 2 \ 2}$	complex of G protein alpha o, beta 2 and gamma 2 subunit
G α_o (G _o)	G protein alpha o subunit
G $\alpha_{o \ 2 \ 8}$	complex of G protein alpha o, beta 2 and gamma 8 subunit
G α_{olf}	G protein alpha olfactory subunit
G /G γ -complex	complex of G protein beta and gamma subunit
G γ_2	G protein gamma 2 subunit
G γ_8	G protein gamma 8 subunit
GC-D	guanylyl cyclase D
GFP+	GFP-expressing
GFP	green fluorescence protein
GG	Grüneberg ganglion
GIRK	G protein-coupled inwardly-rectifying potassium channel
GPCR	G protein-coupled receptor
Gucy1B2	guanylyl cyclase 1B2
h	hour
H2-Mv	major histocompatibility complex molecule

H2-Mv+	<i>H2-Mv</i> -expressing cells
H2-Mv-	<i>H2-Mv</i> -non-expressing cells
H2-Mv/ 2-microglobulin	complex of a major histocompatibility complex molecule and 2-microglobulin
HANA3A	HEK293T-derived cell system
HBSS	Hankø balanced salt solution
HEK293	human embryonic kidney cell line 293
HeLa/Olf	HeLa-derived cell line
HEPES	4-(2-hydroxyethyl)-1-piperazineethane-sulfonic acid
HMW	high molecular weight fraction of urine
HSV-1	herpes simplex virus type 1
HSV-1 a/pac	herpes simplex virus type 1 packaging sequence
IE 4/5	immediate early 4/5 viral promoter sequence
IP ₃	inositol 1,4,5-trisphosphate
IPTG	isopropyl -D-1-thiogalactopyranoside
IRES	internal ribosomal entry site
kDa	kilodalton
LB	Luria-Broth medium
LB/Amp	Luria-Broth medium supplemented with 100 µg/ml ampicillin
l	liter
LMW	low molecular weight fraction of urine
Lucy-tag	17 amino acids of the membrane protein LRRC32 added to N-terminus of proteins
M1/9/10/11	<i>H2-Mv</i> families
MBP	maltose binding protein
mCherry	mCherry fluorophore
MCS	multiple cloning site
MHC	major histocompatibility complex
MHC I	major histocompatibility complex class I
min	minute
ml	milliliter
mM	millimolar
MOB	main olfactory bulb
MOE	main olfactory epithelium

MOPS	3-(N-morpholino) propanesulfonic acid
MOS	main olfactory system
mRNA	messenger ribonucleic acid
MS4A	membrane-spanning 4-domain family, subfamily A
MTMT	(methylthio) methanethiol
MUP	major urinary protein
mV	millivolt
N=	number of cells or performed experiments
N-	N-terminus of a protein
NC	nasal cavity
NCBI	national center for biotechnology information
ND1	mitochondria-derived peptide (f-MFFINTLTL)
NEB	New England Biolabs
ng	nanogram
NG	necklace glomeruli
Non-GFP	cells not expressing GFP
NP-40	Nonidet P-40
n/r	non-responder cells in single cell RT-PCR
NT	not tested
OlfR	olfactory receptor
OMP	olfactory marker protein
Opti-MEM®	cell culture medium (Invitrogen)
Or	olfactory receptor
oriS	origin of replication sequence
OSN	olfactory sensory neuron
P0/P1/P2	supernatant fraction during viral amplicon preparation
PBS	phosphate-buffered saline
pcDNA3.1/hChR2 (H134R)	plasmid equipped with <i>mCherry</i> fluorophore sequence
PCR	polymerase chain reaction
PDE4A	phosphodiesterase 4A
pfu	plaque-forming unit
pHSV-IRES-GFP/mCherry	herpes simplex virus-based plasmid containing IRES sequence and fluorescent marker protein sequence (GFP or mCherry)
PIP ₂	phosphatidylinositol-4,5-bisphosphate

PLC	phospholipase C
PLC	phospholipase C
pMal-2cx	plasmid for protein expression and purification
poly(A)	polyadenylation sequence
RAMP	receptor activity-modifying proteins
REEP1	receptor expression-enhancing protein
rFeld4	recombinant major urinary protein Feld4
Rho-tag	the first 20/39 amino acids of bovine rhodopsin
Ric8B	guanine nucleotide exchange factor B
rMUP	recombinant major urinary protein
RNA	ribonucleic acid
ROI	region of interest
rpm	revolutions per minute
RT	room temperature
RTP1	receptor-transporting protein 1
RTP2	receptor-transporting protein 2
RT-PCR	reverse transcription polymerase chain reaction
s	second
SBT	2-sec-butyl-4,5-dihydrothiazole
SDS	sodium dodecyl sulfate
SDS-PAGE	sodium dodecyl sulfate polyacrylamide gel electrophoresis
SEM	standard error of mean
Sf9	insect cell line from <i>Spodoptera frugiperda</i> pupal ovarian tissue
SK3	small conductance calcium-activated potassium channel
SNP	single-nucleotide polymorphism
SOC	super optimal broth with catabolite repression
SOM	septal organ of Masera
SYF	MHC-peptide (SYFPEITHI)
Taar	trace amine-associated receptor
TBE	Tris-Borat-EDTA buffer
TdT	terminal deoxynucleotidyl transferase
TM	transmembrane domain
TMEM16A	transmembrane member 16A
TMEM16B	transmembrane member 16B

Tris	2-amino-2-(hydroxymethyl) propane-1,3-diol
Tris-HCl	tris hydrochloride
Trp	transient receptor potential
Trpc2	transient receptor potential cation channel, subfamily c, member 2
Trpc6	transient receptor potential cation channel, subfamily c, member 6
Trpm5	transient receptor potential cation channel, subfamily m, member 5
UCSC	University of California, Santa Cruz
U	unit
μl	microliter
μM	micromolar
UV	ultraviolet
V1rj	vomeronasal type 1 receptor subfamily j
Vmn1r, V1r	vomeronasal type 1 receptor
Vmn2r, V2r	vomeronasal type 2 receptor
VNO	vomeronasal organ
VSN	vomeronasal sensory neuron
wc1	water control 1; from 1 st amplification PCR
wc2	water control 2; from 2 nd gene-specific PCR
w-pep (w-peptide)	synthetic hexapeptide (WKYMVm)
X-Gal	5-bromo-4-chloro-3-indolyl-β-D-galactopyranoside
YT	yeast extract and tryptone
Z5-14: OH	(Z)-5-tetradecen-1-ol

1 INTRODUCTION

1.1 The olfactory system

Animals must constantly make decisions about food, resources, predators, competitors, and mates. Correct processing of environmental information is essential for making these appropriate decisions and to maximize survival. Therefore, animals are equipped with different perception systems to sense, facilitate, and decode the information emerging from their surroundings. Most nocturnal animals, such as mice, have a highly developed olfactory system to detect chemosignals enabling them to communicate with the environment. These chemosignals convey information about predators, food as well as reproductive status and gender of conspecifics. To process this huge variety of chemical information, the olfactory system in mice has evolved into several distinct subsystems, some of which are anatomically segregated (Fig. 1) (Munger *et al.*, 2009). These subsystems are comprised of the canonical main olfactory system and the accessory olfactory system (also known as the vomeronasal system). Other known smaller olfactory subsystems also exist in the nose, such as the septal organ of Maserà, the GC-D cell system, the trace-amine-associated receptor cell system, and the Grüneberg ganglion (GG).

Anatomical separation is accompanied by functional divergence and is executed by specialized chemoreceptors, signaling mechanisms, and neural projections to olfactory processing nuclei in the brain. However, many of the receptors identified are orphan-receptors, particularly those in the vomeronasal system with its 400 receptor genes, where only a few receptors have been matched with suitable ligands. To overcome this limitation, a novel expression system was developed to deorphanize receptor-ligand interactions in the vomeronasal system. Knowledge of chemostimuli detected by the vomeronasal organ may also help to decipher the logic of chemodetection in other subsystems, as some ligands activate more than one subsystem. Due to this partially overlapping activation pattern, the following sections will introduce the reader to the most prominent olfactory subsystems and their receptors.

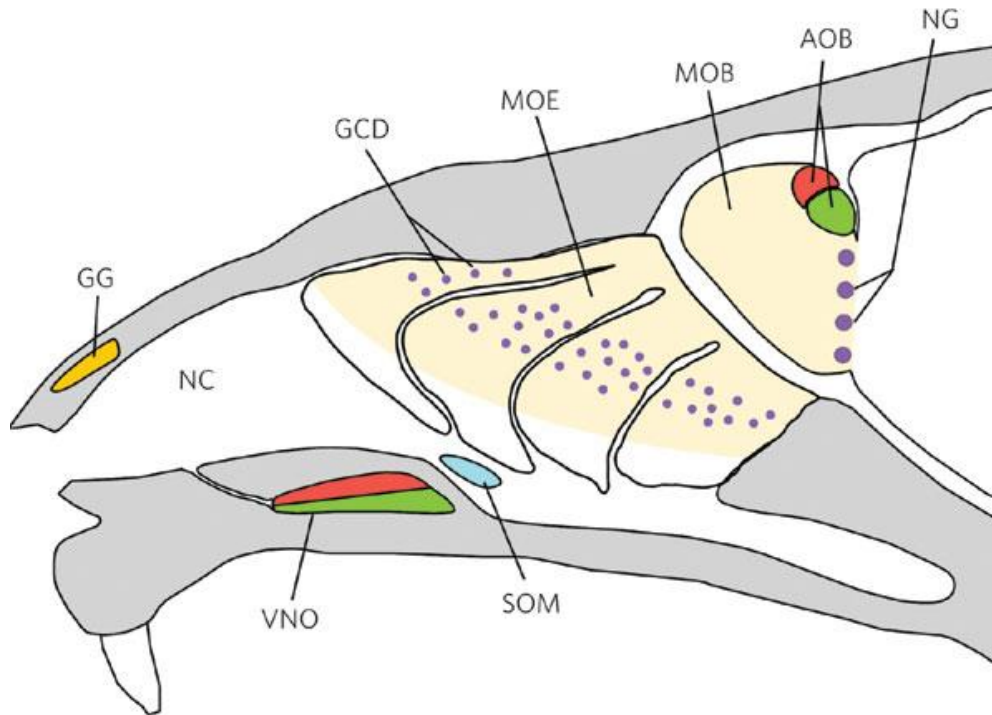


Figure 1: Schematic sagittal section of the mouse head with its different olfactory subsystems.

The tip of the nose hosts the Grüneberg ganglion (GG) neurons (yellow). The vomeronasal organ (VNO) is separated into at least two molecular distinct zones called the apical and basal zones (green and red). The nasopalatine duct enables contact to the nasal cavity (NC) and is filled with mucus. The main olfactory epithelium (MOE) is separated into four turbinates and equipped with different sensory neurons: the guanylyl-cyclase D neurons (GCD; purple dots), trace amine-associated receptor neurons (Taars), and canonical odorant receptor-expressing neurons (OSNs). The septal organ of Masera (SOM; light blue) is located in the septum, ventral to the MOE. The main olfactory bulb (MOB), the necklace glomeruli (NG), and the accessory olfactory bulb (AOB) form the olfactory bulb in the mouse forebrain. These structures are innervated by different sensory olfactory neuron types and send further projections to higher brain areas. Figure adapted from Leinders-Zufall T, Ma M (2009) Olfactory Epithelium. In: Squire L, Albright T, Bloom F, Gage F, Spitzer N (eds) Encyclopedia of Neuroscience, 4th edition. Elsevier Science, Amsterdam, pp. 113-118.

1.1.1 Main olfactory system (MOS)

Among different perception systems, the sense of smell is one of the most fascinating senses for humans, probably due to broad emotional associations (Krusemark *et al.*, 2013). Humans may discriminate up to one trillion stimuli (Bushdid *et al.*, 2014). Although the exact number remains controversial (Meister, 2015), olfaction enables animals to sense and evaluate a huge number of chemical signals present in the environment. The MOS consists of the main olfactory epithelium (MOE), the main olfactory bulb (MOB), and higher olfactory centers of the brain (Munger *et al.*, 2009). The MOE is composed of a heterogeneous group of sensory cells characterized by the expression of receptors, signaling components, and ion channels (Zufall and Munger, 2001).

1.1.1.1 Canonical olfactory sensory neurons (OSNs)

The vast majority of sensory neurons in the MOE express one member of the odorant receptor (*Or*) gene family, termed classical or canonical olfactory sensory neurons (OSNs). Canonical OSNs are ciliated, bipolar in shape, and have been proposed to detect odorants (Munger *et al.*, 2009). Ors were identified in the early 1990s by Buck and Axel and belong to the class A rhodopsin-like G protein-coupled receptors (GPCRs) (Buck and Axel, 1991).

GPCRs are coupled to G proteins and participate in initial signaling mechanisms, leading to opening of ion channels (Imai and Sakano, 2008). Activation of G protein-coupled signaling cascades may also affect transcriptional regulation (Sorkin and Von Zastrow, 2009). *Ors* account for 364% of the mammalian genome, whereas the number of *Or* genes varies between species: humans possess 3006400 intact genes and almost the same number of pseudogenes (Niimura and Nei, 2003; Matsui *et al.*, 2010; Verbeurgt *et al.*, 2014). *Or* genes are distributed on almost every human chromosome (except chromosomes 20 and Y) with a high degree of individual diversity. This diversity is further increased by different mechanisms, such as single-nucleotide polymorphisms and insertions/deletions of *Or* loci. The mouse genome contains about 1430 total *Or* genes, of which almost 1200 are intact (Niimura, 2009). GPCRs have a high relevance in medical drug design studies, as they are involved in the regulation of many physiological processes in the body. The Ors are particularly interesting as they make up the largest family of GPCRs.

These receptors have a conserved N-terminal glycosylation site and several conserved motifs in transmembrane regions 3 (TM3), 5 (TM5), 6 (TM6), and 7 (TM7) (Fig. 2) (Fleischer *et al.*, 2009). Computational homology modeling and side-directed mutagenesis studies on the structure of Ors have revealed that TM3, TM5, TM6, and TM7 build a ligand binding site formed by hydrophobic amino acids, which is important for receptor-ligand interactions (Katada *et al.*, 2005; Abaffy *et al.*, 2007). Such hydrophobic interactions are weaker than ionic- or hydrogen-based interactions observed in non-olfactory GPCRs and could explain the relatively high tolerance in the tuning profile and overlapping receptive range of many Ors (Araneda *et al.*, 2000; Kajiya *et al.*, 2001; Abaffy *et al.*, 2006; Repicky and Luetje, 2009; Saito *et al.*, 2009). Furthermore, studies in humans and *Drosophila melanogaster* suggest that Ors may form homo- or heterooligomers for signal transduction (Neuhaus *et al.*, 2005; Belloir *et al.*, 2017).

Each OSN typically expresses only one *Or* (Chess *et al.*, 1994; Touhara, 2001), using one allele (monoallelic expression) (Ishii *et al.*, 2001; Serizawa *et al.*, 2003; Lewcock and Reed, 2004); thus, following the ðone receptor-one neuron rule.ö However, the mechanism of how

individual OSNs facilitate this monogenic/monoallelic *Or* expression remains unclear. Recent studies favor a stochastic model (in contrast to a deterministic model), based on the orchestration of epigenetic chromatin modifications as well as transcription factors and enhancers (Dalton and Lomvardas, 2015). *Or* expression is not restricted to the olfactory tissue (Kang and Koo, 2012), as Ors are found in ganglia of the autonomic nervous system (Weber *et al.*, 2002), insulin-secreting cells (Blache *et al.*, 1998), carotid body (Chang *et al.*, 2015), and in testis (Fukuda *et al.*, 2004), among other tissues. The functions of Ors in non-olfactory tissues are unclear, as expression levels seem to be low; although some may have important physiological functions (Fukuda *et al.*, 2004; Chang *et al.*, 2015; Ferrer *et al.*, 2016).

Ors normally show lower affinity compared to non-olfactory GPCRs and detect chemically different structures in a combined manner (Malnic *et al.*, 1999): one receptor can detect several components and one stimulus can activate several Ors (Kajiya *et al.*, 2001; Malnic *et al.*, 1999; Saito *et al.*, 2009). This tuning profile may allow detection of a vast number of chemostimuli with a limited number of Ors. However, how this combined activation pattern is transduced into a specific odor quality remains elusive. OSNs expressing a given *Or* project their axons to specific neural structures (glomeruli) in the olfactory bulb (OB), leading to a topographic activation map in the OB (Ressler *et al.*, 1993; Vassar *et al.*, 1993; Mombaerts *et al.*, 1996; Mori *et al.*, 1999). Even similar odors, such as those elicited by enantiomers differing only in their three-dimensional structure, induce a slightly different (by one activated glomerulus) activation pattern (Rubin and Katz, 2001).

Guidance of the axon to the correct glomerulus in the OB is hereby dependent on the expressed *Or* itself (Wang *et al.*, 1998) and at least partially on cyclic adenosine-3',5'-monophosphate (cAMP), a key signaling component in canonical OSNs (Imai *et al.*, 2006; Chesler *et al.*, 2007). Specialized neurons in the OB, also known as mitral and tufted cells, further transduce and represent the information to the olfactory cortex, where signals are further processed (Poo and Isaacson, 2009; Stettler and Axel, 2009). Subsets of OB mitral cells also send projections to the anterior medial amygdala, a region that is richly innervated by the accessory olfactory bulb (AOB) and important for processing innate behaviors and emotions. The amygdala offers a first platform to integrate information transduced by the main and accessory olfactory system (Pérez-Gómez *et al.*, 2015; Brennan and Kendrick, 2006; Mucignat-Caretta *et al.*, 2012). Indeed, individual neurons in the amygdala appear to be stimulated by both systems and sensory neurons from other systems, which will be introduced in the following sections (Licht and Meredith, 1987).

inducing entry of calcium and sodium ions, which cause depolarization (Frings and Lindemann, 1991). Additionally, other channels expressed in OSNs can augment the depolarization event (Stephan *et al.*, 2009; Rasche *et al.*, 2010). Cyclic guanosine-3',5'-monophosphate (cGMP) is another second messenger that increases in response to odor stimulation (Breer *et al.*, 1992). cGMP is synthesized from guanosine triphosphate (GTP) either by soluble or particulate guanylyl cyclases (sGC or pGC). cGMP may be linked to regulation of the CNG channel and therefore connected to odor adaption (Zufall and Leinders-Zufall, 2000; Pifferi *et al.*, 2006; Zufall and Leinders-Zufall, 1997). Furthermore, cGMP is also linked with cAMP production and cAMP signaling (Moon *et al.*, 2005; Pietrobon *et al.*, 2011; Kroner *et al.*, 1996), providing an additional signaling pathway in OSNs to facilitate odor responses. cAMP and cGMP signaling interplay (Pietrobon *et al.*, 2011) and therefore may act in parallel in one cell.

It is likely that additional pathways exist in the MOE and are used by specific subpopulations of cells; some have been already identified (see *1.1.1.2* *1.1.1.4*).

1.1.1.2 The guanylyl cyclase D (GC-D) system and necklace glomeruli

Apart from sGCs (*1.1.1.1*), a subpopulation of ciliated OSNs express membrane bound pGC from the subtype D (*GC-D*), which is enriched in the cilia (Fülle *et al.*, 1995; Juilfs *et al.*, 1997; Walz *et al.*, 2007). These neurons are also known as GC-D neurons.

GC-D neurons detect the peptide hormones uroguanylin and guanylin, which are present in mouse feces and urine. How this activation is processed remains unclear, but detection likely occurs either via direct contact of the extracellular peptides with the pGC or by another, yet unknown, receptor.

GC-D neurons also detect CS₂ and CO₂ (Munger *et al.*, 2010; Hu *et al.*, 2007), which can act intracellularly. CO₂ enters the cell via passive transport through the plasma membrane and is converted into bicarbonate. The enzymatic activity of carbonic anhydrase type II, present in OSNs (Hu *et al.*, 2007), accelerates conversion to bicarbonate.

CS₂ and guanylin/uroguanylin may be important for detecting food and evaluating the safety of a food source during socially transmitted food preference (Arakawa *et al.*, 2013; Munger *et al.*, 2010). In contrast to canonical OSNs, this subpopulation of cells lacks expression of classical *O_rs* and common cAMP signaling pathway components.

GC-D neurons innervate a group of up to 40 connected glomeruli, spatially arranged in a necklace-like structure surrounding the OB (Juilfs *et al.*, 1997; Shinoda *et al.*, 1989).

More recently, it was suggested that members of the four-pass transmembrane proteins (MS4A), a class of potential non-GPCR receptors, may contribute to ligand detection in GC-D neurons (Greer *et al.*, 2016). MS4A proteins are expressed in every GC-D neuron and are localized to the dendritic knobs. They are proposed to play a role in the detection of steroids, fatty acids, and nitrogenized cyclic molecules (Greer *et al.*, 2016). It is not yet clear if MS4A acts only as a receptor or more as a receptor-ion channel (ionotropic receptor).

1.1.1.3 Trace amine-associated receptor (Taar) neurons

Vertebrate GPCRs detect trace amines and were originally identified in 2001 and called Taars (Borowsky *et al.*, 2001; Bunzow *et al.*, 2001; Lindemann *et al.*, 2005). Taars were later found to be expressed in the olfactory epithelium (Liberles and Buck, 2006). Mice possess 15 *Taar* genes that are expressed almost exclusively in the nose, except *Taar1*, which is present in many cell types, including the brain (Lindemann *et al.*, 2008). Expression of a particular *Taar* does not overlap with expression of any other *Taar* or *Or*, maintaining the ðone neuron-one receptorö rule of olfactory neurons. Similar to most canonical OSNs, *Taar*-expressing neurons also use the the canonical cAMP-dependent odorant transduction cascade (Liberles and Buck, 2006; Zhang *et al.*, 2013). Olfactory Taars detect primary or tertiary amines, such as trimethylamine or -phenylethylamine (Zhang *et al.*, 2013), which is present in carnivore urine, activates the mouse *Taar4* receptor, and induces avoidance in mice (Ferrero *et al.*, 2011; Dewan *et al.*, 2013). Other Taars induce attraction in response to other compounds (Li *et al.*, 2013).

Interestingly, one study suggested that different ligands activating a particular *Taar* receptor can elicit opposite behaviors, such as attraction and aversion (Saraiva *et al.*, 2016). This study also indicated that the MOE with its Taars may contribute to innate behaviors, which was originally thought to be exclusively facilitated by the accessory olfactory system.

1.1.1.4 Other OSN subgroups

Beside expression of *Ors* and *Taars*, some cells in the MOE seem to express vomeronasal type 1 (*V1rs/Vmn1rs*) and type 2 receptors (*V2rs/Vmn2rs*) (Karunadasa *et al.*, 2006; Pascarella *et al.*, 2014; Kanageswaran *et al.*, 2015), which are mainly found in the accessory olfactory epithelium (1.1.2). Expression of *Vrs* in the MOE has also been reported in humans (Rodriguez *et al.*, 2000), lemurs (Hohenbrink *et al.*, 2014), goats (Wakabayashi *et al.*, 2002,

2007; Ohara *et al.*, 2013), and *Xenopus laevis* (Date-Ito *et al.*, 2008). The functional relevance of *Vr*-expressing cells in the MOE, particularly in the context of a potential interaction with the VNO, remains to be determined.

Another vomeronasal sensing component has been recently identified in the MOE. A subgroup of MOE cells expresses the transient receptor potential channel, subfamily c, member 2 (*Trpc2*) (Omura and Mombaerts, 2014, 2015). These cells also express a *CNG* channel (*CNGA2*), whereas expression of *ACIII* allows further subdivision into type A cells (positive for *ACIII*) and type B cells (negative for *ACIII*) (Omura and Mombaerts, 2014). In contrast to type B, some type A cells express *Ors*. However, type B cells express the sGC *Gucy1B2* and have been linked to the detection of oxygen in a concentration-dependent manner (Bleymehl *et al.*, 2016).

Other Trp channel subtypes, including transient receptor potential cation channel, subfamily m, member 5 (*Trpm5*) and transient receptor potential channel, subfamily c, member 6 (*Trpc6*), are also expressed in the MOE and may play a role in olfaction (Zufall F [2014] TRPs in Olfaction. In: Nilius B, Flockerzi V (eds) Mammalian Transient Receptor Potential (TRP) Cation Channel Volume II, 1st edition. Springer, Berlin, pp. 917-933).

1.1.1.5 Behavior mediated by the MOE

The MOE is tuned to detect a diverse array of odorants, ranging from food odors to compounds released by predators and conspecifics. Thus, the MOE can detect chemostimuli that could induce innate behaviors (Wang *et al.*, 2006, 2007; Zufall and Leinders-Zufall, 2007; Tirindelli *et al.*, 2009; Baum, 2012; Saraiva *et al.*, 2016). This is consistent with studies in other species where pheromones and socially relevant chemosignals are largely sensed by the MOE (Charra *et al.*, 2012; Dorries *et al.*, 1997).

Chemostimuli detected by both systems raise the question of why this overlap exists and how information from both systems is integrated to form the behavioral output. For example, the ligand 2-heptanone is detected by the apical zone of the VNO (Leinders-Zufall *et al.*, 2000) and by the MOE (Gaillard *et al.*, 2002; Spehr *et al.*, 2006). Segregation is also present at the level of the OB: 2-heptanone activates the MOB and the AOB (Xu *et al.*, 2005).

1.1.2 Grüneberg ganglion (GG)

This subsystem is located in the dorsal tip of both sides of the nose (Fig. 1) with no direct contact to the nasal cavity lumen, but is located adjacent to the naris opening (Grüneberg, 1973). The GG was first described and named by Hans Grüneberg in the early 1970s (Grüneberg, 1973). It comprises 3006500 ciliated cells arranged in a cluster-like structure with a length of about 1 mm (Brechtbühl *et al.*, 2008; Schmid *et al.*, 2010). GG cells have been suggested to detect components released by conspecifics or predators that elicit aversive or aversive-like behaviors (Pérez-Gómez *et al.*, 2015; Brechtbühl *et al.*, 2008, 2013; Debiec and Sullivan, 2014). Moreover, the GG may also act as a sensor for cool temperatures similar to certain sensory neurons found in *Caenorhabditis elegans* (Komatsu *et al.*, 1996; Kuhara *et al.*, 2008; Biron *et al.*, 2008).

1.1.3 Septal organ of Masera (SOM)

The SOM is located at the base of the nasal septum close to the nasopharynx opening. It was described and named by Rodolfo Masera in 1943 and is present in many mammals (Rodolfo-Masera, 1943; Adams and McFarland 1971; Bojsen-Moller, 1975; Katz and Merzel, 1977; Kratzing, 1984; Taniguchi *et al.*, 1993). The SOM is similar to the MOE system in terms of cellular composition: It is comprised of one to three layers of canonical OSNs and also contains microvillar cells, supporting cells, and Bowman's glands (Miragall *et al.*, 1984; Kratzing, 1984; Adams, 1992; Taniguchi *et al.*, 1993; Giannetti *et al.*, 1995). SOM neurons express several *Or* family genes (Kaluza *et al.*, 2004; Tian and Ma, 2004). The function of this secondary sensory structure that shares a similar and overlapping receptor composition with the MOE is unclear.

1.1.4 Vomeronasal organ (VNO)

1.1.4.1 VNO structure

The VNO is located on top of the palate and has a bilateral cigar-shaped structure (Jacobson *et al.*, 1998). The VNO is encapsulated in bone for protection. In many species, the organ has contact with the outer world mainly via the nasopalatine duct to the olfactory cavity. The VNO is composed of a sensory epithelium that partially surrounds a liquid-filled lumen and a non-sensory cuboidal epithelium (Fig. 3). The laterally located non-sensory cuboidal

epithelium contains vascularized erectile tissue, which has been proposed to actively fill the VNO lumen with liquid (Trotier, 2011). Induction of the pumping process is probably facilitated by sympathetic innervation (Meredith, 1994; Meredith and O`Connell, 1979). This active pumping can be induced by social interactions, such as during detection of volatile stimuli by the MOE (Martínez-García *et al.*, 2009).

The size of the organ can vary from species to species, but cetaceans, some bats, crocodylians, and most haplorrhine primates have lost this organ (Eisthen, 1992; Bhatnagar and Meisami, 1998; Halpern and Martínez-Marcos, 2003). Humans acquire a VNO-like structure during early development (Smith and Bathanagar, 2000), but no functional VNO is present in adults (Meredith, 2001).

In mice, the VNO is first visible around day 11 of gestation as a condensed structure in the olfactory placode (Cuschieri and Bannister, 1975). After embryonic day 18, the VNO is vascularized, and seems to be functional at birth, although microvilli composition is completed 8-10 days after birth. Interestingly, the AOB seems to be already functional *in utero* (Pedersen *et al.*, 1983). The sensory epithelium is composed of bipolar glutamatergic neurons (Dudley and Moss, 1995), supporting (sustentacular cells), progenitor, and stem cells. The VNO is constantly renewed during the lifetime (Brann and Firestein, 2010, 2014), and is enhanced by sex hormones under certain physiological conditions (Oboti *et al.*, 2015). Most of the vomeronasal sensory neurons (VSNs) detect semiochemicals, using different types of GPCRs, such as V1rs, V2rs and formyl peptide receptors (Fprs). A semiochemical is defined as chemical component involved in the chemical interaction between organisms of the same species (Wyatt TD [ed] [2014] Pheromones and Animal Behavior-Chemical Signals and Signatures, 2nd edition. Cambridge University Press, Cambridge, p. 1).

1.1.4.2 Vomeronasal receptor family 1 (V1r)

V1rs were first identified in the mid-1990s by Catherine Dulac and Richard Axel using a subtractive single cell PCR approach (Dulac and Axel, 1995). These newly identified *V1r* genes (also known as *Vmn1rs*) belong to the rhodopsin-like family of GPCRs and share sequence homology with bitter taste receptors. *V1r* genes are distributed as clusters in the genome and usually contain one coding exon and a highly conserved promoter region (Young *et al.*, 2005; Lane *et al.*, 2002; Stewart and Lane, 2007). The mouse genome contains almost 240 intact *V1r* genes (Young *et al.*, 2010), grouped into 12 subfamilies according to their sequence similarities (Rodríguez *et al.*, 2002). The number of *V1rs* and the ratio of intact

genes to pseudogenes (mice genome contains almost 150 *Vlr* pseudogenes) can vary from species to species, indicating an evolutionary active set of receptors, which are probably adapted to specific ecological habitats. *Vlr* expression follows a monoallelic and monogenic pattern (Rodriguez *et al.*, 1999), which means that only one receptor is expressed per VSN, either from the maternal or parental allele. It has been proposed that VSNs select their receptor randomly and suppress expression of other *Vlrs* (Dalton and Lomvardas, 2015). The underlying mechanism for the monogenic *Vlr* choice is unclear, although *Vlr* expression itself could prevent further activity of enhancer elements within a single *Vlr* gene cluster, hereby suppressing expression of other *Vlrs* (Roppolo *et al.*, 2007). This model is called the *ö*cluster lock*ö* model and is based on a feedback loop mechanism, similar to the one described for *Or* expression (Chess *et al.*, 1994).

Responses in sensory VSNs (Tucker, 1963) and the AOB from hamsters suggested activation of the VNO by volatile stimuli. Almost 40 years later, Leinders-Zufall and coworkers showed that mouse VSNs can sense volatiles in an ultra-low concentration range (Leinders-Zufall *et al.*, 2000). The volatile components detected in this study are present in mouse urine and were proposed previously to be pheromones (Novotny *et al.*, 1999a; Jemiolo *et al.*, 1986). The response profile patterns of individual VSNs showed a high degree of chemosensitivity to different stimuli with no overlapping responses (Leinders-Zufall *et al.*, 2000). The number of responding cells could not be increased by higher stimulus concentrations, suggesting a narrow detection profile, in contrast to the broad activation pattern observed in many OSNs. Other studies confirmed that *Vlrs* are specialized to sense small organic stimuli (Leinders-Zufall *et al.*, 2000; Boschat *et al.*, 2002; Isogai *et al.*, 2011; Haga-Yamanaka *et al.*, 2014). Potential VSN ligands could be either released from conspecifics or from individuals of other species (e.g. predators) (Isogai *et al.*, 2011).

Mouse urine is a rich source of chemosignals and activates almost 40% of VSNs (He *et al.*, 2008). Activation seems to be dependent on a downstream signaling cascade that includes phospholipase C (PLC), inositol-1,4,5-triphosphate (IP₃), and Trpc2 (Lucas *et al.*, 2003; Leybold *et al.*, 2002; Holy *et al.*, 2000; Inamura *et al.*, 1997; Stowers *et al.*, 2002). Mouse urine contains a large number of sulfated steroids which account for ~80% of VSN activation in female mouse urine (Nodari *et al.*, 2008). These sulfated steroids are mainly derivatives of androgens, estrogens, pregnenolone, and glucocorticoids (Nodari *et al.*, 2008). Only 12 sulfated steroids activate about 25% of the apical VSNs in calcium imaging measurements using objective-coupled planar illumination microscopy (Turaga and Holy, 2012). VSNs that are activated by sulfated steroids cover a broad range of selectivity and specificity: some

detect only a limited number of sulfated steroids, whereas others seem to be tuned to detect various groups of steroids (Turaga and Holy, 2012). Responses to sulfated steroids can also be functionally organized into different classes, indicating combined detection. This clustered activity pattern is also present in the AOB, as shown in *ex vivo* AOB preparations (Meeks *et al.*, 2010; Hammen *et al.*, 2014). The role of V1rs in the detection of sulfated steroids is not completely understood, although a mapping study and a gene targeting approach showed a correlation between activation and *V1r* expression (Isogai *et al.*, 2011; Haga-Yamanaka *et al.*, 2014). Circulating steroids are sulfated to increase their solubility and to clear them in the urine (Mueller *et al.*, 2015). Urinary steroids can reach micromolar levels depending on the physiological status of the urine donor (Nodari *et al.*, 2008). Some contribute to transmit information about stress, sexual, or social status. Interestingly, at least some enzymes that modulate steroids have higher activity in females (Lewis, 1969), suggesting an association with the estrous cycle. Additionally, female mouse urine contains the steroid carboxylic acid, which was recently identified as a potential VSN activator that promotes mounting behavior (Fu *et al.*, 2015).

1.1.4.3 Vomeronasal receptor family 2 (V2r)

A second class of GPCRs was identified independently in the VNO by three groups (Herrada and Dulac, 1997; Matsunami and Buck, 1997; Ryba and Tirindelli, 1997). The V2rs (also known as Vmn2rs) are part of the group C GPCRs (known as the metabotropic glutamate receptor group). V2rs are located in the basal layer of the vomeronasal sensory epithelium and are coexpressed with the G protein subunit $G_{\alpha o}$ (Matsunami and Buck, 1997; Jia and Halpern, 1996). G proteins are proposed to initiate the first step of a downstream signaling cascade conveying ligand binding into an electrical signal, as shown conclusively by Chamero *et al.* (2011).

V2rs are characterized by a long extracellular N-terminal tail, which is important for ligand binding (Matsunami and Buck, 1997). Their primary amino acid sequence length is about twice as long as that of V1rs (V1r: 300 amino acids; V2r: 600 amino acids). *V2r* genes contain multiple exons located along the whole genome. The mouse genome comprises ~122 intact genes, which can be further divided into the A, B, C, and D subfamilies. The ABD subfamilies have about 115 members and subfamily C has seven members (Young and Trask, 2007). The number of *V2rs* varies highly between species: rodents, amphibians, the opossum, and some snakes possess a high number of active genes, whereas other species, including

humans, have few or even no *V2r* repertoire (Shi and Zhang, 2007; Young and Trask, 2007). *V2rs* evolved independently of *V1rs* and differ functionally, as *V2rs* are proposed to detect peptides and proteinaceous components (Chamero *et al.*, 2007, 2011; Leinders-Zufall *et al.*, 2014), whereas *V1rs* detect small organic compounds (Leinders-Zufall *et al.*, 2000) as well as steroids (Haga-Yamanaka *et al.*, 2014, 2015; Turaga and Holy, 2012). Functional and spatial segregation between *V1rs* and *V2rs* is also reflected in their VNO expression properties. Unlike *V1rs*, *V2rs* do not follow monogenetic receptor expression and are expressed in a non-randomly combined manner with one receptor of the ABD subfamily together with at least one receptor of subfamily C (Ishii and Mombaerts, 2011; Martini *et al.*, 2001; Silvotti *et al.*, 2007, 2011).

The functional relevance of a subfamily organization of *V2rs* is undetermined, although different families could be linked to detection of specific ligands (Isogai *et al.*, 2011). Furthermore, multiple receptors of one subfamily may facilitate a combined detection pattern, as suggested for major urinary proteins (MUPs) and major histocompatibility complex class I peptides (MHC-peptides) (Kaur *et al.*, 2014; Leinders-Zufall *et al.*, 2009).

Additionally, some basal *V2r*-expressing VSNs coexpress at least one (often two or three) member of non-classical major histocompatibility complex 1b proteins (*H2-Mv* molecules) (Ishii and Mombaerts, 2008; Ishii *et al.*, 2003; Leinders-Zufall *et al.*, 2014; Loconto *et al.*, 2003). *H2-Mv* is composed of nine genes- *M1*, *M9*, *M11*, and six members of the *M10* family. Expression in the dendritic knob and microvilli of VSNs indicates a potential role in signal transduction or ligand binding (Leinders-Zufall *et al.*, 2014). From a functional point of view, *H2-Mv* molecules may form a functional complex with β 2-microglobulin and *V2rs* to act as a chaperone or coreceptor and/or contribute to ligand sensitivity of *V2rs* (Loconto *et al.*, 2003; Leinders-Zufall *et al.*, 2014). The mechanism of the *V2r*-combined receptor choice is unclear, but it seems that VSNs first express a class A, B, or D receptor followed by the expression of the family C receptor and finally by expression of *H2-Mv*/ β 2-microglobulin. Expression of the *H2-Mv* molecules is restricted to the lower sublayer of basal VSNs, reflecting a tripartite organization (apical layer, basal-upper layer without *H2-Mv*, basal layer with *H2-Mv* expression) (Fig. 3), which is also maintained at the AOB level. Thus, not all receptors need *H2-Mv* expression to detect ligands: *Vmn2r26* (*V2r1b*) positive VSNs detect prototypic MHC-peptides without *H2-Mv* expression (Fig. 3B).

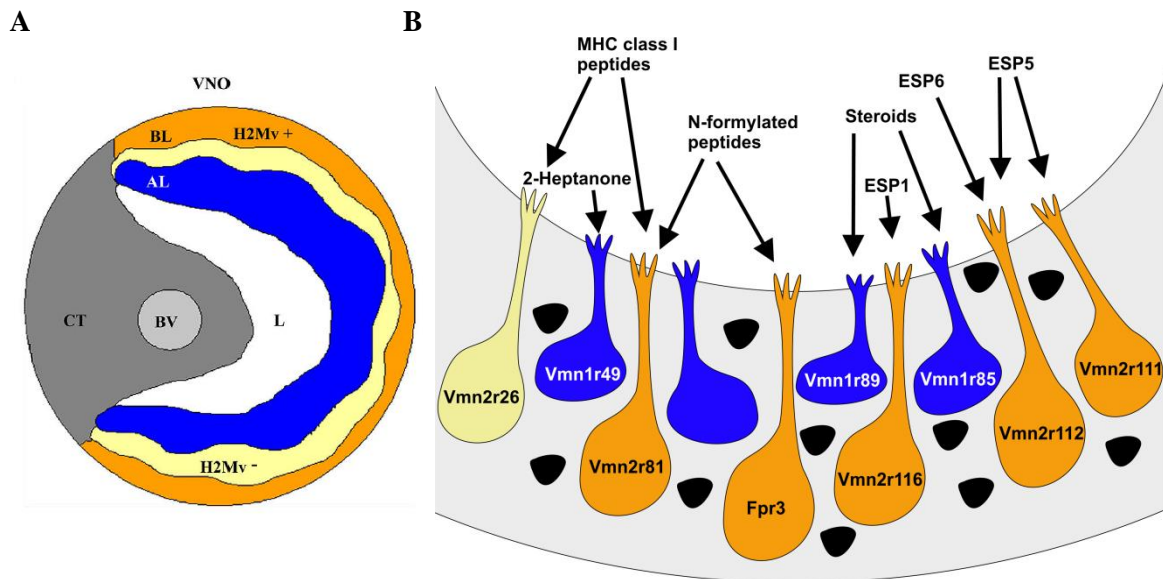


Figure 3: Schematic coronal section of the VNO and receptors located in the sensory epithelium.

A. Tripartite organization of the mouse VNO: AL, apical layer of the sensory epithelium (blue); BL, basal layer (yellow/orange), which can be further divided into two proposed molecular distinct sublayers, depending on expression or lack of one of the nine known *H2-Mv* genes (*H2-Mv* + or *H2-Mv* -). CT, cavernous tissue; BV, blood vessel; L, mucus filled lumen. **B.** Schematic drawing of VSNS expressing specific receptors with their proposed ligands. Color code is equal to A, indicating location of the VSNS. Black geometric figures show additional non-sensory cells in the VNO, including progenitor and sustentacular cells. Figure 3A is adapted from Pérez-Gómez *et al.*, 2014.

The first identified ligands for basal VSNS were 9-mer MHC-peptides at very low concentrations with high selectivity and high specificity (Leinders-Zufall *et al.*, 2004). Experiments in gene-targeted mice identified *Vmn2r26* (*V2r1b*) and *Vmn2r81* (*V2rf2*) detecting MHC-peptides (Leinders-Zufall *et al.*, 2009, 2014). Individual VSNS could distinguish between peptides varying in single amino acid residues, whereas modified anchor residues led to an elimination or diminution of the response. Some VSNS were activated by more than one peptide, and structurally dissimilar ones give rise to the idea of multiple *V2r* expression within these neurons (Leinders-Zufall *et al.*, 2004). A combined detection pattern seems to be likely, as VSNS can detect several peptides, and a given peptide can be recognized by more than one receptor-neuron (Leinders-Zufall *et al.*, 2009; He *et al.*, 2008). Detection of MHC-peptides may have a role in social recognition and pregnancy failure/termination (Leinders-Zufall *et al.*, 2004; Spehr *et al.*, 2006). Overall, the exact function of VSN-based MHC-peptide activation is unknown, as MHC-peptides can also be detected by the MOE (Spehr *et al.*, 2006).

A second family of peptides recognized by *V2rs* are the exocrine gland-secreting peptides (ESP). The mouse genome holds 24 intact *ESP* genes and pseudogenes (Kimoto *et al.*, 2007). These peptides have a mass of 5615 kDa and are expressed in various exocrine glands.

Exocrine glands produce substances and secrete them via a duct onto an epithelial surface. For example, mice use their submaxillary, lacrimal, harderian, and extraorbital glands to secrete this group of peptides (Kimoto *et al.*, 2007). The peptide expression profile differs among inbred mouse strains and seems to follow a gender-specific pattern; ESP1 is only present in males, whereas ESP36 appears to be female specific (Kimoto *et al.*, 2007).

The male-specific ESP1 is secreted in the tears of male mice and induced activation of the VNO, as shown by electrovomeranosogram (EVG) measurements, calcium imaging measurements, and c-Fos immunostaining (Kimoto *et al.*, 2005, 2007; Chamero *et al.*, 2011). ESP1 has been matched to the Vmn2r116 (V2Rp5) receptor (Haga *et al.*, 2010). Similar to MHC-peptides, signal transduction to detect ESP1 in VSNs is dependent on G_o (Chamero *et al.*, 2011). Another member of the ESP family, ESP22, functions as a juvenile-specific pheromone secreted from lacrimal glands into tear fluid of young mice. *ESP22* expression in tears of adult mice (>12 weeks) is almost completely absent (Ferrero *et al.*, 2013). ESP22 activates the VNO on EVG recordings (Ferrero *et al.*, 2013), although the receptor for this juvenile pheromone remains unknown.

Two other ESP peptides, ESP5 and ESP6, activate Vmn2r111 and Vmn2r112 receptors in a heterologous expression system (Dey and Matsunami, 2011). The Vmn2r111 receptor detects ESP5, whereas Vmn2r112 is activated by both peptides. These two receptors as well as the Vmn2r116 receptor belong to the V2rp subfamily.

Another important group of non-volatile components linked to activation of V2rs comprises MUPs. MUPs belong to the lipocalin family of proteins, a group of hydrophobic ligand binding proteins with a molecular mass of about 20 kDa. Although lipocalins have diverse functions, they share a similar glove-like spatial (tertiary) structure (Flower *et al.*, 2000). This shape is characterized by a β -barrel, built up with eight anti-parallel β -sheets and α -helices at the C- and N-termini (Flower, 1995). The barrel structured protein is opened at one end to enable binding of small molecules inside the core.

MUPs are mainly produced in the liver and are extensively secreted into the urine at high concentrations of 20640 mg/ml (Beynon and Hurst, 2003; Szoka and Paigen, 1978). *MUP* expression is sex- and strain-dependent; urine of male mice is more enriched than that of females (Hastie *et al.*, 1979). Expression of *MUPs* is regulated by different hormones, including testosterone, growth hormone, and thyroxine (Knopf *et al.*, 1983; Hastie *et al.*, 1979). Mice typically express from 4 to 12 *MUPs* with dynamic and flexible expression profiles dependent on the age of the animal (Robertson *et al.*, 1996, 1997; Hurst *et al.*, 2001; Thoß *et al.*, 2015). MUPs are also present in different bodily secretions, such as saliva and

milk, due to secretion by glands, including the parotid, sublingual, submaxillary, and the lacrimal gland (Shaw *et al.*, 1983).

The mouse genome encodes for 21 *MUP* genes, which are extremely similar to each other and differ only in a few amino acids (Logan *et al.*, 2008; Mudge *et al.*, 2008). These highly similar *MUP* genes are clustered together on chromosome 4, indicating rapid evolution of this gene cluster. A genome analysis revealed gene coexpansion of *MUPs* and *V2rs* in the mouse, rat, and opossum (Chamero *et al.*, 2007), supporting the idea that specific *V2rs* can detect MUPs. Thus far, no specific *V2r* has been linked to MUP detection. Small volatile molecules can bind to the protein core, some of which are recognized by apical *V1r*-expressing VSNs (Leinders-Zufall *et al.*, 2000). The two volatiles 2-*sec*-butyl-4,5-dihydrothiazole (SBT) and 2,3-dehydro-*exo*-brevicomine (DHB) bind to MUPs of C57BL/6 inbred mice (Sharlow *et al.*, 2002; Kwak *et al.*, 2016). Additionally, farnesenes are found in MUPs of swiss albino mice (Marchlewska-Koj *et al.*, 2000). These volatile components are proposed to function as pheromones independent of MUP binding (Novotny *et al.*, 1985; Novotny *et al.*, 1999b). Thus, MUPs may function as passive carriers of these small volatiles through the mucus to the VNO, stabilizing them and helping preserve the signals longer in the environment (Hurst *et al.*, 1998).

Apart from a carrier function, MUPs themselves have been proposed to function as pheromones. MUPs derived from small molecule-bound components induce calcium and electrical responses in *V2r*-expressing VSNs. These responses depend on G_{α} and *Trpc2* (Chamero *et al.*, 2007, 2011). MUPs play a role in the display of many different social behaviors, including countermarking behavior in male mice, which has been suggested to be dependent on combined sensory coding of MUPs in a correct composition and concentration (Kaur *et al.*, 2014). Some MUPs elicit aggressive behaviors in mice and one MUP in particular present in male mouse urine, MUP20 or darcin, stimulates memory in female mice and sexual attraction to males (Roberts *et al.*, 2010). Due to the variability of the MUPs in urine of individual wild mice, MUPs may play a role in individual recognition of conspecifics (Hurst *et al.*, 2001), postulated as the barcode hypothesis (Thoß *et al.*, 2015).

MUP orthologs are also present in the genome of many species. Interestingly, MUPs from other species can be detected by mice inducing avoidance or fearful behavior in a *Trpc2*- and G_{α} -dependent manner (Papes *et al.*, 2010; Pérez-Gómez *et al.*, 2015).

1.1.4.4 *Formyl peptide receptors (Fprs)*

Fprs are candidates to detect specific pathogenic ligands (Kretschmer *et al.*, 2010; Bufe *et al.*, 2015). They were originally described as expressed in the immune system to facilitate defense mechanisms against pathogens. A high throughput screening for GPCRs in VSNs revealed the expression of five (*Fpr3*, *Fpr-rs3*, *Fpr-rs4*, *Fpr-rs6*, and *Fpr-rs7*) of the seven known *Fprs* (Liberles *et al.*, 2009). *Fpr* expression is dispersed into different small subsets of neurons and does not overlap with the expression of *Vrs* (Rivière *et al.*, 2009). Calcium imaging measurements of single dendritic knobs support a potential role for ligand detection in VSNs (Rivière *et al.*, 2009). One of the five *Fprs* present in VSNs (*Fpr3*) is expressed in basal VSNs (*G_o*-expressing), whereas the remaining four *Fprs* (*Fpr-rs3*, 4, 6, and 7) overlap with *G_{i2}* (Liberles *et al.*, 2009).

Immune *Fprs* are tuned to detect a wide range of chemically diverse ligands (Bufe *et al.*, 2012). Most of the known classical *Fpr* agonists are N-formylated, including the well-characterized tripeptide N-formyl-methionine-leucine-phenylalanine (f-MLF), originally described as a chemoattractant (Showell *et al.*, 1976; Schiffmann *et al.*, 1975), and the specific mitochondria-derived chemoattractant peptide ND1 (f-MFFINTLTL) (Shawar *et al.*, 1995). Interestingly, ND1 also activates VSNs expressing the vomeronasal receptor *Vmn2r81* (*V2rf2*) (Leinders-Zufall *et al.*, 2014). Human and mouse immune *Fprs* have similar activation profiles in a heterologous expression system, although the species separated about 100 million years ago. This indicates functional conservation between human and mouse *Fprs* (Bufe *et al.*, 2012). Yet, it remains unclear how a limited number of receptors can detect such a variety of chemically different ligands with high selectivity.

In contrast to broadly tuned immune *Fprs*, VNO *Fprs* seems to be more narrowly tuned. *Fpr3* is activated by the N-formylated and C-amidated synthetic hexapeptide W-peptide (w-pep; WKYMVm) (Bufe *et al.*, 2012). The w-pep is a known activator of immune *Fprs*. *Fpr3* recognizes a much more limited number of ligands and signal peptides compared to classical *Fprs*. This narrowly tuned activation profile may be a consequence of a neo-functionalization of *Fpr3* in the VNO (Bufe *et al.*, 2012), perhaps used to detect ill conspecifics (Boillat *et al.*, 2015).

Putative activators for the four *Fprs* expressed in the apical layer of the VNO (*Fpr-rs3*, *Fpr-rs4*, *Fpr-rs6* and *Fpr-rs7*) comprise the prototypical human immune *Fpr* agonist f-MLF, the antimicrobial CRAMP peptide, the inflammatory modulator lipoxin A4, and the urokinase-type plasminogen activator receptor (Rivière *et al.*, 2009). However, other studies could not confirm these observations (Bufe *et al.*, 2012; Gao *et al.*, 2007).

1.1.4.5 Canonical olfactory receptors in the VNO

Additionally, several studies have revealed expression of *Ors* in the VNO (Lévai *et al.*, 2006; Nakahara *et al.*, 2016). *Ors* present in the VNO are also expressed in the MOE, although expression is higher in the VNO than in the MOE (Nakahara *et al.*, 2016). Two studies using deep sequencing confirmed the finding of Lévai *et al.* (Ibarra-Soria *et al.*, 2014; Nakahara *et al.*, 2016). Both identified strong expression of the mouse *Or36-1* (*Olf692*) receptor in the VNO. *Or36-1* detects pup odors and is involved in mediating pup-oriented behaviors in mice (Nakahara *et al.*, 2016). These data are consistent with early experiments, indicating that the VNO is involved in the detection of conventional odorants (Sam *et al.*, 2001; Trinh and Storm, 2004).

1.1.4.6 Signal transduction

The accessory olfactory system (AOS) in mice shows a functional and anatomical dichotomy within the sensory epithelium as well as in the AOB (Kumar *et al.*, 1999; Belluscio *et al.*, 1999; Rodriguez *et al.*, 1999). *V1r*-expressing VSNs are located more apically within the sensory epithelium, which is a zone that expresses G_{i2} and the phosphodiesterase isoform *PDEA4* (Berghard and Buck, 1996; Cherry and Pho, 2002; Chamero *et al.*, 2011; Leinders-Zufall *et al.*, 2004). *V2r*-expressing VSNs are located in the basal layer of the VNO and coexpress G_o (Berghard and Buck, 1996; Jia and Halpern, 1996). Both G protein subunits are present in the dendritic tip and microvilli of VSNs (Berghard and Buck, 1996; Halpern *et al.*, 1995; Matsuoka *et al.*, 2001), suggesting a role in signal transduction. Indeed, conditional G_o deletion abolishes sensitivity of VSNs to different peptide stimuli, such as MHC-peptides, ESP, or MUPs in calcium imaging measurements and EVG recordings (Chamero *et al.*, 2011).

G_{α} subunits form a G protein complex together with beta and gamma subunits, consisting of $G_{\alpha 28}$ in basal VSNs and $G_{i2 22}$ in apical VSNs (Montani *et al.*, 2013). The expression profile can be heterogeneous depending on the developmental stage (Sathyanesan *et al.*, 2013). After receptor-ligand binding, conformational changes lead to activation of isoforms of PLC through the dissociated $G_{\beta/\gamma}$ -complex (Smrcka and Sternweis, 1993; Camps *et al.*, 1992; Smrcka, 2008). It is not yet clear which PLC isoforms participate in signal transduction for receptor-ligand interactions. PLC 2 is the only one suggested to contribute partially in the signal transduction to detect MUPs (Dey *et al.*, 2015).

PLC proteins cleave phosphatidylinositol-4,5-bisphosphate (PIP₂) into diacylglycerol (DAG) and IP₃ (Fig. 4). Membrane-bound DAG interacts directly with Trpc2 gating calcium and sodium flux (Lucas *et al.*, 2003). DAG can also be enzymatically metabolized to fatty acids, potentially arachidonic acid, which could also influence membrane-bound channels and therefore facilitate signal transduction (Spehr *et al.*, 2002; Zhang *et al.*, 2010). IP₃ is soluble and important for calcium release from internal stores, although a direct role of IP₃ in vomeronasal transduction is still unclear.

Trpc2 is present in the dendritic knobs of VSNs and facilitates the influx of calcium and sodium into the cell, which generates an electrical signal (depolarization). Genetic ablation of the *Trpc2* channel induces defects in socio-sexual behaviors in mice (Leypold *et al.*, 2002; Stowers *et al.* 2002; Kimchi *et al.*, 2007; Ferrero *et al.*, 2013; Wu *et al.*, 2014), suggesting a role for Trpc2 in chemotransduction. *Trpc2* expression in the olfactory system was initially thought to be exclusive to VSNs. However, recent findings showed that Trpc2 is also present in the MOE (Omura and Mombaerts, 2014; 2015). Trpc2-mediated ionic influx seems to gate additional channels in VSNs, including the calcium-activated chloride channels TMEM16A/anoctmin1 and TMEM16B/anoctamin2 (ANO1 and 2), the small conductance calcium-activated potassium channel (SK3), large conductance calcium-sensitive potassium channels (BK channels), the G protein-activated inwardly rectifying potassium channel GIRK, and calcium-activated cation channels (CAN) (Dibattista *et al.*, 2012; Amjad *et al.*, 2015; Kim *et al.*, 2012; Zhang *et al.*, 2008; Liman, 2003; Spehr *et al.*, 2009).

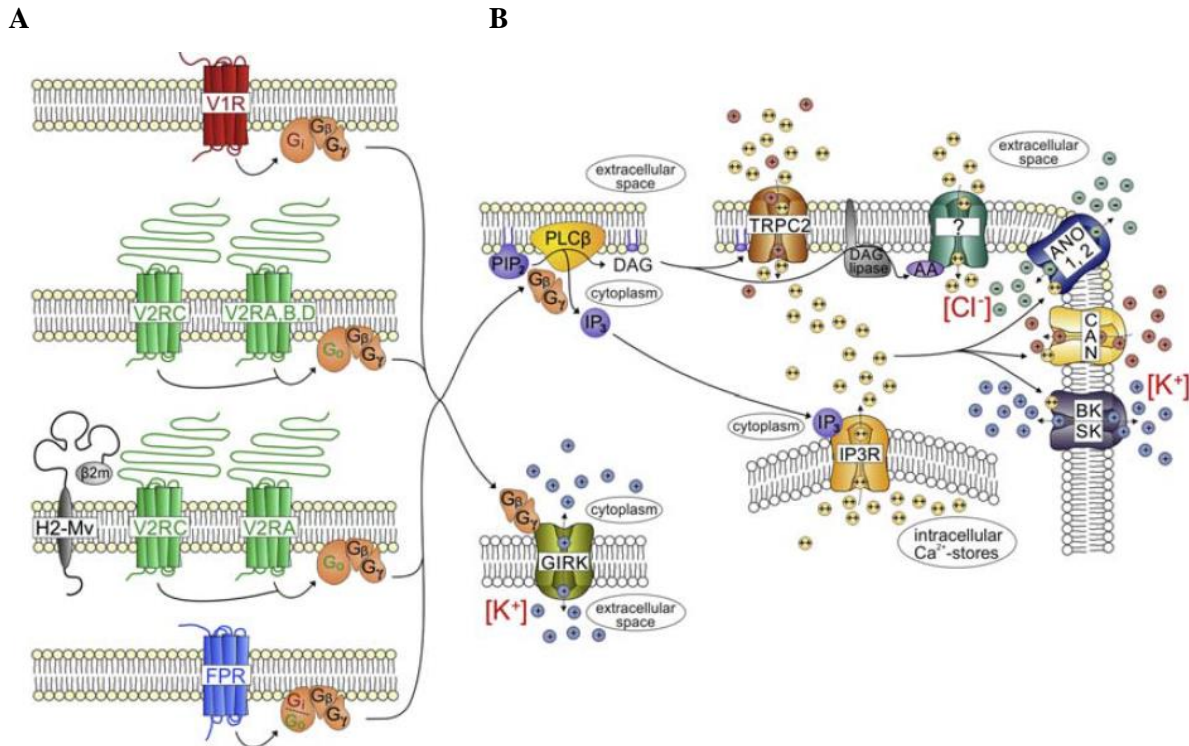


Figure 4: Proposed VNO signal transduction pathway.

A. Schematic drawing of proposed receptors in the VNO and their coupling to different G protein subunits (G_o / G_{i2} , G_s , and G_{12}). *V1r*-expressing VSNs express the G protein subunit G_{i2} ; VSNs located in the basal layer of the VNO express at least one member of the *V2r* family C, with one member of the *V2r* A, B, or D family in a non-randomly combined pattern, and the G_o subunit. Some basal VSNs express one member of the family C *V2rs* with one of the *V2r* A subfamily together with one of the nine known *H2-Mv* genes in combination with *2-microglobulin*. *Fpr*-expressing neurons may express either G_o or G_{i2} subunits. **B.** Changes in conformation during receptor-ligand interactions induce activation of the PLC, which degrades PIP_2 into soluble IP_3 and membrane-bound DAG. DAG is proposed to activate *Trpc2* inducing depolarization via cation influx. Increased level of the second messenger calcium can further gate other channels, including the calcium-activated chloride channels ANO1, 2, as well as CANs and BK/SK channels. Figure adapted from Spehr M (2016) *Vomeronasal Transduction and Cell Signaling*. In: Munger S, Zufall F (eds) *Chemosensory Transduction- The Detection of Odors, Tastes, and Other Chemostimuli*, 1st edition. Academic Press, London, p. 194.

1.1.4.7 Projection of VSNs

The dichotomy in the organization of the vomeronasal sensory epithelium is also maintained in the AOB, which is the first station for processing stimulus information for the brain. VSN axons are condensed into nerve bundles, which are sent dorsally through the cribriform plate to the AOB located dorso-caudally of the MOB. Apical neurons target areas in the anterior part of the AOB, whereas basal VSNs project to the posterior AOB (Jia and Halpern, 1996). Mitral/tufted cells form segregated structures called glomeruli that are synapsed as second order neurons by VSNs. In contrast to the MOB, VSNs carrying one receptor type contact several different glomeruli. This induces a combined activation pattern of different glomeruli dependent on ligand-receptor interactions (Hammen *et al.*, 2014). The glomeruli can be modulated by inhibitory interneurons, suggesting that the AOB is not only a passive relay station but also a plastic area of integration (Wagner *et al.*, 2006; Brennan and Kendrick,

2006). Information is further sent to areas of the limbic system (amygdala and hypothalamus) (Martinez-Marcos, 2009; Kang *et al.*, 2011). Although the MOB mainly targets higher cortical areas (Miyamichi *et al.*, 2011; Ghosh *et al.*, 2011; Stettler and Axel, 2009; Sosulski *et al.*, 2011), projections from the MOB and AOB overlap in some areas of the medial amygdala (Pro-Sistiaga *et al.*, 2007; Kang *et al.*, 2009), indicating functional integration of inputs from both systems (Kang *et al.*, 2009).

1.1.4.8 Behavior mediated by the VNO

The VNO is responsible for several social behaviors in mice (Table 1), such as avoidance of predator signals, sick avoidance of conspecifics, aggression, and sexual behaviors (Leypold *et al.*, 2002; Papes *et al.*, 2010; Boillat *et al.*, 2015; Chamero *et al.*, 2007). A link between a chemosignal and a proposed receptor is thus far only known for a limited number of receptors (Table 1). The connection between the VNO and specific behavioral outputs has been elucidated by genetic deletion of major components in the VNO signaling cascade (Del Punta *et al.*, 2002; Stowers *et al.*, 2002; Leypold *et al.*, 2002; Norlin *et al.*, 2003; Kelliher *et al.*, 2006; Kimchi *et al.*, 2007; Chamero *et al.*, 2011; Kim *et al.*, 2012; Leinders-Zufall *et al.*, 2014; Oboti *et al.*, 2014; Pérez-Gómez *et al.*, 2015; Nakahara *et al.*, 2016), surgical disruption of the VNO (Clancy *et al.*, 1984; Beauchamp *et al.*, 1985; Lepri *et al.*, 1985; Maruniak *et al.*, 1986; Lepri and Wysocki, 1987; Bean and Wysocki, 1989; Labov and Wysocki, 1989; Wysocki and Lepri, 1991; Wysocki *et al.*, 2004; Pankevich *et al.*, 2004, 2006a, 2006b; Kelliher *et al.*, 2006; Kimchi *et al.*, 2007), or by using specific VSN activators (Chamero *et al.*, 2007; Haga *et al.*, 2010; Papes *et al.*, 2010; Kaur *et al.*, 2014; Haga-Yamanaka *et al.*, 2014; Fu *et al.* 2015; Nakahara *et al.*, 2016; Xu *et al.*, 2016).

Table 1. List of selected signaling molecules with proposed receptors and behavioral output.

Chemosignal	Source	Receptor	Behavioral effects	Reference
ESP1	Male mouse tears	Vmn2r116	Lordosis	Kimoto <i>et al.</i> , 2007; Haga <i>et al.</i> , 2010
			Aggression	Hattori <i>et al.</i> , 2016
ESP5	Mouse tears	Vmn2r111	?	Kimoto <i>et al.</i> , 2007; Dey and Matsunami, 2011
		Vmn2r112		
ESP6	Mouse tears	Vmn2r112	?	Kimoto <i>et al.</i> , 2007; Dey and Matsunami, 2011

ESP22	Juvenile mouse tears	?		Inhibition of male sexual behavior	Ferrero <i>et al.</i> , 2013
HMW/MUPs	Mouse urine	?		Intermale aggression	Chamero <i>et al.</i> , 2007, 2011
				Maternal aggression	Martín-Sánchez <i>et al.</i> , 2015
				Preference in females	Cheetham <i>et al.</i> , 2007; Roberts <i>et al.</i> , 2010
				Countermarking behavior	Kaur <i>et al.</i> , 2014
				Puberty acceleration	Mucignat-Caretta <i>et al.</i> , 1995
				Ovulation	Morè, 2006
MUP3		?		Intermale aggression countermarking	Kaur <i>et al.</i> , 2014
MUP20		?		Attraction in females	Roberts <i>et al.</i> , 2010, 2012
				Conditioned place preference	
				Countermarking behavior	Kaur <i>et al.</i> , 2014
Feld4	Cat saliva	?		Avoidance/Defensive behavior	Papes <i>et al.</i> , 2010; Pérez-Gómez <i>et al.</i> , 2015
MUP13	Rat urine			Defensive behavior	Papes <i>et al.</i> , 2010
LMW	Mouse urine	?		Intermale aggression	Chamero <i>et al.</i> , 2007, 2011
				Maternal aggression	
MHC class I peptides	Mouse urine		Vmn2r26 Vmn2r81	Bruce effect	Leinders-Zufall <i>et al.</i> , 2009, 2014
N-formylated peptides	Bacteria or mitochondria		Fpr3 Vmn2r81	?	Rivière <i>et al.</i> , 2009; Bufe <i>et al.</i> , 2012; Leinders-Zufall <i>et al.</i> , 2014
Steroids	Female mouse urine		Vmn1r89 Vmn1r85	Mounting behavior?	Haga-Yamanaka <i>et al.</i> , 2014
, farnesene	Preputial gland	?		Estrus induction	Ma <i>et al.</i> , 1999
				Intermale aggression	Novotny <i>et al.</i> , 1990
				Puberty acceleration	Novotny <i>et al.</i> , 1999b
				Female attraction	Jemiolo <i>et al.</i> , 1991
2-heptanone	Female mouse urine		Vmn1r49	Puberty delay	Boschat <i>et al.</i> , 2002; Novotny <i>et al.</i> , 1986
<i>trans</i> -5-hepten-2-one	Female mouse urine	?		Puberty delay	Novotny <i>et al.</i> , 1986
<i>trans</i> -4-hepten-2-one	Female mouse urine	?		Puberty delay	Novotny <i>et al.</i> , 1986
<i>n</i> -pentyl acetate	Female mouse urine	?		Puberty delay	Novotny <i>et al.</i> , 1986
<i>cis</i> -2-penten-1-yl-acetate	Female mouse urine	?		Puberty delay	Novotny <i>et al.</i> , 1986

2,5-dimethylpyrazine	Female urine	mouse	?	Puberty delay	Novotny <i>et al.</i> , 1986
2- <i>sec</i> -butyl-4,5-dihydrothiazole	Male urine	mouse	?	Puberty acceleration	Novotny <i>et al.</i> , 1999b; Kelly, 1996
				Aggression	Novotny <i>et al.</i> , 1985
				Female attraction	Jemiolo <i>et al.</i> , 1991
				Whitten effect	Jemiolo <i>et al.</i> , 1986
2,3-dehydro- <i>exo</i> -brevicommin	Male urine	mouse	?	Puberty acceleration	Novotny <i>et al.</i> , 1999b; Kelly, 1996
				Aggression	Novotny <i>et al.</i> , 1984, 1985
				Female attraction	Jemiolo <i>et al.</i> , 1991
				Whitten effect	Jemiolo <i>et al.</i> , 1986

1.1.5 Deorphanizing receptor-ligand interactions

1.1.5.1 Heterologous system

Identifying ligands for GPCRs is of great interest because of its relevance to drug development and involvement in many important physiological functions. Of the nearly 1200 *Ors* encoded in the mouse genome, most have not been deorphanized. Only nine receptors (*Vmn2r111*, *Vmn2r112*, *Vmn2r116*, *Vmn2r26*, *Vmn2r81*, *Vmn1r49*, *Vmn1r89*, *Vmn1r85* and *Fpr3*) of almost 400 functional VNO receptor genes have been deorphanized using different experimental approaches. Knowledge of precise receptor-ligand interactions is a fundamental step to decipher the logic of chemical communication. A major bottleneck to deorphanize Vrs and to proof their functionality seems to be the lack of suitable heterologous expression systems. Reasons for poor receptor expression are unclear but it seems to be due to receptor retention in the endoplasmic reticulum (ER) or a lack of suitable chaperone proteins (see Discussion).

A functional heterologous expression system requires appropriate receptor transport to the plasma membrane as well as functional coupling to a signal transduction system, conveying and processing stimulus-induced receptor activation. Heterologous expression studies in *Ors* have revealed that they are often retained in the ER (Lu *et al.*, 2003, 2004). A special expression environment, including accessory components, seems to be needed to functionally express *Ors* on the cell surface (McClintock and Sammeta, 2003; Gimelbrant *et*

al., 1999, 2001). This environment may be provided only by specific neurons and not by heterologous cells. Coexpression of receptor-transporting proteins, such as RTP1 or RTP2, receptor expression-enhancing proteins REEP1 (Saito *et al.*, 2004), and the guanine nucleotide exchange factor for G_{olf} Ric8B (Von Dannecker *et al.*, 2005, 2006; Kerr *et al.*, 2008) improve the heterologous expression of *Ors* in HEK293 cells. Additionally, coexpressed components also seem to have a functional effect on *Ors* (Li and Matsunami, 2011). For *Vrs*, it was recently described that calreticulin4, a chaperone-like protein, enhances proper surface expression of some *V2rs* (Dey and Matsunami, 2011). The N-terminal amino acid tags, such as rhodopsin (Krautwurst *et al.*, 1998) or the 17-amino acid leucine rich N-terminal signal peptide (Lucy-tag) (Shepard *et al.*, 2013), enhance receptor expression, although such modifications may alter the response profile of the receptor (Zhuang and Matsunami, 2007). The most common used heterologous systems to deorphanize *Ors* include HEK293 cells, the HANA3A system, which is derived from HEK293T cells (Saito *et al.*, 2004), and the HeLa/Olf expression system (Shirokova *et al.*, 2005). These systems are coupled to various approaches to monitor receptor activity indirectly by measuring second messengers or subsequent ionic currents (Katada *et al.*, 2003; Saito *et al.*, 2004). Other expression systems include *Xenopus laevis* oocytes (Katada *et al.*, 2003; Abaffy *et al.*, 2006, 2007), the insect cell line *Sf9* (Matarazzo *et al.*, 2005), yeast (Minic *et al.*, 2005), and a baculovirus system (Mitsui *et al.*, 2012). The advantage of a heterologous system lies mainly in its technical/experimental simplicity as well as in its high throughput capacity. Disadvantages mainly refer to less physiological environments for receptor expression, which may limit functional expression.

Thus far, heterologous expression has yielded only modest success in deorphanizing *Vrs*: ESP5 and ESP6 were proposed as potential ligands for *Vmn2r111* and *Vmn2r112* (Dey and Matsunami, 2011), *Vmn2r1* as a low-sensitivity receptor for hydrophobic amino acids (DeMaria *et al.*, 2013), and *Fpr3* as the receptor for the synthetic hexapeptide *w-pep* (Bufe *et al.*, 2012). The human *V1rb2* receptor was linked to the detection of aliphatic alcohols using the HeLa/Olf system (Shirokova *et al.*, 2008).

To overcome the limitations and drawbacks of a heterologous expression, Zhao and coworkers developed a virus-based expression system in rat OSNs as a natural and physiological environment to enable efficient and functional receptor expression (Zhao *et al.*, 1998). They used an adenovirus vector containing an expression cassette with the *Or-I7* odorant receptor combined with an internal ribosomal entry site (IRES) and a green fluorescent protein (*GFP*) to transfer the *Or* gene to OSNs. The IRES sequence enables

bicistronic expression of the receptor with *GFP* in the same cell. Infected cells were stimulated with odorants and the responses were analyzed by whole cell patch clamp recordings and electroolfactograms. Zhao and coworkers used this virus-based assay to identify octyl aldehyde as potential ligand for Or-I7. This *ex vivo* approach was also used in other studies to deorphanize mouse Or23 (Olf16) (Touhara *et al.*, 1999; Araneda *et al.*, 2000). However, this virus-based expression system has not been used in the VNO with a single *Vr*.

1.1.5.2 Gene delivery in sensory neurons by viral vectors

Several methods, including electroporation, nucleofection, calcium-phosphate coprecipitation, microinjection, biolistics, and lipofection have been described to transfer genes into cells; with different efficiencies based on the viability and expression levels of the transgene (Karra and Dahm, 2010). Neurons are postmitotic cells that are particularly challenging for introducing and expressing gene constructs. Virus-based gene transduction is widely used in neurons because of its high efficiency and suitability *in vitro* and *in vivo*. Different viral systems are available, depending on the transgene, the target cell type, and the experimental application. The most commonly used systems are herpes simplex virus (HSV), lentivirus, adenovirus (AV), and adeno-associated virus (AAV).

AVs infect mitotic and postmitotic cells, including neurons, with high efficiency and do not integrate into the host genome. Expression of the transgene starts a few days postinfection and can last for several weeks. The main disadvantages of AVs are their preferential infection of glia cells and limited transgene size capacity. AAVs infect neurons with high efficiency (Royo *et al.*, 2008) and low toxicity but suffer from late transgene expression onset and random integration into the host genome. Lentiviruses are RNA viruses that belong to the retrovirus family, such as the human immunodeficiency virus, and can be used *in vivo* and *in vitro*. Lentiviruses infect non-dividing cells (including neurons) with high efficiency, but transgene expression may last several days.

Herpes Simplex Virus type 1 (HSV-1) is an excellent tool to transduce neurons because of its huge capacity, fast and robust expression, and natural tropism for neurons and epithelial cells. HSV-1 is an enveloped virus that carries a 150 kb genome divided into 75 genes, but 40 of these genes are not essential for virus replication. HSV-1 has a natural tropism for various cell types, facilitated by different glycoproteins on the surface. HSV-1 invades a host by retrograde transport along the axon of a neuron. HSV-1 can either enter a latent state or

induce a lytic infection, which causes reproduction and propagation of the virus. Several strategies for a HSV-1-derived gene transfer are available, including replication of defective and competent viruses as well as HSV-1-derived amplicons (Simonato *et al.*, 2000; Spaete and Frenkel, 1982, 1985; Andersen *et al.*, 1993). Viral amplicons are helper-dependent defective HSV-1-derived vectors indistinguishable from intact viruses in terms of structure and functionality. Viral amplicons are produced using an *Escherichia coli* (*E. coli*)-derived amplicon plasmid, equipped with one origin of replication and a packaging sequence plus the transgene of interest, which is packed into a viral amplicon as a concatemer of tandem repeats (Spaete and Frenkel, 1982). The capacity of the viral amplicon is up to 150 kb (Spaete and Frenkel, 1982), allowing delivery of whole genes.

Extra genetic information is provided by a helper virus to package the viral amplicon with the plasmid. In this study, I used the replication defective HSV-1 mutant *5dl1.2*, lacking an immediate early gene combined with a special cell line (see Material and Methods). Other amplicon-derived systems are available, such as Epstein-Barr virus (EBV)-derived systems or a combination of two herpes viruses, including a HSV-EBV hybrid amplicon system. Such modifications can be used to adapt the amplicon system to the target cell and to modify its tropism. Due to its versatile properties, the HSV-1-derived amplicon system is widely used to study expression of different genes linked to various neurodegenerative disease, such as Alzheimer's disease, Parkinson's disease, cancer, and learning and memory (Jerusalinsky *et al.*, 2012).

1.1.5.3 Gene-targeted mouse models as a Vr-deorphanizing tool

Given the complexity of functional *Or/Vr* expression in heterologous systems, some studies have used gene-targeted mice to deorphanize olfactory and vomeronasal receptors. Leinders-Zufall and coworkers identified that *Vmn2r26* is activated with certain MHC-peptides (Leinders-Zufall *et al.*, 2009) and *Vmn2r81* is activated with both, MHC-peptides and the formylated peptide f-MFFINTLTL (Leinders-Zufall *et al.*, 2014), using GFP-labeled cells. *Vmn1r49-GFP* transgenic cells are activated by 2-heptanone (Boschat *et al.*, 2002) and sulfated steroids induce activation of cells expressing *Vmn1r85*- and *Vmn1r89-TdTomato* transgenes (Haga-Yamanaka *et al.*, 2014). Genetically modified mice have also been used extensively in studies to deorphanize several *Ors* (Bozza *et al.*, 2002; Grosmaître *et al.*, 2006). These tools are often complemented and utilized in combination with single cell RT-PCR and imaging approaches (Touhara, 2001; Kajiyama *et al.*, 2001; Nara *et al.*, 2011).

2 AIMS

Vomer nasal sensory neurons (VSNs) of the accessory olfactory epithelium compose three main groups of GPCRs: V1rs (Vmn1rs), V2rs (Vmn2rs) and Fprs. Function and tuning properties of most of the receptors present in the VNO remain poorly understood. Only a few receptors have been matched with their ligands. A major bottleneck in the identification of possible ligands for individual receptors is their inefficient expression *in vitro* due to retention in cellular compartments or non-functional coupling to the signal transduction machinery. However, knowledge of receptor-ligand interactions in the VNO is an important prerequisite to understand the logic of VNO ligand detection.

To overcome this limitation, I hypothesize that native VSNs themselves provide the most capable cellular environment to express and localize *Vrs*. To prove this hypothesis, I aim to develop and validate a Herpes Simplex Virus type 1 (HSV-1)-derived amplicon delivery system allowing a functional expression of *Vrs* in native VSNs.

1. First, I aim to set up a protocol that allows combining culture of primary VSNs with viral transgene transduction and subsequent calcium imaging measurements.
2. Determine a critical time point regarding optimal cell survival and transgene expression for suitable functional analysis (calcium imaging measurements).
3. Prepare viral amplicons either equipped with a green fluorescent marker protein (GFP) or a mCherry protein as fluorescent tag, to combine derived amplicon system with genetically marked VSNs.
4. Test response profile of VSNs infected with one representative receptor of each of the three major groups of GPCRs present in the VNO to get insights into the functionality of amplicon-induced expression.
5. Analyze receptor expression of VSNs responding to specific ligands in calcium imaging measurements, using a single cell RT-PCR approach.
6. Identify potential receptors for the MUP-containing high molecular weight urine fraction (HMW) by amplicon-induced receptor expression and calcium imaging measurements.
7. Since orthologous MUPs are sensed via the VNO, I aim to determine the signal transduction mechanism of one orthologous MUP (Feld4).

3 MATERIALS AND METHODS

3.1 Molecular cloning

3.1.1 RNA extraction from tissue

Two to three adult mice (for liver preparation male mice were used) older than eight weeks were anesthetized and sacrificed (see 3.9.1). Liver and/or VNO was dissected and tissue immediately homogenized. For RNA extraction the PureLink[®] RNA Mini Kit (Ambion) was used. RNA isolation was performed according to the manufacturer's instructions. Briefly: tissue was transferred to an RNase-free Biosphere[®] SafeSeal tube 1.5 ml (reaction tube; Sarstedt) and a suitable amount (dependent on tissue weight) of lysis buffer (Ambion) containing 1% [v/v] 2-mercaptoethanol (Sigma Aldrich) was added. Tissue was homogenized using an RNase-free pestle. After centrifugation at 12000 g for 2 min at RT (Room Temperature) the supernatant was transferred to a reaction tube. One volume of 70% [v/v] ethanol was added to homogenized tissue, mixed, and transferred to a spin-cartridge (Ambion). Samples were centrifuged at 12000 g for 15 s at RT, and flow-through was disposed. To wash column-bound RNA, 350 μ l wash buffer I (Ambion) were added and centrifuged at 12000 g for 15 s at RT. Subsequently, 80 μ l of a DNase mix were added (8 μ l 10x DNase reaction buffer [Fermentas], 30 U DNase I [Fermentas] adjusted to 80 μ l with diethyl dicarbonate [DEPC] treated water [Invitrogen]). To digest rests of genomic DNA, reaction was incubated for 15 min at RT. The reaction was stopped, and column washed by adding 500 μ l wash buffer II (Ambion) followed by subsequent centrifugation at 12000 g for 15 s at RT. Purification step was repeated once. The membrane was dried for 5 min at RT. To elute RNA, 30 μ l DEPC treated water (Invitrogen) were added centrally to the column membrane and centrifuged at 12000 g for 1 min at RT. RNA was collected in a 1.5 ml reaction tube and stored at -80°C until further procedure.

3.1.2 cDNA synthesis

To transcribe extracted RNA into complementary DNA (cDNA), the SuperScript[™] III Reverse Transcriptase Kit (Invitrogen) was used according to manufacturer's instructions. Eight μ l of total RNA extracts (see 3.1.1) were mixed with 1 μ l of a 50 μ M oligo(dT)₂₀ mix and 1 μ l of a 10 mM 2'-deoxynucleoside 5'-triphosphate (dNTP) mix and incubated for 5 min at 65°C followed by 1 min on ice. To perform reverse transcription, 10 μ l of a cDNA

synthesis mix (2 μ l 10x Reverse transcription buffer [Invitrogen], 4 μ l of a 25 mM $MgCl_2$ solution [Invitrogen], 2 μ l of a 0.1 M dithiothreitol (DTT) solution [Invitrogen], 40 U RNaseOutTM [Invitrogen], and 200 U SuperscriptTM III reverse transcriptase [Invitrogen]) were added and incubated for 50 min at 50°C. Reaction was stopped by a heating cycle of 5 min at 85°C. Samples were subsequently cooled on ice before adding 2 U Ribonuclease H (Invitrogen), which eliminates RNA complementary to cDNA. Reaction was performed for 20 min at 37°C before cDNA samples were stored at -20°C or used immediately.

3.1.3 Vomeronasal receptor cloning into pHSV-IRES-GFP vector

Full-length coding regions of selected *V1rs*, *V2rs*, and *Fpr3* were amplified from cDNA library of C57BL/6 mice (see 3.1.2) and cloned into either TOPO®-TA (Invitrogen) or pGEM®-T Easy (Promega) cloning vector. They were further subcloned into the pHSV-IRES-GFP expression vector (kindly provided by Prof. M.T. Alonso, University of Valladolid, Spain).

3.1.3.1 Amplification of receptor genes

Full-length coding regions of receptors were amplified by PCR with gene-specific primers (Table 2) using whole VNO (male and female) cDNA library (see 3.1.2) as template. Primers were selected to span the entire gene sequence. PCR was performed with the Stratagene Herculase II Fusion DNA Polymerase System (Agilent Technologies). PCR conditions were optimized for each gene, containing the following components: 0.5 μ l-4 μ l cDNA, 10 μ l 5x Herculase II reaction buffer (Agilent Technologies), 1 μ l Herculase II Fusion DNA polymerase (Agilent Technologies), 0.25 μ M of each primer and 250 μ M of each dNTP (dATP, dTTP, dGTP, dCTP; see abbreviation list). Dimethyl sulfoxide (DMSO; Agilent Technologies) was added at 3% [v/v] of the final reaction volume, which was adjusted to a final volume of 50 μ l with H₂O_{bidest.} (autoclaved).

Table 2. Gene-specific primers.

Gene	Accession Numbers*	Gene-Specific Primer Sequences [5'→ 3']
<i>Fpr3</i>	NM_008042.2	Forward: CATAAGCTTATGGAAACCAACTACTCTATCCCTT Reverse: CAAGTCGACTCATATTGCCTTTATTTC AATGTCTT
<i>Vmn2r26</i>	NM_019917.2	Forward: ATGAAATACTCACTGCTTTCTCTC Reverse: TCATTTAAAGAACTTCTTTCTTGAATG
<i>Vmn2r74</i>	NM_001105187.1	Forward: ATGTTCTTCTTGAACTCTGTCTTCTG Reverse: TTAGGTGGTTAAATTTAACTCACGTC
<i>Vmn2r66</i>	NM_001033878.3	Forward: ATGTTCACTTTGATCTCTGTCTTCT Reverse: TTAACTTATATTTTCAGCTTTAGCATGT
<i>Vmn2r65</i>	NM_001105180.1	Forward: ATGTTATCTTTCATGTCTTTCTTCTCCT Reverse: TTAATGGTTATATTCAATTTTAGAATGTG
<i>Vmn1r237</i>	NM_134200.1	Forward: ATGGAAAACAGTGACATTGTAATTAGTGT Reverse: TTAACTGGAGATCACCAGAAAGGGA
<i>Vmn1r89</i>	NM_134226.1	Forward: ATGTTTTCAAGTGACACATTCTTCCAGA Reverse: TCAGCCATGCAGTGAACCTTGTATG

* = National center for biotechnology information (NCBI)

PCR reactions were mixed on ice and ran on a Mastercycler gradient (Eppendorf).

3.1.3.2 Gel electrophoresis

To purify, separate, and assess quality and size of linearized DNA molecules, 1% [w/v] agarose (Sigma Aldrich) gels supplemented with ethidium bromide (Carl Roth®) were used. After polymerization at RT gels were ready to be loaded.

DNA samples were mixed with 6x DNA loading dye (Fermentas) and loaded on a gel together with 10 µl of 0.1-10 kb DNA standards (PEQLAB and Thermo Scientific).

Electrophoretic separation was performed in 100-250 ml 1x TBE buffer (Ambion) at 100 mV for 40 min. Detection and gel documentation was done with the ChemiDoc™ system (BioRad) or with a UV-Transilluminator (= 254 nm).

3.1.3.3 Gel Band extraction

Plasmid and PCR products were loaded on a 1% [w/v] agarose (Sigma Aldrich) gel and purified with the MiniElute Gel Extraction Kit (Qiagen) following manufacturer's instructions. Gel bands of interest were carefully excised under UV-light and transferred to 1.5 ml reaction tubes. According to the specific weight of the gel band, three volumes of solubilization buffer (Qiagen) were added and immediately incubated for 10 min at 50°C until bands were entirely solubilized. One gel volume of isopropanol (Sigma Aldrich) was added. Samples were mixed by pipetting up and down, transferred to a MiniElute spin-column (Qiagen), and centrifuged at 12000 g for 1 min. The flow-through was removed and spin-column was washed once with 500 µl solubilization buffer (Qiagen). Afterward, the column was washed with washing buffer (Qiagen) and dried via centrifugation to remove remaining ethanol. 10-30 µl H₂O_{bidest.} (autoclaved) were put on the column, and the DNA was eluted via centrifugation at 12000 g for 2 min at RT. Purified products were stored at -20°C until use.

3.1.3.4 DNA and RNA concentration measurements

To measure purity and concentration of DNA- and RNA-solutions, light absorption at 260 nm wavelength (A_{260}) and 280 nm wavelength (A_{280}) was measured with an Ultrospec 2100 *pro* spectrophotometer (Amersham Biosciences). Solutions were diluted either 1:25 or 1:100 in H₂O_{bidest.} (autoclaved), mixed, and measured in a 10 mm quartz cuvette (path length: 10 mm). DNA-solutions were characterized by $A_{260/280}$ quotient of 1.6 to 2.0, RNA-solutions with a quotient between 1.8 and 2.1.

3.1.3.5 Sequencing

Sequencing of DNA constructs was performed by SeqLab Co. (Göttingen, Germany) according to their internal quality standards.

3.1.3.6 Subcloning into pGEM®-T Easy and TOPO®-TA vectors

PCR fragment insertion into pGEM®-T Easy vector was performed according to manufacturer's information. In brief: 5 µl of 2x Rapid ligation buffer (Promega) were mixed with 50 ng pGEM®-T Easy vector, 3 U T4 DNA ligase (Promega), and an adapted volume of PCR fragment, usually following an insert:vector molar ratio of 3:1. As background control,

reactions were prepared without insert (C1) and/or without T4 DNA ligase (C2). Reactions were incubated either for 3 h at RT or overnight at 4°C.

Subcloning in TOPO®-TA vector (Invitrogen) was performed according to manufacturer's protocol either. Up to 4 µl PCR product were mixed with 1 µl of a salt solution (Invitrogen) and 1 µl TOPO®-TA vector (Invitrogen) and incubated for 3 h at RT. Control reaction lacks the PCR fragment (insert).

3.1.3.7 Preparation of competent *Escherichia coli* (*E. coli*)

To prepare chemically competent bacteria (*E.coli*) for transformation (see 3.1.3.8), a starter culture of 6 ml LB medium (see 3.12) was inoculated with 10 µl TOP10 cells (Invitrogen) and incubated overnight (shaking; 220 rpm) at 37°C. Next day, 100 ml LB/Amp medium (see 3.12) were inoculated with 1 ml of the starter culture and incubated at 37°C until absorbance at 600 nm wavelength (A_{600}) of the bacteria mixture reaches a value of around 0.5. Subsequently, mixture was incubated on ice for 15 min. Cells were collected by centrifugation (1200 g for 15 min at 4°C) and resuspended in 30 ml competency buffer I (see 3.12). After 1 h incubation on ice, cells were collected by centrifugation, dissolved in 25 ml competency buffer II (see 3.12), and incubated on ice for 15 min. Afterward, *E.coli* were shock-frosted with liquid nitrogen (-196°C) and stored at -80°C.

3.1.3.8 Transformation of *E. coli*

For transformation of ligation products either One Shot® TOP10 chemically competent *E.coli* (transformation efficiency > 10⁹; Invitrogen) or TOP10 *E.coli* (Invitrogen), which were made competent in our laboratory (see 3.1.3.7), were used.

Competent *E.coli* were stored at -80°C and thawed on ice for 10 min. 1-5 µl ligation product were carefully added to 50 µl competent *E.coli* and incubated for 20 min on ice. Heat-shock was performed for 30 s at 42°C followed by 2 min incubation on ice. Afterward, 150 µl super optimal broth with catabolite repression (SOC) medium (see 3.12) were added and *E.coli* incubated for 1 h shaking at 220 rpm. The mixture was spread on agar plates supplemented with 100 µg/ml ampicillin (Sigma Aldrich) and incubated overnight at 37°C. In some cases, transformation mixture was spread on agar plates supplemented with ampicillin and 5-bromo-4-chloro-3-indolyl-β-D-galactopyranoside (X-Gal; Sigma Aldrich) solution for blue-white screening. X-Gal is a chromogenic substrate for β-gal, a sequence present in the pGEM®-T

Easy and TOPO®-TA vector. If DNA fragment is inserted, β -gal is not functional and positive clones appear as white colonies. To prepare LB/Amp agar plates, 40 μ l X-Gal (20 mg/ml, Sigma Aldrich) and 40 μ l isopropyl -D-1-thiogalactopyranoside (IPTG) solution (100 mM; Sigma Aldrich) were added on the surface of agar plates and incubated for 30 min at RT.

3.1.3.9 Isolation of bacterial clones and plasmid amplification

To control fragment insertion, usually 12 bacterial clones were isolated from agar plates and plasmid DNA was purified according to Miniprep Purification Protocol (Qiagen). Three ml LB/Amp medium (see 3.1.2) were inoculated with one picked clone, incubated at 37°C overnight (shaking; 220 rpm), and bacteria collected by centrifugation (12000 g for 2 min at RT). After bacteria lysis, neutralization, and precipitation, plasmid DNA was dissolved in 20 μ l H₂O_{bidest.} (autoclaved). To increase the amount of plasmid DNA, 250 ml LB/Amp medium (see 3.1.2) were inoculated with a single clone or with 1 ml an overnight starter culture (6 ml LB/Amp medium with a single picked clone). The mixture was incubated at 37°C overnight (shaking; 220 rpm). Plasmid DNA was isolated with the HiSpeed® Plasmid Midi Kit (Qiagen). Briefly: bacteria were harvested by centrifugation at 6000 g for 15 min at 4°C, resuspended, and lysed. The suspension was purified by a QIAfilter Midi Catridge (Qiagen), and plasmid DNA was collected using a HiSpeed® Midi Tip (Qiagen). After washing, plasmid DNA was eluted with buffer QF (Qiagen), concentrated with the QIAprecipitator Midi Module (Qiagen), and solved in 500 μ l H₂O_{bidest.} (autoclaved).

3.1.3.10 Restriction analysis for receptor cloning

Insertion of receptor sequence into cloning vector (pGEM®-T Easy or TOPO®-TA vector) was evaluated by enzymatic restriction analysis. To analyze insertion into the vector, purified plasmid DNA was digested with *EcoRI* restriction enzyme (Fermentas) or independently with *EcoRI* and *PstI* restriction enzymes (Fermentas) according to manufacturer's instructions. In brief: ~1 μ g plasmid DNA was digested with 0.5-1 μ l restriction enzyme and 2 μ l 10x Restriction buffer (Fermentas). Mixture was adjusted with H₂O_{bidest.} (autoclaved) to a final volume of 20 μ l. Enzymatic reaction was performed for 1 h at 37°C. Digestion reactions were analyzed on agarose gels (see 3.1.3.2).

3.1.3.11 Subcloning into *pHSV-IRES-GFP* expression vector

Purified plasmid DNA of pGEM®-T Easy or TOPO®-TA insertion-positive clones was digested in parallel with the *pHSV-IRES-GFP* vector, using the following restriction enzymes (Fermentas): *Sall/XbaI* (*Vmn2r26*), *HindIII/Sall* (*Vmnr2r65*, *Vmnr2r66*, *Vmnr2r74* and *Fpr3*) and *HindIII/XbaI* (*Vmn1r89* and *Vmn1r237*). Digestion conditions were the following: 25 µl 2x Tango buffer (Fermentas), ~1µg plasmid DNA and 2 µl of each restriction enzyme. Reaction volume was adjusted to 50 µl with H₂O_{bidest.} (autoclaved). Reactions were incubated for 30 min at 37°C, purified, and used for the ligation reaction.

3.1.3.12 Ligation

Ligations were performed for 3 h at RT with the digested insert and vector, 5 U T4 DNA ligase (Thermo Scientific), and 1 µl 10x Ligation reaction buffer (Thermo Scientific). As controls, two reactions were performed either without insert or without insert and T4 DNA ligase.

3.1.3.13 Preparation of glycerol stocks

To store bacteria equipped with specific plasmid DNA, 3 ml of an overnight culture were centrifuged at 1200 g for 5 min at RT, resuspended in 3 ml LB medium (see 3.12) supplemented with 15 % [v/v] glycerol (Sigma Aldrich), and stored at -80°C.

3.1.4 Cloning procedure mCherry

3.1.4.1 Cloning *pHSV-IRES-mCherry* constructs

The *mCherry* sequence was amplified by PCR (Forward primer: 5'-TGAATTCATGGTGAGCAAGGGCGAGGAGG-3'; Reverse primer: 5'-TTCTCGAGTTACTTGTACAGCTCGTCCAT-3') from the pcDNA3.1/hChR2(H134R)-*mCherry* plasmid (Addgene plasmid #20938), kindly provided by Prof. Karl Deisseroth (Stanford University, Stanford, United States). The IRES sequence was amplified by PCR from the *pHSV-IRES-GFP* expression vector (kindly provided by Prof. M.T. Alonso, University of Valladolid, Valladolid Spain; Forward primer: 5'-AAGACATTGAAATAAAGGCAATATGA-3'; Reverse primer: 5'-

TGAATTCGGTGGCGATGGATCCCAGCTTGA-3'). To combine both sequences, an assembly PCR was performed and PCR product subcloned into pGEM®-T Easy vector. Sequences were further cloned into pHSV-IRES-*GFP* vector using the *Sall* restriction enzyme (Fermentas). A polyadenylation site from the pHSV-IRES-*GFP* vector was amplified by PCR (Forward primer: 5'-AAGGTACCTTCTCGAGCTGAGCGCCGGTC-3'; Reverse primer: 5'-GGTCTAGAGCTTTATTTGTGAAATTTGTG-3') and inserted downstream of the *mCherry* sequence, using *XhoI*/*XbaI* restriction sites. Plasmid DNA of positive clones was isolated using a Miniprep Purification Protocol (Qiagen). Restriction analysis was performed as double restrictions according to manufacturer's protocol with several restriction enzymes flanking the inserted fragment. Restriction products were evaluated by agarose gel electrophoresis (see 3.1.3.2). Plasmid DNA of positive clones was amplified by HiSpeed® Plasmid Midi Kit (Qiagen) (see 3.1.3.9), dissolved in 500 µl of H₂O_{bidest.} (autoclaved), and used for sequencing analysis (see 3.1.3.5).

3.1.4.2 pHSV-*Vmn2r74*-IRES-*mCherry* construct

Vmn2r74 sequence was excised from the pHSV-*Vmn2r74*-IRES-*GFP* vector using *HindIII* and *Sall* restriction sites, which flank the receptor sequence. Digestions were performed independently (*HindIII* and *Sall* restriction enzyme; Fermentas) and purified with the MiniElute Gel Extraction Kit (Qiagen) (see 3.1.3.3). *Vmn2r74* sequence was ligated into *HindIII*- and *Sall*-restricted (Fermentas) pHSV-IRES-*mCherry* vector. Correct insertion was controlled by restriction analysis using *HindIII* and *Sall* restriction enzymes (Fermentas) and monitored by gel electrophoresis (see 3.1.3.2). After ligation (see 3.1.3.12) and transformation (see 3.1.3.8), plasmid DNA from positive clones was amplified using the HiSpeed® Plasmid Midi Kit (Qiagen) (see 3.1.3.9).

3.1.5 Cloning of the recombinant major urinary protein 20 (MUP20)

The coding sequence of the major urinary protein *MUP20* was amplified by PCR (Forward primer: 5'-ATGAAGCTGCTGGTGCTG-3'; Reverse primer: 5'-TCATTCTCGGGCCTCAAG-3') from a cDNA library of male mice liver. PCR product was ligated into pGEM®-T Easy vector (see 3.1.3.6). After transformation (see 3.1.3.8), positive clones were isolated, and plasmid DNA was extracted (see 3.1.3.9). Restriction analysis was performed with *CspI* restriction enzyme (Fermentas) for 45 min at 37°C. Linearized plasmid

DNA was excised from agarose gel, purified (see 3.1.3.3), and eluted into 20 μ l H₂O_{bidest.} (autoclaved). Linearized plasmid DNA was further digested with FastDigest® *RsaI* restriction enzyme (Fermentas) according to manufacturer's instructions and purified by agarose gel electrophoresis (see 3.1.3.2). Both restriction steps induced fragmentation of the plasmid DNA into two characteristic fragments. Fragment with inserted *MUP20* sequence was confirmed by sequencing (Sequencing primer: 5'-ATGAAGCTGCTGGTGCTG-3').

For subcloning into pMAL-2cX vector (NEB), *MUP20* sequence was amplified from pGEM®-T Easy vector by PCR using primers, which include *BamHI* and *HindIII* restriction sites (Forward primer: 5'-AGGATCCATGAAGCTGCTGGTGCTG-3', Reverse primer: 5'-CAAAGCTTTCATTCTCGGGCCTCAAG-3'). To insert purified PCR products (insert) into pMAL-2cX vector, insert and vector were digested with FastDigest® *HindIII* and FastDigest® *BamI* restriction enzymes (Fermentas). Plasmid DNA was further used to prepare a glycerol stock (see 3.1.3.13) or used to express and purify the MUP (see 3.1.6). Plasmid DNA containing *rFeld4* sequence was kindly provided by Prof. Lisa Stowers (The Scripps Research Institute, San Diego, United States), *MUP7*, *MUP10*, *MUP19*, and *MUP3* were kindly provided by Dr. Pablo Chamero (University of Tours, Nouzilly, France).

3.1.6 Production of recombinant major urinary proteins (MUPs)

To prepare recombinant MUPs (rMUPs), the pMal Protein Fusion and Purification System (NEB) was used. For a starter culture, 10 ml LB/Amp medium (see 3.12) were inoculated with a pipette tip scratched over the surface of a glycerol stock and grown overnight at 37°C (shaking; 220 rpm). Next day, the starter culture was diluted in 1 l LB/Amp medium and grown for 1 h at 37°C (shaking; 220 rpm). Gene expression in *E.coli* was induced adding 0.3 mM IPTG (Sigma Aldrich) for 2 h at 37°C (shaking; 220 rpm). Bacteria were collected by centrifugation at 4000 g for 20 min at 4°C. Bacteria pellet was dissolved in 25 ml column buffer (see 3.12) supplemented with a protease inhibitor cocktail tablet (cOmplete™ Tablets EASYpack; Roche) and incubated for 30 min on ice with 1 mg/ml lysozyme (Sigma Aldrich). Samples were sonicated for 10 min on ice (90% Duty cycle, 100% output control; Branson Sonifier 250) and centrifuged at 9000 g for 30 min at 4°C. Supernatant was removed and incubated with 2 ml bed volume of amylose resin (NEB) overnight at 4°C. Emulsion was washed twice with 50 ml pre-cooled column buffer (see 3.12) and amylose resin was collected by centrifugation at 100 g for 5 min at 4°C. To elute recombinant protein, amylose resin was

transferred to a 15 ml centrifuge tube (Greiner) and incubated with 2 ml column buffer (see 3.1.2) supplemented with 25 mM maltose (Sigma Aldrich) for 2 h at RT.

3.1.7 Sodium dodecyl sulfate polyacrylamide gel electrophoresis (SDS-PAGE)

Purity and concentration of rMUPs were evaluated by SDS-PAGE. Therefore, 1 μ l and 5 μ l of 2 ml elution volume (see 3.1.6) were mixed with 1 μ l SDS-sample buffer (20 μ l 6x DNA loading dye [Fermentas] were mixed with 1 μ l 2-mercaptoethanol [Sigma Aldrich] and adjusted with H₂O_{bidest.} [autoclaved] to a final volume of 6 μ l). To estimate concentration of rMUPs, standard samples with defined amounts (usually: 0.5 μ g-15 μ g) of bovine serum albumin (BSA; NEB) were used and treated equal to rMUP samples. Samples were boiled for 10 min at 95°C and cooled down on ice briefly. They were loaded on a precast RunBlue SDS protein gel 10% (Expedeon). SDS-PAGE run was performed in a Mini-PROTEAN® 3 Cell Chamber (Bio-Rad) in ~1 l of 1x SDS run buffer (Expedeon) at ~170 mV for 45 min. SDS-PAGE was stained with 20 ml of InstantBlue™ protein stain solution for 2 h shaking (220 rpm) at RT.

3.2 Calcium imaging measurements using ratiometric calcium indicator dye fura-2 AM

To monitor activation of VSNs, OSNs, and HEK293 cells, the calcium dye fura-2 AM (fura-2; Molecular Probes) (Grynkiewicz *et al.*, 1985) was used. The neutrally charged acetoxymethyl (AM) ester form of the dye (fura-2 AM) was used to load the cells by passive diffusion over the plasma membrane. After diffusion into cytoplasm, cellular esterase cleaves off AM ester. This induces a shift to the anionic form, which keeps the dye trapped in the cell. The anionic form, in contrast to the neutral form, can bind free calcium ions. Fura-2 excitation was performed at 340 nm and 380 nm wavelength, respectively. Fluorescence emission was collected at ~510 nm wavelength.

3.2.1 Fura-2 loading

Lyophilized fura-2 was dissolved according to manufacturer's manual in DMSO to a final concentration of 5 mM. Cells attached to concanavalin A type V coated coverslips (see 3.5.1)

were washed with imaging buffer (see 3.12) and immediately incubated with 250 μ l imaging buffer supplemented with 5 μ M fura-2 for 30 min at RT in the dark.

3.2.2 Live cell calcium imaging measurement

Coverslips with fura-2-loaded cells were placed into a laminar flow-perfusion chamber (Warner Instruments) under constant perfusion with imaging buffer (see 3.12). Chemostimuli were applied for 30 s with 2 min washing (imaging buffer; see 3.12) intervals in between. Calcium imaging measurements were performed with an inverted Olympus IX71 microscope equipped with a charge-coupled device (CCD) camera (Hamamatsu) and 10x and 20x fluar 0.75 objectives (Olympus). Image pairs after 340 nm and 380 nm wavelength excitation were acquired at a frequency of 0.25 Hz. Fluorescence ratio images at 340 nm and 380 nm wavelength (F340/F380) were calculated after background fluorescence subtraction, using XcellencePro software (Olympus). Acquisition of bright field and fluorescence images was performed with XcellencePro software (Olympus).

3.2.3 Data processing and analysis

Data analysis of fluorescence ratio images was performed with ImageJ 1.50i software (NIH) and Origin 8.6 software (OriginLab). Cells were selected and labeled manually as a region of interest (ROI) and intensities of fluorescence ratio images (F340/F380) were calculated. Intensity values were plotted as line diagrams and visualized with Origin 8.6 software (OriginLab). Peak signals were defined as ligand-induced response when deviation in fluorescence ratio exceeds 1.5 the standard deviation of the mean of the baseline. Response analysis was performed manually. To compare response amplitudes, peak fluorescence ratio value (F_P) and baseline fluorescence ratio value (F_0) were measured and calculated as a quotient (F_P/F_0). Usually, F_P/F_0 quotients of associated cells were averaged and presented as arithmetic mean (\pm SEM). For comparison of individual variability of response amplitudes, F_0 was subtracted from F_P values, normalized to the highest F_P ($\text{ratio}_{\text{norm}}$) and plotted as color-coded heatmap.

3.2.4 Chemostimuli

Chemostimuli were prepared immediately before calcium imaging measurements and used for one experiment. The MHC-peptide SYFPEITHI (SYF) and the mitochondria-derived peptide f-MFFINTLTL (ND1) were dissolved to 100 μ M stocks in the following solution: 120 mM NaCl, 25 mM NaHCO₃, 5 mM KCl, 5 mM N, N-bis (2-hydroxyethyl)-2-aminoethanesulfonic acid (BES), 1 mM MgSO₄, 1 mM CaCl₂ and 10 mM D-glucose. They were further diluted with imaging buffer (see 3.12) to a final experimental concentration of 10⁻¹¹ M and 10⁻⁷ M. Both peptides were kindly provided by Prof. Trese Leinders-Zufall (Saarland University, Homburg, Germany). Synthetic hexapeptide W-peptide (w-pep; WKYMVm) was initially dissolved in a solution (130 mM NaCl, 5 mM KCl, 2 mM CaCl₂, 5 mM D-glucose, 10 mM HEPES) to a concentration of 1 mM and was further diluted in calcium imaging buffer (see 3.12) to a final experimental concentration of 10⁻⁷ M. W-peptide was kindly provided by Dr. Bernd Bufe (Saarland University, Homburg, Germany). A mix of sulfated steroids (E mix) was composed of individual sulfated estrogens (Steraloid): E1050 (1,3,5(10)-estratrien-3, 17 -diol disulphate, E1100 (1,3,5(10)-estratrien-3, 17 -diol 3-sulphate), E0893 (1,3,5(10)-estratrien-3, 17 -diol 3-sulphate), E0588 (1,3,5(10)-7-estratetraen-3, 17 -diol 3-sulphate) each component at a final experimental concentration of 100 μ M. In some experiments, E1050 was used as individual stimulus at a concentration of 100 μ M. Androgen A7864 (5-androsten-3 , 17 -diol disulphate; Steraloid) and sulfated steroid E2734 (1,3,5(10)-estratrien-3, 16 , 17 -triol 17-sulphate; Steraloid) were used and diluted to a final experimental concentration of 100 μ M. All individual steroids were diluted in DMSO to a stock concentration of 50 or 100 mM. As a negative control in calcium imaging measurements, a solution containing 0.2% [v/v] DMSO was used. Potassium chloride (KCl; Sigma Aldrich) was dissolved with imaging buffer (see 3.12) to a 1 M stock solution and further diluted to 100 mM for experimental usage. An adenosine triphosphate solution (ATP; Sigma Aldrich) was used at a final experimental concentration of 60 μ M. Maltose binding protein (MBP; NEB) was used at 10⁻⁷ or 500 nM. Recombinant mouse major urinary proteins (rMUPs) were diluted to a final concentration of 10⁻⁷ M. The recombinant MBP-Feld4 fusion protein (rFeld4) was used at a final experimental concentration of 500 nM. For the preparation of rMUPs see 3.1.6. Cat fur odor solution (CFO) was used undiluted. High molecular weight urine fraction (HMW) from C57BL/6 (B6) and BALB/c (B/c) mice were used in dilutions from 1:10000-1:1000-1:500-1:300 and 1:100. For HMW preparation see 3.2.4.1. All stimuli for fura-2 calcium imaging measurements were diluted with imaging buffer (see 3.12) to their final concentration.

3.2.4.1 High molecular weight urine fraction (HMW) preparation

Mouse urine of adult B6 or B/c male mice (8-15 weeks old; sexually naïve) was collected (~3 mice per collection session) in accordance with the guidelines of the animal welfare committee of the University of Saarland. Collected urine (in average between 0.5 ml and 1 ml) was size-fractionated via centrifugation (14000 g for 30 min at RT) using Nanosep® (Pall) or Microcon® (Millipore) 10 kDa molecular mass cutoff ultrafiltration columns. Flow-through of the first centrifugation represents molecular components lower than 10 kDa (low molecular weight fraction of urine; LMW). Retentate representing urine components larger than 10 kDa (high molecular weight urine fraction; HMW) was washed three times with 0.5 ml 1x phosphate-buffered saline (PBS; Sigma Aldrich) and resuspended in 1x PBS to the initial urine volume. HMW fraction was stored at 4°C not longer than 4 weeks.

3.2.4.2 Cat fur odor solution (CFO) preparation

A sterile (autoclaved) cotton pad was rubbed on a cat's neck (four different domestic cats of both gender) and stored until usage at -80°C in a plastic bag. Cat odor solution was prepared freshly before use in calcium imaging measurements. Therefore, one cotton pad was incubated in 20 ml imaging buffer (see 3.12) shaking (220 rpm) for 2 h at 4°C. Afterward, the cotton pad was separated from the solution by centrifugation at 3000 g for 15 min at 4°C. Supernatant was transferred to a fresh 50 ml centrifuge tube (Greiner) and used undiluted in calcium imaging measurements (see 3.12).

3.3 Single cell RT-PCR

VSNs responding to a certain stimulus or non-responding control cells identified in calcium imaging measurements were isolated individually by a glass capillary (~10 µm diameter; Kwik-Fill™ Borosilicate glass capillaries; World Precision Instruments Inc.) in 1 µl imaging buffer (see 3.12). Cells were transferred into 1 µl DEPC treated water (Invitrogen) in a 1.5 ml reaction tube. As control (-RT) one sample contained 1 µl DEPC treated water (Invitrogen) instead of an individual cell in 1 µl imaging buffer. Cells were immediately frozen in liquid nitrogen (-196°C) and stored at -80°C until usage. To perform RT-PCR, 5 µl pre-cooled cell lysis mix, consisting of 47 µl lysis buffer (100 µl 10x Reverse transcription buffer [Invitrogen], 60 µl 25 mM MgCl₂ [Invitrogen], 5 µl NP-40 [Invitrogen], 50 µl of a 0.1 M DTT solution [Invitrogen] adjusted with 725 µl DEPC treated water [Invitrogen]), 1 µl

RNaseOUT™ (Invitrogen), 1 µl of a 2 mM dNTP mix (Invitrogen) and 0.01 µg Anchor-T primer (5'-TATAGAATTCGCGGCCGCTCGCGA[T]₂₄-3'; Eurofins Genomic) were added and sample was incubated for 1 min at 65°C to unfold mRNA. Samples were cooled on ice for at least 1 min before adding 0.5 µl Reverse transcription mix (RT-mix; 3 µl [600 U] Superscript® III reverse transcriptase [Invitrogen] and 0.5 µl RNaseOUT™ [Invitrogen]). The reaction was incubated for 90 min at 37°C followed by 15 min at 50°C. Incubation for 10 min at 70°C stopped reaction and samples were cooled on ice for at least 1 min. To extend mRNAs with a poly(A)-tail, 5 µl of a terminal deoxynucleotidyl transferase (TdT) mix consisting of 0.15 µl 100 mM 2'-deoxyadenosine 5'-triphosphate (dATP; Fermentas), 0.5 µl 10x Reverse transcription buffer (Invitrogen), 0.3 µl 25 mM MgCl₂ (Invitrogen), 0.25 µl RNaseOUT™ (Invitrogen), 0.25 µl (5 U) TdT (Fermentas), and 3.55 µl DEPC treated water (Invitrogen) were added. Reactions were incubated for 20 min at 37°C and heat-inactivated for 10 min at 65°C. For cooling, samples were kept on ice. RT-tailed products were first amplified (first amplification PCR) with EX-Taq® HS DNA polymerase (TaKaRa) and Anchor-T primer (see above), using the following conditions: 2 µg Anchor-T primer (see above), 5 µl RT-tailed products and 25 µl Premix Taq® DNA polymerase (TaKaRa Taq® Version 2.0). PCR steps: 95°C for 2 min --> 37°C for 5 min --> 72°C for 20 min --> 30 cycles of 95°C for 30 s, 67°C for 1 min, 72°C for 6 min with 6 s extension on each cycle finalized at 72°C for 10 min. Expression analysis was performed by PCR using gene-specific primers (second amplification PCR) (Table 3). PCRs were performed as described above with 2-4 µl PCR product of the first amplification PCR and 0.5-2 µl whole VNO cDNA (see 1.2) as positive control. Amplification was analyzed by gel electrophoresis (see 3.1.3.2). In both PCR reactions (first and second amplification PCR), a sample containing water instead of cDNA was used as a negative control.

Table 3. Gene-specific primers for Single and Low cell RT-PCR.

Gene	Accession Numbers*	Gene-Specific Primer Sequences [5'→ 3']	Annealing temperature [°C]	Internal Primer name
<i>Omp</i>	NM_011010.2	Forward: CGTCTACCGCCTCGATTTCA Reverse: CAGAGGCCTTTAGGTTGGCA	53	<i>Omp1</i>
<i>Omp</i>	NM_011010.2	Forward: GCACAGTTAGCAGGTTTCAGCT Reverse: GGTTTGCAGTCCTGGCAGC	55	<i>Omp2</i>
<i>Vmn2r1</i>	NM_019918.2	Forward: TTGTGGGCTGTATTGGGTGC Reverse: TGATCCCCCTGATCCAACCA	55	<i>Vmn2r1</i>
<i>Trpc2</i>	NM_001109897.2	Forward: ATGTTTCGGCATGGAAGAGCA Reverse: GATGACTCGAAGGCGGTAGG	53	<i>Trpc2</i>
<i>G_o</i>	NM_010308.3	Forward: CTCCACGAGGACGAAACCAC Reverse: GCCCGGAGATTGTTGGCA	56	<i>G_o</i>
<i>G_{i2}</i>	NM_008138.4	Forward: GAGCATGAAGCTGTTTGACAGC Reverse: CTCCTTGGTGTCTTTGCGC	53	<i>G_{i2}</i>
<i>V1rj subfamily</i>	NM_145847.1 NM_001167536.1 NM_134226.1	Forward: CATCACTCCCAGTAAYTCTAAGTGGGC Reverse: GCTGGGMTCTCTTGRRRTGYCTGTAGAG	61	<i>V1rj subfamily</i>

* = National center for biotechnology information (NCBI)

Gene-specific PCRs were performed as followed:

Initial denaturation	94°C 5 min	} 35-40 cycles
Denaturation	94°C 30s	
Annealing	see Table 2	
Extension	72°C 1 min	
Final extension	72°C 10 min	

3.3.1 Low cell RT-PCR

To prepare mRNA from 5 to >50 VNSs isolated with glass capillaries (see 3.3), the PureLink™ RNA Mini Kit (Ambion) was used as described (see 3.1.1). Instead of tissue, 5-50 cells were transferred to a 1.5 ml reaction tube (Greiner) and proceeded as described (see 3.1.1). Transcripts were reversely transcribed into cDNA (see 3.1.2) and gene-specific PCRs were performed (see 3.3).

3.4 Cell-line culture

3.4.1 HEK293 cell culture

HEK293T (HEK293; ATCC® #CRL-11268), originated from human kidney tissue, were cultured in 100 mm Cellstar® petri dishes (Greiner) with 10 ml cell culture medium (see 3.12). For cell culture maintenance, HEK293 cells were kept until 80-90% confluency. Cell culture medium (see 3.12) was removed using RNase-, DNase- and pyrogen-free Cellstar® serological pipettes (Greiner) and washed twice with 1x PBS (Sigma Aldrich). Cells were detached by adding 1 ml 1x Trypsin-EDTA (0.05%; Gibco). Subsequently, 9 ml cell culture medium (see 3.12) were added and cell suspension was centrifuged (100 g for 5 min at RT). Supernatant was removed and cells were resuspended in 5-10 ml cell culture medium (see 3.12). One ml cell suspension was used to inoculate a new petri dish containing 9 ml cell culture medium (see 3.12). For further experimental usage, 10^5 HEK293 cells were counted with an improved Neubauer counting chamber (Hausser Scientific) and seeded on round coverslips (Menzel cover glasses; Thermo Scientific), which were previously coated with concanavalin A type V (Sigma Aldrich). Coating was performed via shaking incubation of round coverslips in 10 ml of a concanavalin A type V solution (0.5 mg/ml; dissolved in PBS) at 4°C overnight. In general, cells were kept in an incubator (37°C, 24% [v/v] O₂ and 5% [v/v] CO₂).

3.4.2 2-2 cell-line

To prepare viral amplicons for gene transduction in freshly dissociated VSNs, OSNs, or HEK293 cells, the 2-2 cell-line (Smith *et al.*, 1992) was cultured. 2-2 cells were kept in culture under same conditions than HEK293 cells (see 3.4.1).

3.5 Primary cell culture

3.5.1 Dissociation of mouse vomeronasal sensory neurons (VSNs)

The VNO was removed carefully without disturbing the tissue and moved to 1 ml 1x PBS at 4°C. The cartilaginous capsule and rests of the vomer bone were removed. Following this, each lobe of the VNO was minced with fine forceps into small pieces. Crushing of the VNO was performed in a freshly prepared dissociation buffer containing 2.2 U/ml papain enzyme

(Worthington), 1.1 mM ethylenediaminetetraacetic acid (EDTA; Fermentas) and 5.5 mM D-cysteine-HCl (Sigma Aldrich). All components were dissolved in 1x PBS (Sigma Aldrich). VNO tissue was slightly triturated by pipetting up and down and incubated at 37°C for 20 min. After incubation, 1 ml of a DNase I solution (600 μ l 1x PBS, 10 U DNase I [Fermentas] and 400 μ l of 5x Colorless GoTaq® reaction buffer [Promega]) was added. The reaction was stopped by adding 10 ml of pre-warmed cell culture medium (see 3.12). VSNs were collected by centrifugation (100 g for 5 min at 7°C). Cells were dissolved in 100 μ l cell culture medium (see 3.12), and 25 μ l cell suspension were plated on each round coverslip (Menzel cover glasses; Thermo Scientific) coated with concanavalin A type V (Sigma Aldrich). Coverslips were placed in a 4-well plate (Nunc) and incubated for 1 h at 37°C, 24% [v/v] O₂, and 5% [v/v] CO₂. Cells were either infected with viral amplicons (see 3.7) or loaded with calcium indicator fura-2 (Invitrogen) for calcium imaging measurements.

3.5.2 Dissociation of mouse olfactory sensory neurons (OSNs)

To dissociate olfactory sensory neurons (OSNs), the entire main olfactory epithelium (MOE) of one adult male mouse was removed and transferred to pre-cooled MOE dissociation buffer containing 2.2 U/ml papain enzyme (Worthington), 1.1 mM EDTA (Fermentas), 5.5 mM D-cysteine-HCl (Sigma Aldrich), 10 U DNase I (Fermentas) and 40 mM urea (Sigma Aldrich). All components were dissolved in 1x PBS (Sigma Aldrich). The MOE was carefully minced and dissected. After incubation for 20 min at 37°C, reaction was stopped by adding 10 ml of pre-warmed cell culture medium (see 3.12). Cells were collected by centrifugation and further processed as described for VSNs (see 3.5.1).

3.6 Generation of HSV-1-derived amplicons

To produce high titer HSV-1-derived amplicons, the *5dl1.2* helper virus/2-2 host cell system was used (Lim *et al.*, 1996). First, 5x 10⁵ 2-2 cells were plated on a 60 mm Cellstar® petri dishes (Greiner) in 5 ml cell culture medium (see 3.12). Cells were incubated for 24 h in an incubator (37°C, 24% [v/v] O₂ and 5% [v/v] CO₂) until they reach 80-90% confluency. Afterward, they were transfected (see 3.8 and Fig. 5A) with pHSV-IRES-*GFP* or pHSV-IRES-*mCherry* expression vectors either equipped with receptor cDNA or as empty vectors. The transfection efficiency and health status of cells were monitored by microscopy. Around 24 h post transfection, medium was removed and replaced by 3 ml Dulbecco's modified

MATERIALS AND METHODS

eagle's medium (DMEM-GlutaMAX™-I; Gibco) supplemented with 2% [v/v] heat-inactivated Fetal bovine serum (FBS; Gibco). For superinfection, transfected cells were infected (Fig. 5A) with 60-180 μ l (~6-18x 10⁵ plaque-forming units [pfu]) 5dl1.2 helper virus, which provides packaging sequences *in trans* (McCarthy *et al.*, 1989). Helper virus was kindly provided by Prof. Dr. Teresa Alonso (University of Valladolid, Valladolid, Spain). Cytopathic effect (CPE) was monitored by microscopy and around 30-48 h post infection, cells were harvested by pipetting up and down. To harvest viral particles (amplicons), cells were alternately kept for 5 min in liquid nitrogen at -196°C and for 10 min in a water bath at 37°C. Subsequently, cells were sonicated for 2 min at RT using a water bath sonicator (Bandelin; Sonorex RK 100). To pellet cellular debris, cells were centrifuged at 1000 g for 5min at 4°C and supernatant (P0~3 ml) was collected.

To amplify viral amplicons, 7x 10⁵ fresh 2-2 cells were plated on a 60 mm Cellstar® petri dishes (Greiner) in 5 ml DMEM-GlutaMAX™-I (Gibco) supplemented with 10% [v/v] heat-inactivated FBS (Gibco). After 24 h, medium was replaced by 4 ml DMEM-GlutaMAX™-I (Gibco) supplemented with 2% [v/v] heat-inactivated FBS (Gibco) and 3 ml P0 (see above) were added. Cells were incubated for 24 h at 37°C, 24% [v/v] O₂ and 5% [v/v] CO₂ until CPE was visible. They were collected by pipetting and transferred to a 15 ml centrifuge tube (Greiner). Amplicons were harvested by alternating freeze and thaw cycles (see above) followed by sonication and centrifugation (see above). Collected supernatant (P1~7 ml), which contains amplicons, was used for further amplification.

Fresh 2x 10⁶ 2-2 cells were plated on two 100 mm Cellstar® petri dishes (Greiner) per sample in 10 ml DMEM-GlutaMAX™-I (Gibco) supplemented with 10% [v/v] heat-inactivated FBS (Gibco). After 24 h incubation (37°C, 24% [v/v] O₂ and 5% [v/v] CO₂), medium was replaced by 2 ml DMEM-GlutaMAX™-I (Gibco) supplemented with 2% [v/v] heat-inactivated FBS (Gibco) and 3.5 ml P1 supernatant were added to each of the two dishes. Cells were incubated for additional 24 h (see above) before medium was replaced by 2 ml Opti-MEM® (Gibco) supplemented with 1% [v/v] Bovine serum albumin (BSA; Sigma Aldrich). Cells were incubated until CPE was visible under microscopic control (~30 h). Supernatant (P2 ~2 ml) was harvested by freeze/thaw cycles and centrifugation as described above for P0 and P1. P2 supernatant was further concentrated by centrifugation at 3000 g for 15 min at 7°C using Amicon® Ultra 4 Centrifugal Filter Units (Merck Millipore). Filter units retained components >10 kDa. Retained volume of supernatant (500 μ l-1 ml) was aliquoted and stored at -80°C until usage.

HSV-1-derived amplicons are composed of a glycoprotein-coated envelope, which mediates intake into a host cell, and the tegument coat structure, important for gene activation and down-regulation of the host cell protein synthesis (Fig. 5B).

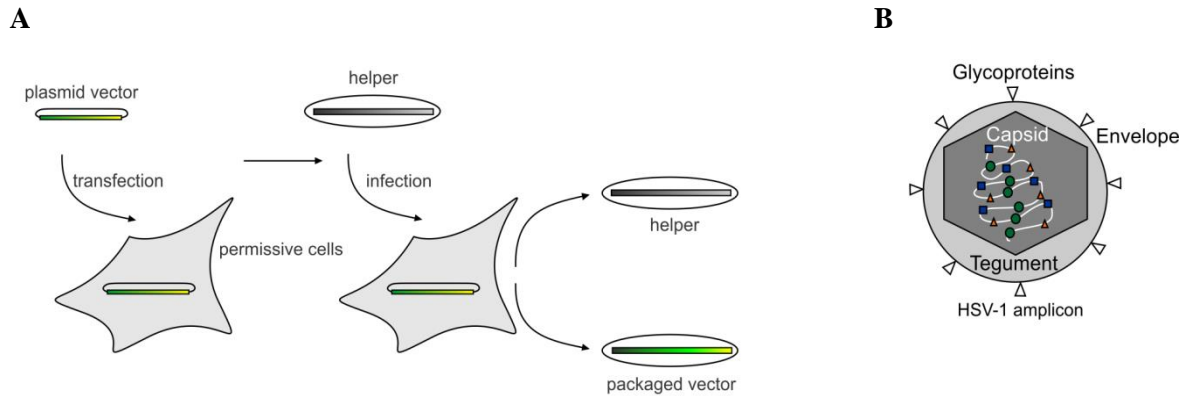


Figure 5. Production of HSV-1-derived amplicons in 2-2 cells.

A. Schematic drawing of the preparation protocol for HSV-1-derived amplicons. 2-2 cells were transfected with pHSV expression vectors (Fig. 7 A-D) and subsequently infected with a replication-defective *5dl1.2* helper virus (helper). Helper enables packaging of multiple pHSV copies into viral particles (amplicons). A mixed culture of helper and amplicons is harvested after three times of amplification. **B.** Schematic drawing of a HSV-1-derived amplicon consisting of an envelope, a tegument structure, and a capsule structure containing the transgene sequence.

3.6.1 Amplification of helper virus stock

To amplify a *5dl1.2* helper virus stock, 10×10^6 2-2 cells were plated on four 100 Cellstar® petri dishes (Greiner) in 5 ml DMEM-GlutaMAX™-I (Gibco) supplemented with 10% [v/v] heat-inactivated FBS (Gibco) and incubated for 24 h at 37°C, 24% [v/v] O₂ and 5% [v/v] CO₂. Medium was replaced by 8 ml DMEM-GlutaMAX™-I (Gibco) supplemented with 2% [v/v] heat-inactivated FBS (Gibco) and cells were infected with 60 μl of a *5dl1.2* seed stock. Infected cells were incubated (37°C, 24% [v/v] O₂ and 5% [v/v] CO₂) until they showed CPE. Helper virus was harvested as described above (see 3.6), aliquoted, and stored at -80°C.

3.6.2 Amplicon titration

To estimate titer of viral amplicon preparations, 50×10^3 HEK293 cells were plated on concanavalin A type V coated coverslips in a 4-well plate (Nunc) and kept overnight at 37°C, 24% [v/v] O₂ and 5% [v/v] CO₂. Next day, HEK293 cells were infected with different volumes (usually: 1 μl-5 μl-10 μl-20μl) of prepared viral amplicons and incubated for 16-20 h (37°C, 24% [v/v] O₂ and 5% [v/v] CO₂). Coverslips were washed one time with 500 μl 1x

PBS (Sigma Aldrich) followed by incubation for 15 min at RT in 500 μ l 4% [v/v] paraformaldehyde solution (Electron Microscopy Sciences). Cells were washed three times with 500 μ l 1x PBS. Afterward, they were placed in 5 μ l Vectorshield® mounting medium (Vector) on a microscopic slide (VWR) and incubated for 30 min in the dark. Infected HEK293 cells were identified by GFP fluorescence microscopy. The relative number of infected cell was calculated dependent on the infection volume. Amplicon titers were between 2×10^5 and 8×10^5 viral amplicons ml^{-1} .

3.7 Viral infection

Freshly dissociated cells (VSNs or OSNs) or HEK293 cells were incubated (37°C, 24% [v/v] O₂ and 5% [v/v] CO₂) in 500 μ l cell culture medium (see 3.12). Cells were infected with 1-25 μ l HSV-1-derived amplicons and incubated for 16-20 h. Before loading with fura-2 (see 3.2.1) cells were washed two times with 500 μ l imaging buffer (see 3.12).

3.8 Transient Transfection

For transfection of primary cells and HEK293 cells, the Lipofectamine® LTX & PLUS™ Reagent Kit (Invitrogen) was used. To transfect cells, 0.5-1 μ g DNA was mixed with 1 μ l Plus™ reagent in 50 μ l Opti-MEM® (Gibco) and incubated for 5 min at RT. Additional 50 μ l Opti-MEM® (Gibco) supplemented with 2 μ l Lipofectamine® LTX were added. The mixture was incubated for 20 min at RT. Subsequently, 100 μ l of the DNA/Lipofectamine® LTX mixture were added to the cells and incubated for 24 h before analysis. Volumes were adjusted according to manufacturer's multiplication factors.

3.9 Mice

3.9.1 Animal care and housing

Animal care and experimental procedures were completed in accordance with the guidelines of the animal welfare committee of the Saarland University (approval number of the Institutional Animal care and Use Committee: H-2.2.4.1.1). Mice were kept under standard light/ dark cycle (12:12) and fed *ad libidum* with sterile water and animal food (Teklad 18%

Protein Rodent Diet, Harlan). Mice were euthanized by CO₂ and cervical dislocation in accordance with the guidelines of the animal welfare committee of the Saarland University.

3.9.2 C57BL/6 wild type mice

For most of the experiments C57BL/6 from Charles River Laboratories were used for organ collection. Used male mice were sexually naïve.

3.9.3 Omp-GFP mice

VSNs of heterozygous *Omp-GFP* mice (B6.OMP^{tm3Mom}MomJ; originally JR# 006667) (Potter *et al.*, 2001) were used for experiments with mCherry amplicons. Since the coding region of the *Omp* gene and part of the 3' non-translated region was replaced by *GFP* (Potter *et al.*, 2001), mature olfactory sensory cells can be visualized by GFP fluorescence microscopy. *Omp-GFP* mice were paired with C57BL/6 mice to produce heterozygous mice.

3.9.4 *Gnao1/OMP-Cre* conditional G_o knockout mice

In some experiments, VSNs from a mutant mouse strain, in which the *Gnao1* gene (coding for the G protein subunit G_o) is deleted, were used. The gene was conditionally deleted under the control of the olfactory marker protein gene (*Omp*) (Chamero *et al.*, 2011; Oboti *et al.*, 2014; Pérez-Gómez *et al.*, 2015). Floxed *Gnao1* mice (*Gnao1*^{fx/fx}) were crossed with a mouse line, in which the coding sequence of the *Cre* recombinase is under the control of the *Omp* promoter (B6;129P2-Omp^{tm4(cre)Mom}/MomJ; Stock #: 006668) (Li *et al.*, 2004). Mutant mice homozygous for *Gnao1* alleles and heterozygous for *Cre* and *Omp* (*cG_o*^{-/-}) and mice heterozygous for deletion (*cG_o*^{+/-}) were used.

3.10 Computational analysis and tools

3.10.1 Software

3.10.1.1 Microsoft office Word 2007

This thesis was written in Microsoft Word 2007.

3.10.1.2 CorelDRAW Graphics suite X7

Figures of this thesis were created in CorelDRAW Graphics suite X7. CorelDRAW was used to adjust brightness, crop, and rotate images.

3.10.1.3 XcellencePro software (Olympus)

Data acquisition of bright field images, fluorescence images, and calcium imaging measurements was performed with XcellencePro software (Olympus).

3.10.1.4 Origin 8.6 (OriginLab) and ImageJ 1.50i (NIH)

Image processing and data analysis of calcium imaging experiments were performed with Origin 8.6 software (OriginLab) and ImageJ 1.50i software (NIH).

3.10.1.5 Chromas Lite (Technelysium Pty Ltd) and AnnHyb (Bioinformatics Organization)

Gene sequences and chromatograms were analyzed with Chromas Lite 2.0 software (Technelysium Pty Ltd) and AnnHyb version 4.946 software (Bioinformatics Organization).

3.10.2 Computational analysis

3.10.2.1 GFP fluorescence intensity comparison

Ten or twenty VSNs or HEK293 cells showing GFP fluorescence at three different time points after amplicon infection (GFP-positive cells) were selected manually and defined as region of interest (ROI). Fluorescence intensity values of selected ROIs were calculated with ImageJ 1.50i software (NIH). The arithmetic mean of the fluorescence intensity values of three randomly selected GFP-negative cells was subtracted from individual intensities of GFP-positive cells. Corrected intensity values were averaged by calculation of the arithmetic mean and visualized as scatter plots using Origin 8.6 software (OriginLab).

3.10.3 Online tools

Information about coding sequences and genes were collected by the U.S. government-funded national resource for molecular biology information (NCBI, <http://www.ncbi.nlm.nih.gov/>). For primer design, the NCBI based Primer-tool (<https://www.ncbi.nlm.nih.gov/tools/primer-blast/>) was used. To perform PCRs *in silico*, the University of California Santa Cruz (UCSC) Genome Browser was used (<https://genome.ucsc.edu/cgi-bin/hgPcr>). The NCBI BLAST® tool (https://blast.ncbi.nlm.nih.gov/Blast.cgi?PROGRAM=blastn&PAGE_TYPE=BlastSearch&LINK_LOC=blasthome) was used to blast sequences.

3.11 Statistics and mathematics

For statistical analysis Origin 8.6 (OriginLab) was used. Mann-Whitney Test was used to evaluate the difference between two independent distributions. Multiple groups were compared with the Kruskal-Wallis analysis of variance (Kruskal-Wallis ANOVA with the Mann-Whitney Test as *post hoc* comparison). The relative amount of responding cells in calcium imaging measurements was calculated for each experiment individually. Relative values of associated experiments were averaged by calculation of the arithmetic mean (denoted as mean percentage). Error bars in figures represent the standard error of the mean percentage (\pm SEM). In some cases, the number of responding cells in calcium imaging measurements was presented as percentage of all responder cells compared to the total amount of analyzed cells (denoted as total percentage).

3.12 Media and buffers

Imaging buffer : 50 ml Hank's balanced salt solution (10x HBBS; Gibco); 5 ml 1 M 4-(2-hydroxyethyl)-1-piperazineethane-sulfonic acid (1 M HEPES; Gibco); adjusted with H₂O_{bidest.} to 500 ml.

Column buffer: 20 ml 1 M Tris-HCl (Sigma Aldrich), adjusted to pH 7.4; 11.7 g NaCl (VWR); 2 ml 0.5 M ethylenediaminetetraacetic acid (EDTA, Sigma Aldrich); adjusted with H₂O_{bidest.} to 1 l.

Competency buffer I: 20 ml 1 M KCl (Sigma Aldrich); 1.2 ml 5 M KCH₃COOH (Sigma Aldrich); 12 ml 1 M CaCl₂ (Sigma Aldrich); 30 ml [v/v] glycerol (Sigma Aldrich); adjusted with H₂O_{bidest.} to 200 ml and adjusted to pH 5.8.

Competency buffer II: 4 ml 0.5 M 3-(N-morpholino)propanesulfonic acid (MOPS; Sigma Aldrich); 2 ml 1 M KCl (Sigma Aldrich); 15 ml 1 M CaCl₂ (Sigma Aldrich); 30 ml [v/v] glycerol (Sigma Aldrich); adjusted with H₂O_{bidest.} to 200 ml and adjust to pH 6.8.

Single cell lysis buffer: 100 μ l 10x Reverse transcription buffer (Invitrogen), 60 μ l 25 mM MgCl₂ (Invitrogen), 5 μ l NP-40 (Invitrogen), 50 μ l 0.1 M DTT (Invitrogen) adjusted with 725 μ l DEPC treated water (Invitrogen) to 1 ml.

Super optimal broth with catabolite repression (SOC) medium : 2% [m/v] casein (Carl Roth®), 5% [m/v] yeast extract (Fluka Analytical/ Sigma Aldrich), 0.05% [m/v] NaCl (VWR), 2.5 mM KCl (Sigma Aldrich), 10 mM MgCl₂ (Sigma Aldrich) and 20 mM D-glucose (Sigma Aldrich), adjusted to pH 7.4.

Luria-Broth (LB) medium: 1% [m/v] casein hydrolyzate (Carl Roth®), 0.5% [m/v] yeast extract (Fluka Analytical/ Sigma Aldrich), 0.5 % [m/v] NaCl (VWR), 0.2 % [m/v] D-glucose (Sigma Aldrich) adjusted to pH 7.4.

LB/Amp medium: 1% [m/v] casein hydrolyzate (Carl Roth®), 0.5% [m/v] yeast extract (Fluka Analytical/ Sigma Aldrich), 0.5 % [m/v] NaCl (VWR), 0.2 % [m/v] D-glucose (Sigma Aldrich) adjusted to pH 7.4 and supplemented with 100 μ g/ml ampicillin (Sigma Aldrich).

Cell culture medium: DMEM-GlutaMAX™-I (Gibco) supplemented with 10% [v/v] heat-inactivated FBS (Gibco) and 100 μ g/ml penicillin plus 10 μ g/ml streptomycin (Gibco).

4 RESULTS

4.1 Functional overexpression of vomeronasal receptors

4.1.1 Heterologous expression of *Vmn1r89* (*V1rj2*) in HEK293 cells

Mice use the vomeronasal organ (VNO) to convey chemosensory information and facilitate social and reproductive behaviors. Around 400 functional vomeronasal receptor (*Vr*) genes have been identified in the mouse VNO. Thus far, only a few receptor-ligand pairs have been identified (Table 1). Most of the receptors have been deorphanized by gene-targeted mice expressing a fluorescent marker protein in specific sensory neurons. In some cases, the results have been verified through genetic deletions. Among identified receptor-ligand pairs are for example: *Vmn1r89* (*V1rj2*) and *Vmn1r85* (*V1rj3*), proposed to be activated by sulfated steroids (Haga-Yamanaka *et al.*, 2014, 2015), *Vmn2r26* (*V2r1b*) and *Vmn2r81* (*V2rf2*) were paired with 9-mer peptides (Leinders-Zufall *et al.*, 2009, 2014), *Vmn2r116* (*V2rp5*) with the ESP1 peptide (Haga *et al.*, 2010), and *Vmn1r49* (*V1rb2*) with 2-heptanone (Boschat *et al.*, 2002). Three receptor-ligand pairs have been identified using a heterologous system (HEK293 cells): *Vmn2r112* (*V2rp1*) and *Vmn2r111* (*V2rp2*) with ESP5 and ESP6 (Dey and Matsunami, 2011) and formyl peptide receptor 3 (*Fpr3*) with signal peptides related to pathogens (Bufe *et al.*, 2015). In most cases, considerable difficulties were found to functionally express *Vrs* in heterologous cells likely as consequence of misled intracellular receptor targeting and/or missing components needed for proper receptor function. No *V1r* has been expressed in a heterologous system, to the best of my knowledge.

First, I aimed to express a *V1r*, namely the *Vmn1r89*, in HEK293 cells. I selected this specific receptor since it was reported that *Vmn1r89* can be robustly activated by sulfated steroids (Haga-Yamanaka *et al.*, 2014). *Vmn1r89* was cloned into a mammalian expression vector (pHSV-IRES-*GFP*). The cloned receptor sequence is hereby followed by an internal ribosomal entry site (IRES) and a green fluorescent marker protein sequence (*GFP*) leading to a bicistronic expression of the *GFP* and the transgene. HEK293 cells were then transfected (see 3.8) with the pHSV-*Vmn1r89*-IRES-*GFP* (*Vmn1r89*-*GFP*) vector. I tracked transfection efficiency by monitoring *GFP* expression in living cells (Fig. 6). *GFP* fluorescence was observed after 24 h with little or no cytotoxic effects (Fig. 6, left panel). Transfected HEK293 cells were loaded with the calcium-sensitive dye fura-2 and calcium imaging measurements were performed. Cells were stimulated with a mix of sulfated steroids (E mix: E1050

[1,3,5[10]-estratrien-3,17 β -diol disulphate]; E1100 [1,3,5[10]-estratrien-3,17 β -diol 3-sulphate]; E0893 [1,3,5[10]-estratrien-3, 17 -diol 3-sulphate] and E0588 [1,3,5[10]-7-estratetraen-3, 17 -diol 3-sulphate, each at 100 μ M), which were previously described as potential activators of *Vmn1r89* (Isogai *et al.*, 2011; Haga-Yamanaka *et al.*, 2014; 2015). Transfected cells failed to show any calcium response to the E mix (Fig. 6), indicating that *Vlr* expression in HEK293 cells was not effective. Since the E mix and the sulfated steroid E2734 were dissolved in DMSO, I applied a solution containing the same amount of dimethyl sulfoxide (denoted as DMSO) as a control. Additionally, the high molecular weight fraction of C57BL/6 mouse urine (HMW) (see 3.2.4.1) and the sulfated steroid E2734 (1,3,5(10)-estratrien-3, 16 , 17 -triol 17-sulphate), which does not activate *Vmn1r89* (Isogai *et al.*, 2011), were used as further control solutions. E2734 is chemically and structurally related to the steroids included in the E mix. No responses to any of the control solutions were detected. As a positive control, a 60 μ M adenosine triphosphate solution (ATP), which activates purinergic receptors, was applied. Most of the HEK293 cells (~90%) showed a response to ATP (Fig. 6), indicating that cells were viable and able to show calcium transients. As a transfection control the empty pHSV-IRES-*GFP* vector containing *GFP* but no receptor cDNA (*GFP* control) was used (Fig. 6). *GFP* control-transfected HEK293 cells showed a similar activity pattern compared to *Vmn1r89-GFP*-transfected cells (Fig. 6, upper panel). No responses to any of the applied stimuli, except for 60 μ M ATP, were monitored. Thus, I was unsuccessful in expressing *Vmn1r89* functionally in HEK293 cells.

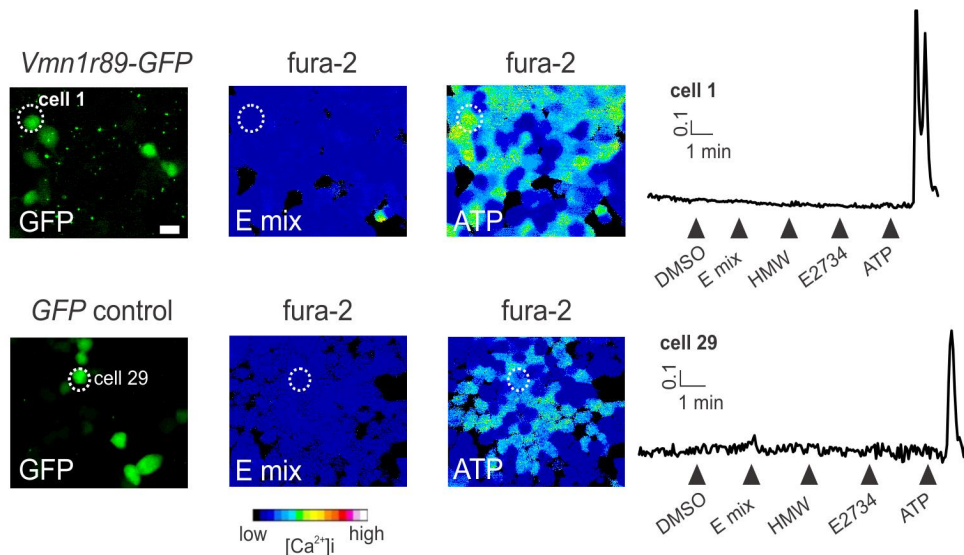


Figure 6. Fura-2 calcium imaging assay of transfected HEK293 cells.

HEK293 cells were transfected either with mammalian expression vector pHSV-*Vmn1r89*-IRES-*GFP* (*Vmn1r89-GFP*; upper panel) or with pHSV-IRES-*GFP* (*GFP* control) expression vector (lower panel) and loaded with fura-2. GFP fluorescence and pseudocolor fura-2 images of transfected HEK293 cells activated by adenosine triphosphate (ATP; 60 μ M) are shown. F340/F380 ratio traces (arbitrary units a.u.) of individual cells (dashed circle) are indicated on the right panel. Transfected HEK293 cells did not show responses to a mix of sulfated steroids (E mix: E1050, E1100, E0893 and E0588; each at 100 μ M), the high molecular weight fraction of C57BL/6 mouse urine (HMW; 1:300), a DMSO control solution (DMSO; containing the same amount of DMSO compared to E mix), and the sulfated steroid E2734 (100 μ M). ATP-induced calcium transients in both HEK293 cell transfections (*Vmn1r89-GFP* and *GFP* control) were monitored. Black arrows indicate start of stimulation. Scale bar: 20 μ m.

4.1.2 Herpes Simplex Virus type 1 (HSV-1)-derived amplicon system

I hypothesized that native VSNs themselves could provide the most capable cellular environment to express *Vrs*. Thus, I aimed to develop a Herpes Simplex Virus type 1 (HSV-1)-derived amplicon delivery system to functionally express *Vrs* in native VSNs.

4.1.2.1 Cloning strategy

To circumvent expression difficulties in HEK293 cells, I developed an uncomplicated and rapid *Vr/Fpr3* expression system using a Herpes Simplex Virus type 1 (HSV-1)-derived amplicon system.

To generate viral amplicons that cover all three major groups of *Vrs*, receptor cDNA from four different *V2rs* (*Vmn2r74*, *Vmn2r66*, *Vmn2r65*, and *Vmn2r26*; Fig. 7A), two *V1rs* (*Vmn1r89* and *Vmn1r237*; Fig. 7B) and *Fpr3* were cloned into a pHSV-IRES-*GFP* vector (Fig. 7A, B). The cloning cassette consists of a *GFP* sequence, an internal ribosomal entry site (IRES), and the receptor cDNA (Fig. 7A, B) to enable bicistronic expression of *Vrs* and *GFP*. Thus, receptor and marker protein are expressed as separate proteins within the same cell,

avoiding potential interferences in the conformation of the receptor protein by GFP. Infected cells were then monitored by green fluorescence and selected for further analysis in calcium imaging measurements.

The mammalian expression vector pHSV-IRES-*GFP* contains prokaryotic sequences, including an ampicillin-resistance gene (*Amp*) to enable selective amplification in bacteria and a ColE1 sequence to facilitate vector replication. Additionally, this vector construct contains a HSV-1-based origin of replication (HSV-1 ori; Fig. 7A-D) together with a short packaging sequence (HSV-1 a/pac). These enable amplification of a high number of viral amplicon copies per cell, resulting in a high transgene expression. To amplify and produce viral amplicons, additional gene sequences are delivered *in trans* using a helper virus and the dedicated host cell line 2-2 (see 3.6). To evaluate the influence of the viral amplicon infection as well as the effect of the marker protein, I used control amplicons (*GFP*-only) equipped with pHSV-IRES-*GFP* vector, which expresses *GFP* but no receptor (Fig. 7C).

I also generated a new pHSV-IRES expression vector, in which the *GFP* sequence was substituted by the one of *mCherry* (Fig. 7D). Two pHSV-IRES-*mCherry* vectors were cloned: one with the *mCherry* cDNA alone and a second with *mCherry* and *Vmn2r74* cDNA (Fig. 7D). Amplicons with these vectors could be used to infect VSNs from gene-targeted mouse lines, e.g. expressing *GFP* under *Omp* promoter control in mature sensory neurons.

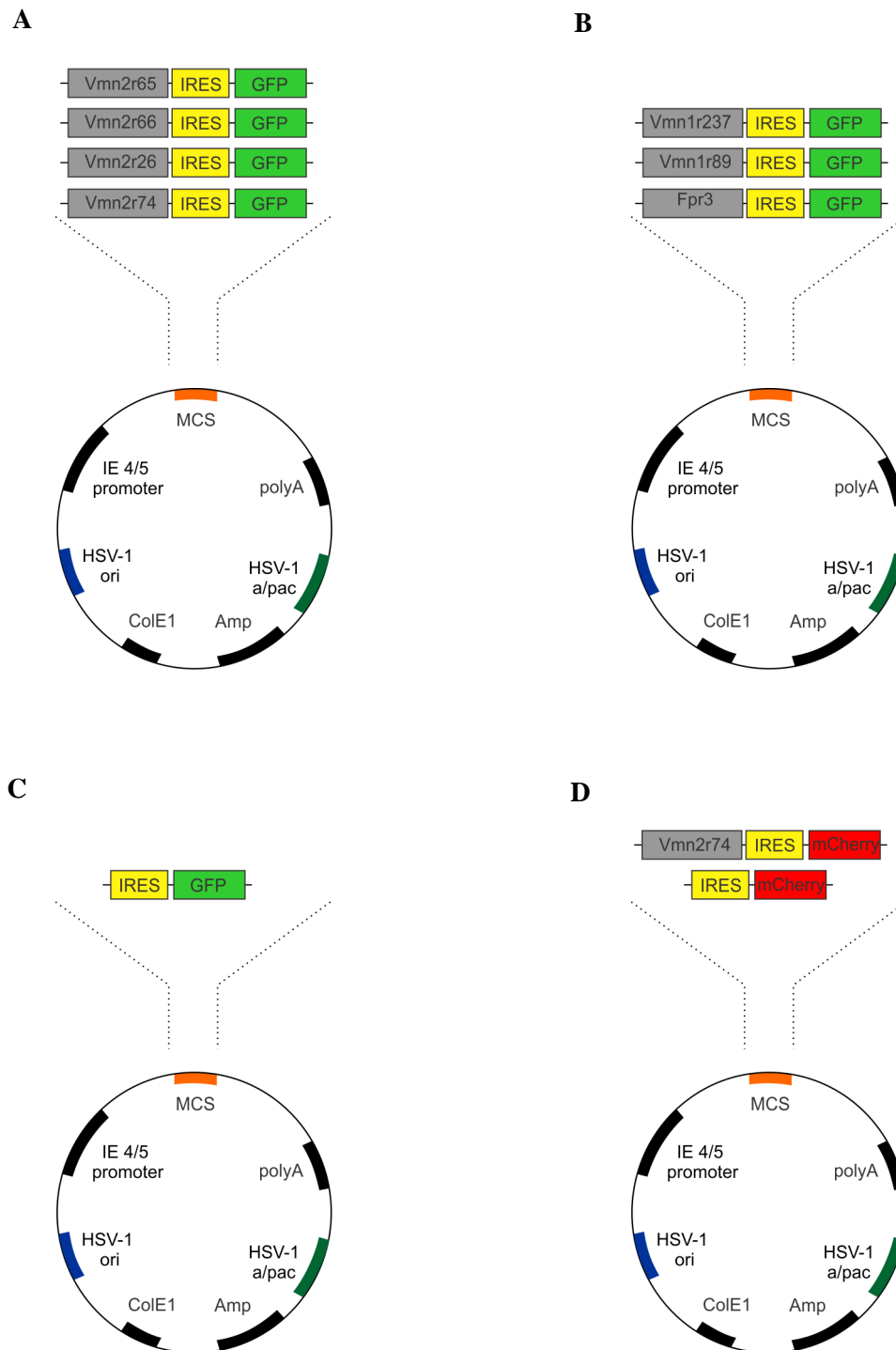


Figure 7. pHSV expression vectors.

A-D. Schematic drawing of 10 pHSV expression vectors (not in actual scale). Receptors are coexpressed with *GFP* using an internal ribosomal entry site (IRES). Expression vectors contain a prokaryotic ampicillin-resistance gene sequence (*Amp*) and an origin of replication sequence (ColE1) for amplification and selection of the plasmid vector in bacteria. A packaging sequence (HSV-1 a/pac) is used to pack transgenes into viral amplicons. The transgenic cassette is equipped with a strong viral promoter sequence (IE 4/5) and a polyadenylation sequence (polyA) finalizing transcription. Additionally, the expression vector contains a HSV-1-based origin of replication (HSV-1 ori) to amplify expression vector in mammalian cells. Various pHSV-IRES-*GFP* vectors encoding either *V2rs* (*Vmn2r74*, *Vmn2r65*, *Vmn2r66*, and *Vmn2r26*; **A**), *V1rs* (*Vmn1r89*; *Vmn1r237*; **B**), or *Fpr3* (**B**) were cloned. A pHSV-IRES-*GFP* expression vector containing no receptor cDNA was used as control (**C**). For viral transduction in *Omp-GFP*-marked VSNs (see 3.9.3), receptor cDNA was cloned into a pHSV-IRES-*mCherry* expression vector containing *mCherry* instead of *GFP* (**D**).

4.1.2.2 Time course of GFP expression in amplicon-infected HEK293 cells

To test HSV-1-derived amplicon properties, the time course of *GFP* expression in infected HEK293 cells was determined. HEK293 cells infected with HSV-1-derived amplicons carrying *GFP* (HSV-1-*GFP*) were monitored by their GFP fluorescence at three different time points: 6, 24 and 48 h (Fig. 8). GFP fluorescence was observed 6 h post infection with a peak in fluorescence intensity after 48 h (Fig. 8). Cytotoxic effects (indicated by morphological alterations) were not observed at these time points. Average GFP fluorescence intensity showed a slight increase from 6 h to 24 h but a sharp (~50%) increase from 24 h to 48 h (Fig. 8B). From this *GFP* expression profile in HEK293 cells, I conclude that 24-48 h post infection could be a suitable time frame to monitor functional *Vr* expression in native VSNs.

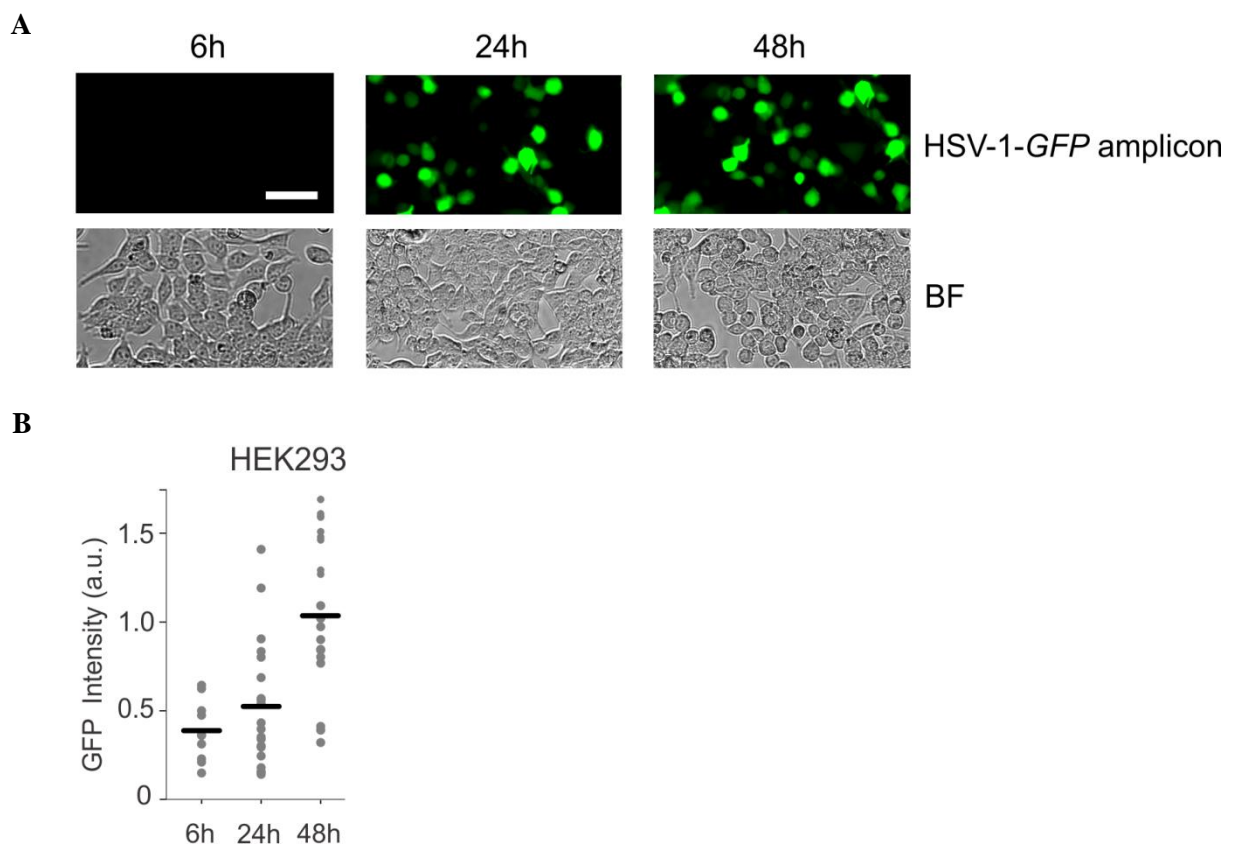


Figure 8. *GFP* expression in infected HEK293 cells.

A. GFP fluorescence and bright field (BF) images of HEK293 cells infected with HSV-1-*GFP* amplicons. GFP fluorescence was monitored at 6, 24 and 48 h post infection. **B.** The background-corrected GFP fluorescence intensity (arbitrary units a.u.) at three different time points was measured in HEK293 cells infected with HSV-1-*GFP* amplicons. Gray circles represent individual cells. Mean values of GFP fluorescence intensity for each time point are indicated as black bars. Intensity increases constantly from 6 h with a peak after 48 h. N= 10 cells (6 h); N= 20 cells (24 h); N= 48 cells (48 h). Scale bar: 50 μ m.

4.1.2.3 *HSV-1-Vmn1r89-GFP amplicon infection in HEK293 cells*

Since transfection failed to induce functional expression of *Vmn1r89* in HEK293 cells, I sought to determine whether an increase of receptor expression level via an amplicon-derived delivery system is functional in HEK293 cells. Thus, HEK293 cells were infected either with HSV-1-derived amplicons carrying *Vmn1r89-GFP* or with control amplicons just carrying *GFP* (*GFP*-only; no receptor DNA) (Fig. 9). At 24 h post infection, HEK293 cells were loaded with fura-2 and calcium imaging measurements were performed. Clear *GFP* fluorescence could be observed, indicative of efficient infection (Fig. 9A), but no response to E mix (Fig. 9). Similarly, no responses were observed to any other tested stimuli (HMW and DMSO). Occasional responses to the sulfated steroid E2734 were found in both, *Vmn1r89-GFP* (three cells out of 333 infected cells) and *GFP*-only (two cells out of 240 infected cells) amplicon-infected HEK293 cells (Fig. 9). This indicates that these responses are likely unspecific and driven by a mechanism different from *Vmn1r89*. In *Vmn1r89-GFP* and control (*GFP*-only) amplicon-infected HEK293 cells I observed a similar response profile to ATP (~80% of infected cells), indicating that viral infection does not alter cell viability and response to ATP (Fig. 9). These experiments indicate, that amplicon-induced expression does not seem to facilitate functional *Vr* expression in HEK293 cells. Probably due to ineffective receptor transport to the membrane or missing coupling to a suitable signal transduction machinery.

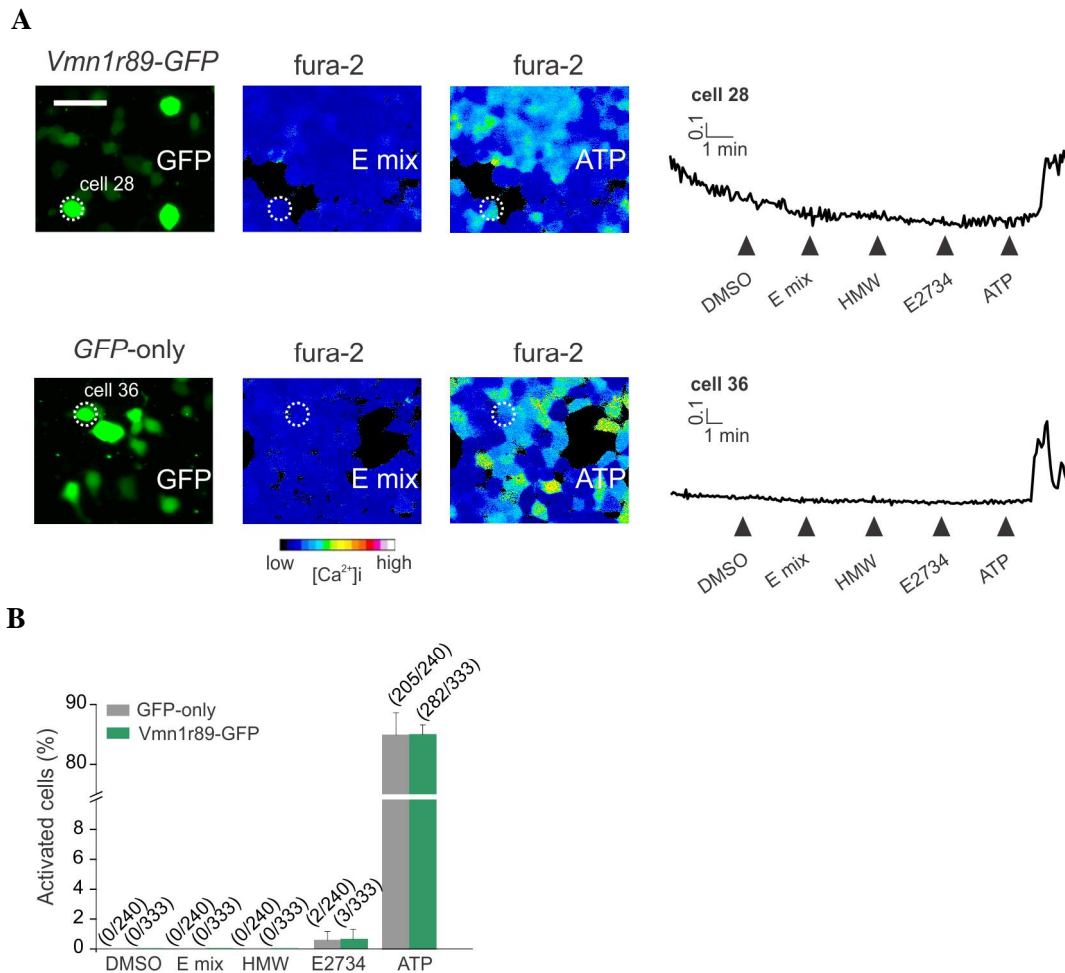


Figure 9. Viral transduction of *Vmn1r89-GFP* in HEK293 cells.

A. GFP fluorescence (left) and pseudocolor fura-2 (center, right) images of HEK293 cells infected with HSV-1-*Vmn1r89-GFP* amplicons (*Vmn1r89-GFP*) or HSV-1-*GFP* amplicons (*GFP-only*) and loaded with fura-2. F340/F380 ratio traces (arbitrary units a.u.) of selected cells (dashed circle) are shown on the right. Stimuli: a DMSO control solution (DMSO, containing the same amount of DMSO compared to E mix), E mix: (E1050; E1100; E0893 and E0588; each at 100 μ M); the high molecular weight fraction of C57BL/6 mouse urine (HMW; 1:300); E2734 (100 μ M) and ATP (60 μ M). Infected cells showed robust activation to ATP (60 μ M) but no responses to HMW, DMSO control solution, and E mix. Black arrows indicate start of stimulation. Scale bar: 50 μ m. **B.** Summary of GFP-positive (GFP+; infected) cell activation of HEK293 cells either infected with HSV-1-*Vmn1r89-GFP* amplicons (*Vmn1r89-GFP*; green) or HSV-1-*GFP* amplicons (*GFP-only*; gray). Mean percentage of activated GFP+ cells by each stimulus (DMSO, E mix, HMW, E2734, and ATP) is indicated. Infected cells showed robust activation to ATP (*Vmn1r89-GFP* amplicon: mean percentage: 85.05% \pm 1.63% SEM; *GFP-only* amplicon: mean percentage: 84.98% \pm 3.73% SEM) but no responses to HMW, a DMSO control solution, and E mix. Responses to E2734: *Vmn1r89-GFP* amplicon: mean percentage: 0.68% \pm 0.68% SEM; *GFP-only* amplicon: mean percentage: 0.60% \pm 0.60% SEM). N= 333 *Vmn1r89-GFP* amplicon-infected cells and 240 *GFP-only* amplicon-infected cells in 4 infection experiments for each amplicon. Numbers in parentheses denote activated cells out of all infected cells in 4 infection experiments for each amplicon (*Vmn1r89-GFP* or *GFP-only*). Data expressed as mean \pm SEM.

4.1.2.4 Culture of vomeronasal sensory neurons (VSNs)

Since HEK293 cells failed to functionally express *Vrs*, I reasoned that a more natural cellular microenvironment would be a better system to facilitate functional receptor expression. Receptors need to be correctly localized to the cell surface and coupled to a second messenger system to allow generation of measurable responses after ligand binding. Native VSNs themselves would be good candidates to provide this suitable cellular environment to properly express and localize *Vrs*. Further support for this assumption comes from the presence of only

two main signaling cascades: one involves G_{i2} coupled to *V1r*-expressing VSNs and most Fprs localized in the apical layer of the sensory epithelium; the second involves G_o used by V2rs and Fpr3 localized in the basal cell layer.

To transfer a *Vr* sequence into native VSNs, HSV-1-derived amplicons, which were previously tested for their expression capabilities in HEK293 cells (Fig. 8), were used. The HSV-1-derived amplicon system is characterized by a high specificity for VSNs since it uses the VNO to invade the central nervous system of rodents under natural conditions (Mori *et al.*, 2005).

To culture VSNs *in vitro* and enable amplicon infection, I developed a protocol for a mouse VSN culture (see 3.5). After dissociation, cells were seeded on glass coverslips and incubated at 37°C in cell culture medium (see 3.12). After 1 h, cells were infected with HSV-1-*GFP* or -*mCherry* amplicons and expression was monitored after 24 h by fluorescence microscopy (Fig. 10). I did not observe a decrease in cell abundance and any obvious morphological alterations. Using this method, allowed me to maintain acutely dissociated VSNs *in vitro* for 24-48 h under standard cell culture conditions without cell loss and almost intact morphology (Figs. 10, 11).

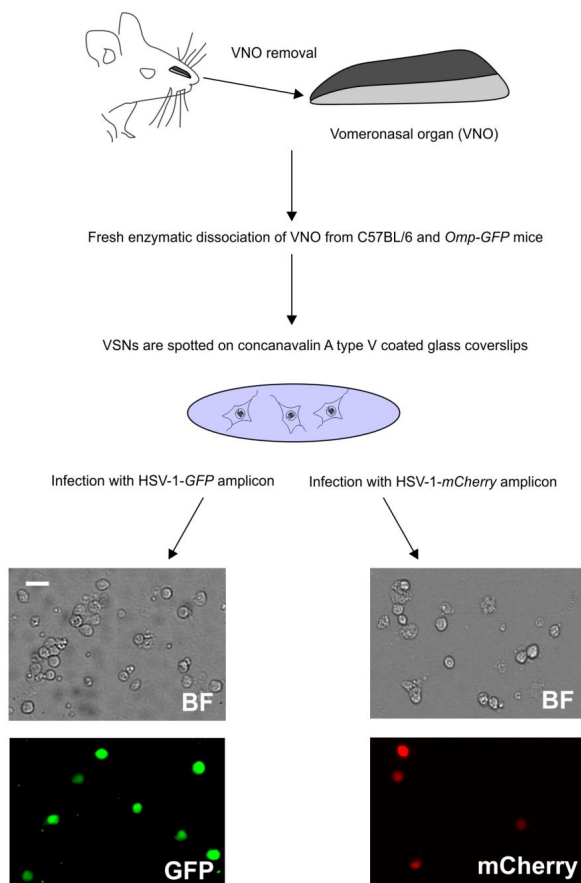


Figure 10. Culture of freshly dissociated VSNs and infection with HSV-1-derived amplicons.

The VNO, located at the bottom of the mouse nasal cavity, is removed, enzymatically dissociated, and plated on concanavalin A type V coated glass coverslips. Cells were either infected with HSV-1-*GFP* or with HSV-1-*mCherry* amplicons. Bright field (BF), GFP and mCherry fluorescence images of amplicon-infected cells (bottom). Scale bar: 20 μ m.

Longer incubation periods resulted in increased cell death since 72 h post infection I found a sharp increase in morphological changes, such as compartmentalization, swelling, and bursting, indicative of cell death (Fig. 11).

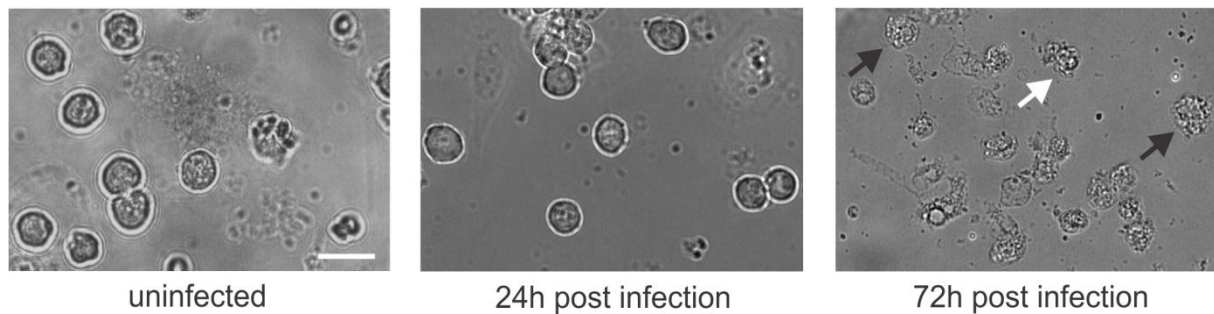


Figure 11. VSN culture after amplicon infection.

C57BL/6 VSNs were freshly dissociated (0 h; uninfected) or infected with HSV-1-*GFP* amplicons and cell morphology was monitored after 24 h and 72 h using bright field microscopy. Cells maintained for 24 h in culture (central panel) showed intact morphology. 72 h post infection (right panel) cells showed clear alterations in cell shape and morphology, such as compartmentalization and swelling (black arrows), typical morphological features of cell death. Some cells bursted and collapsed (white arrow). Scale bar: 20 μ m.

The previous observations regarding the morphology of infected cells indicated that 24 h post infection could provide a suitable time point for functional measurements. Thus, I asked if robust transgene expression could be monitored in cells after 24 h. To test this, acutely dissociated VSNs were infected with HSV-1-*GFP* amplicons and GFP fluorescence intensity and relative cell abundance after 6, 24, and 48 h were analyzed (Fig. 12A). GFP fluorescence intensity could be observed at 6 h, sharply increasing in intensity at 24 h post infection (Fig. 12B). After 48 h of incubation, GFP fluorescence intensity was still high but lower compared to 24 h (Fig. 12B), perhaps as a consequence of reduced cell fitness. To further characterize transgene expression in VSNs, I calculated the abundance of GFP positive cells in HSV-1-derived amplicon-infected VSNs at the three time points: 6, 24 and 48 h (Fig. 12C). A steep increase in the relative number of cells expressing *GFP* from 19% at 6 h to 72% at 24 h was monitored. After 48 h, the number of *GFP*-expressing cells seems to stabilize. This high abundance of *GFP*-expressing cells matched with the observed increase in GFP fluorescence intensity, pointing to 20-24 h as the optimal time interval for infection efficiency and transgene expression in VSNs. From these experiments, I draw the conclusion that infected VSNs can express a virally transduced transgene in a suitable amount of cells. Furthermore, the best time point for further cell processing (calcium imaging measurements) seems to be 24

h post infection since fluorescence intensity decreases after 48 h. This decrease could indicate a reduced activity of the expression machinery due to infection or a general reduction of cellular fitness.

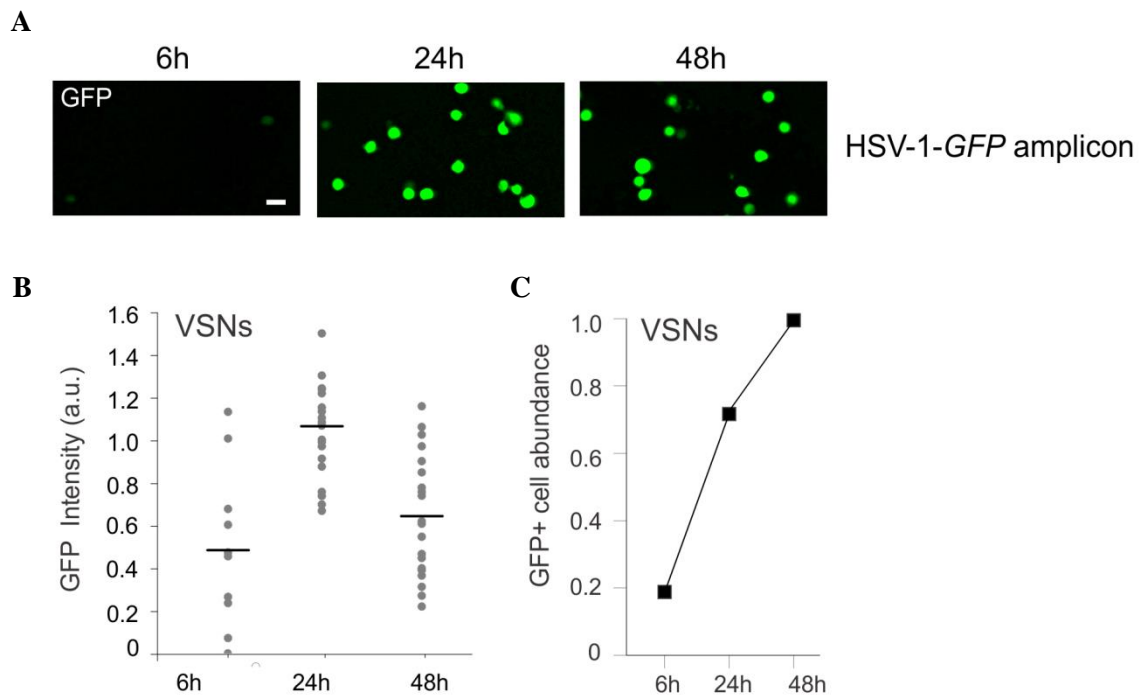


Figure 12. HSV-1 transgene expression profile at different time points in VSNs.

A. Fluorescence (HSV-1-GFP amplicon) images of dissociated C57BL/6 VSNs infected with HSV-1-GFP amplicons. GFP fluorescence was monitored at 6, 24 and 48 h post infection. Scale bar: 20 μ m. **B.** Background-corrected GFP fluorescence intensity measured in arbitrary units (a.u.) on HSV-1-GFP amplicon-infected cells. For each time point 10-20 GFP-positive cells (GFP+; infected) were analyzed (gray dots). Black lines represent mean values of GFP fluorescence intensity. Number of GFP+ cells for each time point: N= 10 cells (6 h); N= 20 cells (24 h); N= 20 cells (48 h). **C.** Normalized abundance of GFP+ cells is plotted at 6, 24 and 48 h. Number of cells: 6 h: 10 GFP+ cells out of 209 total cells; 24 h: 35 GFP+ cells out of 192 total cells; 48 h: 29 GFP+ cells out of 114 total cells.

Overall, the HSV-1-derived amplicon system is feasible to infect and deliver transgenes to VSNs. However, this prompted the question of whether lipofection can recapitulate similar levels of GFP expression efficiency in VSNs. I analyzed GFP expression after 6, 24 and 48 h in VSNs transfected with the pHSV-IRES-GFP expression vector using lipofectamine® (Invitrogen). No GFP-positive cell at any time point was observed (Fig. 13). This indicates that lipofectamine®-induced transfection is not effective in VSNs. This further underlines the relevance of the newly developed HSV-1-derived amplicon system to deliver transgenes to native VSNs and identify receptor-ligand interactions.

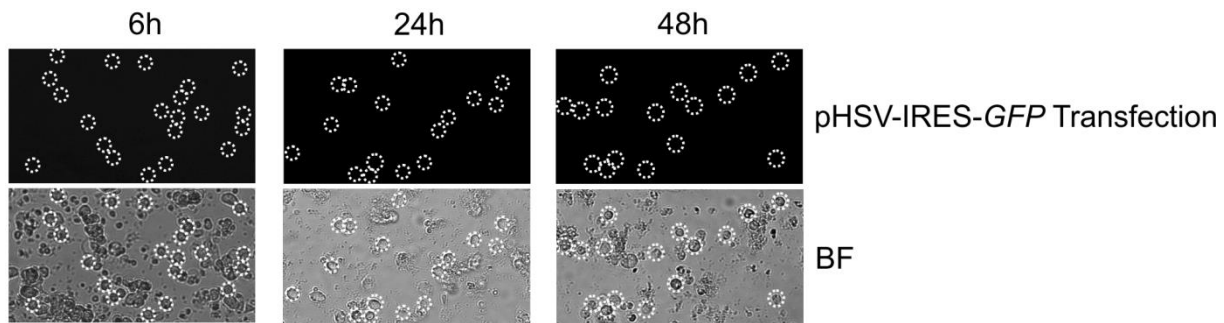


Figure 13. Alternative gene delivery system in VSNs.

GFP fluorescence (pHSV-IRES-*GFP* Transfection) and bright field (BF) images of C57BL/6 VSNs at three different time points (6, 24 and 48 h). Cells were transfected with a pHSV-IRES-*GFP* vector (upper panel) using lipofectamine® (Invitrogen). No GFP-positive cell was found in transfected VSNs. Transfection was performed according to manufacturer's protocol. Scale bar: 20 μ m.

4.1.2.5 *HSV-1-GFP amplicon infection of native VSNs*

To identify receptor-ligand pairs in native VSNs, changes in intracellular calcium were measured using the calcium indicator fura-2. First, I tested whether infected VSNs can be loaded with the dye efficiently. To test this, acutely dissociated VSNs were infected with HSV-1-*GFP* amplicons for 24 h and subsequently incubated in a fura-2-containing solution for 30 min. Infection efficiency was monitored by *GFP* expression and dye uptake (Fig. 14). Cells infected with the amplicon could also be loaded with fura-2, as exemplarily shown for one native VSN (Fig. 14A). After 30 min, a robust dye uptake in GFP-positive (infected) cells could be observed without major influence on the plasma membrane integrity (Fig. 14A). Infection rates of amplicons used in this study were calculated as percentage of *GFP*-expressing cells relative to the total number of cells (Fig. 14B). Both, single receptor amplicon-infected VSNs (denoted as *Vmn1r89-GFP*, *Vmn1r237-GFP*, *Fpr3-GFP*, *Vmn2r26-GFP*, *Vmn2r74-GFP*, *Vmn2r65-GFP*, *Vmn2r66-GFP* in Fig. 14B) as well as VSNs infected with control amplicons with no receptor sequence (denoted as *GFP-only* in Fig. 14B), showed infection rates in the range between ~8% and ~35% of all cells (Fig. 14B). Some amplicons showed higher infection rates than others (Fig. 14B) likely because of varying amplicon titer between preparations as well as differences in amplicon-helper ratio. Nevertheless, I observed no obvious differences based on the receptor type (V1rs, V2rs and Fprs) (Fig. 14B). Furthermore, the number of infected cells is large enough to be analyzed by calcium imaging measurements, even with varying infection rates.

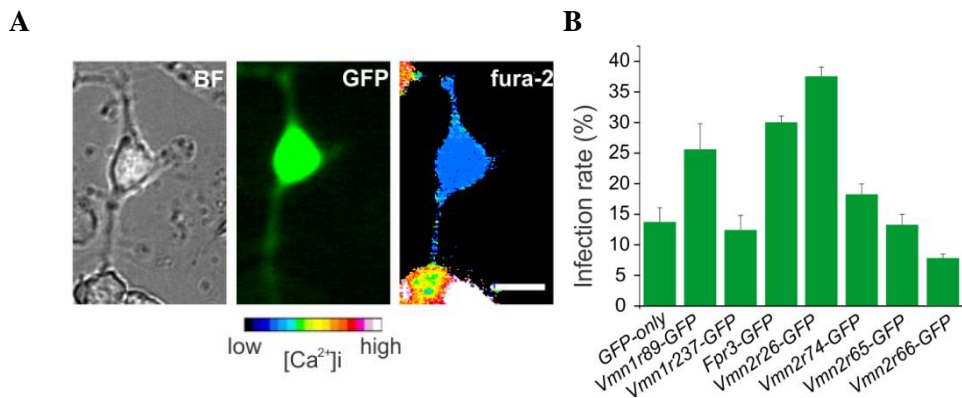


Figure 14. HSV-1-GFP amplicon infection of VSNs followed by fura-2 loading.

A. Bright field (BF), GFP fluorescence and pseudocolor fura-2 images of a single C57BL/6 VSN infected with HSV-1-*GFP* (*GFP*-only) amplicons. Individual VSN showed robust *GFP* expression and effective fura-2 dye uptake. Scale bar: 20 μ m. **B.** Infection rates of different HSV-1-derived amplicons. Infection rates were calculated as the mean percentage of GFP-positive cells (GFP+; infected) relative to all C57BL/6 VSNs in associated experiments. Numbers: *GFP*-only amplicon: 193 GFP+ cells out of 1415 total cells, *Vmn1r89-GFP* amplicon: 436 GFP+ cells out of 1828 total cells, *Vmn1r237-GFP* amplicon: 299 GFP+ cells out of 2499 total cells, *Fpr3-GFP* amplicon: 104 GFP+ cells out of 342 total cells, *Vmn2r26-GFP* amplicon: 271 GFP+ cells out of 723 total cells, *Vmn2r74-GFP* amplicon: 261 GFP+ cells out of 1462 total cells, *Vmn2r65-GFP* amplicon: 12 GFP+ cells out of 89 total cells, *Vmn2r66-GFP* amplicon: 136 GFP+ cells out of 1795 total cells. N= 3-4 infection experiments for each amplicon. Data expressed as mean \pm SEM.

4.1.2.6 HSV-1-mCherry amplicon infection in native VSNs

Dissociation of the VNO leads to a mixed culture consisting of mature and immature VSNs, supporting cells, and progenitor cells. To determine whether infected cells are indeed VSNs, cells from heterozygous *Omp-GFP* mice (Potter *et al.*, 2001) were used for infection experiments. These mice express *GFP* under the control of the olfactory marker protein (*Omp*) gene promoter, which is expressed in all mature VSNs. Following VNO dissociation, GFP fluorescence in ~70% of the cells in culture was monitored, thus identifying them as mature VSNs (Fig. 15B).

Heterozygous *Omp-GFP* VSNs were infected with HSV-1-derived amplicons carrying either an *mCherry* (*mCherry*-only) (Fig. 15A) or a receptor-*mCherry* (*Vmn2r74-mCherry*) expression cassette. The number of cells positive for *mCherry* (*mCherry*+; indicating infected VSNs) and GFP (*GFP*+; indicating mature VSNs) 24 h post infection was analyzed to estimate the percentage of *mCherry*+ cells, which were also positive for GFP. Out of all counted *mCherry*+ cells (infected with *mCherry*-only amplicons) 81% were also positive for GFP (Fig. 15C). In receptor-*mCherry* amplicon-infected VSNs 65% of the *mCherry*+ cells were also positive for GFP. These data indicate that the majority of infected cells in my VSN preparation protocol are likely mature VSNs. Therefore, I could assume that functional expression measurements (calcium imaging) to test my hypothesis that native VSNs would be the most competent cells for functional *Vr* and *Fpr* expression are mainly performed in VSNs.

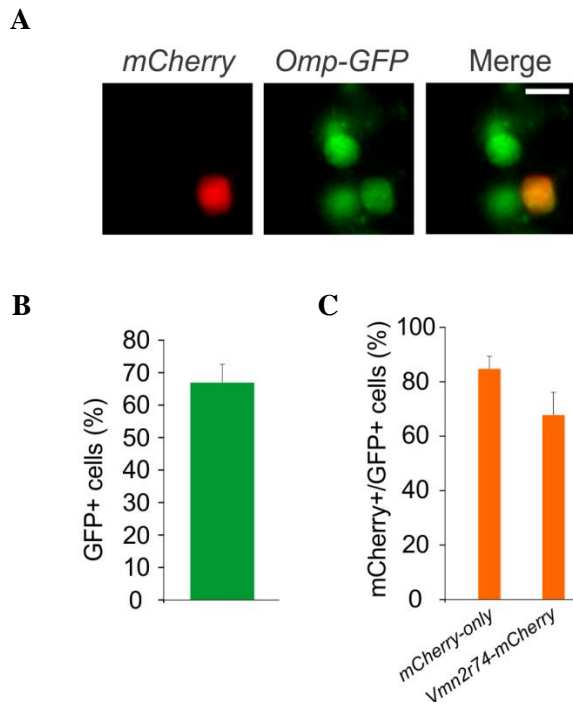


Figure 15. HSV-1-derived amplicon infection of heterozygous *Omp-GFP* VSNs.

A. GFP, mCherry and merged fluorescence images of three individual cells. VSNs were dissociated from the VNO of heterozygous *Omp-GFP* mice and infected with HSV-1-*mCherry* amplicons. One cell of the three GFP-positive cells (GFP+) was also positive for mCherry. Scale bar: 20 μ m. **B.** Around 70% (mean percentage) of the cells in culture (prepared from heterozygous *Omp-GFP* mice) were positive for GFP (2179 GFP+ cells out of 3134 total cells, N= 6 infection experiments). **C.** Heterozygous *Omp-GFP* cells were infected either with HSV-1-*mCherry* (*mCherry-only*) or HSV-1-*Vmn2r74-mCherry* (*Vmn2r74-mCherry*) amplicons. Mean percentage of cells positive for mCherry and GFP (mCherry+/GFP+ cells) relative to all mCherry+ cells. Of all *mCherry+* cells infected with HSV-1-*mCherry* amplicons 81% (289 mCherry+/GFP+ cells out of 335 mCherry+ cells, N= 3 infection experiments) also expressed GFP, indicative of mature VSNs. In *Vmn2r74-mCherry* amplicon-infected cells 65% of the mCherry+ cells did also express GFP (158 mCherry+/GFP+ cells out of 221 mCherry+ cells, N= 3 infection experiments). Data expressed as mean \pm SEM.

4.1.3 Functional validation of the HSV-1-derived expression system in VSNs

4.1.3.1 *Vmn1r89* expression in VSNs

After showing that native mature VSNs can be infected with HSV-1-derived amplicons, I asked if amplicon-induced expression of *Vrs* is functional in cultured VSNs. To test functionality, I stimulated virally transduced cells with already known ligands for specific receptors. I selected two V1rs (*Vmn1r89* and *Vmn1r237*), which were proposed to be activated by sulfated steroids (Isogai *et al.*, 2011; Haga-Yamanaka *et al.*, 2014, 2015). I started with *Vmn1r89* and infected freshly dissociated VSNs from male C57BL/6 mice with two HSV-1-derived amplicons: HSV-1-*Vmn1r89-GFP* (*Vmn1r89-GFP*) or as control HSV-1-*GFP* (*GFP-only*). After 24 h incubation with viral amplicons, cells were loaded with fura-2 and calcium imaging measurements were performed (Fig. 16A). As stimulus, I selected four sulfated steroids, which were previously shown to activate *Vmn1r89*, and applied them as a mix (E mix: E1050 [1,3,5[10]-estratrien-3,17 β -diol disulphate]; E1100 [1,3,5[10]-estratrien-3,17 β -diol 3-sulphate]; E0893 [1,3,5[10]-estratrien-3, 17 -diol 3-sulphate] and E0588

[1,3,5[10]-7-estratetraen-3, 17 -diol 3-sulphate, each at 100 μ M). As a negative control, I used the related sulfated steroid E2734 (1,3,5(10)-estratrien-3, 16 , 17 -triol 17-sulphate; 100 μ M). E2734 is chemically and structurally related to the E mix components. I opted for stimuli concentrations in the high end of the dose-response curves for *Vmn1r89* to maximize discernability of the responses (Haga-Yamanaka *et al.*, 2014, 2015). Similar steroid concentrations were already successfully used in calcium imaging measurements of dissociated VSNs (Celsi *et al.*, 2012). Since steroids are dissolved in DMSO, I used a DMSO control solution (containing the same amount of DMSO compared to E mix) to detect potential false-positive responder cells. HMW of freshly prepared C57BL/6 mouse urine, which activates *V2rs*, was used as an additional control in a 1:300 dilution. As a positive control, a high potassium chloride solution (KCl; 100 mM), which induces a depolarization of the cell, was used. VSNs infected with *Vmn1r89-GFP* amplicons showed robust responses to the E mix (Fig. 16A). This observation was in sharp contrast to previous experiments performed in HEK293 cells (Figs. 6, 9). In these cells, neither transfection nor virally induced expression of *Vmn1r89* revealed any responsivity to the E mix.

VSNs infected with control amplicons (*GFP*-only) were used to address the influence of *GFP*, infection, and endogenous receptor composition on cell responses. Mean percentage of responding cells (relative to all *GFP*-positive cells) to each tested stimulus was compared between cells infected with *Vmn1r89-GFP* and *GFP*-only amplicons (Fig. 16B). VSNs infected with *Vmn1r89-GFP* amplicons showed a 7-fold higher number of responsive cells to the E mix compared to *GFP*-only amplicon-infected cells (Mann-Whitney Test: * $p < 0.05$) (Fig. 16B). To exclude false-positive E mix responders, cells that showed responses to the DMSO control solution and E mix were not considered as positive responses. Importantly, cells infected with *Vmn1r89-GFP* amplicons did not show an increase in responsivity to the control solutions, including the chemically related steroid E2734, the DMSO control solution, and HMW (Mann-Whitney Test: $p = 0.17-0.6$). However, both groups of infected cells (*Vmn1r89-GFP* and *GFP*-only amplicons) showed a comparable percentage of responder cells to high KCl (Fig. 16B), indicating that cells are viable and excitable. These data reveal that the HSV-1-derived amplicon system is a feasible tool for functional expression of *Vmn1r89* in VSNs. I could monitor a significant responsivity of this individual *V1r* to sulfated steroids in VSNs, which is independent of *GFP* expression and amplicon infection. Thus, I could confirm previous observations matching *Vmn1r89* with sulfated steroids on the single cell level. In contrast to HEK293 cells showing no responsivity to the E mix, I could observe

robust responses to applied E mix in *Vmn1r89-GFP*-expressing VSNs. This matches my hypothesis that VSN could provide a functional system to overexpress receptors.

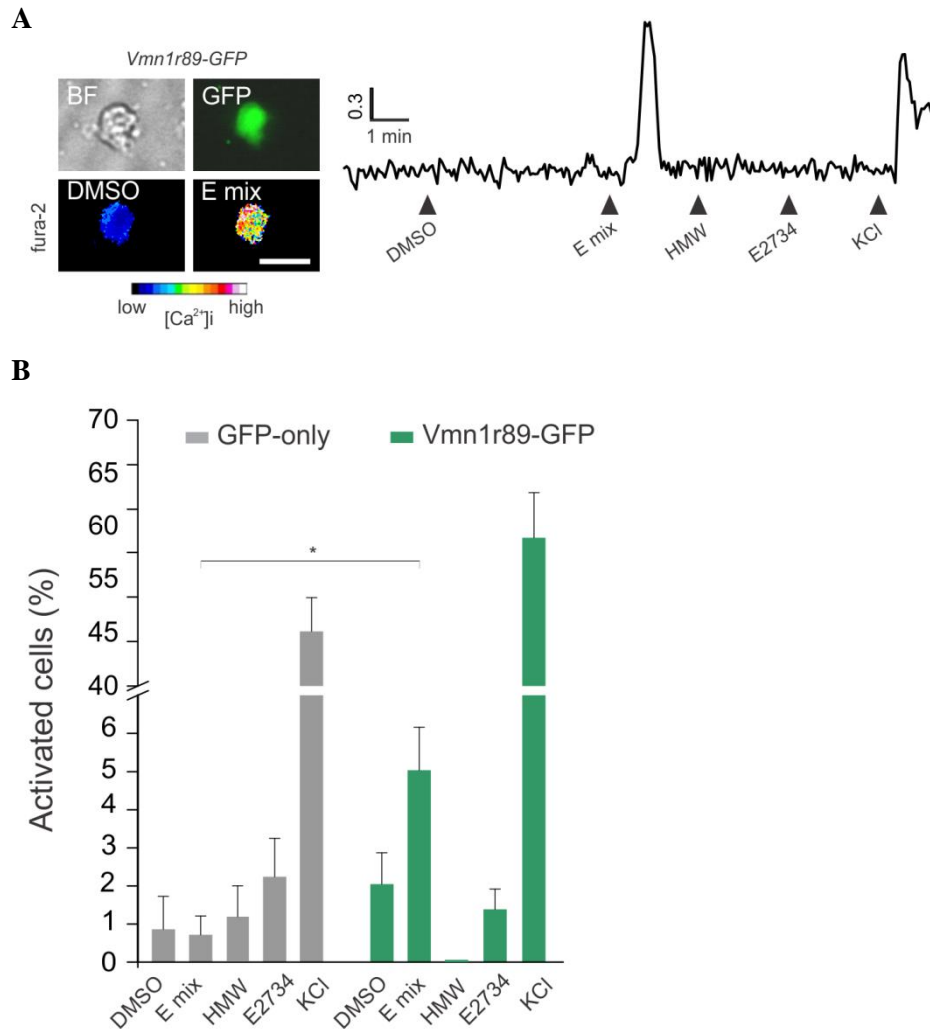


Figure 16. Functional expression of *Vmn1r89* in HSV-1-derived amplicon-infected VSNs.

A. Left, bright field (BF), GFP fluorescence and pseudocolor fura-2 images of a single C57BL/6 VSN infected with HSV-1-*Vmn1r89-GFP* (*Vmn1r89-GFP*) amplicons. The cell is activated by a mix of four sulfated steroids (E mix: E1050; E1100; E0893 and E0588; each at 100 μ M). Right, F340/F380 ratio traces expressed as arbitrary units (a.u.) of the activated cell are shown. The cell was not responding to a DMSO control solution (containing the same amount of DMSO than E mix), the high molecular weight fraction of C57BL/6 mouse urine (HMW; 1:300) and the chemically related sulfated steroid E2734 (100 μ M). Black arrows indicate start of stimulation. Scale bar: 20 μ m. **B.** Summary of GFP-positive cell (GFP+; infected) activation (mean percentage of activated GFP+ cells) for each stimulus in C57BL/6 VSNs either infected with *Vmn1r89-GFP* amplicons (green) or with *GFP-only* control amplicons (gray). VSNs expressing *Vmn1r89-GFP* showed increased responsivity to E mix (E1050; E1100; E0893 and E0588; each at 100 μ M) compared to *GFP-only* amplicon-infected VSNs (*Vmn1r89-GFP* amplicon: mean percentage: 5.03% \pm 0.12% SEM; *GFP-only* amplicon: mean percentage: 0.71% \pm 0.48% SEM; Kruskal-Wallis ANOVA, DF (9), $p = 9.36 \times 10^{-11}$; *post hoc* comparison: Mann-Whitney Test: * $p < 0.05$). No significant increase in activation was found for E2734 (100 μ M), the high molecular weight fraction of C57BL/6 mouse urine (HMW; 1:300), a DMSO control solution (containing the same amount of DMSO than E mix) or a high potassium chloride solution (KCl; 100 mM) (Mann-Whitney Test: $p = 0.09-0.6$). N= 436 *Vmn1r89-GFP* amplicon-infected cells: 25 E mix responder cells, 9 DMSO responder cells, 0 HMW responder cells, 6 E2734 responder cells and 258 high KCl responder cells in 8 infection experiments. 334 *GFP-only* amplicon-infected cells: 3 E mix responder cells, 2 DMSO responder cells, 3 HMW responder cells, and 153 high KCl responder cells in 8 infection experiments; 229 *GFP-only* amplicon-infected cells: 5 E2734 responder cells and 106 high KCl responder cells in 8 infection experiments Data expressed as mean \pm SEM.

Monitored responsiveness to the E mix prompted the question how specific *Vmn1r89-GFP*-expressing VSNs detect the E mix solution. To answer this question, calcium transients of 25 E mix-activated cells previously infected with *Vmn1r89-GFP* amplicons were analyzed. First, I compared peak fluorescence ratio values (F_P) of the 25 E mix responder cells to each applied stimulus, which were normalized to the baseline fluorescence ratio value (F_0) before stimulus application (presented as mean peak fluorescence F_P/F_0 quotient; Fig. 17A). Cells showed similar increased mean peak fluorescence quotient (F_P/F_0) to E mix and high KCl (Mann-Whitney Test: $p= 0.95$) (Fig. 17A). The chemically related sulfated steroid E2734, HMW, and DMSO did not induce an increase of F_P/F_0 in *Vmn1r89-GFP*-expressing cells.

To gain insights into the individual variability of peak responses, normalized ratio responses (see 3.2.3) of 25 E mix responder cells to each stimulus were compared and visualized in a color-coded heatmap (Fig. 17B). These cells lacked responses to any other tested stimulus, except to high KCl. Normalized ratio responses of individual E mix responder cells were heterogeneous for E mix and high KCl. Importantly, cells showing a particular level of response to E mix also showed a similar response level to high KCl (Fig. 17C), probably reflecting a cellular variability in terms of cell fitness or maturity. A comparison between E mix and high KCl response amplitudes (expressed as normalized ratio responses) revealed no statistical difference in the cell-to-cell response variability (Mann-Whitney Test: $p= 0.90$) (Fig. 17C). Thus, response amplitudes were comparable for both, which indicates that measured amplitudes reflect calcium transients in a physiological range.

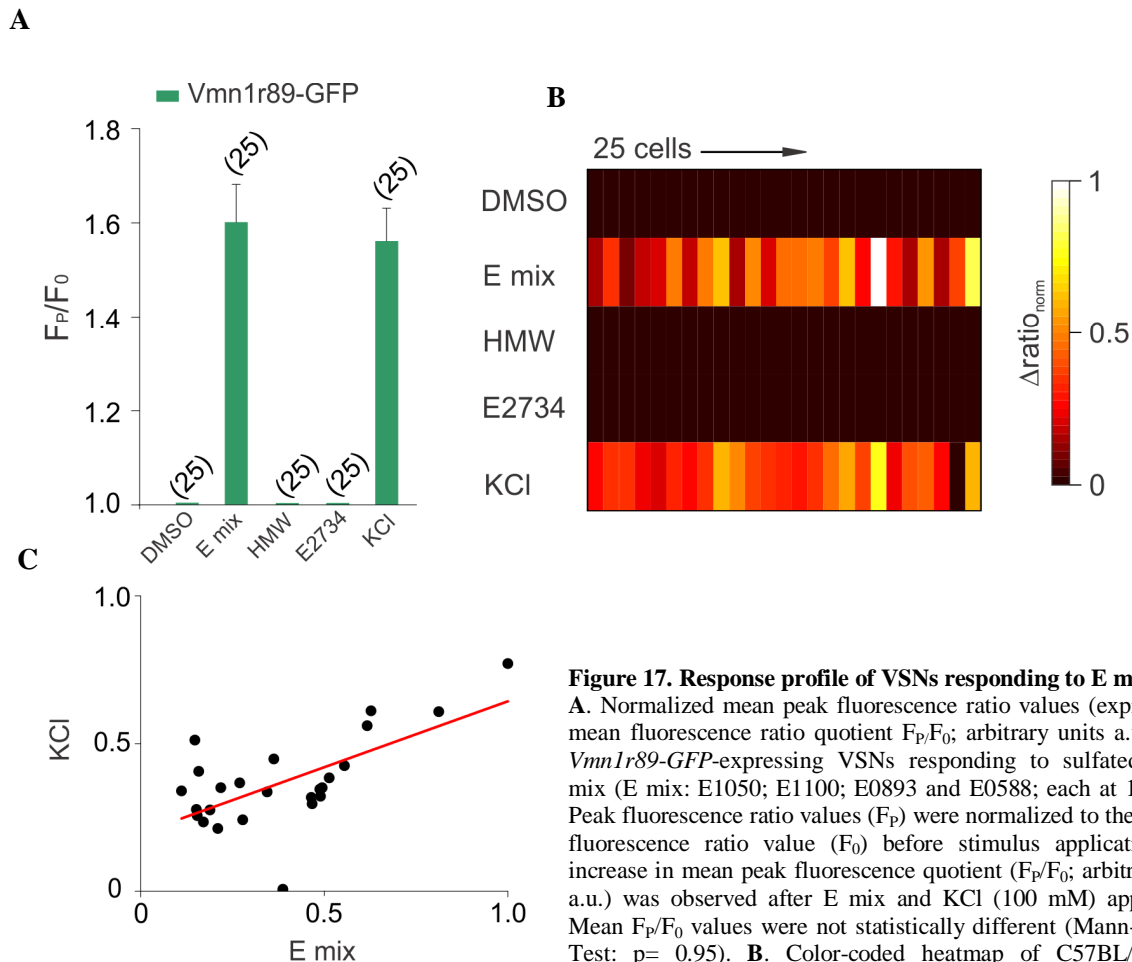


Figure 17. Response profile of VSNs responding to E mix.

A. Normalized mean peak fluorescence ratio values (expressed as mean fluorescence ratio quotient F_p/F_0 ; arbitrary units a.u.) of 25 *Vmn1r89-GFP*-expressing VSNs responding to sulfated steroid mix (E mix: E1050; E1100; E0893 and E0588; each at 100 μ M). Peak fluorescence ratio values (F_p) were normalized to the baseline fluorescence ratio value (F_0) before stimulus application. The increase in mean peak fluorescence quotient (F_p/F_0 ; arbitrary units a.u.) was observed after E mix and KCl (100 mM) application. Mean F_p/F_0 values were not statistically different (Mann-Whitney Test: $p=0.95$). **B.** Color-coded heatmap of C57BL/6 VSNs responding to sulfated steroid mix (E mix). Baseline-subtracted peak fluorescence ratio values were normalized to highest peak in associated experiments ($\Delta ratio_{norm}$; see 3.2.3). All E mix-activated cells did not show responses to any other tested stimuli, except for a high potassium chloride solution (KCl) (24 out of 25 cells). **C.** Comparative analysis of normalized $\Delta ratio_{norm}$ responses on 25 cells responding to E mix and high KCl (except for one cell). Individual cells are visualized as separate circles. Responses to E mix and high KCl were not statistically different (Mann-Whitney Test: $p=0.90$). Red line indicates linear fit of response amplitudes (slope=0.44).

4.1.3.2 Expression of *Vmn1r237* in native VSNs

Other *V1r* receptors different from *Vmn1r89* also have been reported to be sensitive to sulfated steroids. *Vmn1r237*-expressing VSNs were shown to be good candidates in detecting sulfated steroids, including the four present in the E mix (Isogai *et al.*, 2011). To determine whether *Vmn1r237* follows a similar activation profile to E mix in the HSV-1-derived amplicon delivery system, *Vmn1r237* was cloned into the expression cassette of the pHSV-IRES-*GFP* vector and receptor amplicons were prepared. Calcium responses of VSNs infected with HSV-1-*Vmn1r237-GFP* (*Vmn1r237-GFP*) amplicons to a battery of ligands, including the previously used E mix, were monitored (Fig. 18). As negative controls, I used the sulfated androgen A7864 (5-Androsten-3 β , 17 β -Diol disulfate) (Isogai *et al.*, 2011), HMW, a DMSO control solution, and a high KCl solution as positive control (all as described before). A7864 is proposed not to activate *Vmn1r237* (Isogai *et al.*, 2011), similar as E2734

for *Vmn1r89*. A7864 was used at the same concentration as E2734 in previous experiments (100 μ M).

Similar to previous observations, VSNs infected with *Vmn1r237-GFP* amplicons showed robust responses to E mix (Fig. 18A). An almost 5-fold increase in the number of activated cells to the E mix was observed in *Vmn1r237-GFP*-infected cells compared to *GFP-only* amplicon-infected VSNs (Fig. 18B). Importantly, no significant increase in the number of VSNs showing responses to A7864, HMW, and DMSO could be monitored (Mann-Whitney Test: $p= 0.21-0.89$). Nonetheless, a tendency to detect A7864 was observed since 13 out of 653 *Vmn1r237-GFP* amplicon-infected VSNs showed responses to this component. However, this group of cells showed almost no overlap with VSNs responding to E mix. Both groups of infected VSNs (*Vmn1r237-GFP* and *GFP-only* amplicon-infected cells) showed a comparable number of responses to high KCl (*Vmn1r237-GFP* amplicon: 332 cells out of 653 GFP+ cells, *GFP-only* amplicon: 153 cells out of 334 GFP+ cells).

To further characterize E mix responder cells, I compared mean peak fluorescence quotient (F_p/F_0) of 26 *Vmn1r237-GFP* amplicon-infected E mix responder VSNs to all tested stimuli (Fig. 18C). VSNs showed an increased F_p/F_0 to E mix and KCl but only a moderate increase to A7864 and HMW. This indicates, that E mix responder cells are mainly activated by E mix and high KCl, whereas F_p/F_0 for both stimuli was not different (Mann-Whitney Test: $p= 0.15$). Since F_p/F_0 did not deliver information about individual overlapping responder cells, the activation profile of all 26 E mix responder cells was visualized in an activation map (Fig. 18D). This activation map showed that only two E mix responder cells out of 26 were also activated by A7864.

Overall, these experiments indicate an activation of *Vmn1r237-GFP*-expressing cells by the E mix but not by androgen A7684, HMW, or a DMSO control solution. These data further support the assumption that *Vmn1r237* can detect sulfated steroids, which was previously proposed (Isogai *et al.*, 2011). With the detection of this additional proposed receptor-ligand pair, I could further confirm the functionality of this expression system.

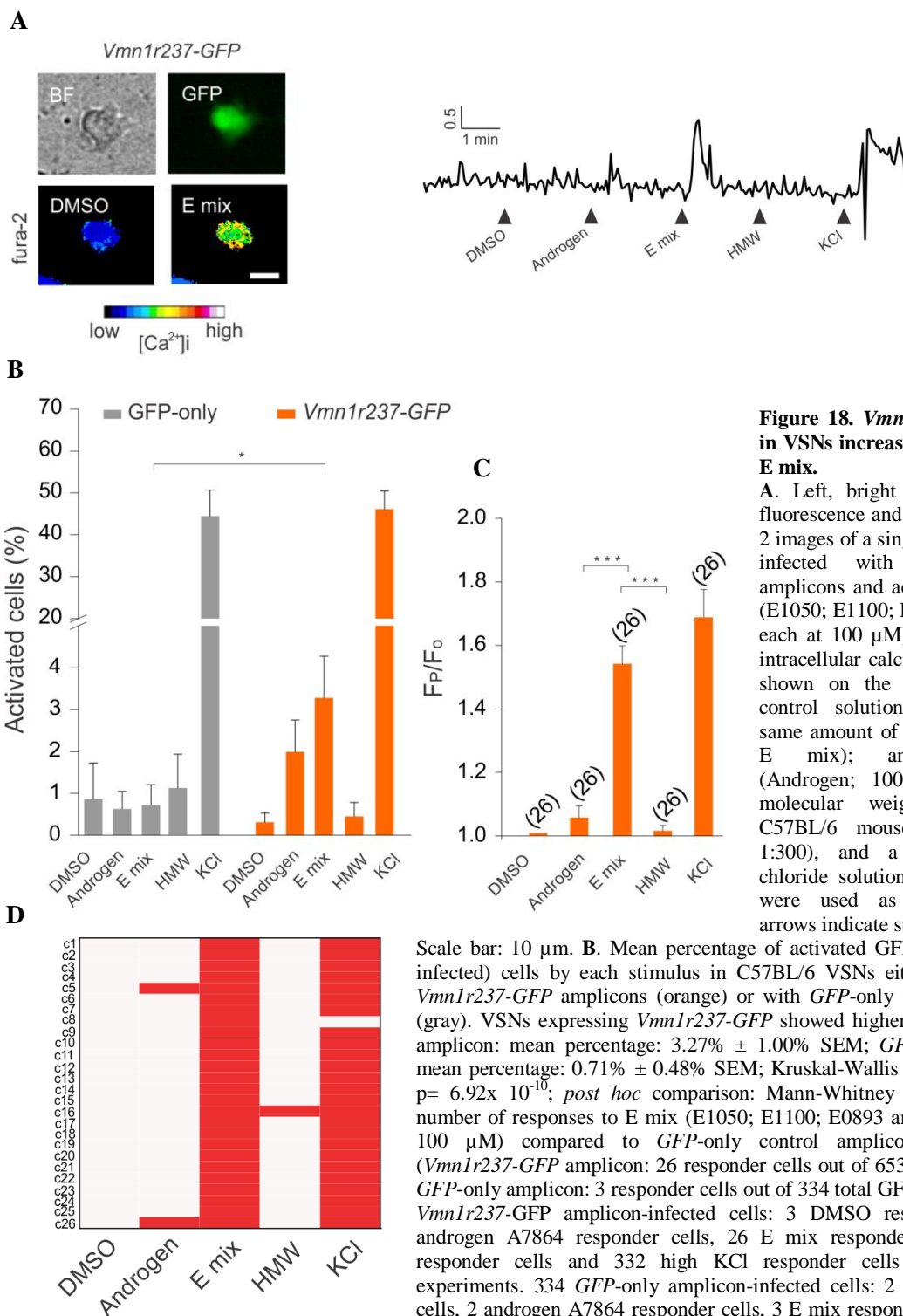


Figure 18. *Vmn1r237* expression in VSNs increases responsivity to E mix.

A. Left, bright field (BF), GFP fluorescence and pseudocolor fura-2 images of a single C57BL/6 VSN infected with *Vmn1r237-GFP* amplicons and activated by E mix (E1050; E1100; E0893 and E0588; each at 100 μ M). Time course of intracellular calcium of this cell is shown on the right. A DMSO control solution (containing the same amount of DMSO present in E mix); androgen A7864 (Androgen; 100 μ M), the high molecular weight fraction of C57BL/6 mouse urine (HMW; 1:300), and a high potassium chloride solution (KCl; 100 mM) were used as controls. Black arrows indicate start of stimulation.

B. Mean percentage of activated GFP-positive (GFP+; infected) cells by each stimulus in C57BL/6 VSNs either infected with *Vmn1r237-GFP* amplicons (orange) or with *GFP-only* control amplicons (gray). VSNs expressing *Vmn1r237-GFP* showed higher (*Vmn1r237-GFP* amplicon: mean percentage: $3.27\% \pm 1.00\%$ SEM; *GFP-only* amplicon: mean percentage: $0.71\% \pm 0.48\%$ SEM; Kruskal-Wallis ANOVA, DF (9), $p = 6.92 \times 10^{-10}$; *post hoc* comparison: Mann-Whitney Test: * $p < 0.05$) number of responses to E mix (E1050; E1100; E0893 and E0588; each at 100 μ M) compared to *GFP-only* control amplicon-infected VSNs (*Vmn1r237-GFP* amplicon: 26 responder cells out of 653 total GFP+ cells; *GFP-only* amplicon: 3 responder cells out of 334 total GFP+ cells). N = 653 *Vmn1r237-GFP* amplicon-infected cells: 3 DMSO responder cells, 13 androgen A7864 responder cells, 26 E mix responder cells, 4 HMW responder cells and 332 high KCl responder cells in 11 infection experiments. 334 *GFP-only* amplicon-infected cells: 2 DMSO responder cells, 2 androgen A7864 responder cells, 3 E mix responder cells, 3 HMW responder cells and 153 high KCl responder cells in 8 infection experiments. Data expressed as mean \pm SEM. **C.** Normalized mean peak fluorescence ratio values (expressed as mean peak fluorescence quotient F_p/F_0 ; arbitrary units a.u.) of 26 *Vmn1r237-GFP*-expressing cells responding to sulfated steroid mix (E mix: E1050; E1100; E0893 and E0588; each at 100 μ M). The increase in F_p/F_0 was observed after E mix and high KCl (100 mM) stimulation, which was not statistically different (Mann-Whitney Test: $p = 0.15$). Mean F_p/F_0 to E mix was significantly different to androgen A7864 and HMW (Kruskal-Wallis ANOVA, DF (4), $p = 2.25 \times 10^{-21}$, *post hoc* comparison: Mann-Whitney Test: 4.93×10^{-9} and 3.40×10^{-10} . *** $p < 0.001$). **D.** Individual activation map of 26 E mix responder cells to different applied stimuli. 25 cells out of 26 E mix responder cells were also activated by KCl. Two cells out of 26 E mix responder cells showed overlapping activity with androgen A7864. One cell was activated by E mix, HMW, and KCl.

4.1.3.3 Functional expression of a V2r (*Vmn2r26*) in native VSNs

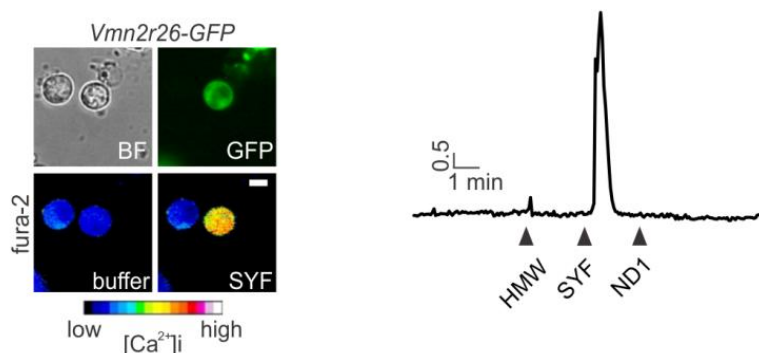
The two examples of *V1r* expression suggest that the use of the HSV-1-derived amplicon system in native VSNs is functional. To verify if this procedure also works for V2rs, an already known receptor-ligand pair was tested. I used the *Vmn2r26* receptor with its proposed peptide ligand SYFPEITHI (SYF). Previous studies in VNO tissue slices using *V2r1b* (*Vmn2r26*)-IRES-*tauGFP* gene-targeted mice revealed that more than half of VSNs expressing this receptor were activated by the peptide SYF.

I monitored responsivity to SYF in VSNs infected with HSV-1-*Vmn2r26-GFP* (*Vmn2r26-GFP*) amplicons using calcium imaging measurements (Fig. 19A). To stimulate infected cells with SYF, I used a concentration of 10^{-11} M, which was previously reported to activate *Vmn2r26-GFP*-expressing VSNs. As controls, I used HMW (as described before), the mitochondria-derived peptide ND1 (f-MFFINTLTL; 10^{-7} M), and high KCl (100 mM). ND1 is proposed to activate another V2r, namely the *Vmn2r81*, and therefore a suitable control to assess the specificity of functional V2r expression in this HSV-1-derived amplicon system. ND1 was used in the same concentration as previously described for calcium imaging measurements in tissue slice preparations (Leinders-Zufall *et al.*, 2014).

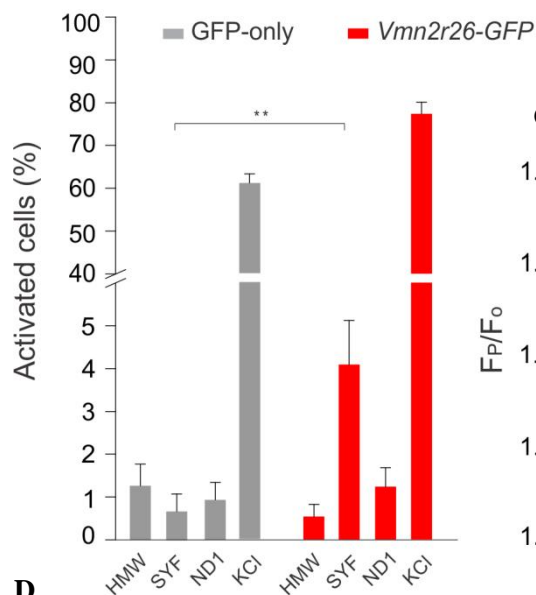
A 6-fold increase in the number of *Vmn2r26-GFP* amplicon-infected VSNs responding to SYF compared to *GFP*-only control amplicon-infected VSNs was observed (Mann-Whitney Test: ** $p < 0.005$) (Fig. 19B). Other tested ligands such as ND1 and HMW did not induce a higher responsivity in *Vmn2r26-GFP* amplicon-infected VSNs compared to control amplicon-infected VSNs (Mann-Whitney Test: $p = 0.3-0.7$). Additionally, the mean peak fluorescence quotient F_p/F_0 of 19 cells was analyzed (Fig. 19C). SYF responder cells showed significant higher F_p/F_0 to SYF compared to HMW and ND1 (Mann-Whitney Test: *** $p < 0.001$). An activation map of individual responder cells further revealed that SYF responder cells showed almost no activation overlap to ND1 or HMW (Fig. 19D).

With this experiments, I could show the functionality of the HSV-1-derived amplicon system to detect potential V2r ligands and confirm an already proposed receptor-ligand interaction. Furthermore, response analysis reveals a high specificity of the system at least for the ligand battery tested in this assay. Since I could show detection of a ligand at very low concentration, I assume that this system provides a high degree of sensitivity even to very low stimulus concentrations.

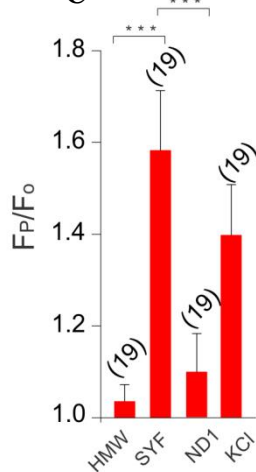
A



B



C



D

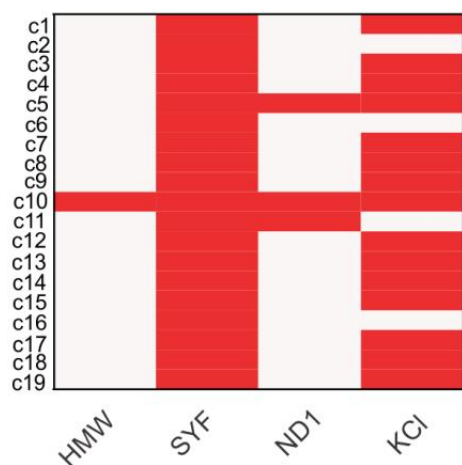


Figure 19. Viral transduction of *Vmn2r26* in VSNs.

A. Bright field (BF), GFP fluorescence and pseudocolored fura-2 images of a single VSN infected with *Vmn2r26-GFP* amplicons and activated by the MHC-peptide SYFPEITHI (SYF; 10^{-11} M) but not by a buffer control solution (imaging buffer; see 3.12), the high molecular weight fraction of C57BL/6 mouse urine (HMW; 1:300) and the ND1 peptide (f-MFFINTLTL; 10^{-7} M). A neighboring non-infected GFP-negative cell did not show any calcium increase during peptide stimulation. Changes in the intracellular calcium level of the stimulated cell are shown on the right. Black arrows indicate start of stimulation. Scale bar: 10 μ m. B. Mean percentages of activated GFP-positive (GFP+; infected) cells by the MHC-peptide SYFPEITHI (SYF; 10^{-11} M), the high molecular weight fraction of C57BL/6 mouse urine (HMW; 1:300), the ND1 peptide (f-MFFINTLTL; 10^{-7} M) and a high potassium chloride solution (KCl; 100 mM) in C57BL/6 VSNs either infected with *Vmn2r26-GFP* amplicons (red) or *GFP*-only control amplicons (gray) are shown. VSNs expressing *Vmn2r26-GFP* showed increased responsiveness to SYF (*Vmn2r26-GFP* amplicon: mean percentage: $4.08\% \pm 1.03\%$ SEM; *GFP*-only amplicon: mean percentage: $0.67\% \pm 0.40\%$ SEM; Kruskal-Wallis ANOVA, DF (7), $p = 3.49 \times 10^{-15}$, post hoc comparison: Mann-Whitney Test: ** $p < 0.005$) compared to *GFP*-only control amplicon-infected VSNs (*Vmn2r26-GFP* amplicon: 19 cells out of 469 total GFP+ cells; *GFP*-only amplicon: 6 cells out of 1224 total GFP+ cells). No increase in the number of activated cells (Mann-Whitney Test: $p = 0.3-0.7$) was observed for HMW (*Vmn2r26-GFP* amplicon: 3 HMW responder cells out of 469 total GFP+ cells; *GFP*-only amplicon: 9 HMW responder cells out of 1224 total GFP+ cells) or ND1 (*Vmn2r26-GFP* amplicon: 3 ND1 responder cells out of 469 total GFP+ cells; *GFP*-only amplicon: 10 ND1 responder cells out of 1224 total GFP+ cells). Responder cells to

high KCl (*Vmn2r26-GFP* amplicon: 363 cells out of 469 total GFP+ cells; *GFP*-only amplicon: 766 cells out of 1224 total GFP+ cells). N = 469 *Vmn2r26-GFP* amplicon-infected cells and 1224 *GFP*-only amplicon-infected cells, in 9 and 21 infection experiments. Data expressed as mean \pm SEM. C. Normalized mean peak fluorescence ratio values (expressed as mean peak fluorescence quotient F_p/F_0 ; arbitrary units a.u.) of 19 *Vmn2r26-GFP*-expressing cells responding to SYF. The increase in F_p/F_0 was observed after SYF (10^{-11} M) and high KCl (100 mM) stimulation and was not statistically different (Mann-Whitney Test: $p = 0.11$). F_p/F_0 to SYF was significantly different to ND1 peptide- and HMW-induced responses (Kruskal-Wallis ANOVA, DF (3), $p = 2.58 \times 10^{-9}$, post hoc comparison: Mann-Whitney Test: 1.03×10^{-6} and 2.51×10^{-7}). D. Individual activation map of 19 SYF responder cells to different applied stimuli. 15 out of 19 SYF responder cells were also activated by KCl. 3 cells out of 19 SYF responder cells showed overlapping activity with ND1. 1 cell was activated by HMW, SYF, ND1, and high KCl.

Previous studies revealed that the G protein subunit G_{α_o} is required to induce electrical and calcium responses in the VNO, evoked by SYF and some formylated peptides (Chamero *et al.*, 2011). To gain insight into the signaling properties of amplicon-induced *V2r* expression, cells obtained from the *Gnao1/Omp*-Cre conditional G_{α_o} knockout mouse line were infected with *Vmn2r26-GFP* amplicons. Calcium responses to SYF were drastically reduced (Fig. 20) (2 responder cells out of 193 total GFP+ cells), now reaching similar values as those evoked by HMW and ND1 (~1% of GFP+ cells). Normal calcium transients were observed in response to KCl, indicating viability and excitability (Fig. 20). Overall, these results indicate that G_{α_o} is necessary to induce enhanced responsiveness to SYF in amplicon-induced *Vmn2r26* expression in VSNs.

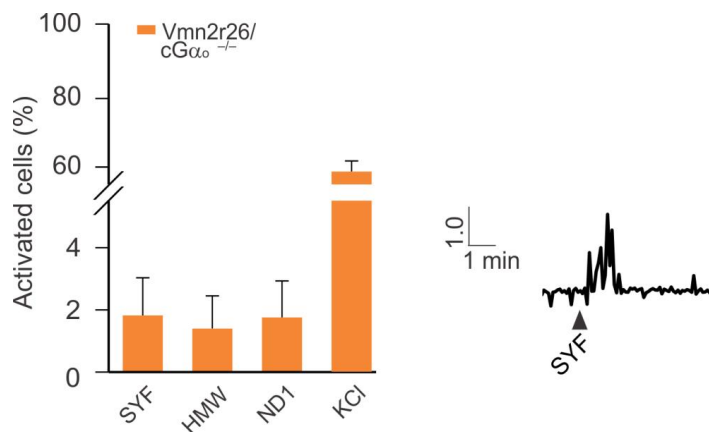


Figure 20. Viral transduction of *Vmn2r26* in $cG_{\alpha_o}^{-/-}$ VSNs.

Mean percentage of activated cells in *Vmn2r26-GFP* amplicon-infected VSNs from *Gnao1/Omp*-Cre conditional G_{α_o} knockout mice ($cG_{\alpha_o}^{-/-}$). For stimuli and concentrations see Fig. 19. Mean percentage of activated GFP-positive cells by SYF (2 cells out of 193 GFP-positive cells) was similar to response levels to HMW (2 cells out of 193 GFP-positive cells) and ND1 (3 cells out of 193 GFP-positive cells). Data expressed as mean \pm SEM. An example of a cell showing changes in the intracellular calcium level due to stimulation with SYF is shown on the right.

4.1.3.4 Expression of *Fpr3* in native VSNs

The third group of GPCRs in the VNO is comprised of *Fprs*. Thus, VSNs were infected with amplicons carrying the *Fpr3* receptor, for which a ligand is known. This receptor can be expressed in HEK293 cells (Bufe *et al.*, 2012). Heterologous expression of *Fpr3* demonstrated that the receptor can be activated by a synthetic formylated 6-mer peptide, also known as W-peptide (w-pep). Interestingly, the related ND1 peptide is an activator of immune *Fprs*, but does not activate *Fpr3* (Bufe *et al.*, 2012). In addition, ND1 peptide can activate *V2r*-expressing VSNs, likely the *Vmn2r81* receptor. Thus, I used the ND1 peptide as a negative control to assess specific activation of *Fpr3-GFP*-expressing VSNs. I used the same concentration as previously applied in *Vmn2r26* expression experiments (10^{-7} M). VSNs were either infected with HSV-1-*Fpr3-GFP* (*Fpr3-GFP*) amplicons (Fig. 21A) or with HSV-1-*GFP* (*GFP*-only) control amplicons. Stimulating infected VSNs with w-pep, gave robust

calcium responses having a 20-fold increase in the number of activated cells compared to *GFP*-only amplicon-infected cells (*Fpr3-GFP* amplicon: mean percentage : $2.49\% \pm 1.30\%$ SEM, 4 w-pep responder cells out of 163 total *Fpr3-GFP* amplicon-infected cells; *GFP*-only amplicon: mean percentage : $0.09\% \pm 0.06\%$ SEM, 2 w-pep responder cells out of 1224 total *GFP*-only amplicon-infected cells; Mann-Whitney Test: * $p < 0.05$) (Fig. 21B). No increase in the number of activated cells was observed for HMW and ND1 (Mann-Whitney Test: $p = 0.48-0.91$). Together, these results indicate that the HSV-1-derived amplicon system is also applicable to *Fpr3-GFP*-expressing VSNs. Overall, I could confirm already known receptor-ligand interactions for all three groups of receptors (*V1r*, *V2r* and *Fpr*), thus indicating that this newly developed system is functional and a suitable tool to deorphanize *Vrs* and *Fprs*. I could also show that this system can detect ligands at nanomolar concentrations.

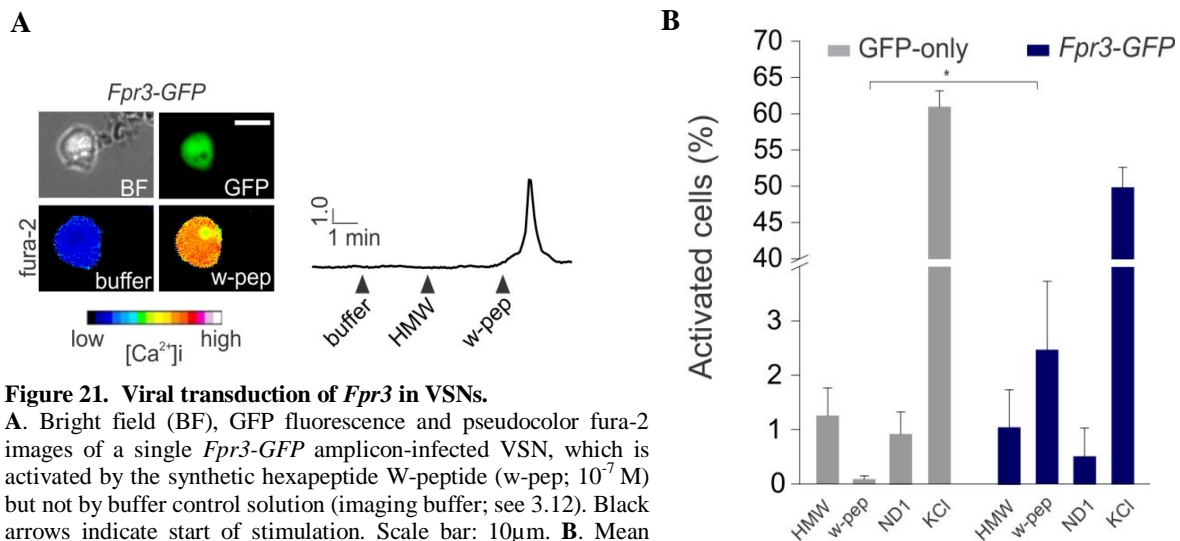


Figure 21. Viral transduction of *Fpr3* in VSNs.

A. Bright field (BF), GFP fluorescence and pseudocolor fura-2 images of a single *Fpr3-GFP* amplicon-infected VSN, which is activated by the synthetic hexapeptide W-peptide (w-pep; 10^{-7} M) but not by buffer control solution (imaging buffer; see 3.12). Black arrows indicate start of stimulation. Scale bar: $10\mu\text{m}$. **B.** Mean percentage of activated GFP-positive (GFP+; infected) cells in C57BL/6 VSNs either infected with *Fpr3-GFP* amplicons (blue) or *GFP*-only control amplicons (gray). Cells expressing *Fpr3-GFP* showed an increased number of activated cells to the W-peptide (w-pep; 10^{-7} M) (*Fpr3-GFP* amplicon: 4 cells out of 163 total GFP+ cells; *GFP*-only amplicon: 2 cells out of 1224 total GFP+ cells) compared to *GFP*-only amplicon-infected cells (Kruskal-Wallis ANOVA, DF (7), $p = 1.67 \times 10^{-13}$, *post hoc* comparison: Mann-Whitney Test: * $p < 0.05$) but not to the high molecular weight fraction of C57BL/6 mouse urine (HMW; 1:300) (*Fpr3-GFP* amplicon: 2 cells out of 163 total GFP+ cells; *GFP*-only amplicon: 9 cells out of 1224 total GFP+ cells) and the ND1 peptide (f-MFFINTLTL; 10^{-7} M) (*Fpr3-GFP* amplicon: 1 cell out of 163 total GFP+ cells; *GFP*-only amplicon: 10 cells out of 1224 total GFP+ cells) (Mann-Whitney Test: $p = 0.48-0.91$). Responses to a high potassium chloride solution (KCl; 100 mM): *Fpr3-GFP* amplicon: 81 cells out of 163 total GFP+ cells; *GFP*-only amplicon: 766 cells out of 1224 total GFP+ cells). N = 163 *Fpr3-GFP* amplicon-infected cells and 1224 *GFP*-only amplicon-infected cells, in 6 and 21 infection experiments. Data expressed as mean \pm SEM.

4.2 A putative high molecular weight fraction (HMW) receptor

4.2.1 HMW-induced activation of *Vmn2r74*

Mouse urine contains chemosignals sufficient to promote robust social behaviors, such as intermale territorial aggression (Chamero *et al.*, 2007), reproductive-associated behaviors (Novotny *et al.*, 1999b), and countermarking (Kaur *et al.*, 2014). Mice secrete unusually large amounts of protein (in the range of several milligrams per milliliter) in urine (Beynon and Hurst, 2003). The larger fraction of proteins in urine corresponds to major urinary proteins (MUPs), a family of 21 proteins belonging to the lipocalin superfamily. Size fractionation experiments using urine from lab mice revealed that the high molecular weight fraction (HMW: urine components > 10 kDa) is primarily composed of 4-5 major urinary proteins (MUPs) (Chamero *et al.*, 2007). Further characterization determined that MUPs are detected by a VSN subclass that expresses *G_o* (Chamero *et al.*, 2007). Like other lipocalins, MUPs are capable of binding small organic compounds, such as 2-*sec*-butyl-4,5-dihydrothiazole (SBT) and 2,3-dehydro-*exo*-brevicommin (DHB), among others, which may have pheromonal activity (Novotny *et al.*, 1985; Novotny *et al.*, 1999b). Therefore, it has been speculated that MUPs may function as mere passive pheromone carriers. However, MUPs produced as recombinant proteins in bacteria and without any urinary ligand present are able to activate VSNs with a similar activation rate to that observed by native (purified from urine) HMW fractions (Chamero *et al.*, 2007). Recombinant MUPs (rMUPs) are reportedly sufficient to induce robust intermale aggression (Chamero *et al.*, 2007; Kaur *et al.*, 2014), indicating that MUPs themselves may have a role as pheromones/semiochemicals.

Receptors involved in MUP recognition by VSNs have thus far not been identified. A parallel expansion in the gene numbers occurred for both, *V2rs* and MUPs in mice, rats, and opossums (Chamero *et al.*, 2007), suggesting that *V2rs* may be involved in detecting MUPs. Together with my practical supervisor Dr. Pablo Chamero, I speculated that the clade 3 of family A *V2rs* comprising a total of 10 receptors (*Vmn2r65*, *Vmn2r66*, *Vmn2r67*, *Vmn2r69*, *Vmn2r70*, *Vmn2r74*, *Vmn2r76*, *Vmn2r77*, *Vmn2r78*, *Vmn2r79*) could be a good candidate to detect some or all of the 21 mouse MUPs. The idea that one clade may be specific for the detection of one class of ligands is further supported by the observation that another family of peptide pheromones, the exocrine gland secretory peptides (ESP), appears to be detected by one specific *V2r* subfamily (clade 4) as well.

To test whether *V2rs* from clade 3 can be activated by the MUP-containing HMW urine fraction, three different receptors from this clade were selected (*Vmn2r74*, *Vmn2r66*, and

Vmn2r65) and cloned into pHSV-IRES-*GFP* expression vectors, which were used to prepare HSV-1-derived amplicons (Fig 5).

Freshly dissociated VSNs from C57BL/6 mice were either infected with amplicons carrying one of the three receptors (*Vmn2r74-GFP*, *Vmn2r65-GFP*, and *Vmn2r66-GFP*) or *GFP*-only control amplicons. VSNs were loaded with fura-2 (Fig. 22) and responses to different ligands were monitored in calcium imaging measurements. I stimulated cells initially with HMW (1:300), SYF (10^{-11} M), w-pep (10^{-7} M), and with high KCl (100 mM). I selected the peptide SYF, which activates the *Vmn2r26* receptor (Fig. 19), and the Fpr3-activating hexapeptide w-pep (Fig. 21) as controls to exclude unspecific responses to any proteinaceous components. I used the same concentrations as I used successfully in previous experiments. VSNs infected with *Vmn2r74-GFP* amplicons showed robust responses to HMW and high KCl but not to buffer control solution (imaging buffer; see 3.12), SYF, or w-pep (Fig. 22). These initial calcium imaging measurements propose for the first time a potential receptor, being *Vmn2r74*, to detect MUP-containing HMW.

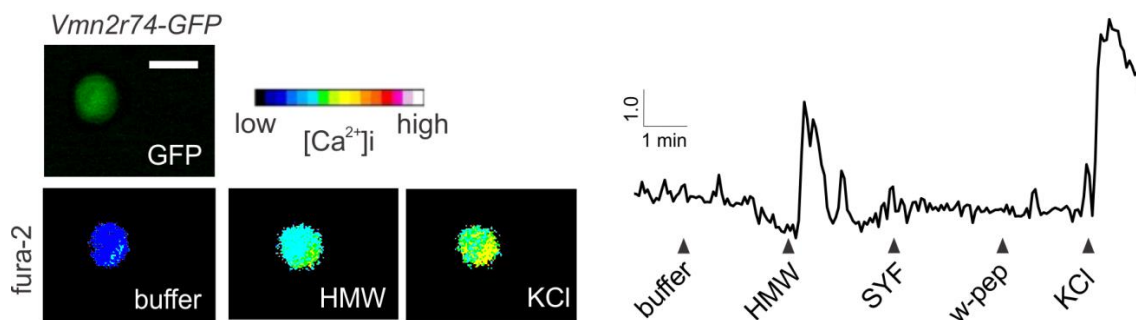


Figure 22. Expression of *Vmn2r74* in HSV-1-derived amplicon-infected VSNs.

GFP fluorescence and pseudocolor fura-2 images of a single cell infected with *Vmn2r74-GFP* amplicons. The cell showed robust responses to the high molecular weight fraction of C57BL/6 mouse urine (HMW; 1:300) and a high potassium chloride solution (KCl; 100 mM). F340/F380 ratio traces (arbitrary units a.u.) of the selected individual cell are shown on the right. No responses were observed to the buffer control solution (imaging buffer), to SYFPEITHI (SYF; 10^{-11} M), and the hexapeptide W-Peptide (w-pep; 10^{-7} M). Black arrows indicate start of stimulation. Scale bar: 10 μ m.

To determine if *Vmn2r74* shows increased responsivity to HMW compared to *GFP*-only, *Vmn2r65-GFP*, and *Vmn2r66-GFP* amplicon-infected VSNs, I compared the mean percentage of responding cells (Fig. 23A-C) and the total percentage of activated cells (Fig. 23D-F). *GFP*-only control amplicons were used to control the influence of infection on responsivity as well as to control background activation due to potentially endogenous receptor expression in monitored VSNs.

I found that cells infected with *Vmn2r74-GFP* amplicons showed a 9-fold higher number of responding cells to HMW compared to cells infected with *GFP*-only control amplicons (Mann-Whitney Test: * $p < 0.05$) (Fig. 23A). I observed no increase in responsivity to the peptides SYF and w-pep (Mann-Whitney Test: $p = 0.17-0.22$). This indicates that *Vmn2r74-GFP*-expressing cells specifically detect HMW but not any other tested ligand.

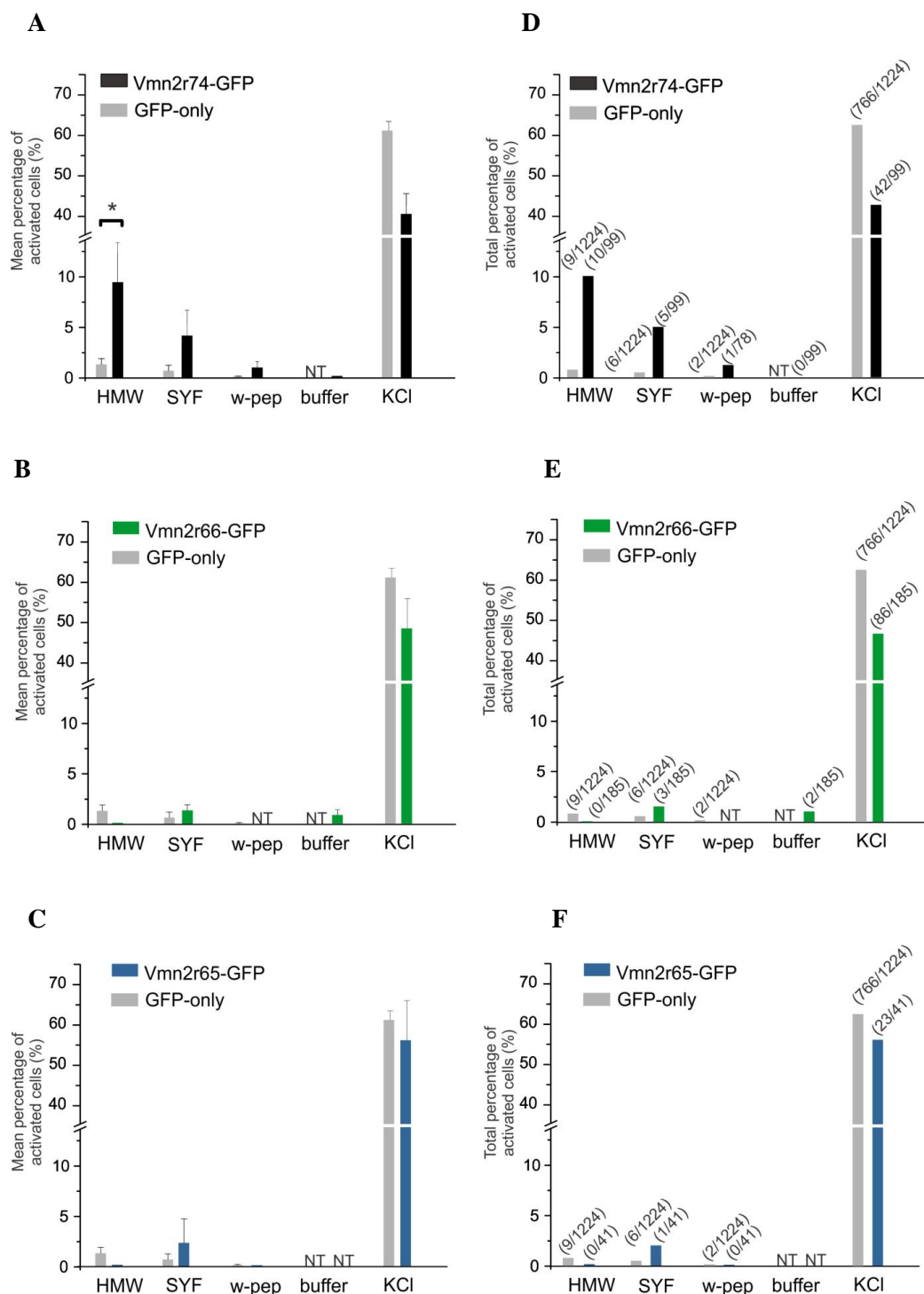


Figure 23. Viral transduction of 3 V2rs in native VSNs.

A.-C. Mean percentage of activated GFP-positive (GFP+; infected) cells by five different ligands: the high molecular weight fraction of C57BL/6 mouse urine (HMW; 1:300), SYFPEITHI (SYF; 10^{-11} M), the hexapeptide W-Peptide (w-pep; 10^{-7} M), buffer control solution (imaging buffer; see 3.12) and a high potassium chloride solution (KCl; 100 mM). C57BL/6 VSNs were either infected with *Vmn2r74-GFP* amplicons (black), *Vmn2r65-GFP* amplicons (blue), *Vmn2r66-GFP* amplicons (green) or *GFP-only* control amplicons (gray). Cells expressing *Vmn2r74-GFP* showed increased responsivity to HMW (10 cells out of 99 total GFP+ cells; mean percentage: $9.53\% \pm 3.89\%$ SEM) compared to *GFP-only* control amplicon-infected cells (8 cells out of 1224 total GFP+ cells; mean percentage: $1.28\% \pm 0.52\%$ SEM) (Kruskal-Wallis ANOVA, DF (9), $p = 1.24 \times 10^{-12}$, *post hoc* comparison: Mann-Whitney Test: * $p < 0.05$). Cells expressing either *Vmn2r65-GFP* or *Vmn2r66-GFP* showed no increased number of activated cells to any of the tested stimuli. The number of activated GFP+ cells to high KCl was similar for all four groups. NT= not tested. **D.-E.** Total percentage of activated GFP+ cells, indicating the percentage of all responder cells to a tested stimulus relative to all GFP+ cells. NT= not tested. Numbers in parentheses denote the number of activated cells out of all GFP+ cells. N= 99 *Vmn2r74-GFP* amplicon-infected cells, 1224 *GFP-only* amplicon-infected cells, 185 *Vmn2r66-GFP* amplicon-infected cells and 41 *Vmn2r65-GFP* amplicon-infected cells. N= 4 (3), 21, 21 and 5 infection experiments. Data expressed as mean \pm SEM.

To determine the level of specificity to HMW in *Vmn2r74-GFP*-expressing cells, I further analyzed the mean peak fluorescence quotient F_P/F_0 of 10 cells responding to HMW (1:300) (Fig. 24A). HMW responder cells showed significant higher F_P/F_0 to HMW compared to the two other applied peptides w-pep and SYF (Kruskal-Wallis ANOVA, DF (4), $p=2.06 \times 10^{-5}$, *post hoc* comparison: Mann-Whitney Test: ** $p < 0.005$). To determine the reason for low mean F_P/F_0 to high KCl, I plotted all cells on an activation map revealing that only five HMW responder cells showed an overlap to KCl (Fig. 24B). Only three cells out of 10 HMW responder cells showed an overlapping activation with SYF. Response to SYF could be generated by an endogenously expressed receptor in this cell. This would indicate that two individual *Vrs*, one native and one transduced, could be functionally expressed in the same cell. From these experiments, I conclude that *Vmn2r74* could be a candidate receptor to detect HMW.

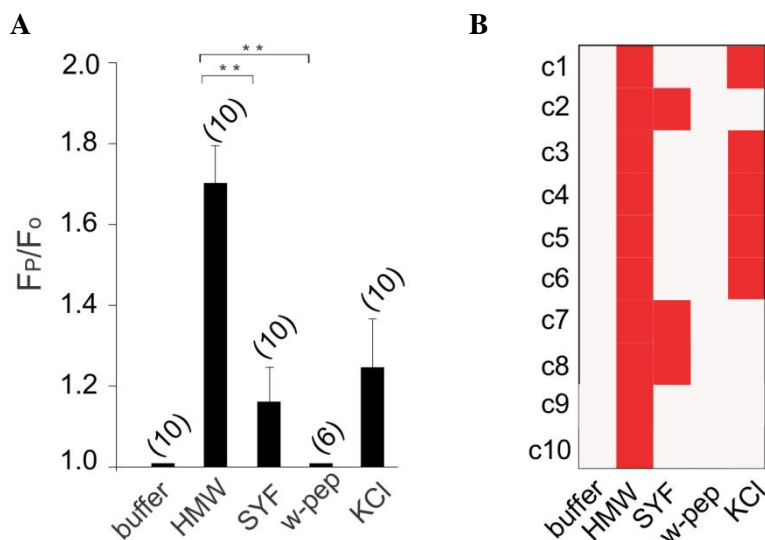


Figure 24. Response profile of *Vmn2r74-GFP* amplicon-infected VSNs.

A. Normalized mean peak fluorescence ratio values (expressed as mean peak fluorescence quotient F_P/F_0 ; arbitrary units a.u.) of 10 (6) *Vmn2r74-GFP*-expressing cells responding to HMW. Increase in F_P/F_0 was observed after stimulation with the high molecular weight fraction of C57BL/6 mouse urine (HMW; 1:300), which was statistically different to SYFPEITHI- (SYF; 10^{-11} M) and hexapeptide W-Peptide- (w-pep; 10^{-7} M) induced increase in F_P/F_0 (Kruskal-Wallis ANOVA, DF (4), $p=2.06 \times 10^{-5}$, *post hoc* comparison: Mann-Whitney Test: ** $p < 0.005$). **B.** Response profile of 10 (6) *Vmn2r74-GFP* amplicon-infected VSNs to the high molecular weight fraction of C57BL/6 mouse urine (HMW; 1:300), SYFPEITHI (SYF; 10^{-11} M), the hexapeptide W-Peptide (w-pep; 10^{-7} M), buffer control solution (imaging buffer; see 3.12), and a high potassium chloride solution (KCl; 100 mM). Three cells out of 10 HMW-activated cells overlapped with SYF activation.

To determine if responsivity of *Vmn2r74-GFP*-expressing VSNs is linked to G_o signaling, I repeated the experiment in G_o deficient VSNs obtained from $cG_o^{-/-}$ mice (see 3.9). I observed no detectable responses to HMW in *Vmn2r74-GFP*-expressing VSNs (Fig. 25),

indicating that increased responsivity to HMW in VSNs is strongly dependent on G_{α_o} expression.

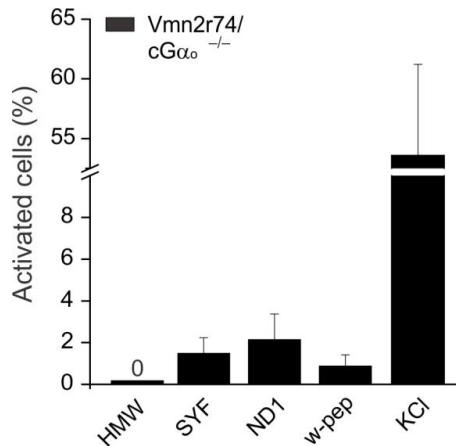


Figure 25. Viral transduction of *Vmn2r74* in $cG_{\alpha_o}^{-/-}$ VSNs.

Mean percentage of activated GFP-positive (GFP+; infected) cells by the high molecular weight fraction of C57BL/6 mouse urine (HMW; 1:300), SYFPEITHI (SYF, 10^{-11} M), ND1 peptide (f-MFFINTLTLL; 10^{-7} M), and a high potassium chloride solution (KCl; 100 mM) in cG_{α_o} deficient VSNs infected with *Vmn2r74-GFP* amplicons. VSNs expressing *Vmn2r74-GFP* showed no responses to HMW (0/189 GFP+ cells). 5 cells out of 189 total GFP+ cells responded either to SYF or ND1; 3 to the peptide w-pep (3/189). Most of the cells (124/189 GFP+ cells) showed robust responses to high KCl. N= 189 *Vmn2r74-GFP* amplicon-infected cells in 11 infection experiments. Data expressed as mean \pm SEM.

4.2.2 Dose-dependent activation of *Vmn2r74-GFP* amplicon-infected cells

In my initial study, I could show that an increased number of *Vmn2r74-GFP*-expressing cells responded to a 1:300 HMW dilution compared to cells infected with *GFP*-only amplicons. Therefore, I asked if this observed difference would also persist using various HMW dilutions. This could provide further information regarding the sensitivity of *Vmn2r74-GFP*-expressing cells. To answer this, freshly dissociated VSNs were either infected with *Vmn2r74-GFP* amplicons or with *GFP*-only control amplicons and five different dilutions of HMW (1:10000, 1:1000, 1:500, 1:300 and 1:100) were tested in calcium imaging measurements. I observed responses to any tested HMW dilution in receptor and control amplicon-infected cells. A comparison of the number of activated cells between *GFP*-only and *Vmn2r74-GFP* amplicon-infected VSNs revealed that low HMW concentrations (1:10000-1:500) activate a comparable amount of cells (*Vmn2r74-GFP* amplicon: 4 out of 376 infected cells to HMW 1:10000, 6/376 to HMW 1:1000, 6/376 to HMW 1:500; *GFP*-only amplicon: 4/360 to HMW 1:10000, 3/360 to HMW 1:1000, 7/360 to HMW 1:500) (Fig. 26A). This indicates that viral amplicon-induced *Vmn2r74* expression is likely to have no influence on the detection of low HMW concentrations and that responses observed at low concentrations are mediated by endogenous receptors. Another possibility is that the HSV-1-derived amplicon system is not suitable to detect slight differences between receptor and control amplicon-infected VSNs at these concentrations. At higher HMW concentrations (HMW 1:300 and HMW 1:100) a difference in the number of activated cells between both

groups of cells became obvious. Regarding the number of responding cells, activation of *Vmn2r74-GFP*-expressing VSNs is dependent on the HMW concentration. This observation prompted the question if the receptor response itself also follows a dose-dependent activation. Therefore, I compared F_P/F_0 values after stimulation with HMW 1:300 and HMW 1:100 in *Vmn2r74-GFP* amplicon-infected cells. I observed an increase in F_P/F_0 comparing HMW 1:300- and HMW 1:100-induced peak responses (Mann-Whitney Test: * $p < 0.05$). These results suggest that HMW-induced responses are dose-dependent in *Vmn2r74-GFP* cells, assuming that *Vmn2r74* is solely responsible for HMW-induced activation. Overall, these experiments suggest that at low concentrations likely one or more endogenous receptors may detect components present in the HMW, leading to a similar number of activated cells in *Vmn2r74-GFP* and *GFP-only* amplicon-infected cells, whereas at higher HMW concentrations, *Vmn2r74* is specifically activated. Overall, I conclude that *Vmn2r74* expression increases the sensitivity to HMW in a dose-dependent manner.

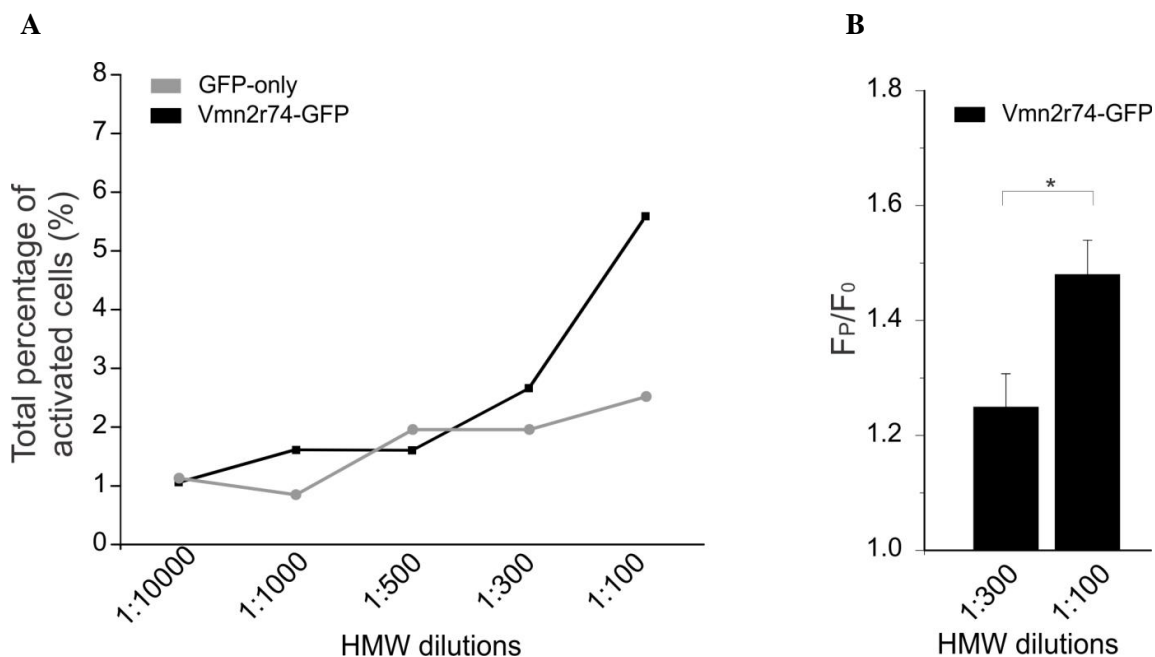


Figure 26. Summary of GFP-positive cell activation for different dilutions of HMW.

A. Total percentage of activated GFP-positive (GFP+; infected) cells either infected with *Vmn2r74-GFP* amplicons (black) or *GFP-only* amplicons (gray). Activity after application of different HMW dilutions was monitored by calcium imaging measurements. *Vmn2r74-GFP* amplicon-infected VSNs showed the following response profile: 4 responder cells out of 376 *Vmn2r74-GFP* amplicon-infected cells to HMW 1:10000, 6/376 to HMW 1:1000, 6/376 to HMW 1:500, 10/376 to HMW 1:300 and 21/376 to HMW 1:100. *GFP-only* control amplicon-infected cells: 4/360 to HMW 1:10 000, 3/360 to HMW 1:1000, 7/360 to HMW 1:500, 7/360 to HMW 1:300 and 9/360 to HMW 1:100. N= 376 *Vmn2r74-GFP* amplicon-infected cells, 360 *GFP-only* amplicon-infected cells, in 6 and 7 infection experiments, respectively. **B.** Normalized mean peak fluorescence ratio values (expressed as mean peak fluorescence quotient F_P/F_0 ; arbitrary units a.u.) of *Vmn2r74-GFP*-expressing cells (black) responding HMW 1:300 or HMW 1:100. An increase in F_P/F_0 between HMW 1:300- and HMW 1:100-responding cells was observed (Mann-Whitney Test: * $p < 0.05$).

To further analyze the response profile of *Vmn2r74-GFP* amplicon-infected cells, I monitored original F340/F380 ratio traces of infected cells and compared their response profile in an activation map (Fig. 27B). I identified a heterogeneous population of cells based on their responses to different HMW dilutions. Most of them responded to 1:300 or 1:100 HMW dilutions (Fig. 27). Since I assumed that only responses to higher HMW concentrations (HMW 1:300 and HMW 1:100) are induced by *Vmn2r74* expression, I focussed on cells responding to these dilutions. I saw that most of the cells respond to a single dilution (cell 22, cell 45 in Fig. 27A). Cell 22 showed only a response to the 1:300 dilution but not to 1:100. It may be that this cell was already fully saturated by this HMW dilution leading to a receptor-ligand internalization, which would explain missing activation to the 1:100 HMW dilution. Cell 45 in contrast, was only responding to the 1:100 HMW dilution, indicating that activating compound was too low concentrated in the 1:300 HMW dilution. These results suggest that *Vmn2r74-GFP*-expressing VSNs detect HMW depending on its concentration.

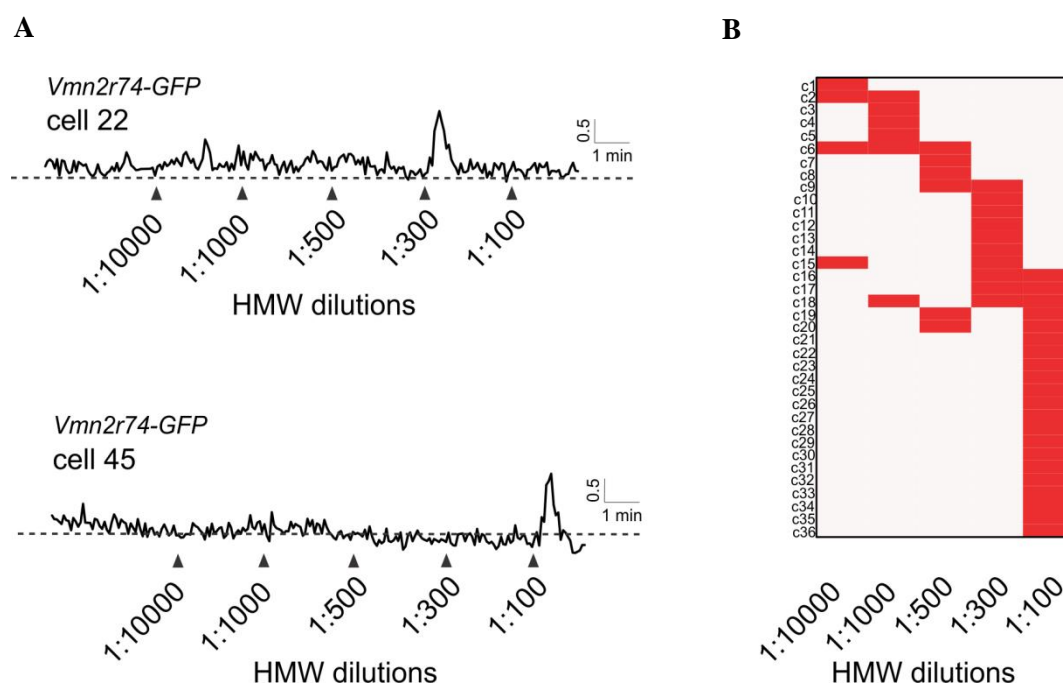


Figure 27. Calcium imaging of VSNs infected with *Vmn2r74-GFP* amplicons and stimulated with different HMW dilutions.

A. F340/F380 ratio traces (arbitrary units a.u.) of *Vmn2r74-GFP* amplicon-infected VSNs stimulated with different HMW dilutions (1:10000-1:100). VSNs showed responses to a single stimulus (cell 21, 45). Black arrows indicate start of stimulation. **B.** Activation map of *Vmn2r74-GFP* amplicon-infected cells after application of different HMW dilutions (1:10000-1:100). 36 cells out of 376 total *Vmn2r74-GFP* amplicon-infected cells responded to tested HMW dilutions. 21 cells out of 36 cells were activated by a 1:100 HMW dilution. Only 3 cells showed responses to a 1:300 and a 1:100 HMW dilution.

4.2.3 HMW activation of *Vmn2r74-GFP* amplicon-infected *Omp-GFP* VSNs

In previous experiments, I observed that *Vmn2r74-GFP*-expressing VSNs showed an increased number of responding cells to HMW. However, VNO dissociation yields a heterogeneous cell mix composed of VSNs, supporting glia cells, and immature progenitors. To determine whether HMW-activated *Vmn2r74-GFP*-expressing cells are indeed VSNs, I repeated experiments in dissociated cells from heterozygous *Omp-GFP* mice (see 3.9). VSNs were infected either with *Vmn2r74-mCherry* or with *mCherry*-only control amplicons. Calcium imaging measurements were performed in cells positive for both, GFP (indicative of mature VSNs) and mCherry (indicative of infection) (Fig. 28A).

I observed responses to HMW (diluted 1:100) in around 3% of VSNs positive for GFP and mCherry (*Vmn2r74-mCherry* amplicon: mean percentage: $3.15\% \pm 1.28\%$ SEM; 7 cells out of 220 total GFP+/mCherry+ cells) (Fig. 28B, C). In contrast, no responses to HMW were observed in *mCherry*-only control amplicon-infected VSNs (0 cells out of total 315 GFP+/mCherry+ cells). These results reveal that *Vmn2r74-GFP*-expressing cells activated by HMW are indeed mature VSNs.

A

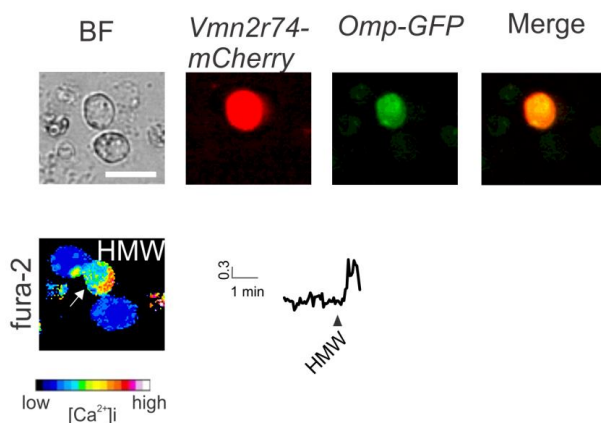
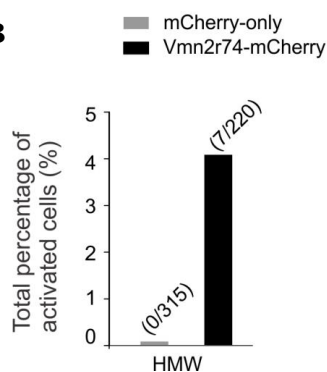


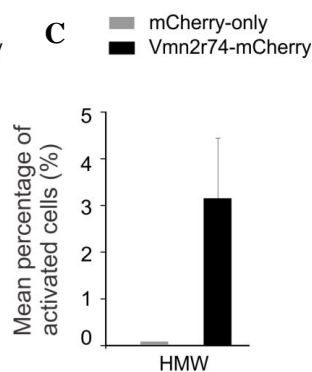
Figure 28. Expression of *Vmn2r74* in *Omp-GFP* cells.

A. Bright field (BF), mCherry, GFP fluorescence, and pseudocolored fura-2 ratio images from heterozygous *Omp-GFP* VSNs infected with *Vmn2r74-GFP* amplicons and F340/F380 ratio traces (arbitrary units a.u.) of a selected VSN responding to the high molecular weight fraction of C57BL/6 mouse urine (HMW; 1:100). Scale bar: 20 μ m. Black arrow indicates start of stimulation. B. Total percentage of activated cells by HMW (1:100) in GFP- and mCherry-positive (GFP+/mCherry+) cells either infected with *Vmn2r74-mCherry* amplicons (black) or *mCherry*-only control amplicons (gray). Numbers in parentheses denote activated cells out of all monitored GFP+/mCherry+ cells. N= 220 and 315 GFP+/mCherry+ cells were screened in 6 and 10 infection experiments. C. Mean percentage of HMW-activated cells (*Vmn2r74-mCherry* amplicon: mean percentage: $3.15\% \pm 1.28\%$ SEM; 7 cells out of 220 total GFP+/mCherry+ cells; *mCherry*-only amplicon: 0 cells out of 315 total GFP+/mCherry+ cells). Data expressed as mean \pm SEM.

B



C



4.2.4 *Vmn2r74* expression in olfactory sensory neurons (OSNs)

The main olfactory system (MOS) is the major chemodetection subsystem in the mouse nose and is located in the dorsal nasal cavity (Fig. 29A) of the mouse, housing olfactory sensory neurons (OSNs). Although OSNs and VSNs use different signal transduction mechanisms, vomeronasal signal transduction molecules, originally thought to be expressed exclusively in VSNs, have also been found in subsets of OSNs, including the cation channel *Trpc2* (Omura and Mombaerts, 2014), $G_{\alpha o}$, and $G_{\alpha i2}$ (Berghard and Buck, 1996); yet, their physiological role in OSNs is still unclear. This raises the question if OSNs, which can even express *Vrs*, could provide a suitable and functional cellular environment to express *Vmn2r74*, as previously observed in VSNs. Interestingly, Zhao and coworkers (Zhao *et al.*, 1998) used successfully a virus-based expression system for a functional *Or* study. This study showed that viral infection and overexpression is working in OSNs, at least for *Ors*.

To test this, freshly dissociated OSNs from heterozygous *Omp-GFP* mice were infected with *Vmn2r74-mCherry* amplicons (Fig. 29A) and calcium imaging measurements were performed. In my analysis, I focused on cells that were positive for GFP (GFP+; indicative of mature OSNs) and positive for mCherry (mCherry+; indicative of infection). First, I compared the infection rate between OSNs and VSNs derived from heterozygous *Omp-GFP* mice (Fig. 29B). I calculated the number of GFP+ cells that were also positive for mCherry and compared the mean percentages (Fig. 29B). I observed a lower infection rate in OSNs (mean percentage: $4.02\% \pm 1.26\%$ SEM; 29 GFP+/mCherry+ cells out of 943 GFP+ cells) compared to VSNs (mean percentage: $11.47\% \pm 3.16\%$ SEM; 124 GFP+/mCherry+ cells out of 1187 GFP+ cells). These experiments indicate that infection efficiency is lower in OSNs compared to VSNs because of decreased specificity or differences in reporter protein expression.

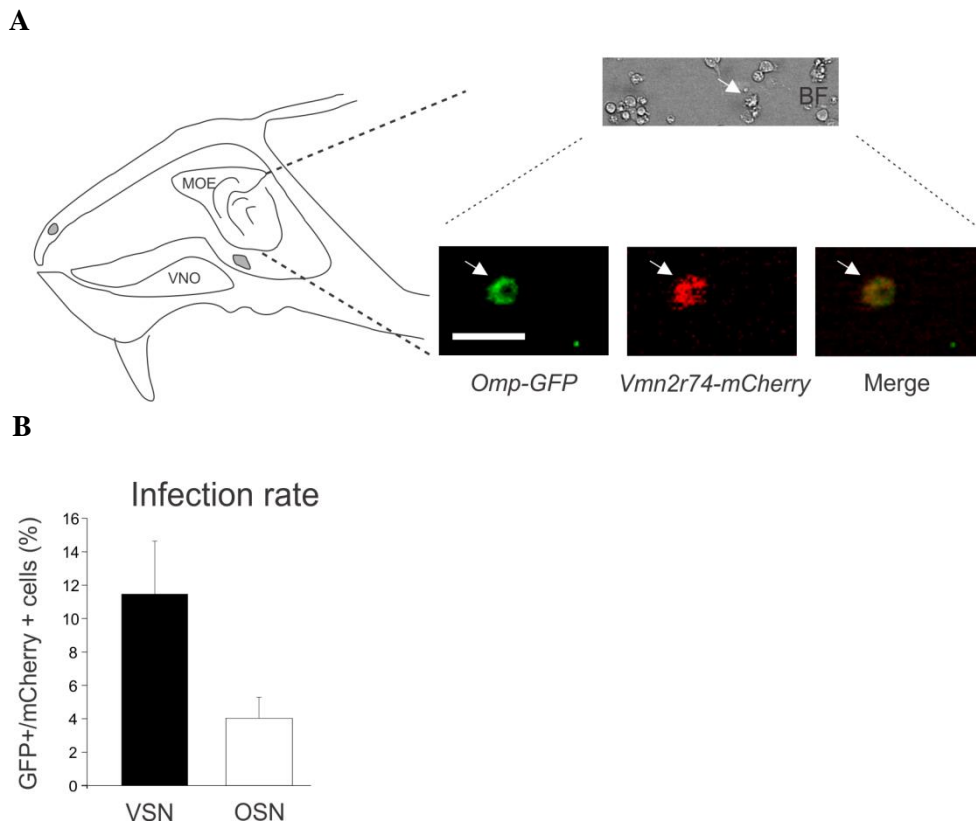


Figure 29. HSV-1-derived amplicon infection in olfactory sensory neurons (OSNs).

A. Schematic drawing of the mouse nose, which houses the VNO and the MOE. Bright field (BF), GFP, and mCherry fluorescence images from freshly dissociated OSNs from heterozygous *Omp-GFP* mice infected with *Vmn2r74-mCherry* amplicons. Merged image of GFP and mCherry fluorescence indicated a cell (white arrow) positive for both markers. **B.** The infection rate in freshly dissociated VSNs (black) and OSNs (white), showing the mean percentage of cells positive for *GFP* and *mCherry* expression. Infected VSNs were almost three times more abundant than OSNs (VSNs: 11.47% ± 3.16% SEM; 124 GFP+/mCherry+ cells out of 1187 total GFP+ cells in 5 infection experiments; OSNs: 4.02% ± 1.26% SEM; 29 GFP+/mCherry+ cells out of total 943 GFP+ cells in 5 infection experiments). Data expressed as mean ± SEM. Scale bar: 20 μ m.

Although the infection rate is limited in OSNs, I was interested in determining if *Vmn2r47-GFP* amplicon-infected OSNs could induce responses to different HMW dilutions (1:500, 1:300 and 1:100). Therefore, calcium imaging measurements in GFP+ and mCherry+ OSNs were performed (Fig. 30A, B). I could not detect any response to any of the three different tested HMW dilutions (1:500, 1:300 and 1:100) (Fig. 30). In contrast, more than 50% of cells (28 KCl responder cells out of 55 GFP+/mCherry+ cells) responded to high KCl (100 mM) (Fig. 30C). These experiments indicate that OSNs do not provide a suitable cellular environment to functionally express *Vmn2r74*. These findings back my hypothesis that VSNs offer the best environment for *Vr* expression. I could further conclude that OSNs (like HEK293 cells) may lack key components for functional *Vr* expression. It is likely that *Vrs* need a very narrowly tuned cellular environment that can only be provided by VSNs themselves *in vitro*.

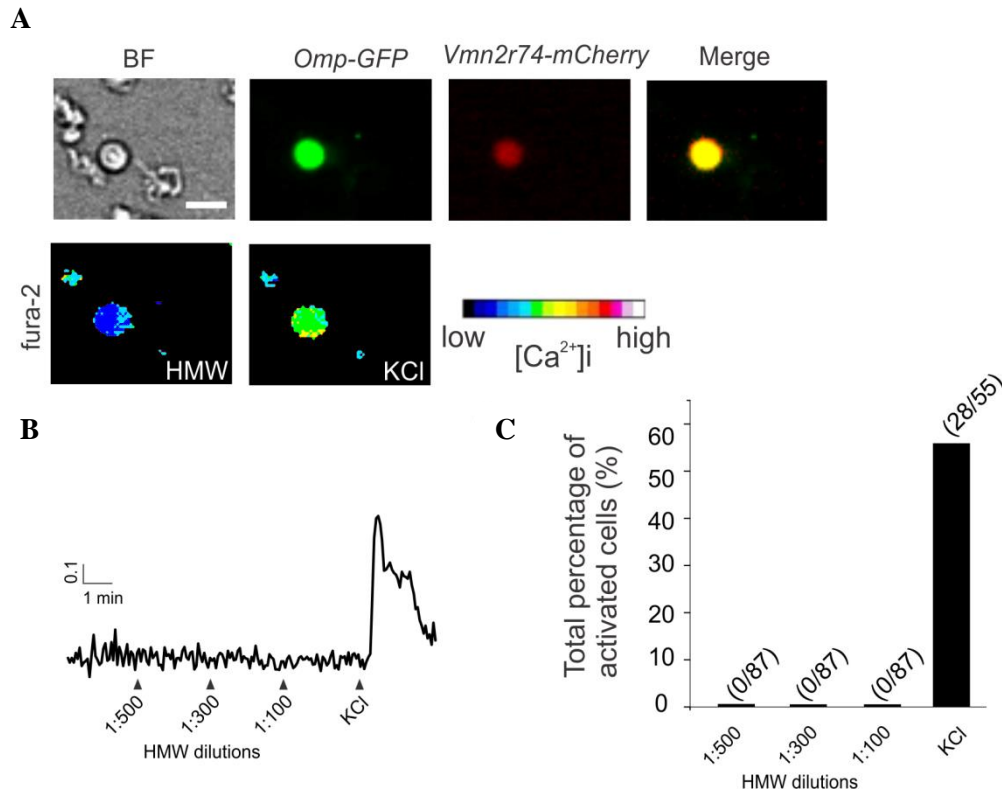


Figure 30. Viral transduction of *Vmn2r74* in OSNs.

A. Bright field (BF), GFP, mCherry fluorescence, and pseudocolor fura-2 ratio images from a single OSN infected with *Vmn2r74-mCherry* amplicons. Scale bar: 10 μ m. **B.** F340/F389 ratio traces from cell in **A** showing a robust response to a high potassium chloride solution (KCl; 100 mM) but not to the high molecular weight fraction of C57BL/6 mouse urine (HMW; 1:500, 1:300 and 1:100). Black arrows indicate start of stimulation. **C.** Total percentage of activated cells. Number in parentheses denote activated cells out of all infected cells. No cell out of 87 total GFP+/mCherry+ cells responded to any HMW dilution (see **B**) in 13 infection experiments. 28 cells out of 55 total GFP+/mCherry+ cells responded to high KCl (total percentage: 50.90%) in 7 infection experiments.

4.2.5 Strain-dependent difference in HMW activation of *Vmn2r74*-GFP-expressing VSNs

Thus far, I could show that HMW derived from adult male C57BL/6 (B6) mouse urine induces responses in *Vmn2r74-GFP*-expressing cells. Since HMW from B6 mice is a mixture of five MUPs (MUP7, 10, 19, 20, 3), it is not yet clear which of the MUPs indeed activate *Vmn2r74*. It is possible that several MUPs activate *Vmn2r74*. Since lab mice typically express between 4-5 MUPs out of the 21 functional genes in a gender- and strain-dependent manner (Logan *et al.*, 2008; Mudge *et al.*, 2008), I prepared the HMW fraction from urine of BALB/c (B/c) mice. B/c male mice secrete four MUPs (MUP7, 10, 12, 19) into urine and share the expression of three MUPs (MUP7, 10, 19) with B6 mice, but lack the expression of MUP20 and MUP3. Additionally, B/c mice express MUP12, which is missing in B6 HMW and an allelic variant of MUP10 different from that expressed in B6.

Thus, comparing stimulation of *Vmn2r74-GFP*-expressing cells with HMW from both strains could reveal if MUP3 and/or MUP20 play a role in *Vmn2r74* activation. To test whether these two MUPs may alter the response profile of *Vmn2r74-GFP*-expressing cells, VSNs were infected with *Vmn2r74-GFP* amplicons and responses to B/c and B6 HMW were compared. I could observe robust responses to both HMW fractions in receptor-infected VSNs (Fig. 31A, B).

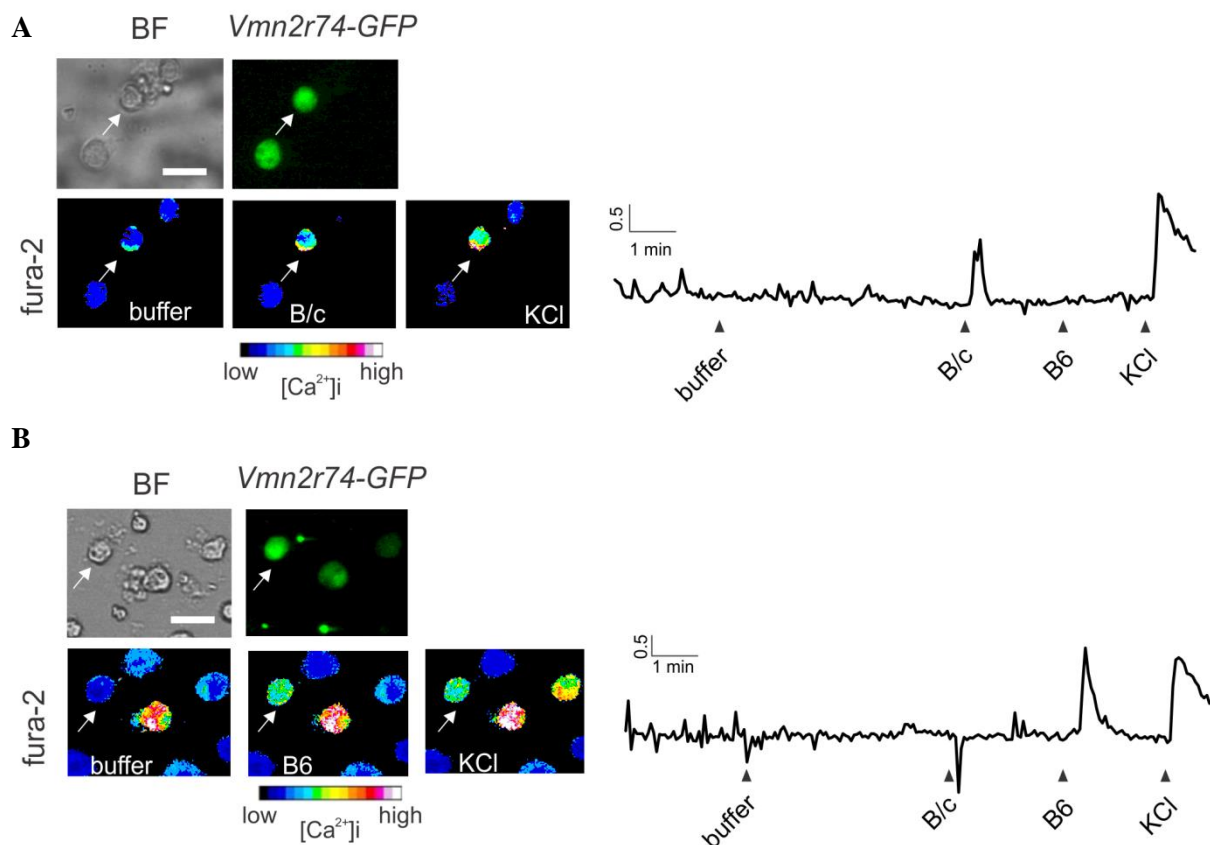


Figure 31. Calcium imaging measurements of *Vmn2r74-GFP*-expressing cells to HMW from different mouse strains. A. and B. Bright field (BF), GFP fluorescence, pseudocolor fura-2 ratio image, and F340/F380 ratio traces (arbitrary units a.u.) from VSNs infected with *Vmn2r74-GFP* amplicons. I applied HMW (1:100) from male B/c or B6 mice. As controls, a buffer control solution (imaging buffer; see 3.12) and a high potassium chloride solution (KCl; 100 mM) were used. Robust responses to both, B6 HMW (A.) and B/c HMW (B.), were monitored with no overlap with control buffer solution, but clear overlap with high KCl. Black arrows indicate start of stimulation. Scale bar: 20 μ m.

Next, I compared the number of activated cells by B6 and B/c HMW fractions. I observed a significantly (Kruskal-Wallis ANOVA, DF (9), $p = 2.17 \times 10^{-24}$, *post hoc* comparison: Mann-Whitney Test: * $p < 0.05$) higher amount of activated cells to B6 HMW compared to HMW from B/c (Fig. 32A, B). Thirty VSNs out of 728 *Vmn2r74-GFP* amplicon-infected cells responded to B6 HMW, whereas only 6 cells to B/c HMW (Fig. 32B). This difference

suggests that MUP3 and/or MUP20, which are missing in B/c HMW, are potential activators of the *Vmn2r74* receptor or alternatively that concentration differences of single MUPs, which are present in both fractions, are responsible for the higher amount of activated cells. I also detected a fraction of cells showing responses to both HMW fractions (Fig. 32C). These cells could sense MUPs present in both mice strains (MUP7, 10, 19). However, no significant differences could be observed compared to *GFP*-only control amplicon-infected VSNs (Mann-Whitney Test: $p = 0.47$). This indicates that it is unlikely that *Vmn2r74* increases sensitivity to MUPs present in both strains. Interestingly, I also observed a tendency of a higher amount of activated cells to B/c HMW compared to *GFP*-only control amplicon-infected VSNs, suggesting that *Vmn2r74* may also detect MUPs that are exclusively present in B/c HMW fraction (MUP12 and perhaps an allelic variant of MUP10). Importantly, the number of *Vmn2r74-GFP* amplicon-infected VSNs that showed responses to buffer control solution was significantly lower (Kruskal-Wallis ANOVA, DF (9), $p = 2.17 \times 10^{-24}$, *post hoc* comparison: Mann-Whitney Test: ** $p < 0.005$) compared to the number of cells activated by B6 HMW. The number of *GFP*-only amplicon-infected VSNs that showed responses to B6 HMW was also significantly lower compared to *Vmn2r74-GFP* amplicon-infected VSNs (Kruskal-Wallis ANOVA, (9), $p = 2.17 \times 10^{-24}$, *post hoc* comparison: Mann-Whitney Test: * $p < 0.05$).

Overall, I could conclude from this combinatorial experiments that MUP3 and/or MUP20 are candidates for the activation of the *Vmn2r74* receptor since more cells respond to B6 HMW compared to B/c HMW, which lacks these MUPs. However, I cannot exclude from these experiments that concentration differences of single MUPs in B6 and B/c HMW are responsible for different activation profiles and therefore mask the activation profile of *Vmn2r74*. A logic continuation would be to test single recombinant MUPs to decipher activation logic of the potential MUP receptor *Vmn2r74*.

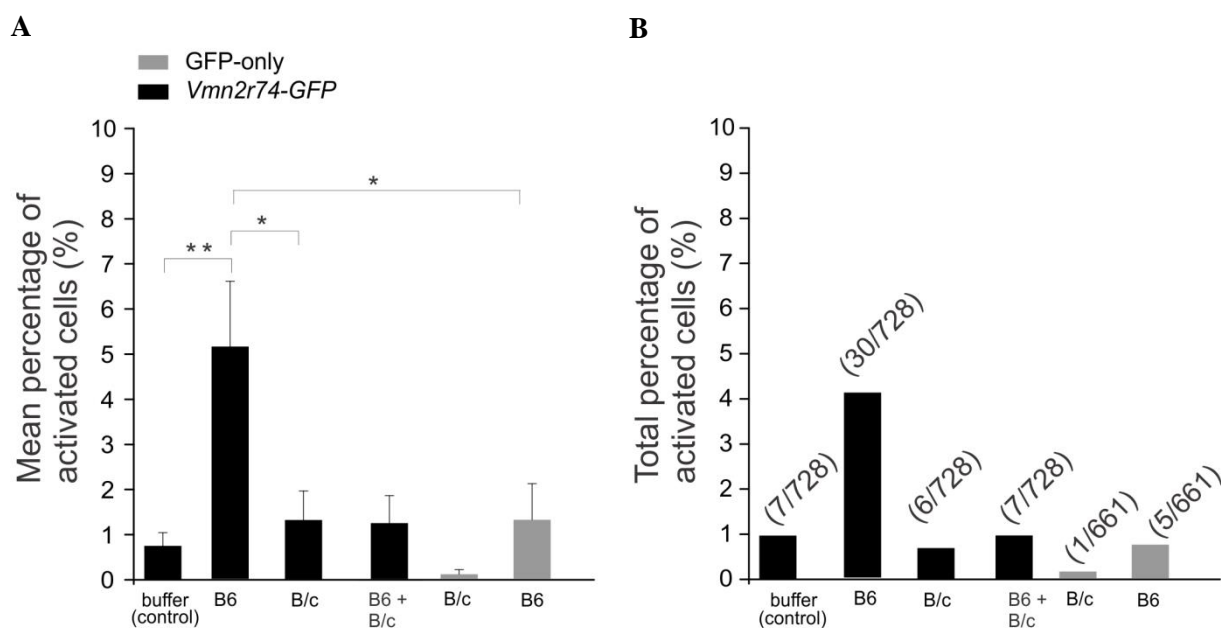


Figure 32. Summary of GFP+ cell activation by HMW fractions from different mouse strains.

A. Mean percentage of activated GFP-positive (GFP+; infected) cells either infected with *Vmn2r74-GFP* amplicons (black) or with *GFP-only* control amplicons (gray bars) to different stimuli. High molecular weight (HMW; 1:100) fraction of BALB/c (B/c) and C57BL/6 (B6) mouse urine was tested. VSNs infected with *Vmn2r74-GFP* amplicons showed increased responsiveness to B6 HMW compared to B/c HMW (B6 HMW: mean percentage: $5.16\% \pm 1.45\%$ SEM; 30 responder cells out of 728 total *Vmn2r74-GFP* amplicon-infected cells; B/c HMW: $1.30\% \pm 0.63\%$ SEM; 6 responder cells out of 728 total *Vmn2r74-GFP* amplicon-infected cells; Kruskal-Wallis ANOVA, DF (9), $p = 2.17 \times 10^{-27}$, *post hoc* comparison: Mann-Whitney Test: * $p < 0.05$). Responsivity to B6 HMW compared to buffer control solution: B6 HMW: mean percentage: $5.16\% \pm 1.45\%$ SEM; 30 responder cells out of 728 total *Vmn2r74-GFP* amplicon-infected cells; buffer control: $0.74\% \pm 0.29\%$ SEM; 7 responder cells out of 728 total *Vmn2r74-GFP* amplicon-infected cells; Kruskal-Wallis ANOVA, DF (9), $p = 2.17 \times 10^{-27}$, *post hoc* comparison: Mann-Whitney Test: ** $p < 0.005$. Responsivity to B6 HMW in *Vmn2r74-GFP* amplicon-infected cells compared to *GFP-only* control amplicon-infected cells: mean percentage: $5.16\% \pm 1.45\%$ SEM; 30 responder cells out of 728 total *Vmn2r74-GFP* amplicon-infected cells; *GFP-only* amplicon: $1.31\% \pm 0.80\%$ SEM; 5 responder cells out of 661 total *GFP-only* amplicon-infected cells; Kruskal-Wallis ANOVA, DF (9), $p = 2.17 \times 10^{-27}$, *post hoc* comparison: Mann-Whitney Test: * $p < 0.05$. Comparison of B/c HMW-induced responsiveness in *Vmn2r74-GFP* and *GFP-only* control amplicon-infected VSNs: *Vmn2r74-GFP* amplicon: mean percentage: $1.30\% \pm 0.63\%$ SEM; 6 responder cells out of 728 total *Vmn2r74-GFP* amplicon-infected cells; *GFP-only* amplicon: $0.10\% \pm 0.10\%$ SEM; 1 responder cell out of 661 total *GFP-only* amplicon-infected cells. **B.** Total percentage of activated GFP+ cells. Most of the activated VSNs responded to B6 HMW (30 cells out of 728 total GFP+ cells). *Vmn2r74-GFP* infected VSNs also showed following responses: 7/728 cells to buffer control solution (imaging buffer; see 3.12), 6/728 to B/c HMW and 7/728 responded to both HMW fractions. Out of 661 total *GFP-only* control amplicon-infected cells, 5 cells responded to B6 HMW and 1 cell responded to B/c HMW. N = 728 *Vmn2r74-GFP* amplicon-infected cells and 661 *GFP-only* amplicon-infected cells in 27 and 16 infection experiments, respectively. Numbers in parentheses denote the number of activated GFP+ cells out of all infected cells. **C.** Activation profile of *Vmn2r74-GFP* amplicon-infected cells. 30 cells responded to B6 HMW, 7 to BALB/c HMW, and 7 to both.

4.2.6 Single MUP activation of *Vmn2r74*-GFP-expressing VSNs

From the previous experiments, I deduced that MUP3 and MUP20 could be candidates to activate the *Vmn2r74* receptor.

To determine if this is the case, five B6 MUPs (rMUP7, 10, 19, 20, 3) were produced as recombinant maltose binding fusion proteins (MBP-MUP fusion protein; see 3.1.6). VSNs infected with *Vmn2r74*-GFP amplicons were stimulated with these five different single recombinant MUPs (rMUP7, 10, 19, 20 and 3); each diluted to a final concentration of 10^{-7} M. This concentration was used in previous studies, inducing robust responses in uninfected native VSNs (Chamero *et al.*, 2011; Leinders-Zufall *et al.*, 2014). All rMUPs gave robust responses in receptor-infected VSNs, except for MUP20 (Fig. 33A, B). To exclude false-positive responders among rMUP activated cells, MBP was used as a negative control at the same concentration than individual rMUPs (diluted 10^{-7} M). I observed a similar amount of cells responding to MBP than found for individual rMUPs (~1% of all infected cells). Nevertheless, none of the rMUP-activated responder cells overlapped with MBP activation, suggesting that rMUP-induced responses are likely not due to the MBP fusion (Fig. 33C). To determine the role of *Vmn2r74* in rMUP-induced activation, VSNs were infected with GFP-only control amplicons and their activation profile was compared to that of *Vmn2r74*-GFP amplicon-infected VSNs. The number of rMUP-activated cells in GFP-only amplicon-infected cells was indistinguishable from receptor-infected VSNs- for almost all rMUPs. These results differ from experiments with the natural MUP source, the HMW fraction, in which I observed an increase in responsivity to HMW in *Vmn2r74*-GFP-expressing VSNs. The reason for this is not known. One explanation could be that rMUP concentration is too low to activate the *Vmn2r74* receptor. Further studies using a dose-dependent approach may solve this issue (for further explanation see Discussion).

My previous data suggested MUP3 and/or MUP20 as potential activators of *Vmn2r74*. Since MUP20 induced no responses in receptor-expressing cells, I focussed on MUP3 and asked if a difference in the peak responses exists between *Vmn2r74*-GFP and GFP-only amplicon-infected VSNs. Thus, I compared the F_p/F_0 quotient of the 7 *Vmn2r74*-GFP amplicon-infected rMUP3 responder cells with the values from the 5 GFP-only amplicon-infected rMUP3 responder cells (Fig. 33D). I observed no difference between both groups. A concentration-dependent receptor activation study could help to determine if the lack of increased responsivity in *Vmn2r74*-GFP amplicon-infected cells is at least partially due to insufficient rMUP concentrations used in this experiment. Additionally, it is possible that *Vmn2r74* requires a unique mix of different MUPs to be activated, which is only present in the natural

MUP source, the HMW. Furthermore, it cannot be excluded that MUPs need a specific steric structure to activate *Vmn2r74*, which is potentially modified by MBP fusion. Overall, these results are not closing the door for *Vmn2r74* as potential MUP receptor since many parameters have to be determined in future studies (for details see Discussion).

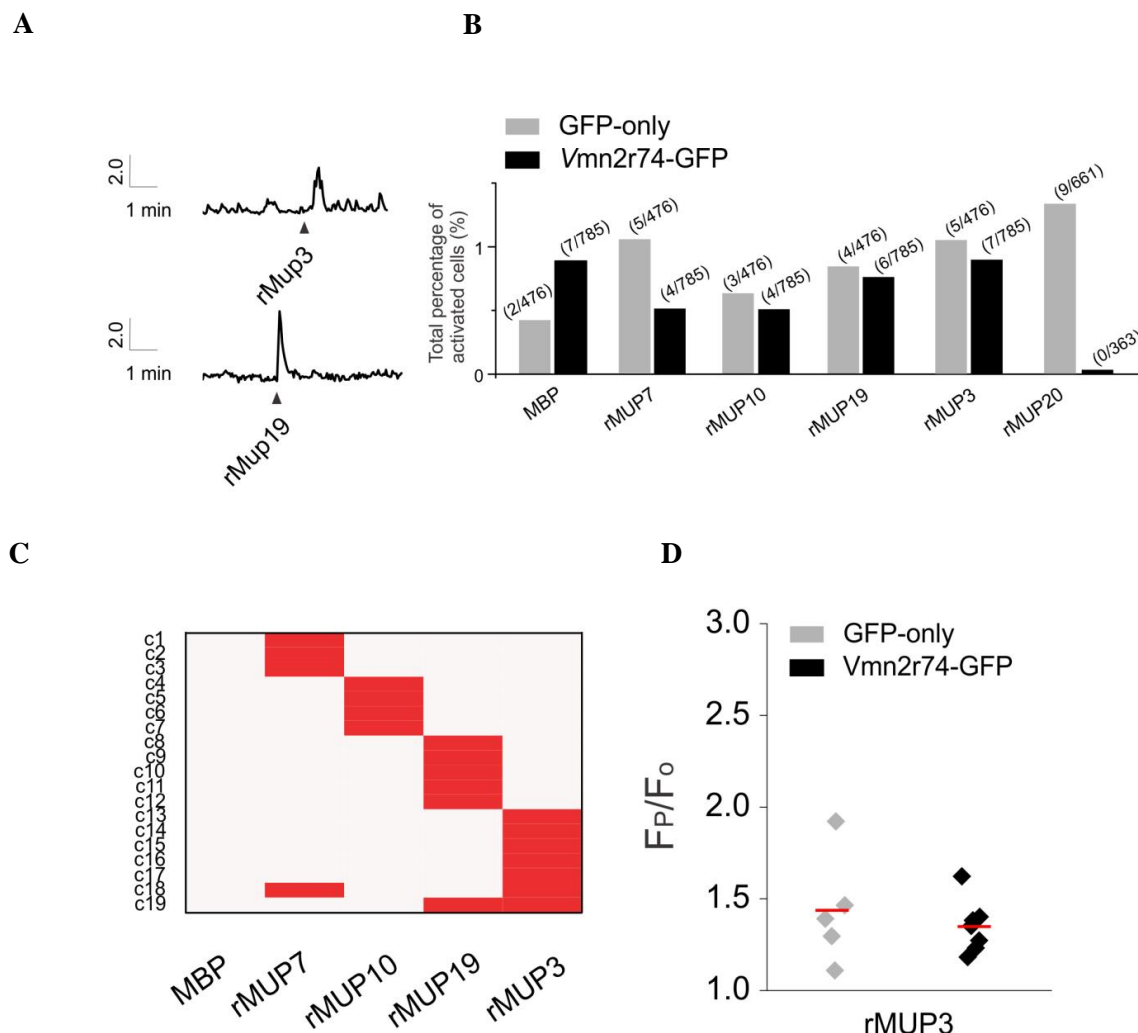


Figure 33. Recombinant MUP (rMUP) stimulation of *Vmn2r74*-transduced VSNs.

A. F340/F380 ratio traces of two individual cells either responding to rMUP3 (10^{-7} M) or rMUP19 (10^{-7} M). **B.** Summary of GFP+ cell activation after stimulation in *Vmn2r74*-GFP or GFP-only amplicon-infected VSNs. The total percentage of activated GFP-positive (GFP+; infected) cells is shown. 5 recombinant proteins (rMUP7, rMUP10, rMUP19, rMUP3 and rMUP20), each at a concentration of 10^{-7} M, were applied. As a negative control, Maltose binding protein (MBP) was used at 10^{-7} M. *Vmn2r74*-GFP amplicon-infected responder cells: 7 cells out of 785 total GFP+ cells responded to MBP, 4/785 to rMUP7, 4/785 to rMUP10, 6/785 to rMUP19, 0/363 to rMUP20 and 7/785 to rMUP3. GFP-only amplicon-infected responder cells: 2 cells out of 476 responded to MBP, 5/476 to rMUP7, 3/476 to rMUP10, 4/476 to rMUP19, 5/476 to rMUP3 and 9/661 to rMUP20. Numbers in parentheses denote the number of activated GFP+ cells out of all infected cells. N= 785 *Vmn2r74*-GFP amplicon-infected cells in 43 infection experiments; MUP20 experiments: N= 363 *Vmn2r74*-GFP amplicon-infected cells in 16 infection experiments. N= 476 GFP-only amplicon-infected cells in 12 infection experiments; MUP20 experiments: N= 661 GFP-only amplicon-infected cells in 11 infection experiments. **C.** Activation profile of 19 *Vmn2r74*-GFP amplicon-infected cells responding to tested rMUP. **D.** Normalized mean peak fluorescence ratio values (expressed as peak fluorescence quotient F_p/F_0 ; arbitrary units a.u.) of 7 *Vmn2r74*-GFP-expressing cells responding to rMUP3 (10^{-7} M). Individual cells are marked as black squares. Mean value is indicated as red line ($1.36\% \pm 0.06\%$ SEM). F_p/F_0 values of 5 individual GFP-only amplicon-infected cells responding to rMUP3 are indicated as gray squares. Mean value is indicated as red line ($1.43\% \pm 0.13\%$ SEM). No difference in F_p/F_0 quotient between both groups was observed.

4.3 Receptor identification by Calcium imaging and single cell RT-PCR

4.3.1 Identification of specific gene transcripts in whole VNO using RT-PCR

To confirm and use an alternative method in identifying ligand-receptor pairs, I set up a single cell reverse transcription-polymerase chain reaction (RT-PCR) approach in combination with calcium imaging measurements. The idea was to identify receptor gene transcripts in individual cells previously activated by a stimulus in calcium imaging measurements. I first tested in an initial approach if gene transcripts, specifically receptor and signal transduction transcripts, can be amplified from whole VNO cDNA.

First, I prepared cDNA from pooled whole VNOs of 2-3 C57BL/6 mice (both genders) and extracted RNA. Prepared cDNA was used to perform PCRs with primers designed to detect *Trpc2*, *Omp*, and *Vmn2r1* transcripts. *Trpc2* encodes for the transient receptor potential cation channel, subfamily c, member 2, which is highly expressed in the VNO and seems to have a direct role in the VNO signaling cascade (Liman *et al.*, 1999; Lucas *et al.*, 2003). The olfactory marker protein (Omp) is present in mature VSNs, which represent around 80% of a dissociated VSN culture (Fig. 15). To identify a *V2r* transcript, I selected a receptor, which is expressed by a high number of VSNs. The *Vmn2r1* receptor, which belongs to family C of *V2rs*, is expressed in around 29% of basal VSNs (Silvotti *et al.*, 2007). Thus, this receptor provides a promising candidate to detect gene transcripts of an individual receptor. I could amplify all selected gene transcripts by PCR using gene-specific primer pairs (Fig. 34A-C). No amplicates were detected in water control samples (wc). Product size was monitored in ethidium bromide agarose gels: *Vmn2r1* specific primers yielded RT-PCR products with a length of 432 bp, *Omp1* of 320 bp, and *Trpc2* of 435 bp. PCR products were verified by DNA sequencing (see 3.1.3.5). This indicates that *Vrs* and signaling components of VSNs can be amplified and detected with a gene-specific PCR approach. These experiments provide the basis to further screen for gene transcripts on the individual cell level.

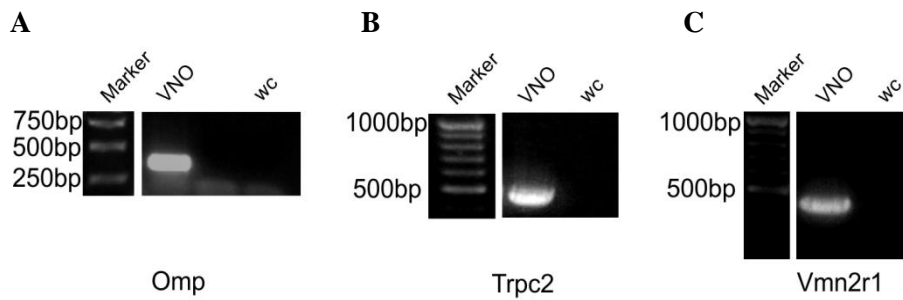


Figure 34. Ethidium bromide-stained agarose gels of RT-PCR products of whole VNO cDNA.

RT-PCR amplification with different gene-specific primers designed to detect *Omp* (A.) (primer *Omp1*; see table 3), *Trpc2* (B.), and *Vmn2r1* (C.) were performed either with whole VNO cDNA (VNO) or water (wc) as a template. PCR products were loaded on 1% ethidium bromide agarose gels. No bands were visible in water control samples (wc). RT-PCR products were identified by size (*Omp*: 320bp; *Trpc2*: 435bp; *Vmn2r1*: 432bp) and confirmed by sequencing reaction.

4.3.2 Detection of gene-specific transcripts from individual VSNs

After showing that specific gene transcripts can be amplified and detected by RT-PCR from whole VNO, the next step towards single cell RT-PCR was to amplify gene transcripts from individual cells. To determine the lowest amount of cells necessary to detect specific gene transcripts, I isolated 5, 10, 25, 50 and more than 50 (>50 cells) cells (VSNs, derived from C57BL/6 mice) using a microcapillary pipette. Cells were collected in lysis buffer and RNA was extracted (see 3.3.1). Prepared cDNA was used as a template to amplify *Omp* and *Trpc2*, which were already used in the previous experiment as a marker for general signaling components. Amplification was visualized in agarose gels stained with ethidium bromide (Fig. 35A, B). I was able to detect PCR products for *Omp* in samples with >50, 50, and 25 cells (white arrow, Fig. 35A). PCRs using 5 and 10 cell samples did not yield any detectable product. RT-PCRs for *Trpc2* yielded positive bands for samples with 25 cells, 50 cells, and whole VNO cDNA (VNO). No bands were detectable in 5 and 10 cell samples (Fig. 35B). To control functionality of PCR, I used whole VNO cDNA, which was successfully used in my previous experiments to amplify *Omp* and *Trpc2* gene transcripts. Water-containing samples were used as negative controls. Since both markers (*Omp* and *Trpc2*) were only detectable in 25 pooled cells, I conclude that this may be the detection threshold for this protocol (see 3.3.1).

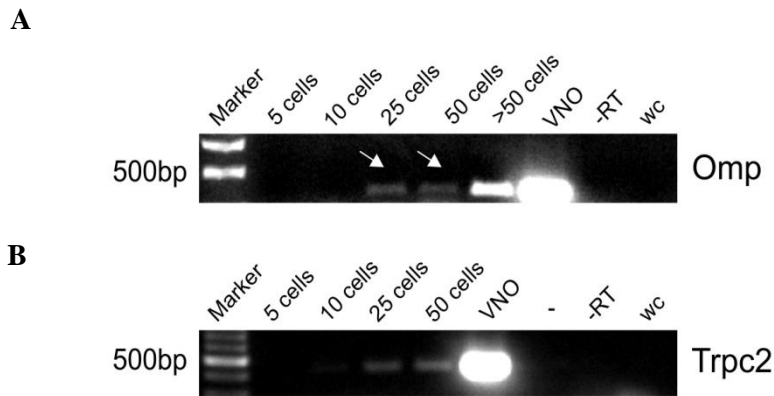


Figure 35. RT-PCRs for olfactory marker protein (*Omp*) and transient receptor potential channel c2 (*Trpc2*).

A. Ethidium bromide-stained agarose gel of RT-PCR amplification with gene-specific primers designed to detect *Omp* transcripts (primer *Omp1*; see table 3) in 5, 10, 25, 50, and more than 50 (> 50 cells) isolated cells. Cells were isolated, pooled, and used as a template for reverse transcription. Whole VNO cDNA (VNO) was used as positive control. Water was used as negative control (wc). -RT indicates a second water control for reverse transcription. *Omp* product size (*Omp*: 320bp) was estimated using a standard DNA ladder (left). **B.** *Trpc2* PCR (product size: 435bp) of 5, 10, 25, and 50 isolated VSNs.

4.3.3 RT-PCR of HMW-activated native VSNs

Since I hypothesized that *Vmn2r74* is a potential candidate to detect HMW/MUPs, I wanted to determine if cells activated by HMW can be further characterized by the developed RT-PCR approach in terms of their transcription profile. The first question that has to be answered is if HMW-responding cells belong to the subgroup of basal VSNs expressing family C *Vmn2r1*. To test this, VSNs from C57BL/6 mice were dissociated and tested in calcium imaging measurements. As stimuli, I selected HMW and as a negative control the sulfated steroid E1050, which induces activation of the *Vmn1r89* receptor (Haga-Yamanaka *et al.*, 2015). I assumed that this component would not activate *V2r*-expressing cells. Since I determined in previous experiments a detection threshold for gene-specific transcripts of at least 25 cells, I collected 27 cells responding to HMW (1:100) but not to the sulfated steroid E1050. To control that potential gene transcripts were specific for HMW-responding cells, I also selected 27 cells, which did not show activation to HMW in calcium imaging measurements (denoted as n/r). Cells were lysed and used as a template for reverse transcription with gene-specific PCRs to detect *Vmn2r1* and *Trpc2* transcripts (Fig. 36A, B).

I observed *Trpc2* products in the HMW responder sample (Fig. 36A; two slots), in non-HMW responder cells (n/r), and in the whole VNO (VNO) (Fig. 36A). Interestingly, I could identify amplification of the *Vmn2r1* gene transcript in the fraction of cells that showed activation after HMW stimulation. This gene transcript was absent in the cell fraction, which was not activated by HMW (Fig. 36B). This indicates that HMW-responding cells belong to the subgroup of basal VSNs expressing the family C *Vmn2r1*. Furthermore, these data also reveal that calcium imaging can be functionally combined with a RT-PCR approach.

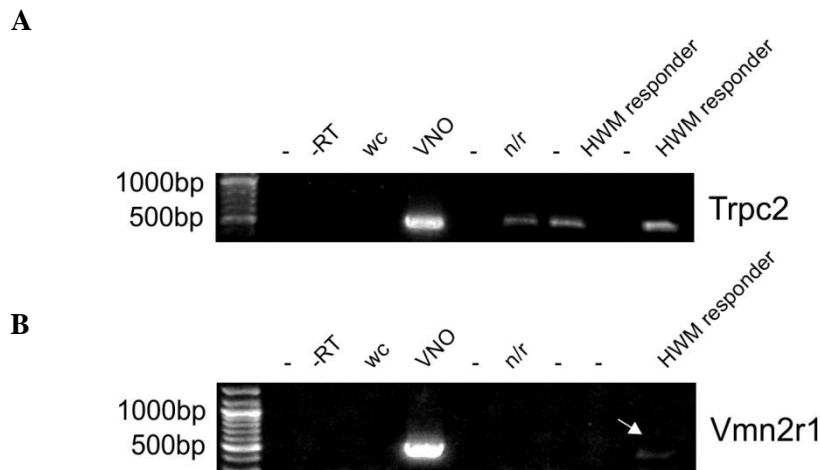


Figure 36. Gene-specific RT-PCR for *Trpc2* and *Vmn2r1* in isolated VSNs after HMW stimulation in calcium imaging. Ethidium bromide-stained agarose gel of RT-PCR amplifications with gene-specific primers designed to detect *Trpc2* (A.) and *Vmn2r1* (B.) transcripts in cells, which were stimulated with HMW (1:100) and sulfated steroid E1050 (100 μ M). 27 cells showing responses to the high molecular weight fraction of C57BL/6 mouse urine (HMW; 1:100) (HMW responder) and 27 cells not showing responses to any of the applied stimuli (n/r) were isolated, pooled, and used as a template for reverse transcription. Sterile water as template (wc) was used as negative control. -RT indicates a second negative control, in which water was added as a template for reverse transcription. Whole VNO cDNA (VNO) was used as positive control. *Vmn2r1* amplification product in HMW responder sample in B. is indicated by a white arrow. Product size: see Fig. 33.

4.3.4 Detection of gene transcripts in single VSNs after stimulus activation

Since I could show that 27 pooled HMW-responding cells likely belong to a subgroup of specific basal VSNs characterized by the expression of a family C *V2r*, I sought to repeat this experiments on the single cell level, which provides more profound and detailed information than a pool of cells. From a pool of responder cells, one cannot exclude the possibility that some individual cells contain the gene transcript of a specific receptor, whereas others do not. To overcome this limitation in transcription profile accuracy, I adapted the receptor identification method for the single cell transcript detection. My aim was to identify *Vmn2r1* expression in HMW responder cells and detect *Vmn2r74* gene transcripts.

To set up and validate the single cell approach, I chose a subgroup of *V1rs* (*V1rj* clade), which were described to detect the sulfated steroid E1050 (100 μ M). Thus, I targeted VSNs that showed robust calcium responses to E1050 but not to HMW (HMW; 1:300) and a DMSO control solution (DMSO; containing the same amount of DMSO compared to E1050 solution) to exclude false-positives. I observed 9 out of 408 cells responding to E1050, 12 to HMW, and one cell to the DMSO control solution (Fig. 37A, B). Single VSNs were picked with a microcapillary pipette after stimulation in calcium imaging, and single cell cDNA was prepared using a previously described procedure (Omura and Mombaerts, 2015) (Fig. 37C).

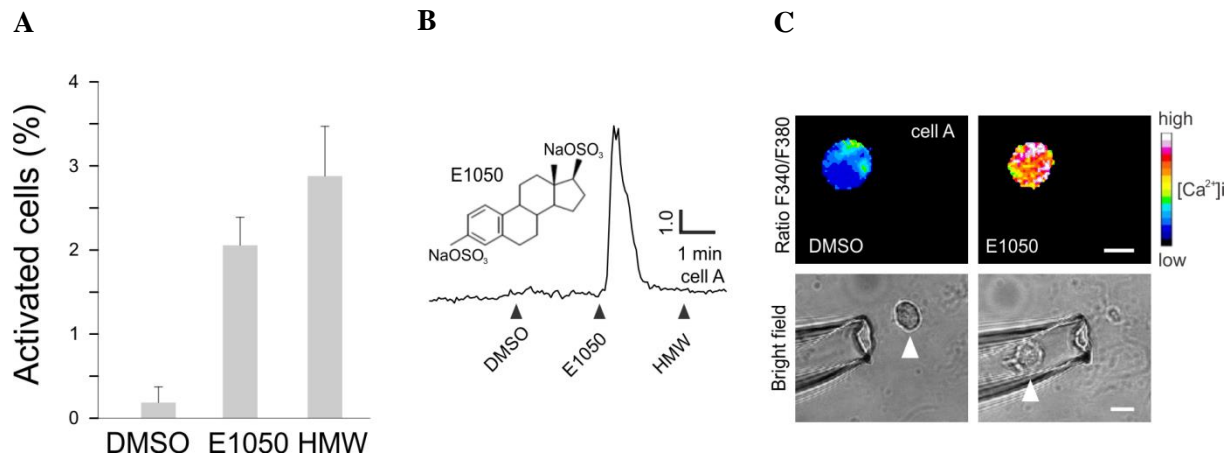


Figure 37. Cell picking of VSNs activated by the sulfated steroid E1050.

A. Mean percentage of activated cells after stimulation with a DMSO control solution (DMSO; containing the same amount of DMSO compared to E1050 solution), the sulfated steroid 1,3,5(10)-estratrien-3, 17 β -diol disulphate (E1050; 100 μ M), and the high molecular weight fraction of C57BL/6 mouse urine (HMW; 1:300). Mean percentages: DMSO responder cells: 0.18% \pm 0.18% SEM; 1 DMSO responder cell out of 408 total cells in 3 infection experiments; E1050 responder cells: 2.05% \pm 0.33% SEM; 9 E1050 responder cells out of 408 total cells in 3 infection experiments, and HMW responder cells: 2.87% \pm 0.59% SEM; 12 HMW responder cells out of 408 total cells in 3 infection experiments. **B.** Representative intracellular calcium increase (F340/F380, arbitrary units a.u.) of a VSN (cell A) loaded with fura-2 in response to E1050 (100 μ M) (chemical structure shown on the side), but not to the high molecular weight fraction of C57BL/6 mouse urine (HMW; 1:300). **C.** Bright field and pseudocolor fura-2 ratio images of the cell shown in A during stimulation with a DMSO control solution (DMSO), HMW, and E1050. Responsive cells were later picked using a microcapillary pipette. Arrowhead points to the cell before and after (inside microcapillary pipette) picking. Scale bar: 10 μ m.

Five single cells responding to E1050 were independently isolated immediately after calcium imaging measurement, lysed, and prepared for RT-PCR to determine if receptors from the *Vlrr* clade can be amplified (Fig. 38). I used degenerated primers for the *Vlrr* subgroup of *Vlrs*, capturing *Vmn1r89*, *Vmn1r85*, and *Vmn1r86* genes. To verify that these cells are indeed VSNs, I further used specific primers to detect *Omp* and the G protein subunits *G_{i2}* and *G_o*. Both G protein subunits are expressed in different layers of the VNO. A control cell, which was not responding to E1050 (n/r), was isolated and its cDNA used for PCR. The (n/r) control cell showed expression of *Omp* and *Gnai2* (gene for *G_{i2}*), indicating that it is likely a VSN of the apical zone. This cell showed no response to E1050 and no detectable expression of *Vlrr* transcripts. Therefore, it is likely that this cell expressed a different *Vlrr*. Four out of five cells responding to E1050 showed a PCR product for *Omp*, and *Gnai2*, which is typically expressed together with *Vlrs* in the apical layer of the sensory VNO epithelium. For *Gnao1* gene transcripts, encoding *G_o* and proposed to be not present in *Vlrr*-expressing VSNs, no detectable expression was monitored in any single cell (Fig. 38). *Vlrr* transcripts were identified in four out of the five E1050-activated cells, but not in the randomly picked cell (n/r), which was not activated by the sulfated steroid E1050. This result was expected since previous studies showed that VSNs responding to E1050 express *Vlrs* of the *Vlrr* subfamily

(Haga-Yamanaka *et al.*, 2014). To identify individual receptor transcripts, PCR-amplified *Vlrf* products were isolated and sequenced. Transcripts for *Vmn1r89* and *Vmn1r85* were identified, which is also consistent with the literature, since both receptors are described to be activated by E1050 (Haga-Yamanaka *et al.*, 2014).

Overall, I could set up a single cell RT-PCR approach that allows identification of individual receptors in single cells responding to a specific ligand in calcium imaging measurements.

This approach was also used to identify the potential HMW receptor *Vmn2r74* in HMW-responding cells. However, I could not detect expression of *Vmn2r74* transcripts in HMW-responding cells (data not shown). The reason for this lack of expression is not clear. It may be that detection of *V2r* specific transcripts, which are longer than *V1r* transcripts, is not working with this approach. To test this, I could stimulate cells in future experiments with the peptide SYFPEITHI, which was matched with the *Vmn2r26* receptor, and perform gene-specific PCR for the *Vmn2r26* receptor. Furthermore, it is not yet clear if different MUPs present in the HMW fraction activate different receptors. This would explain that HMW-responding cells did not show expression of *Vmn2r74* in the single cell RT-PCR approach, but expressed another HMW-detecting receptor. To test this, I could stimulate cells with individual recombinant MUPs and screen for the *Vmn2r74* transcript. A good candidate would be MUP3 since I could show that *Vm2r74-GFP*-expressing cells are mainly activated by HMW fractions that contain MUP3 (Fig. 32). Picking more HMW responder cells to cover a broader amount of cells potentially expressing various receptors may also help to identify individual MUP receptors.

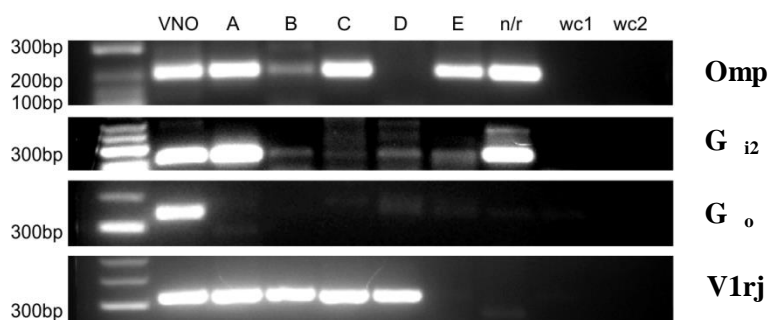


Figure 38. Single cell RT-PCR of VSNS responding to the sulfated steroid E1050 in calcium imaging.

Ethidium bromide-stained agarose gels of RT-PCR products generated from five cells (A to E) showing calcium responses to 1,3,5(10)-estratrien-3, 17 β -diol disulphate (E1050, 100 μ M), a cell lacking a response to E1050 (n/r), and two water controls (wc1 and wc2). cDNA collected from pooled whole VNO tissue was used as positive control (VNO). PCR amplifications of cDNA collected from single cells were performed using gene-specific primers for *Omp* (primer Omp2; see table 3), *Gnai2* (*G_{i2}*), *Gnao1* (*G_o*), and degenerated primers for three members of the *Vlrf* subfamily. Product sizes: *Omp*: 197 bp, *G_{i2}*: 220 bp, *G_o*: 348 bp and *Vlrf*: 320 bp.

4.4 Kairomone activation of VSNs

In addition to pheromones and signals from individuals of the same species, the mammalian olfactory system is also capable of detecting semiochemicals released by other species. One of its modalities consists of signals that may be beneficial for one of the species, such as those enabling identification of a potential predator. These chemostimuli, also called kairomones, provide the receiver species with an invaluable selective advantage for survival. Kairomone-induced behaviors, such as aversion or fear-like behaviors, are proposed to be genetically predetermined. Indeed, it has been shown that innate predator-induced avoidance is driven by kairomones acting on different olfactory subsystems: the VNO, the Grüneberg ganglion (GG), as well as chemosensory neurons within the main olfactory epithelium (MOE) (Pérez-Gómez *et al.*, 2015). Signals are further processed in different areas of the olfactory bulb and converge in limbic areas (in the medial amygdala and the ventromedial hypothalamus) (Pérez-Gómez *et al.*, 2015). However, the contribution of specific VSN subsets to kairomone detection is incompletely understood.

Chamero and coworkers (Chamero *et al.*, 2011) have previously shown that detection of peptides and proteins depends on the presence of $G_{\alpha o}$. Cat fur odor (CFO) and Feld4, a cat MUP orthologue present in saliva, have both been reported to activate mouse VSNs and induce avoidance in mice (Papes *et al.*, 2010). A natural conclusion would be that these compounds are detected by VSNs expressing $G_{\alpha o}$.

Therefore, I tested CFO and recombinant Feld4 (rFeld4) in calcium imaging measurements on freshly dissociated VSNs from $cG_{\alpha o}^{-/-}$ mice, in which the *Gnao1* gene (encoding $G_{\alpha o}$) is conditionally deleted (Chamero *et al.*, 2011) by Cre-mediated excision of the target gene in all *Omp* positive cells. VSNs from heterozygous ($cG_{\alpha o}^{+/-}$) and C57/BL6 (B6) animals were used as controls. Maltose binding protein (MBP) was used as a negative control since rFeld4 is present as a fusion protein with MBP. MBP allows identification of false-positive rFeld4 responder cells. Robust responses to CFO and rFeld4 in B6 and heterozygous ($cG_{\alpha o}^{+/-}$) mice were observed, identifying two main subsets of responder cells: one fraction of cells responded only to CFO and the second group to both, rFeld4 and CFO (Fig. 39, left panel). Each fraction accounts for ~50% of CFO-responding cells (53% CFO-only and 47% CFO + rFeld4). Of all responding cells, 16% were activated by rFeld4 but not by CFO. In VSNs from $cG_{\alpha o}^{-/-}$ mice, responses to CFO were also observed (Fig. 39, right panel). However, VSN activation by rFeld4 was nearly absent in these $cG_{\alpha o}^{-/-}$ VSNs (Fig. 39, right panel).

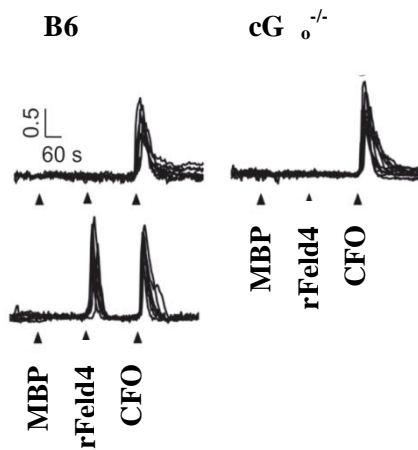


Figure 39. Representative F340/F380 ratio traces from B6 and $cG_{o^{-/-}}$ VSNS.

VSNS from B6 mice and $cG_{o^{-/-}}$ mice were dissociated, loaded with fura-2 dye, and calcium responses to cat fur odor (CFO; 20 ml of 1x HBSS solution incubated with one cat-odorized cotton pad) and recombinant MBP-Feld4 fusion protein (rFeld4; 500 nM) were analyzed. Maltose binding protein (MBP; 500 nM) was used as a negative control. Intracellular calcium increase (F340/F380 ratio traces; arbitrary units [a.u.]) of representative VSNS from both strains (left and right panel) in response to CFO and rFeld4 (B6) or CFO ($cG_{o^{-/-}}$) are shown. Responses to rFeld4 were abolished in $cG_{o^{-/-}}$ VSNS (right panel). 53% of all cells responding to CFO showed only responses to CFO; 47% of CFO-responding cells did also show responses to rFeld4. 16% of all responding cells were activated by rFeld4 but not by CFO. Black arrows indicate start of stimulation.

Next, I compared the mean percentage of responding cells to each stimulus (MBP, CFO, and rFeld4) between VSNS from the three different tested genotypes (Fig. 40): B6, $cG_{o^{-/-}}$, and $cG_{o^{+/+}}$. In VSNS from B6 and $cG_{o^{+/+}}$, I observed that CFO and rFeld4 activated almost 2% of total cells, indicating that VSNS from both strains sense both stimuli in a comparable number of cells. Almost half of the cells responding to CFO showed also robust responses to rFeld4. This indicates that rFeld4 could be a bioactive component present in CFO. In contrast to B6 and $cG_{o^{+/+}}$, VSNS from $cG_{o^{-/-}}$ mice showed a ~50% reduction in the response to CFO, and responses to rFeld4 were nearly absent (LSD: *** $p < 0.001$) (Fig. 40). $cG_{o^{-/-}}$ VSNS activated by CFO showed no overlap with residual rFeld4 responses. This drastic reduction in the response profile for rFeld4 is consistent with the idea that basal (G_{o} -expressing) VSNS detect peptides and proteinaceous components (Chamero *et al.*, 2007, 2011; Leinders-Zufall *et al.*, 2004, 2009; Kimoto *et al.*, 2005).

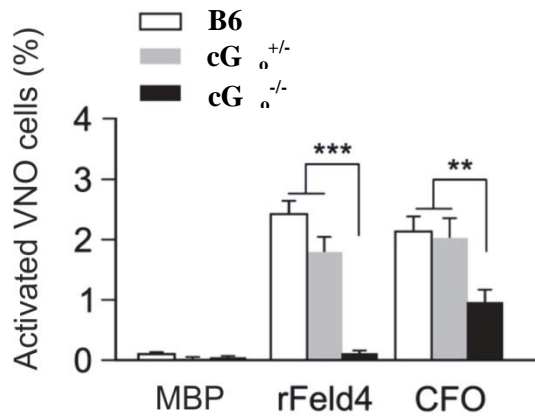


Figure 40. Summary of VSN kairomone activation in mice lacking G_{α} ($cG_{\alpha}^{-/-}$).

Mean percentage of activated B6 (white), $cG_{\alpha}^{+/-}$ heterozygous (gray), and $cG_{\alpha}^{-/-}$ cells (black) with three different stimuli: Maltose binding protein (MBP; 500 nM), cat fur odor (CFO; 20 ml of 1x HBSS solution incubated with one cat-odorized cotton pad), and recombinant MBP-Feld4 fusion protein (rFeld4; 500 nM). VSNs from $cG_{\alpha}^{-/-}$ mice showed strong reduction in response pattern to rFeld4. N= 8115, 12935 and 11282 total VNO cells from 14 B6, 20 $cG_{\alpha}^{+/-}$ and 21 $cG_{\alpha}^{-/-}$ mice. ANOVA: $F_{7,111} = 27.28$, *post hoc* comparison: LSD: ** $p < 0.005$, *** $p < 0.001$, ** $p < 0.005$. Data expressed as mean \pm SEM.

Overall, these experiments reveal that CFO detection in the VNO is both G_{α} -dependent and -independent. Since CFO is a complex stimulus, it is likely to contain other bioactive components different from Feld4 that are detected by VSNs. These components would be transduced in a G_{α} -independent fashion- for example by apical VSNs using a different G protein. rFeld4 seems to be entirely dependent on G_{α} signaling because responses are abolished in $cG_{\alpha}^{-/-}$ VSNs. These data suggest that rFeld4 is a major active component in CFO, responsible for around 50% of its bioactivity in our experimental conditions.

5 DISCUSSION

The main goal of this PhD project was to develop a functional expression system for *Vrs* in native VSNs and identify and match putative ligands with their specific receptor. A Herpes Simplex Virus type 1 (HSV-1)-derived amplicon system was developed, which allows functional gene delivery of different *Vr* types in VSNs. Selected members (*Vmn1r89*, *Vmn1r237*, *Vmn2r26*, and *Fpr3*) from each of the three main vomeronasal receptor families were ectopically expressed in dissociated VSNs. Expression of the receptors increased responsivity to specific ligands that were previously linked to these receptors (Isogai *et al.*, 2011; Bufe *et al.*, 2012, Haga-Yamanaka *et al.*, 2014; Leinders-Zufall *et al.*, 2009). This is the first study that has functionally expressed *Vrs* in VSNs *ex vivo* using a virus-based expression system. This approach overcomes the limitations that heterologous expression systems encounter to express *Vrs*; thus permitting broader investigation of receptor-ligand interactions in VSNs.

Vmn2r74 receptor was identified as a potential detector for the HMW urine fraction, mainly constituted by MUPs. HMW is a highly bioactive component, linked to various social behaviors in mice (Pérez-Gómez *et al.*, 2014). Identifying a HMW receptor could help to understand how chemosensory information is encoded in mice, important for displaying social behaviors.

5.1 *Vr* expression in heterologous cells

A few of the ~150 mouse *V2rs* and one human *V1r* have been matched with potential ligands in a heterologous expression system (Dey and Matsunami, 2011; Shirokova *et al.*, 2008). Some *Vrs* can be expressed in heterologous cell lines, including HEK293 cells (Dey and Matsunami, 2011) and a mouse spermatogonia cell line (Loconto *et al.*, 2003), but with poor performance. They are probably retained in the endoplasmic reticulum (ER) and fail to localize to the membrane surface (Dey and Matsunami, 2011). This inefficient surface expression also affects other GPCR families, including Ors (Lu *et al.*, 2003) and adrenergic receptors (Salahpour *et al.*, 2004). Hence, *Vrs* are particularly difficult to express in heterologous cell systems, indicating that expression of these receptors requires interaction with cell-specific factors and a specific cellular environment. It may be that receptor-specific factors are needed for functional surface expression, as some *V2rs* can be expressed whereas others cannot.

Functional expression of the *Vmn1r89* receptor was tested in a heterologous expression system using lipofection and fura-2 calcium imaging measurements. No positive responses to sulfated steroids were monitored, which are proposed ligands for this receptor (Isogai *et al.*, 2011; Haga-Yamanaka *et al.*, 2014, 2015). Using a viral transduction system (HSV-1-derived amplicon system) to induce high expression of *Vmn1r89* in HEK293 cells did not affect the response to sulfated steroids (Fig. 9), suggesting that the cellular environment of HEK293 cells rather than the higher expression levels provided by HSV-1-derived amplicons may be the limiting factor for functional *Vr* expression. This was likely caused by a lack of surface expression of the receptor due to retention in the ER and/or Golgi apparatus or by non-functional surface expression. ER retention is a major bottleneck in heterologous GPCR expression, including *Ors* (Lu *et al.*, 2003, 2004; Gimelbrant *et al.*, 1999) and *Vrs* (Dey and Matsunami, 2011). Indeed, trafficking of GPCRs to specialized localizations, such as the cilium of an OSN, is a complex mechanism that may involve many GPCR-interacting proteins (Magalhaes *et al.*, 2012). At least some GPCRs are transported via vesicles through the ER and the trans-Golgi network to the ciliary pocket where further anterograde trafficking to the cilium is organized (Schou *et al.*, 2015). An important stage of this mechanism is the coupling of some GPCRs to other GPCRs to form homo- or heterooligomers (Kleinau *et al.*, 2016) or to unrelated accessory proteins that transport the receptor to the plasma membrane. *OlfC* in zebrafish requires coexpression of *OlfCc1* (an orthologue to family C *Vmn2r1* in mice) to be targeted to the surface of HEK293 cells (DeMaria *et al.*, 2013). Additionally, coexpression of major histocompatibility class (MHC) Ib molecules also improves receptor expression, at least for some *V2rs* in a spermatogonia cell line (Loconto *et al.*, 2003). It is not yet clear whether MHC Ib molecules act as chaperones or whether they may have an active function on ligand binding. Although they contribute to *V2r* sensitivity, they seem dispensable for detecting ligands (Leinders-Zufall *et al.*, 2014). Additionally, interactions with different proteins, such as the receptor-activity-modifying proteins (RAMPS), which facilitate the surface expression of the calcitonin-like receptor (McLatchie *et al.*, 1998) and amino acid composition of the receptor itself, could influence poor receptor trafficking and retention in heterologous cells as well (Bubnell *et al.*, 2015). The possibility that *Vmn1r89* is correctly targeted to the surface plasma membrane but is not functional, due to a misled coupling to a signal transduction machinery, cannot be overlooked. Furthermore, missing post-translational modifications and/or interactions with cofactors could cause non-functionality.

Nonetheless, functional surface expression in heterologous cell systems can be improved by cotransfection with receptor-transporting proteins or adding N-terminal extensions. These extensions include amino acids from rhodopsin (Rho-tag) (Krautwurst *et al.*, 1998), a 17-amino acid leucine rich N-terminal peptide tag (Lucy-tag; Shepard *et al.*, 2013), or an octapeptide (Flag-tag). These tags have been proposed to enhance *Or* and *Vr* surface expression *in vitro* (Bufe *et al.*, 2012; Dey and Matsunami, 2011; DeMaria *et al.*, 2013). However, these N-terminal tags may alter responsive profiles, at least proposed for some *Ors* (Zhuang and Matsunami, 2007).

The complexity of conditions used in different *Vr* studies suggests that *Vrs* may need coexpression of a number of factors, some potentially even receptor-specific, to be functional in HEK293 cells. Exceptions are certain vomeronasal *Fprs*, that have been expressed in HEK293 cells without any coexpression of additional proteins or N-terminal extensions (Rivière *et al.*, 2009). Overall, it is likely that *Vrs* require cell-type and receptor-specific components for functional expression in HEK293 cells; therefore, limiting this tool to deorphanize receptor-ligand interactions.

5.2 HSV-1-derived amplicon system to transduce *Vrs* to intact VSNs

A HSV-1-derived amplicon system for *ex vivo* receptor expression in freshly dissociated VSNs was set up to overcome the limitations of *Vr* expression in HEK293 cells. I hypothesized that VSNs would provide an appropriate cellular environment for functional *Vr* expression. Viral transduction approaches are already successfully used in *Or* research, such as adenovirus to infect the MOE. Functionality was tested by calcium imaging measurements or electrical measurements (Zhao *et al.*, 1998; Touhara *et al.*, 1999; Araneda *et al.*, 2000).

In this study, freshly dissociated VSNs were infected and combined with live cell calcium imaging measurements to monitor ligand binding to selected *Vrs*.

5.3 Infection efficiency and natural tropism of HSV-1 for VSNs

Among the large variety of available transduction systems, a HSV-1-derived amplicon system was used to express different *Vrs* in native VSNs because for four main reasons: 1) amplicons are defective gene transfer vectors, in which the amplicon genome does not carry protein-encoding viral sequences; 2) consequently, they are safe for the host and almost nontoxic for the infected cells, yet have the ability to transduce cells at exceedingly high efficiencies; 3)

complete absence of virus genes provides space to accommodate very large foreign DNA sequences, including complete genes and 4) HSV-1 is specifically effective for infecting VSNs because it targets the mouse VNO as a route for neuroinvasion of the rodent central nervous system under natural conditions (Mori *et al.*, 2005). Thus, HSV-1-derived amplicons are adequate candidates for fast and robust ectopic receptor expression in VSNs. A mean of ~20% of all dissociated VSNs were infected (Fig. 14) and 76% of which were neurons (Fig. 15). Infection rates varied, depending on the batch of preparation, but were independent of receptor type (Fig. 14). Variations in infection rate were probably caused by different ratios of helper virus vs. amplified amplicons in different batches. The reason is not clear but it is likely that the status and transfection efficiency of the 2-2 cells could influence the ratio. Nevertheless, these infection rates provided a sufficient amount of infected cells to screen for ligand-induced activity in calcium imaging measurements. Furthermore, infections in dissociated VSNs may be more efficient than any *in vivo* expected infection. Infection rates in the MOE, which is more accessible to external delivery than the VNO, using adenoviruses with higher virus titer compared to HSV-1-derived amplicons, barely reach 1-2% of infected sensory neurons (Zhao *et al.*, 1998).

A lower (almost three-fold) infection rate was observed in OSNs compared to VSNs (Fig. 29). One explanation could be that HSV-1-derived amplicons, which have a natural tropism for VSNs, are not equipped with suitable glycoproteins on their envelope surface to enter OSNs efficiently. Therefore, HSV-1-derived amplicons may have a higher specificity for VSNs. Another reason could be that expression of the transduced cloning cassette consisting of the receptor and the *mCherry* marker protein cDNA was differently expressed and processed in VSNs and OSNs. This could lead to a difference in mCherry fluorescence. Alternatively, this lower rate may only be a consequence of the larger cell density obtained in MOE cultures.

5.4 GFP expression properties of HSV-1-derived amplicon-infected cells

To monitor receptor expression, a *GFP* sequence was inserted into the cloning cassette (Fig. 7). The IRES sequence facilitates bicistronic expression of the receptor and *GFP* as separate proteins within the same cell (Kim *et al.*, 1992). This strategy avoids undesirable side effects of fusion proteins or adding extra residues to the receptor sequence. The HSV-1-derived amplicon infection of VSNs was monitored and 24 h post infection was the best time point to analyze infected VSNs on calcium imaging. GFP fluorescence intensity in infected VSNs peaked at 24 h and decreased after 48 h, probably due to reduced fitness. Furthermore, massive cell death of dissociated VSNs 72 h post infection was detected (Fig. 11), probably

due to virus toxicity and the lack of surrounding glia cells. Fortunately, infected cells could be loaded with fura-2 24 h post infection (Fig. 14), and dye uptake was a direct indicator of an intact plasma membrane integrity. VSNs transfected by lipofection did not show GFP fluorescence. Transfection of primary cells is complex and depends on many different factors like cell membrane composition and health status of the cells. In VSNs, lipofection may be blocked by inappropriate membrane composition or membrane alterations secondary to the dissociation. This disqualifies this widely used and well established gene-delivery tool and further supports the technical relevance of the newly developed HSV-1-derived amplicon system. Overall, a HSV-1-derived amplicon system is suitable for efficient transgene transduction in VSNs and can be used for ligand screening in rapid calcium imaging measurements of several hundred cells in parallel- simplifying the ligand screening remarkably.

5.5 Functional validation of Vr expression

Four members (*Vmn1r89*, *Vmn1r237*, *Vmn2r26*, and *Fpr3*) of all three major VNO receptor families were selected to monitor ligand binding and to test the functionality of this HSV-1-derived expression system in dissociated VSNs combined with fura-2 live cell calcium imaging. Receptor expression induced a significant increase in the number of cells responding to specific ligands (Figs. 16, 18, 19, 21). These receptors have been linked with their ligands using different approaches, including heterologous expression (*Fpr3*- Bufe *et al.*, 2012, 2015), genetically targeted mouse lines (*Vmn2r26* and *Vmn1r89*- Haga-Yamanaka *et al.*, 2014; Leinders-Zufall *et al.*, 2009), and a combination of immunohistochemistry and *in-situ* hybridization (*Vmn1r237*- Isogai *et al.*, 2011). Infection with control amplicons containing only GFP and no receptor (*GFP*-only) was insufficient to increase the response rate, indicating that viral infection and GFP do not contribute to the increased response rate. Closely related ligands for specific receptors were unable to increase responsiveness as well, suggesting a high degree of specificity. Particularly, the response profile of *Vmn1r89-GFP*-expressing VSNs did not overlap with that of the steroid E2734 (Fig. 18), which is similar in terms of structure to the activating steroids. A similar extent of specificity was observed in *V2r-GFP*-infected VSNs: a larger number of VSNs expressing *Vmn2r74-GFP* was activated by the HMW fraction of C57BL/6 (B6) male mouse urine compared to HMW from BALB/c (B/c). Even more, *Vmn2r26-GFP*-expressing VSNs detected the 9-mer peptide SYFPEITHI (SYF) but not the the mitochondria-derived peptide ND1 (f-MFFINTLTL), which seems to be

sensed by another V2r (*Vmn2r81*) (Leinders-Zufall *et al.*, 2014). All three receptor types distinguished related components from their potential ligand. However, in rare exceptions, overlapping response profiles were observed to more than one ligand. This could be a consequence of a parallel expression of an endogenous and ectopically expressed receptor in the same cell. This idea is consistent with previous studies showing that individual VSNs can be activated by different peptides (Leinders-Zufall *et al.*, 2004).

Furthermore, detection of some stimuli was in the nanomolar range (Fig. 19), indicating a high affinity for specific ligands; similar to previously observed ligand detection features in intact slice preparations of mice VNOs (Leinders-Zufall *et al.*, 2004, 2014).

As cells expressing a virally transduced receptor probably maintain expression of an endogenous receptor, I cannot exclude that the endogenous receptor interacted with the ectopically expressed receptor by forming heterodimers or heteromultimers, which may alter the response profile. Further experiments expressing different receptor types ectopically and simultaneously in the same cell are needed to address this question.

Ligand responses of infected cells followed the pattern of transient increases in intracellular calcium measured in untreated cells (Chamero *et al.*, 2011), suggesting that the endogenous second messenger signaling cascade in infected cells is most likely responsible for generating the observed responses. This assumption was further supported by experiments performed in *cG_o^{-/-}* mice lacking a major component (G_o) for signaling in basal VSNs (Chamero *et al.*, 2011): *cG_o^{-/-}* VSNs infected with *Vmn2r26-GFP* or *Vmn2r74-GFP* amplicons failed to show an increase in responses to SYF and HMW, respectively (Figs. 20, 25).

Interestingly, responses were detectable in *Vmn2r26-GFP* amplicon-infected *cG_o^{-/-}* VSNs to SYF, the high molecular weight fraction of mouse urine (HMW), and ND1 (Fig. 25). However, the number of responding cells was very low for all ligands, indicating that responses likely reflected non-specific background activity rather than specific activation.

The overall number of activated cells was relatively low (3-5%), although as many as 76% of the amplicon-infected cells were neurons (Fig. 15). The reasons for this is not known, but several factors may contribute. First, not all of the receptor amplicon-infected cells provide an appropriate access to the correct signaling cascade, as only half of the neurons express either G_{i2} or G_o and further components could be necessary for correct receptor localization (including receptor-modifying proteins, such as Homer-like proteins, calreticulin 4, and phospholipase [PLC]). Second, the requirement for specific molecular partners to form

receptor oligomers. Third, some ligands may act as receptor antagonist, inducing inactivation of the receptor.

Overall, an amplicon-derived delivery system was developed to identify receptor-ligand pairs with high specificity and sensitivity. Amplicons were combined with different fluorescent marker proteins that allowed measurements in genetically labeled cells.

5.6 Vmn2r74 receptor expression increases responses to HMW

Ectopic expression of *Vmn2r74* induces an increase in responsivity to HMW in VSNs (Figs. 23, 28, 32). HMW activation occurred in up to 10% of all infected VSNs by calcium imaging measurements. This activation rate was slightly higher compared to activated cells ectopically expressing *Fpr3-GFP*, *Vmn2r26-GFP*, *Vmn1r89-GFP*, and *Vmn1r237-GFP* (3-6% on average). In contrast, activation rates in control amplicon-infected cells were largely similar for all tested ligands, including HMW (1-2% of infected cells), indicating high specificity of the *Vmn2r74* receptor for HMW. This is further supported by a dose-dependent response rate of *Vmn2r74-GFP*-expressing cells (Fig. 26), which showed a higher number of responding cells under stimulation with higher HMW concentrations. The receptor peak response to 1:100 diluted HMW in *Vmn2r74-GFP*-expressing cells was higher compared to the 1:300 HMW dilution. As dose-dependent activation of a receptor is an important requirement for a proposed receptor-ligand interaction, this further backs *Vmn2r74* as potential HMW receptor. Overall, the percentage of *Vmn2r74* receptor amplicon-infected cells responded to HMW was variable (between 3-10%). Importantly, the amount of activated cells compared to control amplicon-infected (*GFP*-only) was always consistently larger, independently of the response rate. The difference in the increased responsivity factor (compared to *GFP*-only responder cells) varied between two-fold and seven-fold. This variation may reflect the heterogeneity of native dissociated VSNs in culture (depending on the individual culture preparation) as well as differences in stimulus application (different stimuli and order of application). Variations in stimuli application may alter background activity of amplicon-infected cells.

HMW of C57BL/6 mouse urine is composed of five different MUPs. However, it is not clear whether *Vmn2r74* expression favors detection of one or several MUPs, or whether other receptors are also involved in detecting the MUPs present in HMW. Consistent with multiple detection of several MUPs are observations that some cells responded to 1:100 HMW

dilutions, whereas others responded to 1:300 HMW dilutions. This suggests that different MUPs may be detected by the same receptor depending on their individual concentration.

Two related receptors of the same clade, *Vmn2r65* and *Vmn2r66*, failed to show increased number of responses to HMW (Fig. 23), indicating that HMW activation may be largely specific for *Vmn2r74*. However, it cannot be excluded that other receptors of the 10 members of this clade or even receptors from different clades could be also tuned to detect HMW. Nonetheless, HMW contained only a fraction (5 of 21) of the mouse MUP pool, not considering dozens of heterospecific MUP orthologues. Responses to other tested proteinaceous components (SYF and W-peptide [w-pep]), which are linked to different receptors (Leinders-Zufall *et al.*, 2009; Bufe *et al.*, 2012), did not increase in *Vmn2r74-GFP*-expressing cells. This indicates moderate specificity to HMW. Three of the HMW-activated cells (*Vmn2r74-GFP*-expressing) showed also activation to SYF (Fig. 24), suggesting coexpression of the *Vmn2r74* transgene with an endogenous receptor that could detect SYF. Interactions between the ectopically expressed *Vmn2r74* and the endogenous receptor may also lead to a broader tuning profile and allow parallel detection of HMW and SYF.

HMW detection in *Vmn2r74-GFP*-expressing cells seemed to follow a concentration-dependent mechanism (Fig. 26). Regarding the number of activated cells, such a mechanism was already described for HMW, pooled MUPs, and urine in uninfected VSNs (Chamero *et al.*, 2007; Leinders-Zufall *et al.*, 2014). As *Vmn2r74-GFP* expression increased the responses to high HMW concentrations (Fig. 26), *Vmn2r74* may be broadly tuned to detect various MUPs at high concentrations, at least for the MUPs present in my HMW preparation. This would be in agreement with a combined coding scenario, in which different VSN subpopulations detect different MUPs, depending on their composition and relative concentrations (Kaur *et al.*, 2014).

However, it could not be excluded that *Vmn2r74* is also being activated by low HMW concentrations, which might not be detected because of the limited sensitivity of this expression system. In this case, the low activation rate and high HMW background in control amplicon-infected cells may uncover subtler variations in activity.

Vmn2r74-GFP-expressing VSNs showed different response rates to HMW from the C57BL/6 (B6) and BALB/c (B/c) mouse strains (Figs. 31, 32). B/c-derived HMW lacked two MUPs (MUP3 and MUP20) present in B6 HMW, but contained one MUP (MUP12)- not present in B6. Thus, MUP3 and MUP20 could be responsible for the increased responsivity to B6 HMW. Alternatively, concentration ratio differences between specific MUPs in each HMW

could induce these different activation profiles. The fraction of infected cells responding to both stimuli (Figs. 31, 32) was small compared to the fraction of cells responding to B6 HMW. This indicates that overlap seems to be a rare event. This further indicates that the *Vmn2r74* receptor could be tuned to detect MUP3 and/or MUP20 and discriminate between other individual MUPs. Another possibility is that *Vmn2r74-GFP*-expressing cells are not tuned to detect individual MUPs (e.g., MUP3 and MUP20), but more to a defined MUP composition as proposed by Kaur *et al.* (2014).

Unfortunately, activation experiments using *Vmn2r74-GFP*-expressing cells with single rMUPs remained inconclusive due to similar background activity in *GFP*-only amplicon-infected cells and high background activity to MBP (Fig. 33). However, responses to all rMUPs were detectable, except MUP20, in *Vmn2r74-GFP*-expressing cells with no overlap to MBP, indicating that rMUP induced responses are not generated by the MBP fusion protein. I compared peak response ratio values of HMW responder cells (either infected with *Vmn2r74-GFP* or *GFP*-only control) but could not detect a difference in the peak responses. The reason for the limited success in the response profile to rMUPs is not yet clear, although one possibility is that rMUP concentrations were insufficient to elicit the same responses as HMW. Future dose-dependent rMUP activation could help determine the influence of the rMUP concentration to activate *Vmn2r74-GFP*-expressing cells. Nonetheless, the lack of overlapping activation profiles for different HMW sources suggests that *Vmn2r74* receptor may be able to distinguish between individual MUPs; although they share a high similarity. This is consistent with a context-dependent activation model for MUPs, as previously proposed (Kaur *et al.*, 2014). Kaur and coworkers showed that different VSN populations can detect different rMUPs. Some VSNs even seemed to be tuned to detect several rMUPs in a mix depending on the concentration and composition. It is likely that more than one receptor participates in this context-dependent detection mechanism.

Furthermore, MUPs, recombinantly produced in bacteria, could be structurally different from natural MUPs or they may carry small molecules in their pocket influencing receptor activation. In future experiments, small molecule displacers, such as menadione, could be used to strip off all bound molecules from rMUPs and HMW and test if response profile changed in *Vmn2r74-GFP*-expressing cells.

5.7 Single cell RT-PCR to decipher receptor-ligand pairs

To access the identity of cells responding to specific ligands in live cell calcium imaging measurements, I used a RT-PCR approach. A microcapillary pipette-mediated cell picking approach was adapted with a suitable mRNA purification system. A commercially available silica-membrane was used to purify mRNA of 5-50 cells, previously isolated and picked from a dissociated VSN culture. The mRNA was reverse transcribed into cDNA and amplified for gene-specific transcripts of the olfactory marker protein (*Omp*) and the transient receptor potential channel, subfamily 2, member 2 (*Trpc2*) (Fig. 35). I selected these two general marker proteins for mature VSNs as they are proposed to be widely expressed in mature rodent VSNs (Berghard *et al.*, 1996; Liman *et al.*, 1999; Barrios *et al.*, 2014). The detection threshold was determined to be 25 cells to amplify gene-specific products (Fig. 35). This threshold was rather due to a limitation of the silica-based membrane to purify mRNA from a few cells (~25 cells) than to an inadequate number of transcripts within individual cells. Independent of this limitation, the protocol was adapted to calcium imaging measurements and *Trpc2* transcripts were amplified in 27 cells that previously responded to HMW and not to the sulfated steroid E1050. To further characterize HMW-responding cells and test their affiliation to a subgroup of V2rs expressing the family C V2r, namely *Vmn2r1*, this gene transcript was amplified in HMW-responding cells.

This family C V2r (*Vmn2r1*), which is widely expressed in basal VSNs, was not present in non-responding cells. *Vmn2r1* may be coexpressed with an ABD family V2r (*Vmn2r74*) essential for detecting HMW. Cells lacking *Vmn2r1* could either detect other components, independent of *Vmn2r1* expression or express a V1r, which is important for detecting non-proteinaceous stimuli.

Increased responsivity of V1r amplicon-infected cells to sulfated steroids was observed, so a single cell RT-PCR approach was set up to confirm these data. Furthermore, this approach could help to confirm receptor identity on the single cell level. A new protocol (different from the protocol described above) was adapted, which was already successfully used for OSNs (Omura and Mombaerts, 2014).

A clade of receptors (transcripts were further characterized by sequencing as *Vmn1r89* and *Vmn1r85*) and basic signal transduction components (G protein subunits) were identified in cells, previously responding to a sulfated steroid (E1050) (Figs. 37, 38). Cells not responding to E1050 did not express any of the two V1rs, suggesting that these cells are equipped with a different receptor tuned to detect other stimuli. Global amplification of all mRNA transcripts rather than separate purification of mRNA via a silica-based membrane was used to avoid loss

of transcripts (Dixon *et al.*, 2000) as individual cells possess a very limited amount of mRNA (in the range of 1pg). To confirm my functional expression data, this new protocol was used to determine and detect *Vmn2r1* (similar to clade-specific PCR for *V1rs*) and *Vmn2r74* transcripts in cells previously responding to HMW. Unfortunately, these transcripts were not detectable in HMW-responding cells. Since HMW is composed of different MUPs, which are potentially detected by various receptors, it might be that the tested HMW-responding cells expressed another HMW receptor apart from *Vmn2r74*. To overcome this issue, further experiments with a single rMUP as stimulus could help to identify *Vmn2r74* transcripts in responding cells. One could test all five MUPs, present in mouse urine, individually and screen for *Vmn2r74* transcripts in the cDNA library of responding cells.

However, independent of the protocol and detection thresholds, specific *V1rs* and *V2rs* (*Vmn2r74*) may have different transcripts levels and are therefore not equally accessible via this RT-PCR approach. It is already known that gene expression can vary between individual cells (Huang, 2009), suggesting that subgroups of basal and/or apical cells could have varying transcript levels of receptors and signaling components. This could be another explanation for the lack of receptor transcripts in HMW-responding cells. The reason for this heterogeneity may have numerous explanations like epigenetic cell status, microenvironment, and circadian rhythm. Recently, it was shown that mice exposed to prolonged odorant stimulation showed a concentration-dependent decrease and circadian adaption of transcript levels of individual *Ors* upon stimulation (Von der Weid *et al.*, 2015). As the mice used for cell picking experiments and RT-PCR analysis were usually housed together in one cage, they may have been exposed to various emitted stimuli, including urine of roommates, which may induced adaptive transcriptional processes. This could potentially lead to a reduction of transcript levels of potential HMW receptors like *Vmn2r74*. It would be interesting to test HMW responder cells from single housed mice.

Furthermore, technical limitations and constraints could cause differences in transcript levels between *V1r*- and *V2r*-expressing cells. Additionally, *V1r* transcripts are shorter and more stable than *V2rs* and therefore more accessible to amplification. As a consequence, gene-specific amplification of short sequence receptors such as *V1rs* could be more efficient, leading to an easier detection.

5.8 VSN detection of the cat MUP Feld4

Mouse VSNs can detect orthologous MUPs, like Feld4, which is present in the saliva of cats. I tested whether recombinant Feld4 (rFeld4) and cat fur odor (CFO) require the G protein subunit $G_{\alpha o}$ for detection. To test this, I performed calcium imaging measurements in different mouse strains. In B6 and heterozygous ($cG_{\alpha o}^{+/-}$) VSNs both stimuli activated around 2% of all cells, indicating that VSNs from both strains sense both stimuli similarly. Nearly half of the cells responding to CFO also responded to rFeld4, pointing to Feld4 as a potential bioactive component present in CFO. In contrast, VSNs from $cG_{\alpha o}^{-/-}$ mice displayed a ~50% reduction in the response (percentage of activated cells) to CFO and responses to rFeld4 were abolished (Figs. 39, 40). This is consistent with the idea that basal ($G_{\alpha o}$ -expressing) VSNs detect peptides and proteinaceous components (Chamero *et al.*, 2007, 2011; Leinders-Zufall *et al.*, 2009, 2014; Kimoto *et al.*, 2005). Interestingly, VSNs from $cG_{\alpha o}^{-/-}$ mice were still partially able to detect CFO, suggesting that CFO contains more bioactive components using a different ($G_{\alpha o}$ -independent) signaling cascade.

Reduced predator detection has important consequences at the behavioral level: $cG_{\alpha o}^{-/-}$ mice were no longer able to display innate avoidance behavior to either rFeld4 or CFO (Pérez-Gómez *et al.*, 2015). Surprisingly, they showed attractive behavior to CFO, perhaps as a consequence of the presence of attractive chemostimuli.

Overall, these experiments revealed that detection of CFO in the VNO is $G_{\alpha o}$ -dependent and -independent, whereas that of rFeld4 seemed to be entirely dependent on $G_{\alpha o}$ signaling. CFO is likely to contain other bioactive components different from Feld4 that are detected by VSNs transduced in a $G_{\alpha o}$ -independent fashion; for example by apical VSNs.

6 CONCLUSIONS

1. In this doctoral project, I introduced a novel HSV-1-derived expression system (*ex vivo*) to identify and characterize activity and tuning properties of individual Vrs. Through dissociated native VSNs my system facilitates ectopic receptor expression in their natural microenvironment, circumventing non-functional Vr expression observed in heterologous systems. Knowledge of potential ligands for individual receptors contributes enormously to understand the function of the VNO in mice. Receptor-ligand interactions identified by my system could be the basis for analyzing a causal link between receptor expression and potential behavioral effects. Since the generation of *knockin* or *knockout* mice is time-consuming and costly, my approach bridges the gap between the lack of suitable heterologous systems and a gene-targeted approach to identify potential receptor-ligand pairs.

2. I could show functional expression for all three types of GPCRs present in the VNO and confirm previously suggested receptor-ligand pairs. To my knowledge, this is the first study showing activation of a single rodent V1r to a specific ligand *in vitro*. Furthermore, I could show ligand-induced activation of the Vmn1r237 receptor to a mix of sulfated steroids, suggesting a direct link between the receptor and the ligand.

3. This study also provides for the first time the identity of a potential receptor to detect the HMW urine fraction, which contributes to a wide range of social behaviors observed in mice. My experiments propose a concentration- and strain-dependent activation profile of Vmn2r74-GFP-expressing cells by HMW. Further experiments using genetically modified mice lacking this specific receptor could help to determine a potential link between Vmn2r74 activation and MUPs *in vivo*. Furthermore, a behavioral analysis will address the question if the lack of this receptor induces a reduction of specific MUP-induced behaviors.

4. I showed for the first time that activation of VSNs by a MUP orthologue secreted by cats, namely Feld4, is dependent on the G protein subunit G_o. This indicates that a subset of VSNs that express G_o is specialized in detecting chemosignals from different species, perhaps important to induce escaping behaviors from potential predators.

5. I established an approach to identify Vr transcripts in single VSNs that respond to specific ligands by combining single cell RT-PCR with calcium imaging measurements. By using this method, I confirmed proposed receptor-ligand interactions on the RNA/DNA level.

7 LITERATURE

1. Abaffy T, Matsunami H, Luetje CW (2006) Functional analysis of a mammalian odorant receptor subfamily. *J Neurochem* 97: 1506-1518
2. Abaffy T, Malhotra A, Luetje CW (2007) The molecular basis for ligand specificity in a mouse olfactory receptor: a network of functionally important residues. *J Biol Chem* 282: 1216-1224
3. Adams DR, McFarland LZ (1971) Septal olfactory organ in *Peromyscus*. *Comp Biochem Physiol A Comp Physiol* 40: 971-974
4. Adams DR (1992) Fine structure of the vomeronasal and septal olfactory epithelia and of glandular structures. *Microsc Res Tech* 23: 86-97
5. Amjad A, Hernandez-Clavijo A, Pifferi S, Maurya DK, Boccaccio A, Franzot J, Rock J, Menini A (2015) Conditional knockout of TMEM16A/anoctamin1 abolishes the calcium-activated chloride current in mouse vomeronasal sensory neurons. *J Gen Physiol* 145: 285-301
6. Andersen JK, Frim DM, Isacson O, Breakefield XO (1993) Herpesvirus-mediated gene delivery into the rat brain: specificity and efficiency of the neuron-specific enolase promoter. *Cell Mol Neurobiol* 13: 503-515
7. Arakawa H, Kelliher KR, Zufall F, Munger SD (2013) The receptor guanylyl cyclase type D (GC-D) ligand uroguanylin promotes the acquisition of food preferences in mice. *Chem Senses* 38: 391-397
8. Araneda RC, Kini AD, Firestein S (2000) The molecular receptive range of an odorant receptor. *Nat Neurosci* 3: 1248-1255
9. Bakalyar HA, Reed RR (1990) Identification of a specialized adenylyl cyclase that may mediate odorant detection. *Science* 250: 1403-1406
10. Barrios AW, Núñez G, Sánchez Quinteiro P, Salazar I (2014) Anatomy, histochemistry, and immunohistochemistry of the olfactory subsystems in mice. *Front Neuroanat* 8: 63
11. Baum MJ (2012) Contribution of pheromones processed by the main olfactory system to mate recognition in female mammals. *Front Neuroanat* 6: 20
12. Bautze V, Bär R, Fissler B, Trapp M, Schmidt D, Beifuss U, Bufe B, Zufall F, Breer H, Strotmann J (2012) Mammalian-specific OR37 receptors are differentially activated by distinct odorous fatty aldehydes. *Chem Senses* 37: 479-493

13. Bautze V, Schwack W, Breer H, Strotmann J (2014) Identification of a natural source for the OR37B ligand. *Chem Senses* 39: 27-38
14. Bean NJ, Wysocki CJ (1989) Vomeronasal organ removal and female mouse aggression: the role of experience. *Physiol Behav* 45: 875-882
15. Beauchamp GK, Wysocki CJ, Wellington JL (1985) Extinction of response to urine odor as a consequence of vomeronasal organ removal in male guinea pigs. *Behav Neurosci* 99: 950-955
16. Belloir C, Miller-Leseigneur ML, Neiers F, Briand L, Le Bon AM (2017) Biophysical and functional characterization of the human olfactory receptor OR1A1 expressed in a mammalian inducible cell line. *Protein Expr Purif* 129: 31-43
17. Belluscio L, Gold GH, Nemes A, Axel R (1998) Mice deficient in G(olf) are anosmic. *Neuron* 20: 69-81
18. Belluscio L, Koentges G, Axel R, Dulac C (1999) A map of pheromone receptor activation in the mammalian brain. *Cell* 97: 209-220
19. Berghard A, Buck LB, Liman ER (1996) Evidence for distinct signaling mechanisms in two mammalian olfactory sense organs. *Proc Natl Acad Sci U S A* 93: 2365-2369
20. Berghard A, Buck LB (1996) Sensory transduction in vomeronasal neurons: evidence for G alpha o, G alpha i2, and adenylyl cyclase II as major components of a pheromone signaling cascade. *J Neurosci* 16: 909-918
21. Beynon RJ, Hurst JL (2003) Multiple roles of major urinary proteins in the house mouse, *Mus domesticus*. *Biochem Soc Trans* 31: 142-146
22. Bhatnagar KP, Meisami E (1998) Vomeronasal organ in bats and primates: extremes of structural variability and its phylogenetic implications. *Microsc Res Tech* 43: 465-475
23. Biron D, Wasserman S, Thomas JH, Samuel AD, Sengupta P (2008) An olfactory neuron responds stochastically to temperature and modulates *Caenorhabditis elegans* thermotactic behavior. *Proc Natl Acad Sci U S A* 105: 11002-11007
24. Blache P, Gros L, Salazar G, Bataille D (1998) Cloning and tissue distribution of a new rat olfactory receptor-like (OL2). *Biochem Biophys Res Commun* 242: 669-672
25. Bleyemehl K, Pérez-Gómez A, Omura M, Moreno-Pérez A, Macías D, Bai Z, Johnson RS, Leinders-Zufall T, Zufall F, Mombaerts P (2016) A Sensor for Low Environmental Oxygen in the Mouse Main Olfactory Epithelium. *Neuron* pii: S0896-6273 (16) 30839-X

26. Boillat M, Challet L, Rossier D, Kan C, Carleton A, Rodriguez I (2015) The vomeronasal system mediates sick conspecific avoidance. *Curr Biol* 25: 251-255
27. Bojsen-Moller F (1975) Demonstration of terminalis, olfactory, trigeminal and perivascular nerves in the rat nasal septum. *J Comp Neurol* 159: 245-256
28. Borowsky B, Adham N, Jones KA, Raddatz R, Artymyshyn R, Ogozalek KL, Durkin MM, Lakhani PP, Bonini JA, Pathirana S, Boyle N, Pu X, Kouranova E, Lichtblau H, Ochoa FY, Branchek TA, Gerald C (2001) Trace amines: identification of a family of mammalian G protein-coupled receptors. *Proc Natl Acad Sci U S A* 98: 8966-8971
29. Boschat C, Pélofi C, Randin O, Roppolo D, Lüscher C, Broillet MC, Rodriguez I (2002) Pheromone detection mediated by a V1r vomeronasal receptor. *Nat Neurosci* 5: 1261-1262
30. Bozza T, Feinstein P, Zheng C, Mombaerts P (2002) Odorant receptor expression defines functional units in the mouse olfactory system. *J Neurosci* 22: 3033-3043
31. Brann JH, Firestein S (2010) Regeneration of new neurons is preserved in aged vomeronasal epithelia. *J Neurosci* 30: 15686-15694
32. Brann JH, Firestein SJ (2014) A lifetime of neurogenesis in the olfactory system. *Front Neurosci* 8: 182
33. Brechbühl J, Klaey M, Broillet MC (2008) Grueneberg ganglion cells mediate alarm pheromone detection in mice. *Science* 321: 1092-1095
34. Brechbühl J, Moine F, Klaey M, Nenniger-Tosato M, Hurni N, Sporkert F, Giroud C, Broillet MC (2013) Mouse alarm pheromone shares structural similarity with predator scents. *Proc Natl Acad Sci U S A* 110: 4762-4767
35. Breer H, Klemm T, Boekhoff I (1992) Nitric oxide mediated formation of cyclic GMP in the olfactory system. *Neuroreport* 3: 1030-1032
36. Brennan PA, Kendrick KM (2006) Mammalian social odours: attraction and individual recognition. *Philos Trans R Soc Lond B Biol Sci* 361: 2061-2078
37. Bubnell J, Jamet S, Tomoiaga D, D'Hulst C, Krampis K, Feinstein P (2015) In Vitro Mutational and Bioinformatics Analysis of the M71 Odorant Receptor and Its Superfamily. *PLoS One* 10(10):e0141712
38. Buck L, Axel R (1991) A novel multigene family may encode odorant receptors: a molecular basis for odor recognition. *Cell* 65: 175-187

39. Bufe B, Schumann T, Zufall F (2012) Formyl peptide receptors from immune and vomeronasal system exhibit distinct agonist properties. *J Biol Chem* 287: 33644-33655
40. Bufe B, Schumann T, Kappl R, Bogeski I, Kummerow C, Podgórska M, Smola S, Hoth M, Zufall F (2015) Recognition of bacterial signal peptides by mammalian formyl peptide receptors: a new mechanism for sensing pathogens. *J Biol Chem* 290: 7369-7387
41. Bunzow JR, Sonders MS, Arttamangkul S, Harrison LM, Zhang G, Quigley DI, Darland T, Suchland KL, Pasumamula S, Kennedy JL, Olson SB, Magenis RE, Amara SG, Grandy DK (2001) Amphetamine, 3,4-methylenedioxymethamphetamine, lysergic acid diethylamide, and metabolites of the catecholamine neurotransmitters are agonists of a rat trace amine receptor. *Mol Pharmacol* 60: 1181-1188
42. Bushdid C, Magnasco MO, Vosshall LB, Keller A (2014) Humans can discriminate more than 1 trillion olfactory stimuli. *Science* 343: 1370-1372
43. Camps M, Carozzi A, Schnabel P, Scheer A, Parker PJ, Gierschik P (1992) Isozyme-selective stimulation of phospholipase C-beta 2 by G protein beta gamma-subunits. *Nature* 360: 684-686
44. Celsi F, D'Errico A, Menini A (2012) Responses to sulfated steroids of female mouse vomeronasal sensory neurons. *Chem Senses* 37: 849-858
45. Chamero P, Marton TF, Logan DW, Flanagan K, Cruz JR, Saghatelian A, Cravatt BF, Stowers L (2007) Identification of protein pheromones that promote aggressive behaviour. *Nature* 450: 899-902
46. Chamero P, Katsoulidou V, Hendrix P, Bufe B, Roberts R, Matsunami H, Abramowitz J, Birnbaumer L, Zufall F, Leinders-Zufall T (2011) G protein G(alpha)o is essential for vomeronasal function and aggressive behavior in mice. *Proc Natl Acad Sci U S A* 108: 12898-12903
47. Chang AJ, Ortega FE, Riegler J, Madison DV, Krasnow MA (2015) Oxygen regulation of breathing through an olfactory receptor activated by lactate. *Nature* 527: 240-244
48. Charra R, Datiche F, Casthano A, Gigot V, Schaal B, Coureaud G (2012) Brain processing of the mammary pheromone in newborn rabbits. *Behav Brain Res* 226: 179-188
49. Cheetham SA, Thom MD, Jury F, Ollier WE, Beynon RJ, Hurst JL (2007) The genetic basis of individual-recognition signals in the mouse. *Curr Biol* 17: 1771-1777.
50. Cherry JA, Pho V (2002) Characterization of cAMP degradation by phosphodiesterases in the accessory olfactory system. *Chem Senses* 27: 643-652

51. Chesler AT, Zou DJ, Le Pichon CE, Peterlin ZA, Matthews GA, Pei X, Miller MC, Firestein S (2007) A G protein/cAMP signal cascade is required for axonal convergence into olfactory glomeruli. *Proc Natl Acad Sci U S A* 104: 1039-1044
52. Chess A, Simon I, Cedar H, Axel R (1994) Allelic inactivation regulates olfactory receptor gene expression. *Cell* 78: 823-834
53. Clancy AN, Coquelin A, Macrides F, Gorski RA, Noble EP (1984) Sexual behavior and aggression in male mice: involvement of the vomeronasal system. *J Neurosci* 4: 2222-2229
54. Cuschieri A, Bannister LH (1975) The development of the olfactory mucosa in the mouse: light microscopy. *J Anat* 119: 277-286
55. Dalton RP, Lomvardas S (2015) Chemosensory receptor specificity and regulation. *Annu Rev Neurosci* 38: 331-349
56. Date-Ito A, Ohara H, Ichikawa M, Mori Y, Hagino-Yamagishi K (2008) *Xenopus* V1R vomeronasal receptor family is expressed in the main olfactory system. *Chem Senses* 33: 339-346
57. Debiec J, Sullivan RM (2014) Intergenerational transmission of emotional trauma through amygdala-dependent mother-to-infant transfer of specific fear. *Proc Natl Acad Sci U S A* 111: 12222-12227
58. Del Punta K, Leinders-Zufall T, Rodriguez I, Jukam D, Wysocki CJ, Ogawa S, Zufall F, Mombaerts P (2002) Deficient pheromone responses in mice lacking a cluster of vomeronasal receptor genes. *Nature* 419: 70-74
59. DeMaria S, Berke AP, Van Name E, Heravian A, Ferreira T, Ngai J (2013) Role of a ubiquitously expressed receptor in the vertebrate olfactory system. *J Neurosci* 33: 15235-15247
60. Dewan A, Pacifico R, Zhan R, Rinberg D, Bozza T (2013) Non-redundant coding of aversive odours in the main olfactory pathway. *Nature* 497: 486-489
61. Dey S, Matsunami H (2011) Calreticulin chaperones regulate functional expression of vomeronasal type 2 pheromone receptors. *Proc Natl Acad Sci U S A* 108: 16651-16656
62. Dey S, Chamero P, Pru JK, Chien MS, Ibarra-Soria X, Spencer KR, Logan DW, Matsunami H, Peluso JJ, Stowers L (2015) Cyclic Regulation of Sensory Perception by a Female Hormone Alters Behavior. *Cell* 161: 1334-1344

63. Dibattista M, Amjad A, Maurya DK, Sagheddu C, Montani G, Tirindelli R, Menini A (2012) Calcium-activated chloride channels in the apical region of mouse vomeronasal sensory neurons. *J Gen Physiol* 140: 3-15
64. Dixon AK, Richardson PJ, Pinnock RD, Lee K (2000) Gene-expression analysis at the single-cell level. *Trends Pharmacol Sci* 21: 65-70
65. Dorries KM, Adkins-Regan E, Halpern BP (1997) Sensitivity and behavioral responses to the pheromone androstenone are not mediated by the vomeronasal organ in domestic pigs. *Brain Behav Evol* 49: 53-62
66. Duan X, Block E, Li Z, Connelly T, Zhang J, Huang Z, Su X, Pan Y, Wu L, Chi Q, Thomas S, Zhang S, Ma M, Matsunami H, Chen GQ, Zhuang H (2012) Crucial role of copper in detection of metal-coordinating odorants. *Proc Natl Acad Sci U S A* 109: 3492-3497
67. Dudley CA, Moss RL (1995) Electrophysiological evidence for glutamate as a vomeronasal receptor cell neurotransmitter. *Brain Res* 675: 208-214
68. Dulac C, Axel R (1995) A novel family of genes encoding putative pheromone receptors in mammals. *Cell* 83: 195-206
69. Eisthen HL (1992) Phylogeny of the vomeronasal system and of receptor cell types in the olfactory and vomeronasal epithelia of vertebrates. *Microsc Res Tech* 23: 1-21
70. Ferrer I, Garcia-Esparcia P, Carmona M, Carro E, Aronica E, Kovacs GG, Grison A, Gustincich S (2016) Olfactory Receptors in Non-Chemosensory Organs: The Nervous System in Health and Disease. *Front Aging Neurosci* 8: 163
71. Ferrero DM, Lemon JK, Fluegge D, Pashkovski SL, Korzan WJ, Datta SR, Spehr M, Fendt M, Liberles SD (2011) Detection and avoidance of a carnivore odor by prey. *Proc Natl Acad Sci U S A* 108: 11235-11240
72. Ferrero DM, Moeller LM, Osakada T, Horio N, Li Q, Roy DS, Cichy A, Spehr M, Touhara K, Liberles SD (2013) A juvenile mouse pheromone inhibits sexual behaviour through the vomeronasal system. *Nature* 502: 368-371
73. Firestein S, Shepherd GM, Werblin FS (1990) Time course of the membrane current underlying sensory transduction in salamander olfactory receptor neurones. *J Physiol* 430: 135-158
74. Fleischer J, Breer H, Strotmann J (2009) Mammalian olfactory receptors. *Front Cell Neurosci* 3: 9

75. Flower DR (1995) Multiple molecular recognition properties of the lipocalin protein family. *J Mol Recognit* 8: 185-195
76. Flower DR, North AC, Sansom CE (2000) The lipocalin protein family: structural and sequence overview. *Biochim Biophys Acta* 1482: 9-24
77. Frings S, Lindemann B (1991) Current recording from sensory cilia of olfactory receptor cells in situ. I. The neuronal response to cyclic nucleotides. *J Gen Physiol* 97: 1-16
78. Fu X, Yan Y, Xu PS, Geerlof-Vidavsky I, Chong W, Gross ML, Holy TE (2015) A Molecular Code for Identity in the Vomeronasal System. *Cell* 163: 313-323
79. Fülle HJ, Vassar R, Foster DC, Yang RB, Axel R, Garbers DL (1995) A receptor guanylyl cyclase expressed specifically in olfactory sensory neurons. *Proc Natl Acad Sci U S A* 92: 3571-3575
80. Fukuda N, Yomogida K, Okabe M, Touhara K (2004) Functional characterization of a mouse testicular olfactory receptor and its role in chemosensing and in regulation of sperm motility. *J Cell Sci* 117: 5835-5845
81. Gaillard I, Rouquier S, Pin JP, Mollard P, Richard S, Barnabé C, Demaille J, Giorgi D (2002) A single olfactory receptor specifically binds a set of odorant molecules. *Eur J Neurosci* 15: 409-418
82. Gao JL, Guillabert A, Hu J, Le Y, Urizar E, Seligman E, Fang KJ, Yuan X, Imbault V, Communi D, Wang JM, Parmentier M, Murphy PM, Migeotte I (2007) F2L, a peptide derived from heme-binding protein, chemoattracts mouse neutrophils by specifically activating Fpr2, the low-affinity N-formylpeptide receptor. *J Immunol* 178 (3): 1450-6.
83. Ghosh S, Larson SD, Hefzi H, Marnoy Z, Cutforth T, Dokka K, Baldwin KK (2011) Sensory maps in the olfactory cortex defined by long-range viral tracing of single neurons. *Nature* 472: 217-220
84. Giannetti N, Pellier V, Oestreicher AB, Astic L (1995) Immunocytochemical study of the differentiation process of the septal organ of Masera in developing rats. *Brain Res Dev Brain Res* 84: 287-293
85. Gimelbrant AA, Stoss TD, Landers TM, McClintock TS (1999) Truncation releases olfactory receptors from the endoplasmic reticulum of heterologous cells. *J Neurochem* 72: 2301-2311
86. Gimelbrant AA, Haley SL, McClintock TS (2001) Olfactory receptor trafficking involves conserved regulatory steps. *J Biol Chem* 276: 7285-7290

87. Greer PL, Bear DM, Lassance JM, Bloom ML, Tsukahara T, Pashkovski SL, Masuda FK, Nowlan AC, Kirchner R, Hoekstra HE, Datta SR (2016) A Family of non-GPCR Chemosensors Defines an Alternative Logic for Mammalian Olfaction. *Cell* 165: 1734-1748
88. Grosmaître X, Vassalli A, Mombaerts P, Shepherd GM, Ma M (2006) Odorant responses of olfactory sensory neurons expressing the odorant receptor MOR23: a patch clamp analysis in gene-targeted mice. *Proc Natl Acad Sci U S A* 103: 1970-1975
89. Grüneberg H (1973) A ganglion probably belonging to the N. terminalis system in the nasal mucosa of the mouse. *Z Anat Entwicklungsgesch* 140: 39-52
90. Grynkiewicz G, Poenie M, Tsien RY (1985) A new generation of Ca²⁺ indicators with greatly improved fluorescence properties. *J Biol Chem* 260:n3440-3450
91. Haga S, Hattori T, Sato T, Sato K, Matsuda S, Kobayakawa R, Sakano H, Yoshihara Y, Kikusui T, Touhara K (2010) The male mouse pheromone ESP1 enhances female sexual receptive behaviour through a specific vomeronasal receptor. *Nature* 466: 118-122
92. Haga-Yamanaka S, Ma L, He J, Qiu Q, Lavis LD, Looger LL, Yu CR (2014) Integrated action of pheromone signals in promoting courtship behavior in male mice. *Elife* 3: e03025
93. Haga-Yamanaka S, Ma L, Yu CR (2015) Tuning properties and dynamic range of type 1 vomeronasal receptors. *Front Neurosci* 9: 244
94. Halpern M, Shapiro LS, Jia C (1995) Differential localization of G proteins in the opossum vomeronasal system. *Brain Res* 677: 157-161
95. Halpern M, Martínez-Marcos A (2003) Structure and function of the vomeronasal system: an update. *Prog Neurobiol* 70: 245-318
96. Hammen GF, Turaga D, Holy TE, Meeks JP (2014) Functional organization of glomerular maps in the mouse accessory olfactory bulb. *Nat Neurosci* 17: 953-961
97. Hastie ND, Held WA, Toole JJ (1979) Multiple genes coding for the androgen-regulated major urinary proteins of the mouse. *Cell* 17: 449-457
98. Hattori T, Osakada T, Matsumoto A, Matsuo N, Haga-Yamanaka S, Nishida T, Mori Y, Mogi K, Touhara K, Kikusui T (2016) Self-Exposure to the Male Pheromone ESP1 Enhances Male Aggressiveness in Mice. *Curr Biol* 26: 1229-1234
99. He J, Ma L, Kim S, Nakai J, Yu CR (2008) Encoding gender and individual information in the mouse vomeronasal organ. *Science* 320: 535-538

100. Herrada G, Dulac C (1997) A novel family of putative pheromone receptors in mammals with a topographically organized and sexually dimorphic distribution. *Cell* 90: 763-773
101. Hohenbrink P, Dempewolf S, Zimmermann E, Mundy NI, Radespiel U (2014) Functional promiscuity in a mammalian chemosensory system: extensive expression of vomeronasal receptors in the main olfactory epithelium of mouse lemurs. *Front Neuroanat* 8: 102
102. Holy TE, Dulac C, Meister M (2000) Responses of vomeronasal neurons to natural stimuli. *Science* 289 (5484): 1569-1572.
103. Hu J, Zhong C, Ding C, Chi Q, Walz A, Mombaerts P, Matsunami H, Luo M (2007) Detection of near-atmospheric concentrations of CO₂ by an olfactory subsystem in the mouse. *Science* 317: 953-957
104. Huang S (2009) Non-genetic heterogeneity of cells in development: more than just noise. *Development* 136: 3853-3862
105. Hurst JL, Robertson DHL, Tolladay U, Beynon RJ (1998) Proteins in urine scent marks of male house mice extend the longevity of olfactory signals. *Anim Behav* 55: 1289-1297
106. Hurst JL, Payne CE, Nevison CM, Marie AD, Humphries RE, Robertson DH, Cavaggioni A, Beynon RJ (2001) Individual recognition in mice mediated by major urinary proteins. *Nature* 414: 631-634
107. Ibarra-Soria X, Levitin MO, Saraiva LR, Logan DW (2014) The olfactory transcriptomes of mice. *PLoS Genet* 10(9): e1004593
108. Imai, T., Suzuki, M., and Sakano, H (2006) Odorant receptor-derived cAMP signals direct axonal targeting. *Science* 314: 6576661
109. Imai T, Sakano H (2008) Odorant receptor-mediated signaling in the mouse. *Curr Opin Neurobiol* 18: 251-260
110. Inamura K, Kashiwayanagi M, Kurihara K (1997) Blockage of urinary responses by inhibitors for IP₃-mediated pathway in rat vomeronasal sensory neurons. *Neurosci Lett* 233: 129-132
111. Ishii T, Serizawa S, Kohda A, Nakatani H, Shiroishi T, Okumura K, Iwakura Y, Nagawa F, Tsuboi A, Sakano H (2001) Monoallelic expression of the odourant receptor gene and axonal projection of olfactory sensory neurones. *Genes Cells* 6: 71-78
112. Ishii T, Hirota J, Mombaerts P (2003) Combinatorial coexpression of neural and immune multigene families in mouse vomeronasal sensory neurons. *Curr Biol* 13: 394-400

113. Ishii T, Mombaerts P (2008) Expression of nonclassical class I major histocompatibility genes defines a tripartite organization of the mouse vomeronasal system. *J Neurosci* 28: 2332-2341
114. Ishii T, Mombaerts P (2011) Coordinated coexpression of two vomeronasal receptor V2R genes per neuron in the mouse. *Mol Cell Neurosci* 46: 397-408
115. Isogai Y, Si S, Pont-Lezica L, Tan T, Kapoor V, Murthy VN, Dulac C (2011) Molecular organization of vomeronasal chemoreception. *Nature*. 478: 241-245.
116. Jacobson L, Trotier D, Døving KB (1998) Anatomical description of a new organ in the nose of domesticated animals by ludvig Jacobson (1813). *Chem Senses* 23: 743-754
117. Jemiolo B, Harvey S, Novotny M (1986) Promotion of the Whitten effect in female mice by synthetic analogs of male urinary constituents. *Proc Natl Acad Sci U S A* 83: 4576-4590
118. Jemiolo B, Xie TM, Novotny M (1991) Socio-sexual olfactory preference in female mice: attractiveness of synthetic chemosignals. *Physiol Behav* 50: 1119-1122
119. Jerusalinsky D, Baez MV, Epstein AL (2012) Herpes simplex virus type 1-based amplicon vectors for fundamental research in neurosciences and gene therapy of neurological diseases. *J Physiol Paris* 106: 2-11
120. Jia C, Halpern M (1996) Subclasses of vomeronasal receptor neurons: differential expression of G proteins (Gi alpha 2 and G(o alpha)) and segregated projections to the accessory olfactory bulb. *Brain Res* 719: 117-128
121. Julifs DM, Fülle HJ, Zhao AZ, Houslay MD, Garbers DL, Beavo JA (1997) A subset of olfactory neurons that selectively express cGMP-stimulated phosphodiesterase (PDE2) and guanylyl cyclase-D define a unique olfactory signal transduction pathway. *Proc Natl Acad Sci U S A* 94: 3388-3395
122. Kajiya K, Inaki K, Tanaka M, Haga T, Kataoka H, Touhara K (2001) Molecular bases of odor discrimination: Reconstitution of olfactory receptors that recognize overlapping sets of odorants. *J Neurosci* 21: 6018-6025
123. Kaluza JF, Gussing F, Bohm S, Breer H, Strotmann J (2004) Olfactory receptors in the mouse septal organ. *J Neurosci Res* 76:442-452
124. Kanageswaran N, Demond M, Nagel M, Schreiner BS, Baumgart S, Scholz P, Altmüller J, Becker C, Doerner JF, Conrad H, Oberland S, Wetzel CH, Neuhaus EM, Hatt H, Gisselmann G (2015) Deep sequencing of the murine olfactory receptor neuron transcriptome. *PLoS One* 10: e113179

125. Kang N, Baum MJ, Cherry JA (2009) A direct main olfactory bulb projection to the 'vomeronasal' amygdala in female mice selectively responds to volatile pheromones from males. *Eur J Neurosci* 29: 624-634
126. Kang N, Baum MJ, Cherry JA (2011) Different profiles of main and accessory olfactory bulb mitral/tufted cell projections revealed in mice using an anterograde tracer and a whole-mount, flattened cortex preparation. *Chem Senses* 36: 251-260
127. Kang N, Koo J (2012) Olfactory receptors in non-chemosensory tissues. *BMB Rep* 45: 612-622
128. Karra D, Dahm R (2010) Transfection techniques for neuronal cells. *J Neurosci* 30: 6171-6177
129. Karunadasa DK, Chapman C, Bicknell RJ (2006) Expression of pheromone receptor gene families during olfactory development in the mouse: expression of a V1 receptor in the main olfactory epithelium. *Eur J Neurosci* 23: 2563-2572
130. Katada S, Nakagawa T, Kataoka H, Touhara K (2003) Odorant response assays for a heterologously expressed olfactory receptor. *Biochem Biophys Res Commun* 305: 964-969
131. Katada S, Hirokawa T, Oka Y, Suwa M, Touhara K (2005) Structural basis for a broad but selective ligand spectrum of a mouse olfactory receptor: mapping the odorant-binding site. *J Neurosci* 25: 1806-1815
132. Katz S, Merzel J (1977) Distribution of epithelia and glands of the nasal septum mucosa in the rat. *Acta Anat (Basel)* 99: 58-66
133. Kaur AW, Ackels T, Kuo TH, Cichy A, Dey S, Hays C, Kateri M, Logan DW, Marton TF, Spehr M, Stowers L (2014) Murine pheromone proteins constitute a context-dependent combinatorial code governing multiple social behaviors. *Cell* 157: 676-688
134. Kelliher KR, Spehr M, Li XH, Zufall F, Leinders-Zufall T (2006) Pheromonal recognition memory induced by TRPC2-independent vomeronasal sensing. *Eur J Neurosci* 23: 3385-3390
135. Kelly DR (1996) When is a butterfly like an elephant? *Chem Biol* 3: 595-602
136. Kerr DS, Von Dannecker LE, Davalos M, Michaloski JS, Malnic B (2008) Ric-8B interacts with G alpha olf and G gamma 13 and co-localizes with G alpha olf, G beta 1 and G gamma 13 in the cilia of olfactory sensory neurons. *Mol Cell Neurosci* 38: 341-348
137. Kim DG, Kang HM, Jang SK, Shin HS (1992) Construction of a bifunctional mRNA in the mouse by using the internal ribosomal entry site of the encephalomyocarditis virus. *Mol Cell Biol* 12: 3636-3643

138. Kim S, Ma L, Jensen KL, Kim MM, Bond CT, Adelman JP, Yu CR (2012) Paradoxical contribution of SK3 and GIRK channels to the activation of mouse vomeronasal organ. *Nat Neurosci* 15: 1236-1244
139. Kimchi T, Xu J, Dulac C (2007) A functional circuit underlying male sexual behaviour in the female mouse brain. *Nature* 448: 1009-1004
140. Kimoto H, Haga S, Sato K, Touhara K (2005) Sex-specific peptides from exocrine glands stimulate mouse vomeronasal sensory neurons. *Nature* 437: 898-901
141. Kimoto H, Sato K, Nodari F, Haga S, Holy TE, Touhara K (2007) Sex- and strain-specific expression and vomeronasal activity of mouse ESP family peptides. *Curr Biol* 17: 1879-1884
142. Kleinau G, Müller A, Biebermann H (2016) Oligomerization of GPCRs involved in endocrine regulation. *J Mol Endocrinol* 57: R59-80
143. Knopf JL, Gallagher JF, Held WA (1983) Differential, multihormonal regulation of the mouse major urinary protein gene family in the liver. *Mol Cell Biol* 3: 2232-2240
144. Komatsu H, Mori I, Rhee JS, Akaike N, Ohshima Y (1996) Mutations in a cyclic nucleotide-gated channel lead to abnormal thermosensation and chemosensation in *C. elegans*. *Neuron* 17: 707-718
145. Kratzing JE (1984) The structure and distribution of nasal glands in four marsupial species. *J Anat* 139: 553-564
146. Krautwurst D, Yau KW, Reed RR (1998) Identification of ligands for olfactory receptors by functional expression of a receptor library. *Cell* 95: 917-926
147. Kretschmer D, Gleske AK, Rautenberg M, Wang R, Köberle M, Bohn E, Schöneberg T, Rabié MJ, Boulay F, Klebanoff SJ, van Kessel KA, van Strijp JA, Otto M, Peschel A (2010) Human formyl peptide receptor 2 senses highly pathogenic *Staphylococcus aureus*. *Cell Host Microbe* 7 (6): 463-473
148. Kroner C, Boehhoff I, Lohmann SM, Genieser HG, Breer H (1996) Regulation of olfactory signalling via cGMP-dependent protein kinase. *Eur J Biochem* 236: 632-637
149. Krusemark EA, Novak LR, Gitelman DR, Li W (2013) When the sense of smell meets emotion: anxiety-state-dependent olfactory processing and neural circuitry adaptation. *J Neurosci* 33: 15324-15332
150. Kuhara A, Okumura M, Kimata T, Tanizawa Y, Takano R, Kimura KD, Inada H, Matsumoto K, Mori I (2008) Temperature sensing by an olfactory neuron in a circuit controlling behavior of *C. elegans*. *Science* 320: 803-807

151. Kumar A, Dudley CA, Moss RL (1999) Functional dichotomy within the vomeronasal system: distinct zones of neuronal activity in the accessory olfactory bulb correlate with sex-specific behaviors. *J Neurosci* 19: RC32
152. Kwak J, Strasser E, Luzynski K, Thoß M, Penn DJ (2016) Are MUPs a Toxic Waste Disposal System? *PLoS One* 11: e0151474
153. Labov JB, Wysocki CJ (1989) Vomeronasal organ and social factors affect urine marking by male mice. *Physiol Behav* 45: 443-447
154. Lane RP, Cutforth T, Axel R, Hood L, Trask BJ (2002) Sequence analysis of mouse vomeronasal receptor gene clusters reveals common promoter motifs and a history of recent expansion. *Proc Natl Acad Sci U S A* 99: 291-296
155. Leinders-Zufall T, Lane AP, Puche AC, Ma W, Novotny MV, Shipley MT, Zufall F (2000) Ultrasensitive pheromone detection by mammalian vomeronasal neurons. *Nature* 405: 792-796
156. Leinders-Zufall T, Brennan P, Widmayer P, S PC, Maul-Pavicic A, Jäger M, Li XH, Breer H, Zufall F, Boehm T (2004) MHC class I peptides as chemosensory signals in the vomeronasal organ. *Science* 306: 1033-1037
157. Leinders-Zufall T, Ishii T, Mombaerts P, Zufall F, Boehm T (2009) Structural requirements for the activation of vomeronasal sensory neurons by MHC peptides. *Nat Neurosci* 12: 1551-1558
158. Leinders-Zufall T, Ma M (2009) Olfactory epithelium. In: Squire L, Albright T, Bloom F, Gage F, Spitzer N (eds) *Encyclopedia of Neuroscience*, 4th edition. Elsevier Science, Amsterdam, pp. 113-118
159. Leinders-Zufall T, Ishii T, Chamero P, Hendrix P, Oboti L, Schmid A, Kircher S, Pyrski M, Akiyoshi S, Khan M, Vaes E, Zufall F, Mombaerts P (2014) A family of nonclassical class I MHC genes contributes to ultrasensitive chemodetection by mouse vomeronasal sensory neurons. *J Neurosci* 34: 5121-5133
160. Lepri JJ, Wysocki CJ, Vandenbergh JG (1985) Mouse vomeronasal organ: effects on chemosignal production and maternal behavior. *Physiol Behav* 35: 809-814
161. Lepri JJ, Wysocki CJ (1987) Removal of the vomeronasal organ disrupts the activation of reproduction in female voles. *Physiol Behav* 40: 349-355
162. Lévai O, Feistel T, Breer H, Strotmann J (2006) Cells in the vomeronasal organ express odorant receptors but project to the accessory olfactory bulb. *J Comp Neurol* 498: 476-490

163. Lewcock JW, Reed RR (2004) A feedback mechanism regulates monoallelic odorant receptor expression. *Proc Natl Acad Sci U S A* 101: 1069-1074
164. Lewis DA (1969) Androgen sulphate formation in male and female mice. *Biochem J* 115: 489-493
165. Leybold BG, Yu CR, Leinders-Zufall T, Kim MM, Zufall F, Axel R (2002) Altered sexual and social behaviors in *trp2* mutant mice. *Proc Natl Acad Sci U S A* 99: 6376-6381
166. Li J, Feinstein P, Mombaerts P (2004) Odorant receptor gene choice is reset by nuclear transfer from mouse olfactory sensory neurons. *Nature* 428: 393-399.
167. Li Q, Korzan WJ, Ferrero DM, Chang RB, Roy DS, Buchi M, Lemon JK, Kaur AW, Stowers L, Fendt M, Liberles SD (2013) Synchronous evolution of an odor biosynthesis pathway and behavioral response. *Curr Biol* 23: 11-20
168. Li YR, Matsunami H (2011) Activation state of the M3 muscarinic acetylcholine receptor modulates mammalian odorant receptor signaling. *Sci Signal* 4:mra1
169. Liberles SD, Buck LB (2006) A second class of chemosensory receptors in the olfactory epithelium. *Nature* 442: 645-650
170. Liberles SD, Horowitz LF, Kuang D, Contos JJ, Wilson KL, Siltberg-Liberles J, Liberles DA, Buck LB (2009) Formyl peptide receptors are candidate chemosensory receptors in the vomeronasal organ. *Proc Natl Acad Sci U S A* 106: 9842-9847
171. Licht G, Meredith M (1987) Convergence of main and accessory olfactory pathways onto single neurons in the hamster amygdala. *Exp Brain Res* 69: 7-18
172. Lim F, Hartley D, Starr P, Lang P, Song S, Yu L, Wang Y, Geller AI (1996) Generation of high-titer defective HSV-1 vectors using an IE 2 deletion mutant and quantitative study of expression in cultured cortical cells. *Biotechniques* 20: 460-469
173. Liman ER, Corey DP, Dulac C (1999) TRP2: a candidate transduction channel for mammalian pheromone sensory signaling. *Proc Natl Acad Sci U S A* 96: 5791-5796
174. Liman ER (2003) Regulation by voltage and adenine nucleotides of a Ca²⁺-activated cation channel from hamster vomeronasal sensory neurons. *J Physiol* 548: 777-787
175. Lin DY, Zhang SZ, Block E, Katz LC (2005) Encoding social signals in the mouse main olfactory bulb. *Nature* 434: 470-477

176. Lindemann L, Ebeling M, Kratochwil NA, Bunzow JR, Grandy DK, Hoener MC (2005) Trace amine-associated receptors form structurally and functionally distinct subfamilies of novel G protein-coupled receptors. *Genomics* 85: 372-385
177. Lindemann L, Meyer CA, Jeanneau K, Bradaia A, Ozmen L, Bluethmann H, Bettler B, Wettstein JG, Borroni E, Moreau JL, Hoener MC (2008) Trace amine-associated receptor 1 modulates dopaminergic activity. *J Pharmacol Exp Ther* 324: 948-956
178. Loconto J, Papes F, Chang E, Stowers L, Jones EP, Takada T, Kumánovics A, Fischer Lindahl K, Dulac C (2003) Functional expression of murine V2R pheromone receptors involves selective association with the M10 and M1 families of MHC class Ib molecules. *Cell* 112: 607-618
179. Logan DW, Marton TF, Stowers L (2008) Species specificity in major urinary proteins by parallel evolution. *PLoS One* 3: e3280
180. Lowe G, Gold GH (1991) The spatial distributions of odorant sensitivity and odorant-induced currents in salamander olfactory receptor cells. *J Physiol* 442: 147-168
181. Lu M, Echeverri F, Moyer BD (2003) Endoplasmic reticulum retention, degradation, and aggregation of olfactory G-protein coupled receptors. *Traffic* 4: 416-433
182. Lu M, Staszewski L, Echeverri F, Xu H, Moyer BD (2004) Endoplasmic reticulum degradation impedes olfactory G-protein coupled receptor functional expression. *BMC Cell Biol* 5: 34
183. Lucas P, Ukhanov K, Leinders-Zufall T, Zufall F (2003) A Diacylglycerol-Gated Cation Channel in Vomeronasal Neuron Dendrites Is Impaired in TRPC2 Mutant Mice: Mechanism of Pheromone Transduction. *neuron* 40: 551-561
184. Ma W, Miao Z, Novotny MV (1999) Induction of estrus in grouped female mice (*Mus domesticus*) by synthetic analogues of preputial gland constituents. *Chem Senses* 24: 289-293
185. Magalhaes AC, Dunn H, Ferguson SS (2012) Regulation of GPCR activity, trafficking and localization by GPCR-interacting proteins. *Br J Pharmacol* 165: 1717-1736
186. Malnic B, Hirono J, Sato T, Buck LB (1999) Combinatorial receptor codes for odors. *Cell* 96: 713-723
187. Marchlewska-Koj A, Cavaggioni A, Mucignat-Caretta C, Olejniczak P (2000) Stimulation of estrus in female mice by male mouse urinary proteins. *J Chem Ecol* 26: 2355-2366

188. Martín-Sánchez A, McLean L, Beynon RJ, Hurst JL, Ayala G, Lanuza E, Martínez-García F (2015) From sexual attraction to maternal aggression: when pheromones change their behavioural significance. *Horm Behav* 68: 65-76
189. Martínez-García F, Martínez-Ricós J, Agustín-Pavón C, Martínez-Hernández J, Novejarque A, Lanuza E (2009) Refining the dual olfactory hypothesis: pheromone reward and odour experience. *Behav Brain Res* 200: 277-286
190. Martínez-Marcos A (2009) On the organization of olfactory and vomeronasal cortices. *Prog Neurobiol* 87: 21-30
191. Martini S, Silvotti L, Shirazi A, Ryba NJ, Tirindelli R (2001) Co-expression of putative pheromone receptors in the sensory neurons of the vomeronasal organ. *J Neurosci* 21: 843-848
192. Maruniak JA, Wysocki CJ, Taylor JA (1986) Mediation of male mouse urine marking and aggression by the vomeronasal organ. *Physiol Behav* 37: 655-657
193. Matarazzo V, Clot-Faybesse O, Marcet B, Guiraudie-Capraz G, Atanasova B, Devauchelle G, Cerutti M, Etiévant P, Ronin C (2005) Functional characterization of two human olfactory receptors expressed in the baculovirus Sf9 insect cell system. *Chem Senses* 30: 195-207
194. Matsui A, Go Y, Niimura Y (2010) Degeneration of olfactory receptor gene repertoires in primates: no direct link to full trichromatic vision. *Mol Biol Evol* 27: 1192-1200
195. Matsunami H, Buck LB (1997) A multigene family encoding a diverse array of putative pheromone receptors in mammals. *Cell* 90: 775-784
196. Matsuoka M, Yoshida-Matsuoka J, Iwasaki N, Norita M, Costanzo RM, Ichikawa M (2001) Immunocytochemical study of G(i)2alpha and G(o)alpha on the epithelium surface of the rat vomeronasal organ. *Chem Senses* 26: 161-166
197. McCarthy AM, McMahan L, Schaffer PA (1989) Herpes simplex virus type 1 ICP27 deletion mutants exhibit altered patterns of transcription and are DNA deficient. *J Virol* 63: 18-27
198. McClintock TS, Sammeta N (2003) Trafficking prerogatives of olfactory receptors. *Neuroreport* 14: 1547-1552
199. McLatchie LM, Fraser NJ, Main MJ, Wise A, Brown J, Thompson N, Solari R, Lee MG, Foord SM (1998) RAMPs regulate the transport and ligand specificity of the calcitonin-receptor-like receptor. *Nature* 393: 333-339
200. Meeks JP, Arnson HA, Holy TE (2010) Representation and transformation of sensory information in the mouse accessory olfactory system. *Nat Neurosci* 13: 723-730

201. Meister M (2015) On the dimensionality of odor space. *Elife* 4: e07865
202. Meredith M, O'Connell RJ (1979) Efferent control of stimulus access to the hamster vomeronasal organ. *J Physiol* 286: 301-316
203. Meredith M (1994) Chronic recording of vomeronasal pump activation in awake behaving hamsters. *Physiol Behav* 56: 345-354
204. Meredith M (2001) Human vomeronasal organ function: a critical review of best and worst cases. *Chem Senses* 26: 433-445
205. Minic J, Persuy MA, Godel E, Aioun J, Connerton I, Salesse R, Pajot-Augy E (2005) Functional expression of olfactory receptors in yeast and development of a bioassay for odorant screening. *FEBS J* 272: 524-537
206. Miragall F, Breipohl W, Naguro T, Voss-Wermbter G (1984) Freeze-fracture study of the plasma membranes of the septal olfactory organ of Maseru. *J Neurocytol* 13:111-125
207. Mitsui K, Sakihama T, Takahashi K, Masuda K, Fukuda R, Hamana H, Sato T, Hamakubo T (2012) Functional reconstitution of olfactory receptor complex on baculovirus. *Chem Senses* 37: 837-847
208. Miyamichi K, Amat F, Moussavi F, Wang C, Wickersham I, Wall NR, Taniguchi H, Tasic B, Huang ZJ, He Z, Callaway EM, Horowitz MA, Luo L (2011) Cortical representations of olfactory input by trans-synaptic tracing. *Nature* 472: 191-196
209. Mombaerts P, Wang F, Dulac C, Chao SK, Nemes A, Mendelsohn M, Edmondson J, Axel R (1996) Visualizing an olfactory sensory map. *Cell* 87: 675-686
210. Mombaerts P (2004) Genes and ligands for odorant, vomeronasal and taste receptors. *Nat Rev Neurosci* 5: 263-278
211. Montani G, Tonelli S, Sanghez V, Ferrari PF, Palanza P, Zimmer A, Tirindelli R (2013) Aggressive behaviour and physiological responses to pheromones are strongly impaired in mice deficient for the olfactory G-protein α -subunit G8. *J Physiol* 591: 3949-3962
212. Moon C, Simpson PJ, Tu Y, Cho H, Ronnett GV (2005) Regulation of intracellular cyclic GMP levels in olfactory sensory neurons. *J Neurochem* 95: 200-209
213. Morè L (2006) Mouse major urinary proteins trigger ovulation via the vomeronasal organ. *Chem Senses* 31: 393-401

214. Mori I, Goshima F, Ito H, Koide N, Yoshida T, Yokochi T, Kimura Y, Nishiyama Y (2005) The vomeronasal chemosensory system as a route of neuroinvasion by herpes simplex virus. *Virology* 334: 51-58
215. Mori K, Nagao H, Yoshihara Y (1999) The olfactory bulb: coding and processing of odor molecule information. *Science* 286: 7116715
216. Mucignat-Caretta C, Caretta A, Cavaggioni A (1995) Acceleration of puberty onset in female mice by male urinary proteins. *J Physiol* 486 : 517-522
217. Mucignat-Caretta C, Redaelli M, Caretta A (2012) One nose, one brain: contribution of the main and accessory olfactory system to chemosensation. *Front Neuroanat* 6: 46
218. Mudge JM, Armstrong SD, McLaren K, Beynon RJ, Hurst JL, Nicholson C, Robertson DH, Wilming LG, Harrow JL (2008) Dynamic instability of the major urinary protein gene family revealed by genomic and phenotypic comparisons between C57 and 129 strain mice. *Genome Biol* 9: R91
219. Mueller JW, Gilligan LC, Idkowiak J, Arlt W, Foster PA (2015) The Regulation of Steroid Action by Sulfation and Desulfation. *Endocr Rev* 36: 526-563
220. Munger SD, Leinders-Zufall T, Zufall F (2009) Subsystem organization of the mammalian sense of smell. *Annu Rev Physiol* 71: 115-140
221. Munger SD, Leinders-Zufall T, McDougall LM, Cockerham RE, Schmid A, Wandernoth P, Wennemuth G, Biel M, Zufall F, Kelliher KR (2010) An olfactory subsystem that detects carbon disulfide and mediates food-related social learning. *Curr Biol* 20: 1438-1444
222. Nakahara TS, Cardozo LM, Ibarra-Soria X, Bard AD, Carvalho VM, Trintinalia GZ, Logan DW, Papes F (2016) Detection of pup odors by non-canonical adult vomeronasal neurons expressing an odorant receptor gene is influenced by sex and parenting status. *BMC Biol* 14: 12
223. Nara K, Saraiva LR, Ye X, Buck LB (2011) A large-scale analysis of odor coding in the olfactory epithelium. *J Neurosci* 31: 9179-9191
224. Neuhaus EM, Gisselmann G, Zhang W, Dooley R, Störtkuhl K, Hatt H (2005) Odorant receptor heterodimerization in the olfactory system of *Drosophila melanogaster*. *Nat Neurosci* 8: 15-17
225. Niimura Y, Nei M (2003) Evolution of olfactory receptor genes in the human genome. *Proc Natl Acad Sci U S A* 100: 12235-12240

226. Niimura Y (2009) Evolutionary dynamics of olfactory receptor genes in chordates: interaction between environments and genomic contents. *Hum Genomics* 4: 107-118
227. Nodari F, Hsu FF, Fu X, Holekamp TF, Kao LF, Turk J, Holy TE (2008) Sulfated steroids as natural ligands of mouse pheromone-sensing neurons. *J Neurosci* 28: 6407-6418
228. Norlin EM, Gussing F, Berghard A (2003) Vomeronasal phenotype and behavioral alterations in G alpha i2 mutant mice. *Curr Biol* 13: 1214-1219
229. Novotny M, Schwende FJ, Wiesler D, Jorgenson JW, Carmack M (1984) Identification of a testosterone-dependent unique volatile constituent of male mouse urine: 7-exo-ethyl-5-methyl-6,8-dioxabicyclo[3.2.1]-3-octene. *Experientia* 40: 217-219
230. Novotny M, Harvey S, Jemiolo B, Alberts J (1985) Synthetic pheromones that promote inter-male aggression in mice. *Proc Natl Acad Sci U S A* 82: 2059-2061
231. Novotny M, Jemiolo B, Harvey S, Wiesler D, Marchlewska-Koj A (1986) Adrenal-mediated endogenous metabolites inhibit puberty in female mice. *Science* 231: 722-725
232. Novotny M, Harvey S, Jemiolo B (1990) Chemistry of male dominance in the house mouse, *Mus domesticus*. *Experientia* 46: 109-113
233. Novotny MV, Jemiolo B, Wiesler D, Ma W, Harvey S, Xu F, Xie TM, Carmack M (1999a) A unique urinary constituent, 6-hydroxy-6-methyl-3-heptanone, is a pheromone that accelerates puberty in female mice. *Chem Biol* 6: 377-383
234. Novotny MV, Ma W, Wiesler D, Zídek L (1999b) Positive identification of the puberty-accelerating pheromone of the house mouse: the volatile ligands associating with the major urinary protein. *Proc Biol Sci* 266: 2017-2022
235. Oboti L, Pérez-Gómez A, Keller M, Jacobi E, Birnbaumer L, Leinders-Zufall T, Zufall F, Chamero P (2014) A wide range of pheromone-stimulated sexual and reproductive behaviors in female mice depend on G protein G α . *BMC Biol* 12: 31
236. Oboti L, Ibarra-Soria X, Pérez-Gómez A, Schmid A, Pyrski M, Paschek N, Kircher S, Logan DW, Leinders-Zufall T, Zufall F, Chamero P (2015) Pregnancy and estrogen enhance neural progenitor-cell proliferation in the vomeronasal sensory epithelium. *BMC Biol* 13: 104
237. Ohara H, Okamura H, Ichikawa M, Mori Y, Hagino-Yamagishi K (2013) Existence of G α i2-expressing axon terminals in the goat main olfactory bulb. *J Vet Med Sci* 75: 85-88
238. Omura M, Mombaerts P (2014) Trpc2-expressing sensory neurons in the main olfactory epithelium of the mouse. *Cell Rep* 8: 583-595

239. Omura M, Mombaerts P (2015) Trpc2-expressing sensory neurons in the mouse main olfactory epithelium of type B express the soluble guanylate cyclase Gucy1b2. *Mol Cell Neurosci* 65:114-124
240. Pankevich DE, Baum MJ, Cherry JA (2004) Olfactory sex discrimination persists, whereas the preference for urinary odorants from estrous females disappears in male mice after vomeronasal organ removal. *J Neurosci* 24: 9451-9457
241. Pankevich DE, Cherry JA, Baum MJ (2006a) Effect of vomeronasal organ removal from male mice on their preference for and neural Fos responses to female urinary odors. *Behav Neurosci* 120: 925-936
242. Pankevich DE, Cherry JA, Baum MJ (2006b) Accessory olfactory neural Fos responses to a conditioned environment are blocked in male mice by vomeronasal organ removal. *Physiol Behav* 87 (4): 781-788
243. Papes F, Logan DW, Stowers L (2010) The vomeronasal organ mediates interspecies defensive behaviors through detection of protein pheromone homologs. *Cell* 141: 692-703
244. Pascarella G, Lazarevic D, Plessy C, Bertin N, Akalin A, Vlachouli C, Simone R, Faulkner GJ, Zucchelli S, Kawai J, Daub CO, Hayashizaki Y, Lenhard B, Carninci P, Gustincich S (2014) NanoCAGE analysis of the mouse olfactory epithelium identifies the expression of vomeronasal receptors and of proximal LINE elements. *Front Cell Neurosci* 8: 41
245. Pedersen PE, Stewart WB, Greer CA, Shepherd GM (1983) Evidence for olfactory function in utero. *Science* 221: 478-480
246. Pérez-Gómez A, Stein B, Leinders-Zufall T, Chamero P (2014) Signaling mechanisms and behavioral function of the mouse basal vomeronasal neuroepithelium. *Front Neuroanat* 8: 135
247. Pérez-Gómez A, Blyemehl K, Stein B, Pyrski M, Birnbaumer L, Munger SD, Leinders-Zufall T, Zufall F, Chamero P (2015) Innate Predator Odor Aversion Driven by Parallel Olfactory Subsystems that Converge in the Ventromedial Hypothalamus. *Curr Biol* 25: 1340-1346
248. Pietrobon M, Zamparo I, Maritan M, Franchi SA, Pozzan T, Lodovichi C (2011) Interplay among cGMP, cAMP, and Ca²⁺ in living olfactory sensory neurons in vitro and in vivo. *J Neurosci* 31: 8395-8405
249. Pifferi S, Boccaccio A, Menini A (2006) Cyclic nucleotide-gated ion channels in sensory transduction. *FEBS Lett* 580: 2853-2859
250. Poo C, Isaacson JS (2009) Odor representations in olfactory cortex: "sparse" coding, global inhibition, and oscillations. *Neuron* 62: 850-861

251. Potter SM, Zheng C, Koos DS, Feinstein P, Fraser SE, Mombaerts P (2001) Structure and emergence of specific olfactory glomeruli in the mouse. *J Neurosci* 21: 9713-9723
252. Pro-Sistiaga P, Mohedano-Moriano A, Ubeda-Bañon I, Del Mar Arroyo-Jimenez M, Marcos P, Artacho-Pérula E, Crespo C, Insausti R, Martinez-Marcos A (2007) Convergence of olfactory and vomeronasal projections in the rat basal telencephalon. *J Comp Neurol* 504: 346-362
253. Rasche S, Toetter B, Adler J, Tschapek A, Doerner JF, Kurtenbach S, Hatt H, Meyer H, Warscheid B, Neuhaus EM (2010) Tmem16b is specifically expressed in the cilia of olfactory sensory neurons. *Chem Senses* 35: 239-245
254. Repicky SE, Luetje CW (2009) Molecular receptive range variation among mouse odorant receptors for aliphatic carboxylic acids. *J Neurochem* 109: 193-202
255. Ressler KJ, Sullivan SL, Buck LB (1993) A zonal organization of odorant receptor gene expression in the olfactory epithelium. *Cell* 73: 597-609
256. Rivière S, Challet L, Fluegge D, Spehr M, Rodriguez I (2009) Formyl peptide receptor-like proteins are a novel family of vomeronasal chemosensors. *Nature* 459: 574-577
257. Roberts SA, Simpson DM, Armstrong SD, Davidson AJ, Robertson DH, McLean L, Beynon RJ, Hurst JL (2010) Darcin: a male pheromone that stimulates female memory and sexual attraction to an individual male's odour. *BMC Biol* 8: 75
258. Roberts SA, Davidson AJ, McLean L, Beynon RJ, Hurst JL (2012) Pheromonal induction of spatial learning in mice. *Science* 338:146261465
259. Robertson DH, Cox KA, Gaskell SJ, Evershed RP, Beynon RJ (1996) Molecular heterogeneity in the Major Urinary Proteins of the house mouse *Mus musculus*. *Biochem J* 316: 265-272
260. Robertson DH, Hurst JL, Bolgar MS, Gaskell SJ, Beynon RJ (1997) Molecular heterogeneity of urinary proteins in wild house mouse populations. *Rapid Commun Mass Spectrom* 11: 786-790
261. Rodolfo-Masera, T. (1943) Su l'esistenza di un particolare organo olfattivo nel setto nasale della cavia e di altri roditori. *Archo Ital Anat Embriol* 48: 157-212
262. Rodriguez I, Feinstein P, Mombaerts P (1999) Variable patterns of axonal projections of sensory neurons in the mouse vomeronasal system. *Cell* 97: 199-208
263. Rodriguez I, Greer CA, Mok MY, Mombaerts P (2000) A putative pheromone receptor gene expressed in human olfactory mucosa. *Nat Genet* 26: 18-19

264. Rodriguez I, Del Punta K, Rothman A, Ishii T, Mombaerts P (2002) Multiple new and isolated families within the mouse superfamily of V1r vomeronasal receptors. *Nat Neurosci* 5: 134-140
265. Roppolo D, Vollery S, Kan CD, Lüscher C, Broillet MC, Rodriguez I (2007) Gene cluster lock after pheromone receptor gene choice. *EMBO J* 26 (14): 3423-3430
266. Royo NC, Vandenberghe LH, Ma JY, Hauspurg A, Yu L, Maronski M, Johnston J, Dichter MA, Wilson JM, Watson DJ (2008) Specific AAV serotypes stably transduce primary hippocampal and cortical cultures with high efficiency and low toxicity. *Brain Res* 1190: 15-22
267. Rubin BD, Katz LC (2001) Spatial coding of enantiomers in the rat olfactory bulb. *Nat Neurosci* 4: 355-356
268. Ryba NJ, Tirindelli R (1997) A new multigene family of putative pheromone receptors. *Neuron* 19: 371-379
269. Saito H, Kubota M, Roberts RW, Chi Q, Matsunami H (2004) RTP family members induce functional expression of mammalian odorant receptors. *Cell* 119: 679-691
270. Saito H, Chi Q, Zhuang H, Matsunami H, Mainland JD (2009) Odor coding by a Mammalian receptor repertoire. *Sci Signal* 2: ra9
271. Salahpour A, Angers S, Mercier JF, Lagacé M, Marullo S, Bouvier M (2004) Homodimerization of the beta2-adrenergic receptor as a prerequisite for cell surface targeting. *J Biol Chem* 279: 33390-33397
272. Sam M, Vora S, Malnic B, Ma W, Novotny MV, Buck LB (2001) Neuropharmacology. Odorants may arouse instinctive behaviours. *Nature* 412: 142
273. Saraiva LR, Kondoh K, Ye X, Yoon KH, Hernandez M, Buck LB (2016) Combinatorial effects of odorants on mouse behavior. *Proc Natl Acad Sci U S A* 113: E3300-6
274. Sathyanesan A, Feijoo AA, Mehta ST, Nimarko AF, Lin W (2013) Expression profile of G-protein subunit gene transcripts in the mouse olfactory sensory epithelia. *Front Cell Neurosci* 7: 84
275. Schiffmann E, Corcoran BA, Wahl SM (1975) N-formylmethionyl peptides as chemoattractants for leucocytes. *Proc Natl Acad Sci U S A* 72: 1059-1062
276. Schmid A, Pyrski M, Biel M, Leinders-Zufall T, Zufall F (2010) Grueneberg ganglion neurons are finely tuned cold sensors. *J Neurosci* 30: 7563-7568

277. Schou KB, Pedersen LB, Christensen ST (2015) Ins and outs of GPCR signaling in primary cilia. *EMBO Rep* 16: 1099-1113
278. Serizawa S, Miyamichi K, Nakatani H, Suzuki M, Saito M, Yoshihara Y, Sakano H (2003) Negative feedback regulation ensures the one receptor-one olfactory neuron rule in mouse. *Science* 302: 2088-2094
279. Sharrow SD, Vaughn JL, Zidek L, Novotny MV, Stone MJ (2002) Pheromone binding by polymorphic mouse major urinary proteins. *Protein Sci* 11: 2247-2256
280. Shaw PH, Held WA, Hastie ND (1983) The gene family for major urinary proteins: expression in several secretory tissues of the mouse. *Cell* 32: 755-761
281. Shawar SM, Rich RR, Becker EL (1995) Peptides from the amino-terminus of mouse mitochondrially encoded NADH dehydrogenase subunit 1 are potent chemoattractants. *Biochem Biophys Res Commun* 211: 812-818.
282. Shepard BD, Natarajan N, Protzko RJ, Acres OW, Pluznick JL (2013) A cleavable N-terminal signal peptide promotes widespread olfactory receptor surface expression in HEK293T cells. *PLoS One* 8: e68758
283. Shi P, Zhang J (2007) Comparative genomic analysis identifies an evolutionary shift of vomeronasal receptor gene repertoires in the vertebrate transition from water to land. *Genome Res* 17: 166-174
284. Shinoda K, Shiotani Y, Osawa Y (1989) Necklace olfactory glomeruli form unique components of the rat primary olfactory system. *J Comp Neurol* 284: 362-373
285. Shirokova E, Schmiedeberg K, Bedner P, Niessen H, Willecke K, Raguse JD, Meyerhof W, Krautwurst D (2005) Identification of specific ligands for orphan olfactory receptors. G protein-dependent agonism and antagonism of odorants. *J Biol Chem* 280: 11807-11815
286. Shirokova E, Raguse JD, Meyerhof W, Krautwurst D (2008) The human vomeronasal type-1 receptor family--detection of volatiles and cAMP signaling in HeLa/Olf cells. *FASEB J* 22: 1416-1425
287. Showell HJ, Freer RJ, Zigmond SH, Schiffmann E, Aswanikumar S, Corcoran B, Becker EL (1976) The structure-activity relations of synthetic peptides as chemotactic factors and inducers of lysosomal secretion for neutrophils. *J Exp Med* 143: 1154-1169
288. Silvotti L, Moiani A, Gatti R, Tirindelli R (2007) Combinatorial co-expression of pheromone receptors, V2Rs. *J Neurochem* 103: 1753-1763

289. Silvotti L, Cavalca E, Gatti R, Percudani R, Tirindelli R (2011) A recent class of chemosensory neurons developed in mouse and rat. *PLoS One* 6: e24462
290. Simonato M, Manservigi R, Marconi P, Glorioso J (2000) Gene transfer into neurones for the molecular analysis of behaviour: focus on herpes simplex vectors. *Trends Neurosci* 23: 183-190
291. Smith IL, Hardwicke MA, Sandri-Goldin RM (1992) Evidence that the herpes simplex virus immediate early protein ICP27 acts post-transcriptionally during infection to regulate gene expression. *Virology* 186, 74-86
292. Smith TD, Bhatnagar KP (2000) The human vomeronasal organ. Part II: prenatal development. *J Anat* 197 : 421-436
293. Smrcka AV, Sternweis PC (1993) Regulation of purified subtypes of phosphatidylinositol-specific phospholipase C beta by G protein alpha and beta gamma subunits. *J Biol Chem* 268: 9667-9674
294. Smrcka AV (2008) G protein subunits: central mediators of G protein-coupled receptor signaling. *Cell Mol Life Sci* 65: 2191-2214
295. Sorkin A, von Zastrow M (2009) Endocytosis and signalling: intertwining molecular networks. *Nat Rev Mol Cell Biol* 10: 609-622
296. Sosulski DL, Bloom ML, Cutforth T, Axel R, Datta SR (2011) Distinct representations of olfactory information in different cortical centres. *Nature* 472: 213-216
297. Spaete RR, Frenkel N (1982) The herpes simplex virus amplicon: a new eucaryotic defective-virus cloning-amplifying vector. *Cell* 30: 295-304
298. Spaete RR, Frenkel N (1985) The herpes simplex virus amplicon: analyses of cis-acting replication functions. *Proc Natl Acad Sci U S A* 82: 694-698.
299. Spehr M, Hatt H, Wetzel CH (2002) Arachidonic acid plays a role in rat vomeronasal signal transduction. *J Neurosci* 22: 8429-8437
300. Spehr M, Kelliher KR, Li XH, Boehm T, Leinders-Zufall T, Zufall F (2006) Essential role of the main olfactory system in social recognition of major histocompatibility complex peptide ligands. *J Neurosci* 26: 1961-1970
301. Spehr J, Hagendorf S, Weiss J, Spehr M, Leinders-Zufall T, Zufall F (2009) Ca²⁺-calmodulin feedback mediates sensory adaptation and inhibits pheromone-sensitive ion channels in the vomeronasal organ. *J Neurosci* 29: 2125-2135

302. Spehr M (2016) Vomeronasal Transduction and Cell Signaling. In: Munger S, Zufall F (eds) *Chemosensory Transduction- The Detection of Odors, Tastes, and Other Chemostimuli*, 1st edition. Academic Press, London, p. 194
303. Stein B, Alonso MT, Zufall F, Leinders-Zufall T, Chamero P (2016) Functional Overexpression of Vomeronasal Receptors Using a Herpes Simplex Virus Type 1 (HSV-1)-Derived Amplicon. *PLoS One* 11: e0156092
304. Stephan AB, Shum EY, Hirsh S, Cygnar KD, Reisert J, Zhao H (2009) ANO2 is the ciliary calcium-activated chloride channel that may mediate olfactory amplification. *Proc Natl Acad Sci U S A* 106: 11776-11781
305. Stettler DD, Axel R (2009) Representations of odor in the piriform cortex. *Neuron* 63: 854-864
306. Stewart R, Lane RP (2007) V1R promoters are well conserved and exhibit common putative regulatory motifs. *BMC Genomics* 8: 253
307. Stowers L, Holy TE, Meister M, Dulac C, Koentges G (2002) Loss of sex discrimination and male-male aggression in mice deficient for TRP2. *Science* 295: 1493-1500
308. Szoka PR, Paigen K (1978) Regulation of mouse major urinary protein production by the Mup-A gene. *Genetics* 90: 597-612
309. Taniguchi K, Arai T, Ogawa K (1993) Fine structure of the septal olfactory organ of Masera and its associated gland in the golden hamster. *J Vet Med Sci* 55:107-116
310. Thoß M, Luzynski KC, Ante M, Miller I, Penn DJ (2015) Major urinary protein (MUP) profiles show dynamic changes rather than individual 'barcode' signatures. *Front Ecol Evol* 3. pii: 71
311. Tian H, Ma M (2004) Molecular organization of the olfactory septal organ. *J Neurosci* 24: 8383-8390
312. Tirindelli R, Dibattista M, Pifferi S, Menini A (2009) From pheromones to behavior. *Physiol Rev* 89: 921-956
313. Touhara K, Sengoku S, Inaki K, Tsuboi A, Hirono J, Sato T, Sakano H, Haga T (1999) Functional identification and reconstitution of an odorant receptor in single olfactory neurons. *Proc Natl Acad Sci U S A* 96: 4040-4045
314. Touhara K (2001) Functional cloning and reconstitution of vertebrate odorant receptors. *Life Sci* 68: 2199-2206

315. Touhara K, Niimura Y, Ihara S (2016) Vertebrate Odorant Receptors. In: Munger S, Zufall F (eds) *Chemosensory Transduction- The Detection of Odors, Tastes, and Other Chemostimuli*, 1st edition. Academic Press, London, p. 51.
316. Trinh K, Storm DR (2004) Detection of odorants through the main olfactory epithelium and vomeronasal organ of mice. *Nutr Rev* 62: S189-192
317. Trotier D (2011) Vomeronasal organ and human pheromones. *Eur Ann Otorhinolaryngol Head Neck Dis* 128: 184-190
318. Tucker D (1963) Physical variables in the olfactory stimulation process. *J Gen Physiol* 46: 453-489
319. Turaga D, Holy TE (2012) Organization of vomeronasal sensory coding revealed by fast volumetric calcium imaging. *J Neurosci* 32: 1612-1621
320. Vassar R, Ngai J, Axel R (1993) Spatial segregation of odorant receptor expression in the mammalian olfactory epithelium. *Cell*. 74: 309-18
321. Verbeurgt C, Wilkin F, Tarabichi M, Gregoire F, Dumont JE, Chatelain P (2014) Profiling of olfactory receptor gene expression in whole human olfactory mucosa. *PLoS One* 9: e96333
322. Von Dannecker LE, Mercadante AF, Malnic B (2005) Ric-8B, an olfactory putative GTP exchange factor, amplifies signal transduction through the olfactory-specific G-protein Galphao1f. *J Neurosci* 25: 3793-3800
323. Von Dannecker LE, Mercadante AF, Malnic B (2006) Ric-8B promotes functional expression of odorant receptors. *Proc Natl Acad Sci U S A* 103: 9310-9314
324. Von der Weid B, Rossier D, Lindup M, Tuberosa J, Widmer A, Col JD, Kan C, Carleton A, Rodriguez I (2015) Large-scale transcriptional profiling of chemosensory neurons identifies receptor-ligand pairs in vivo. *Nat Neurosci* 18: 1455-1463
325. Wagner S, Gresser AL, Torello AT, Dulac C (2006) A multireceptor genetic approach uncovers an ordered integration of VNO sensory inputs in the accessory olfactory bulb. *Neuron* 50: 697-709
326. Wakabayashi Y, Mori Y, Ichikawa M, Yazaki K, Hagino-Yamagishi K (2002) A putative pheromone receptor gene is expressed in two distinct olfactory organs in goats. *Chem Senses* 27: 207-213
327. Wakabayashi Y, Ohkura S, Okamura H, Mori Y, Ichikawa M (2007) Expression of a vomeronasal receptor gene (V1r) and G protein alpha subunits in goat, *Capra hircus*, olfactory receptor neurons. *J Comp Neurol* 503: 371-380

328. Walz A, Feinstein P, Khan M, Mombaerts P (2007) Axonal wiring of guanylate cyclase-D-expressing olfactory neurons is dependent on neuropilin 2 and semaphorin 3F. *Development* 134: 4063-4072
329. Wang F, Nemes A, Mendelsohn M, Axel R (1998) Odorant receptors govern the formation of a precise topographic map. *Cell* 93: 47-60
330. Wang Z, Balet Sindreu C, Li V, Nudelman A, Chan GC, Storm DR (2006) Pheromone detection in male mice depends on signaling through the type 3 adenylyl cyclase in the main olfactory epithelium. *J Neurosci* 26: 7375-7379
331. Wang Z, Nudelman A, Storm DR (2007) Are pheromones detected through the main olfactory epithelium? *Mol Neurobiol* 35: 317-323
332. Weber M, Pehl U, Breer H, Strotmann J (2002) Olfactory receptor expressed in ganglia of the autonomic nervous system. *J Neurosci Res* 68: 176-184
333. Wei J, Wayman G, Storm DR (1996) Phosphorylation and inhibition of type III adenylyl cyclase by calmodulin-dependent protein kinase II in vivo. *J Biol Chem* 271: 24231-24235
334. Wu Z, Autry AE, Bergan JF, Watabe-Uchida M, Dulac CG (2014) Galanin neurons in the medial preoptic area govern parental behaviour. *Nature* 509: 325-330
335. Wyatt TD (ed) (2014) *Pheromones and Animal Behavior-Chemical Signals and Signatures*, 2nd edition. Cambridge University Press, Cambridge, p. 1
336. Wysocki CJ, Lepri JJ (1991) Consequences of removing the vomeronasal organ. *J Steroid Biochem Mol Biol* 39: 661-669
337. Wysocki CJ, Yamazaki K, Curran M, Wysocki LM, Beauchamp GK (2004) Mice (*Mus musculus*) lacking a vomeronasal organ can discriminate MHC-determined odortypes. *Horm Behav* 46: 241-246
338. Xu F, Schaefer M, Kida I, Schafer J, Liu N, Rothman DL, Hyder F, Restrepo D, Shepherd GM (2005) Simultaneous activation of mouse main and accessory olfactory bulbs by odors or pheromones. *J Comp Neurol* 489: 491-500
339. Xu PS, Lee D, Holy TE (2016) Experience-Dependent Plasticity Drives Individual Differences in Pheromone-Sensing Neurons. *Neuron* 91: 878-892
340. Yoshikawa K, Nakagawa H, Mori N, Watanabe H, Touhara K (2013) An unsaturated aliphatic alcohol as a natural ligand for a mouse odorant receptor. *Nat Chem Biol* 9: 160-162

341. Young JM, Kambere M, Trask BJ, Lane RP (2005) Divergent V1R repertoires in five species: Amplification in rodents, decimation in primates, and a surprisingly small repertoire in dogs. *Genome Res* 15: 231-240
342. Young JM, Trask BJ (2007) V2R gene families degenerated in primates, dog and cow, but expanded in opossum. *Trends Genet* 23: 212-215
343. Young JM, Massa HF, Hsu L, Trask BJ (2010) Extreme variability among mammalian V1R gene families. *Genome Res* 20: 10-18
344. Zhang J, Pacifico R, Cawley D, Feinstein P, Bozza T (2013) Ultrasensitive detection of amines by a trace amine-associated receptor. *J Neurosci* 33: 3228-3239
345. Zhang P, Yang C, Delay RJ (2008) Urine stimulation activates BK channels in mouse vomeronasal neurons. *J Neurophysiol* 100: 1824-1834
346. Zhang P, Yang C, Delay RJ (2010) Odors activate dual pathways, a TRPC2 and a AA-dependent pathway, in mouse vomeronasal neurons. *Am J Physiol Cell Physiol* 298: C1253-1264
347. Zhao H, Ivic L, Otaki JM, Hashimoto M, Mikoshiba K, Firestein S (1998) Functional expression of a mammalian odorant receptor. *Science* 279: 237-242
348. Zhuang H, Matsunami H (2007) Synergism of accessory factors in functional expression of mammalian odorant receptors. *J Biol Chem* 282: 15284-15293
349. Zufall F, Leinders-Zufall T (1997) Identification of a long-lasting form of odor adaptation that depends on the carbon Monoxide/cGMP second-messenger system. *J Neurosci* 17: 2703-2712
350. Zufall F, Leinders-Zufall T (2000) The cellular and molecular basis of odor adaptation. *Chem Senses* 25: 473-481
351. Zufall F, Munger SD (2001) From odor and pheromone transduction to the organization of the sense of smell. *Trends Neurosci* 24: 191-193
352. Zufall F, Leinders-Zufall T (2007) Mammalian pheromone sensing. *Curr Opin Neurobiol* 17: 483-489
353. Zufall F (2014) TRPs in Olfaction. In: Nilius B, Flockerzi V (eds) *Mammalian Transient Receptor Potential (TRP) Cation Channel Volume II*, 1st edition. Springer, Berlin, pp. 917-933

8 ACKNOWLEDGEMENTS

First, I want to thank **Prof. Dr. Trese Leinders-Zufall** and **Dr. Pablo Chamero** for initiating this challenging doctoral project and giving me the opportunity to work on the deorphanization of vomeronasal receptors. This thesis allowed me to gain insight into diverse methodological approaches and to develop my scientific personality and find "my way".

I would like to thank **Prof. Dr. Trese Leinders-Zufall** for her constant support of this project and many motivating scientific discussions, especially during the writing of this doctoral thesis. I also want to thank her for regular scientific advice and her friendly commitment for all PhD students and fellows in the laboratory. Further, I would like to thank her for an easy access to all expensive working material and funding my project. Further, I would like to thank her for providing me with the mitochondria-derived peptide ND1 and mice: C57BL/6 from Charles River Laboratories, *Omp-GFP* mice (B6.OMP^{tm3Mom}MomJ; originally JR# 006667) (Potter *et al.*, 2001), and *cG o^{-/-}* mice (Chamero *et al.*, 2011; Oboti *et al.*, 2014; Pérez-Gómez *et al.*, 2015). I also thank her for enabling me to travel to scientific meetings to present and discuss my work with leading international scientists of the field. Finally, I would like to thank her for reviewing this thesis as 1st reviewer.

I also would like to express considerable thanks to **Dr. Pablo Chamero** for his consistent support of this doctoral thesis, funding this project, and his grateful mentoring. He taught me in many advanced experimental techniques and he always had a friendly ear for all the problems. He always encouraged me to "ask the right experimental questions". Further, I would like to thank him for help during the writing and preparing scientific contributions. I also would like to thank him for partially analyzing experimental results and providing me with DNA plasmids. I also would like to thank him for providing the microscope to perform calcium imaging recordings. Finally, I thank him for thoroughly proofreading this thesis.

I thank **Prof. Dr. Niemeyer** for her interest in my doctoral thesis and her willingness to review this thesis as 2nd reviewer.

I would like to thank **Dr. Anabel Pérez-Gómez** for the kind collaboration and for her scientific advice on many issues. I also would like to thank **Johanna Roth** for technical support. I also thank the staff of the animal facility, **Andrea Degreif, Angelika Ströer, Sarah Boll, Kerstin Becker, and Lisa Knieriem** for professional support in all questions regarding mice. I thank **Michael Konzmann** for ordering and providing me with chemicals and technical equipment.

ACKNOWLEDGEMENTS

I thank **Prof. Dr. Dr. Frank Zufall** for his scientific words of advice and his support for this project and its associated scientific publications. I thank **Dr. Martina Pyrski** for her scientific advice and many nice conversations. I thank **PD Dr. Schmid** for his scientific advice in many issues concerning microscopy. Further, I thank **Dr. Jan Weiss** for electrophysiological explanations. I thank **Petra Hammes** and **Monika Vorndran** for practical advice in gel electrophoresis and **Sabine Plant** for professional advice in heterologous cell culture.

I thank **Gabriele Mörschbacher** for helping me with all kinds of bureaucracy. I thank **Holger Frisch** for his help with IT-problems.

I thank **Prof. Dr. Karl Deisserroth** for providing us with the pcDNA3.1/hChR2(H134R)-*mCherry* plasmid (Addgene plasmid #20938).

I thank **Prof. Dr. Alonso** for providing the helper virus for viral amplicon preparation. I would like to thank **Prof. Dr. Lisa Stowers** for providing *rFeld4* Plasmid DNA.

I thank **Dr. Bernd Bufe** for kindly providing me with the W-peptide and for experimental advice.

I also thank all my current and former fellow students **Dr. Timo Schumann, Florian Bolz, Eugenia Eckstein, Dennis Bakker, Katherin Bleyemehl, Dr. Christian Schauer, Yannick Teuchert, Thomas Blum, Tong Tong, Hendrik Stempel, Ana Moreno-Pérez** and **Dr. Philipp Hendrix** for many nice conversations and support.

I am grateful to all the people from my private life, who supported and motivated me.

9 COPYRIGHT PERMISSION

PLOS ONE:

PLOS applies the Creative Commons Attribution (CC BY) license to articles and other works we publish. If you submit your paper for publication by PLOS, you agree to have the CC BY license applied to your work. Under this Open Access license, you as the author agree that anyone can reuse your article in whole or part for any purpose, for free, even for commercial purposes. Anyone may copy, distribute, or reuse the content as long as the author and original source are properly cited. This facilitates freedom in re-use and also ensures that PLOS content can be mined without barriers for the needs of research.

Figures 8, 12 to 17, and 19 to 21, associated figure legends and text passages of this thesis work in hand were in part originally published in PLoS One: **Stein B**, Alonso MT, Zufall F, Leinders-Zufall T, Chamero P. Functional Overexpression of Vomeronasal Receptors Using a Herpes Simplex Virus Type 1 (HSV-1)-Derived Amplicon. PLoS One 11: e0156092.

Elsevier/ Current biology:

Figures 39 and 40 of this thesis work were used with permission (License Number: 4074210022109) and were originally published in Pérez-Gómez A, Bleyemehl K, **Stein B**, Pyrski M, Birnbaumer L, Munger SD, Leinders-Zufall T, Zufall F, Chamero P. Innate Predator Odor Aversion Driven by Parallel Olfactory Subsystems that Converge in the Ventromedial Hypothalamus. Curr Biol 25: 1340-1346.